

UNCLASSIFIED

RRD 1704-16

**RESTRICTED DATA**

THIS DOCUMENT CONTAINS RESTRICTED DATA AS DEFINED IN THE ATOMIC ENERGY ACT OF 1954. ITS TRANSMITTAL OR THE DISCLOSURE OF ITS CONTENTS IN ANY MANNER TO AN UNAUTHORIZED PERSON IS PROHIBITED.

TID 15062

**MASTER**

Classification Canceled  
Or Changed To **UNCLASSIFIED**

By Authority Of D.O.C.  
By F.M. Deckelmann Date 10/20/71

~~RESTRICTED DATA~~  
~~ATOMIC ENERGY ACT - 1954~~  
~~Under Military~~  
~~Clearance of Secret~~  
~~Required for Access~~

UNCLASSIFIED TITLE

**RADIATION EFFECTS  
ON A  
NUCLEAR ROCKET  
ENGINE SYSTEM**

DISTRIBUTION OF THIS DOCUMENT IS UNLIMITED

**IR** ROCKETDYNE • A DIVISION OF NORTH AMERICAN AVIATION, INC.

~~CONFIDENTIAL~~ UNCLASSIFIED

## **DISCLAIMER**

**This report was prepared as an account of work sponsored by an agency of the United States Government. Neither the United States Government nor any agency Thereof, nor any of their employees, makes any warranty, express or implied, or assumes any legal liability or responsibility for the accuracy, completeness, or usefulness of any information, apparatus, product, or process disclosed, or represents that its use would not infringe privately owned rights. Reference herein to any specific commercial product, process, or service by trade name, trademark, manufacturer, or otherwise does not necessarily constitute or imply its endorsement, recommendation, or favoring by the United States Government or any agency thereof. The views and opinions of authors expressed herein do not necessarily state or reflect those of the United States Government or any agency thereof.**

## **DISCLAIMER**

**Portions of this document may be illegible in electronic image products. Images are produced from the best available original document.**

~~CONFIDENTIAL~~

UNCLASSIFIED

RRP 704-16

C-26

~~RESTRICTED DATA~~

THIS DOCUMENT CONTAINS RESTRICTED DATA AS DEFINED IN THE ATOMIC ENERGY ACT OF 1954. ITS TRANSMISSION OR THE DISCLOSURE OF ITS CONTENTS IN ANY MANNER TO AN UNAUTHORIZED PERSON IS PROHIBITED.

R-3007

RADIATION EFFECTS ON A  
NUCLEAR ROCKET ENGINE SYSTEM  
(Unclassified Title)

NOTICE

This report was prepared as an account of work sponsored by the United States Government. Neither the United States nor the United States Atomic Energy Commission, nor any of their employees, nor any of their contractors, subcontractors, or their employees, makes any warranty, express or implied, or assumes any legal liability or responsibility for the accuracy, completeness or usefulness of any information, apparatus, product or process disclosed, or represents that its use would not infringe privately owned rights.

**ROCKETDYNE**

A DIVISION OF NORTH AMERICAN AVIATION, INC

6633 CANOGA AVENUE

CANOGA PARK CALIFORNIA

EXCLUDED FROM AUTOMATIC  
REGISTRATION; DOD DIR 6200.10  
DOES NOT APPLY

AT(29-2)-771

**SPECIAL REREVIEW  
FINAL  
DETERMINATION**  
Class: U

Reviewers	Class.	Date
<u>JRP</u>	<u>U</u>	<u>12-8-81</u>
<u>HFC</u>	<u>U</u>	<u>12-9-81</u>

PREPARED BY

Rocketdyne Engineering  
Nuclionics Subdivision

APPROVED BY

*S. V. Gunn*

S. V. Gunn  
Program Manager  
Rover Program

DISTRIBUTION OF THIS DOCUMENT IS UNLIMITED

1:191  
*Reg*

NO OF PAGES 255 & xi

REVISIONS

DATE 14 July 1961

DATE	REV. BY	PAGES AFFECTED	REMARKS

UNCLASSIFIED

~~CONFIDENTIAL~~

UNCLASSIFIED

**UNCLASSIFIED**

**ROCKETDYNE**  
A DIVISION OF NORTH AMERICAN AVIATION INC

**CONFIDENTIAL**

## FOREWORD

This final report is submitted in fulfillment of the radiation environment study phase of contract AT(29-2)771. It complements the liquid hydrogen feed system development performed under this contract for the Kiwi-B2 experiment.

The radiation environmental analysis of this report was carried out for the preliminary K-1 engine system design to determine requirements for radiation-resistant components, to establish the preliminary engine package configuration, and to recommend tests of components and parts to be performed at the Nevada Test Site as part of the Kiwi test series.

## ABSTRACT

The problems of radiation environment in a nuclear rocket engine system are analyzed for the K-1 preliminary engine design, and an optimum system configuration is obtained which incorporates radiation-resistant components and structure throughout. Pertinent test programs are recommended for inclusion in the Kiwi-B reactor experiments at the Nevada Test Site.

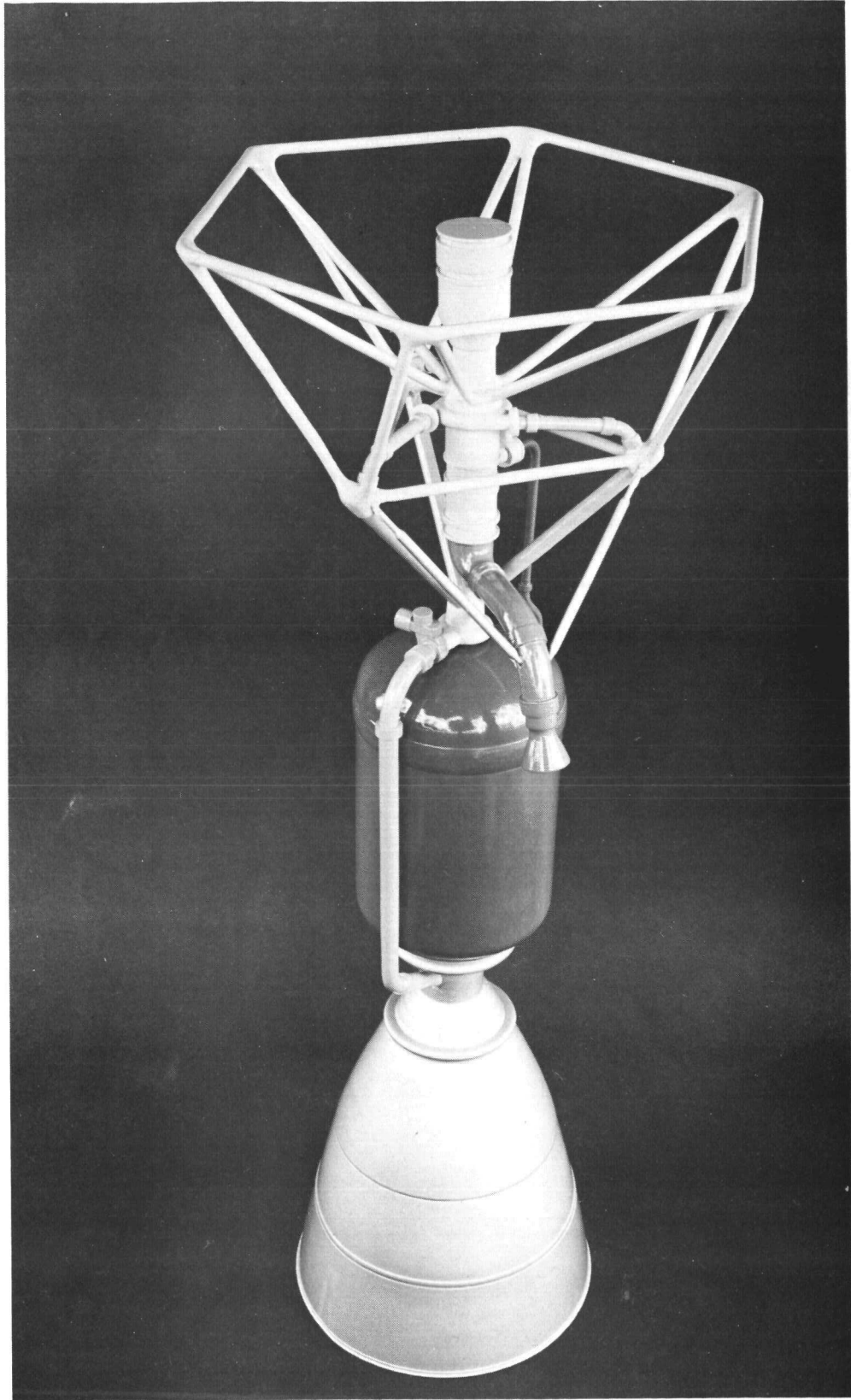
(Unclassified Abstract)

**UNCLASSIFIED**

**CONFIDENTIAL**

UNCLASSIFIED

~~CONFIDENTIAL~~



R-3007

~~CONFIDENTIAL~~

UNCLASSIFIED

~~CONFIDENTIAL~~

CONTENTS

Foreword . . . . . ii

Abstract . . . . . ii

Introduction . . . . . 1

Summary . . . . . 3

Description of Engine System Under Analysis . . . . . 3

    Shield Selection . . . . . 7

    Configuration Optimization . . . . . 8

Summary of Radiation Effects Analysis . . . . . 13

    Requirements . . . . . 13

    Radiation Heating in Tanked Propellant . . . . . 13

    Radiation Heating in Components . . . . . 18

    Radiation Damage . . . . . 27

Recommended Development Test Program . . . . . 35

    Experimental Objectives . . . . . 35

    Areas of Experimental Investigation . . . . . 35

Analysis . . . . . 43

Reactor Radiation Levels . . . . . 43

    Radiation Sources . . . . . 43

    Description of Computer Programs Used in

        Attenuation Calculations . . . . . 60

Shield Material Selection . . . . . 79

    Shield Philosophy . . . . . 79

    Shield Materials . . . . . 81

Radiation Problem Areas and Means of Solution . . . . . 91

    Propellant Heating . . . . . 91

    Reactor, Tank Separation Based on Propellant Heating . . . . . 142

    Component Heating . . . . . 161

    Components in the Flight System . . . . . 170

    Radiation Levels From Radioactivity Induced in

        Materials and Components . . . . . 187

~~CONFIDENTIAL~~

~~CONFIDENTIAL~~

---

Radiation Damage . . . . .	202
<u>Test Programs</u> . . . . .	231
Experimental Objectives . . . . .	231
Areas of Experimental Investigation . . . . .	231
Component Radiation Test Programs . . . . .	242
References . . . . .	253



~~CONFIDENTIAL~~

ILLUSTRATIONS

1. K-1 Engine Layout and Component Identification . . . . .	5
2. K-1 Engine Layout, End View . . . . .	6
3. Change in System Weight vs Separation Distance (Potential Flow Model with 1500 Megawatts of Power) . . . . .	9
4. Change in System Weight vs Separation Distance (Completely Mixed Flow Model with 1500 Megawatts of Power) . . . . .	9
5. Change in System Weight vs Separation Distance (Recirculation Flow Model with 1500 Megawatts of Power) . . . . .	9
6. Isoflux and Isodose Curves for 1500 Megawatt K-1 Engine . . . . .	11
7. Typical Temperature Rise of Propellant Exit Flow as a Function of Engine Operation Time . . . . .	15
8. Pressure Rise (To Prevent Boiling) vs Attenuation Factor and Separation Distance (Potential Flow Model with Power at 1500 Mw) . . . . .	17
9. Pressure Rise (To Prevent Boiling) vs Attenuation Factor and Separation Distance (Completely Mixed Flow Model with Power at 1500 Mw) . . . . .	17
10. Pressure Rise (To Prevent Boiling) vs Attenuation Factor and Separation Distance (Recirculation Flow Model with Power at 1500 Mw) . . . . .	17
11. Engine Thermal Environment . . . . .	19
12. Heat Generation in Components Located Above Reactor Dome. . . . .	20
13. Dose Rates Due to Activation of Some Common Metal Alloys. . . . .	34

~~CONFIDENTIAL~~

~~CONFIDENTIAL~~

14.	Spectrum of Gamma Rays Emitted Within $10^{-6}$ Seconds After Fission Normalized to 7.9 Mev per Fission . . . . .	44
15.	Spectrum of Gamma Rays Emitted by $U^{235}$ Thermal Fission Products . . . . .	44
16.	Capture Gamma-Ray Spectrum for $U^{235}$ , Normalized to 6.42 Mev Per Capture . . . . .	48
17.	Shield Geometry for GRACE-I Code . . . . .	61
18.	Source and Shield Geometry for GRACE-II Code . . . . .	69
19.	Cylindrical Geometry for GRACE-II Code . . . . .	69
20.	Summary of Propellant Heating Curve . . . . .	92
21.	Neutron Flux Distribution in Propellant . . . . .	92
22.	Neutron Flux Distributions in Propellant . . . . .	94
23.	Neutron Flux Distributions in Propellant . . . . .	94
24.	Heat Generation Rate in Propellant . . . . .	97
25.	Heat Generation Rate in Propellant . . . . .	97
26.	Heat Generation Rate in Propellant . . . . .	98
27.	Heat Generation Rate in Propellant . . . . .	99
28.	Heat Generation Rate in Propellant . . . . .	99
29.	Heat Generation Rate in Propellant . . . . .	100
30.	Heat Generation Rate in Propellant . . . . .	100
31.	Shield Attenuation Factor vs Shield Thickness . . . . .	102
32.	Propellant Tank Example 1500 Megawatt Reactor . . . . .	105
33.	Potential Flow Velocity Distribution . . . . .	107
34.	Potential Flow Velocity Distribution (Vertical Components) . . . . .	107

**CONFIDENTIAL**

35. Transformation to a Flat-Bottom Tank . . . . . 109

36. Recirculation Flow Model . . . . . 126

37. Heat Transfer by Turbulent Free Convection to  
Liquid Hydrogen . . . . . 131

38. Comparison of Propellant Heating Models . . . . . 137

39. Tank Baffle to Eliminate Recirculation Currents  
Caused by Radiation Heating . . . . . 139

40. Baffle Velocity Profile . . . . . 140

41. Pressure Rise (To Prevent Boiling) vs Attenuation  
Factor and Separation Distance (Potential Flow Model  
with Power at 1500 Mw) . . . . . 145'

42. Pressure Rise (To Prevent Boiling) vs Attenuation  
Factor and Separation Distance (Completely Mixed Flow  
Model with Power at 1500 Mw) . . . . . 145

43. Pressure Rise (To Prevent Boiling) vs Attenuation  
Factor and Separation Distance (Recirculation Flow  
Model with Power at 1500 Mw) . . . . . 145

44. Shield Weight vs Separation Distance . . . . . 148

45. Residual Gas Weight and Propellant Depletion vs  
Tank Pressure . . . . . 147

46. Tank Weight vs Tank Pressure . . . . . 149

47. Load Diagram Reference Vehicle . . . . . 151

48. Shear and Moment Resulting from Aerodynamic Pressure,  
Control Force, and Inertia Loading . . . . . 152

~~CONFIDENTIAL~~

49. Critical Axial Compression Coefficients for Simply-Supported Sandwich Cylinders with Corrugated Core Oriented in the Axial Direction . . . . .	153
50. Ultimate Element Crippling Curves Alclad 2024-T3, T4 Aluminum Alloy Sheet . . . . .	154
51. Interstage Structure Weight vs Length . . . . .	154
52. Engine Mount Weight vs Separation Distance . . . . .	154
53. General Thrust Structure Mount Arrangement . . . . .	154
54. Change in System Weight vs Separation Distance (Potential Flow Model with 1500 Megawatts of Power) . . . . .	157
55. Change in System Weight vs Separation Distance (Completely Mixed Flow Model with 1500 Megawatts of Power) . . . . .	157
56. Change in System Weight vs Separation Distance (Recirculation Flow Model with 1500 Megawatts of Power). . . . .	157
57. Isoflux and Isodose Curves for 1500 Megawatt K-1 Engine. . . . .	159
58. Heat Generation in Components Located Above Reactor Dome . . . . .	160
59. Heat Generation Rate Along Axial Centerline Below Curve. . . . .	164
60. Component Self-Shielding Factors . . . . .	165
61. Engine Thermal Environment . . . . .	166
62. Effects of Thermal Radiation on End Temperature . . . . .	168
63. Correction Factor for Self-Attenuation and Thermal Conduction . . . . .	169
64. Heat Generation in 3-Inch Zr H <sub>1.8</sub> One-Weight-Percent Boron Shield. Power Level, 1500 Mw . . . . .	184
65. Heat Generation in 5-Inch Zr H <sub>1.8</sub> One-Weight-Percent Boron Shield. Power Level, 1500 Mw . . . . .	184

~~CONFIDENTIAL~~

---

66.	Heat Generation in 9.88-Inch Boronated Graphite Shield. Power Level - 1500 Mw . . . . .	185
67.	Heat Generation in 16.47-Inch Boronated Graphite Shield. Power Level - 1500 Mw . . . . .	185
68.	Dose Rates Due to Activation of Some Common Metal Alloys . . . . .	199
69.	Turbopump Activity After Shutdown . . . . .	200
70.	Temperature-EMF Relationship for Two High-Temperature Thermocouple Combinations, (Reference Junction at 32 F) . . .	206
71.	Temperature-EMF Relationship for Chromel- Constantan (Reference Junction at 32 F) . . . . .	208
72.	Pressure-Actuated Seal . . . . .	226
73.	Gas Evolution by Irradiated Explosives at Ambient Temperatures . . . . .	229
74.	Cavitation Test Facility Schematic . . . . .	239
75.	Cavitating Venturi Test Schematic . . . . .	241

~~CONFIDENTIAL~~

TABLES

1.	Component Activation Levels . . . . .	32
2.	Core Gamma-Ray Sources, Mev Per Fission . . . . .	45
3.	Neutron Economy Table . . . . .	50
4.	Microscopic Removal Cross Sections . . . . .	59
5.	Basic Gamma-Ray Data . . . . .	74
6.	Equivalent Weights and Thicknesses of Possible Shield Materials as Compared to Boronated Graphite . . . . .	82
7.	Shield Materials and Compositions Used . . . . .	87
8.	System Weight, Separation Distance, and Attenuation Factor . . . . .	158
9.	Composition of Alloys (in Percent) . . . . .	190
10.	Nuclear Reactions and Product Isotope Data . . . . .	192
11.	Specific Radiation Levels from Elements per Unit Flux (Fast and Thermal) . . . . .	194
12.	Specific Radiation Levels from Regular and Reactor Grade (R.G.) Alloys (A Comparison) . . . . .	195
13.	Turbopump Materials List . . . . .	197
14.	Component Activation Levels . . . . .	201
15.	Transducer Characteristics . . . . .	210

**CONFIDENTIAL**

---

## INTRODUCTION

The Kiwi-B2 Experiment of the Los Alamos Scientific Laboratory employs a flyable-type feed system mounted 200 ft away from the test reactor, and will utilize a feed system designed, developed and delivered to the test site by Rocketdyne in fulfillment of its obligations under the Atomic Energy Commission contract AT(29-2)771. This report on the effects of radiation environment is also in fulfillment of that contract.

Rocketdyne-developed components in the B2 feed system have been designed to meet all the normal requirements of a flight-weight engine, but the intense radiation fluxes present in a close-coupled flight-configuration engine make necessary a detailed analysis of the operating conditions imposed on the system components by the radiation environment. For this reason, the studies described in this report were performed with the objective of advancing the Kiwi-B2 technology to meet the requirements of a flyable upper-stage engine system.

The scope of radiation environmental analysis must encompass the effects of reactor radiation on all phases of engine system operation and testing. It includes the predominant effects of radiation heating, both in the tanked propellant and in component and structure. It considers the effects of radiation damage to sensitive materials and electronic equipment, and the disrupting effect of ionizing radiation on the operation of electrical systems. Another important consideration is the radioactivity induced by the large neutron fluxes present during engine operation, because posttest maintenance, disassembly and inspection will be seriously hampered by the radiation hazard to personnel. And, although the engine system may operate successfully in ground tests, there must be assurance that the system will function properly in a space environment in the absence of scattered radiation from air, ground, and facility, and without the benefit of convective cooling from the surrounding atmosphere.

~~CONFIDENTIAL~~

---

Analysis of these radiation environment problem areas has been carried out with the objective of moving the Kiwi-B2 technology forward to meet the requirements of a flyable engine system. Foremost among the targets of Rocketdyne's analytical efforts has been the preliminary optimization of over-all engine system configuration to achieve the most favorable balance between reactor-tank separation and shield weight; specification of component designs has been based on these results. Individual component specifications have been developed to meet requirements of light weight, radiation resistance and minimum posttest maintenance hazards. Finally, a specific objective of this analytical effort was to specify those radiation-effects test programs which are required to verify analytical predictions and to provide empirical design data for the development of future nuclear engine systems.



**CONFIDENTIAL**

---

SUMMARY

DESCRIPTION OF ENGINE SYSTEM UNDER ANALYSIS

The rocket engine analyzed in this study characterizes the first flyable nuclear engine capable of performing a useful mission. This engine is referred to as the K-1 throughout the technical analysis and preliminary design which formed the basis for this report. The engine assumes the use of the IASL Kiwi-B3 reactor, the Rocketdyne-developed Mark 9 pump and turbine, and a modified Kiwi B nozzle. By incorporation of a suitable pressure shell and control system, an integrated engine system is obtained. Figures 1 and 2 shows the engine system envelope for nozzle expansion ratios of 50:1, 75:1 and 100:1.

The turbine is driven by hot gases which may be produced either by separate gas generators or by tapping off from the reactor exhaust. The latter type of operation is referred to as the bleed cycle and has been assumed for this study. It is also possible to heat gases to drive the turbine by what is called the topping cycle, in which propellant flows from the pump through the nozzle and reactor and is then expanded through the turbine. The turbine then exhausts into the reactor where the propellant is heated and ejected through the nozzle. While the gas generator system is a proven method of operation, the hot gas bleed system shows performance advantages. The topping cycle provides the highest theoretical engine performance but was rejected for this study because it lacked over-all engine flexibility.

In the engine system shown in Fig. 1 and 2, the propellant, under regulated tank pressure, enters a low NPSH booster stage before entering the main pump. At the main pump exit the propellant flow is distributed through three ducts where it is directed so as to cool the lower thrust structure, propellant transfer lines, the nozzle, and the reflector and pressure shell as it proceeds to the reactor inlet. The propellant is then heated in the reactor

**CONFIDENTIAL**

---

coolant passages and is expanded through the nozzle. Hot gases are bled off upstream of the nozzle throat to drive the turbine, after which they are directed from the turbine exhaust through auxiliary exhaust nozzles to furnish additional thrust. The reactor nozzle assembly can be gimballed to adjust for thrust misalignment. Hydrogen gas is used to operate engine controls, thus utilizing available pneumatic power and taking advantage of the radiation-resistant features of pneumatic systems.

Typical operating parameters which were assumed for this engine study are listed below:

Summary of Engine Data

Reactor Power, Mw	1500
Hydrogen Flowrate through Reactor, lb/sec	83
Chamber Pressure, psia	816
Hydrogen Temperature at Reactor Out- let, R	4500

During preliminary analysis of the engine system, it became apparent that an optimization would be necessary which considered the various ways of reducing the heating effect of reactor leakage radiation on the tanked liquid hydrogen propellant. It appeared that the feed pump must operate with a positive NPSH at its inducer stage to be within the present state of the art and to assure a conservative design. Therefore, an optimum engine system would incorporate a large separation distance and/or a radiation shield to provide radiation protection for its tanked propellant.

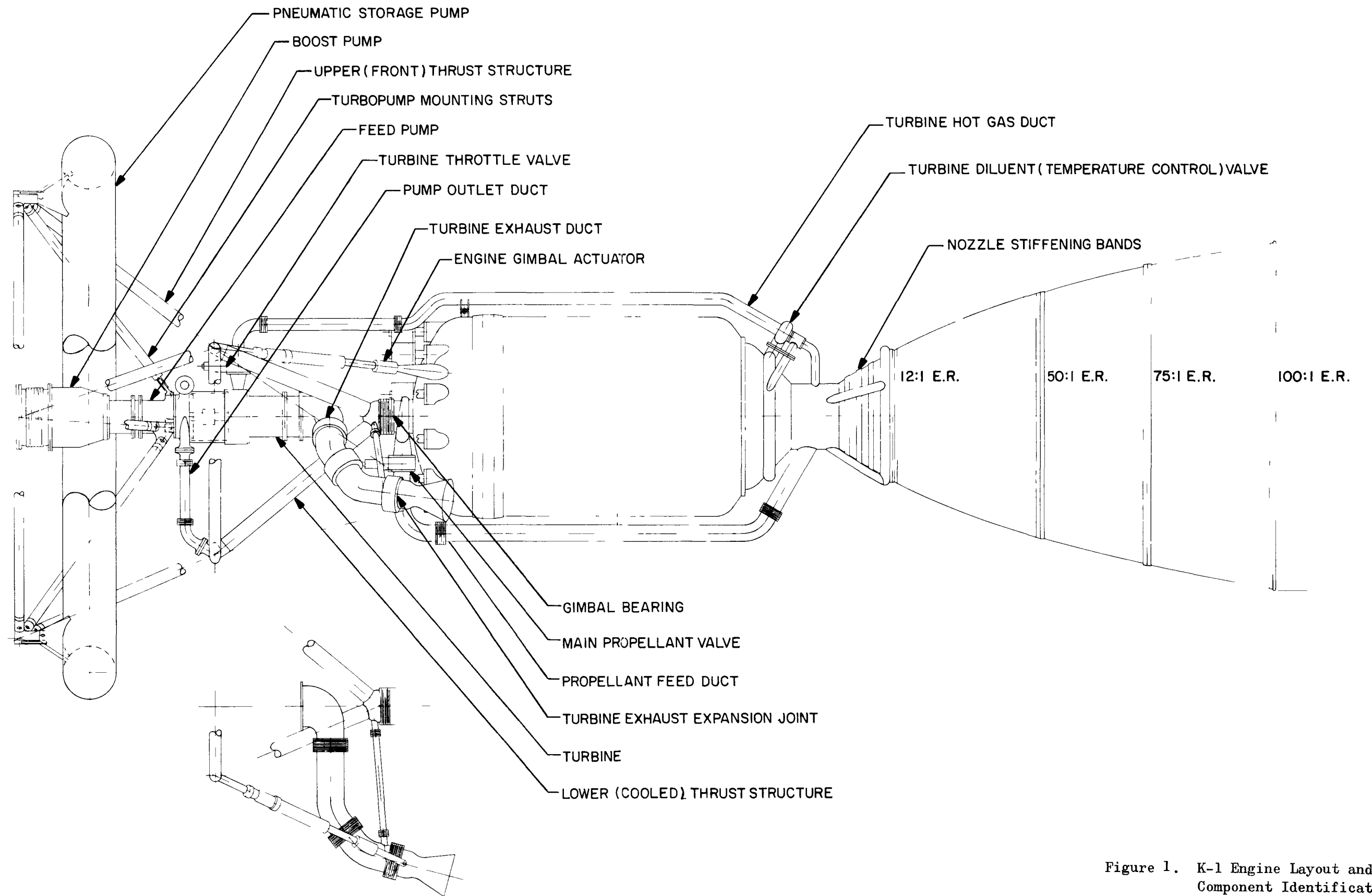


Figure 1. K-1 Engine Layout and Component Identification

**CONFIDENTIAL**

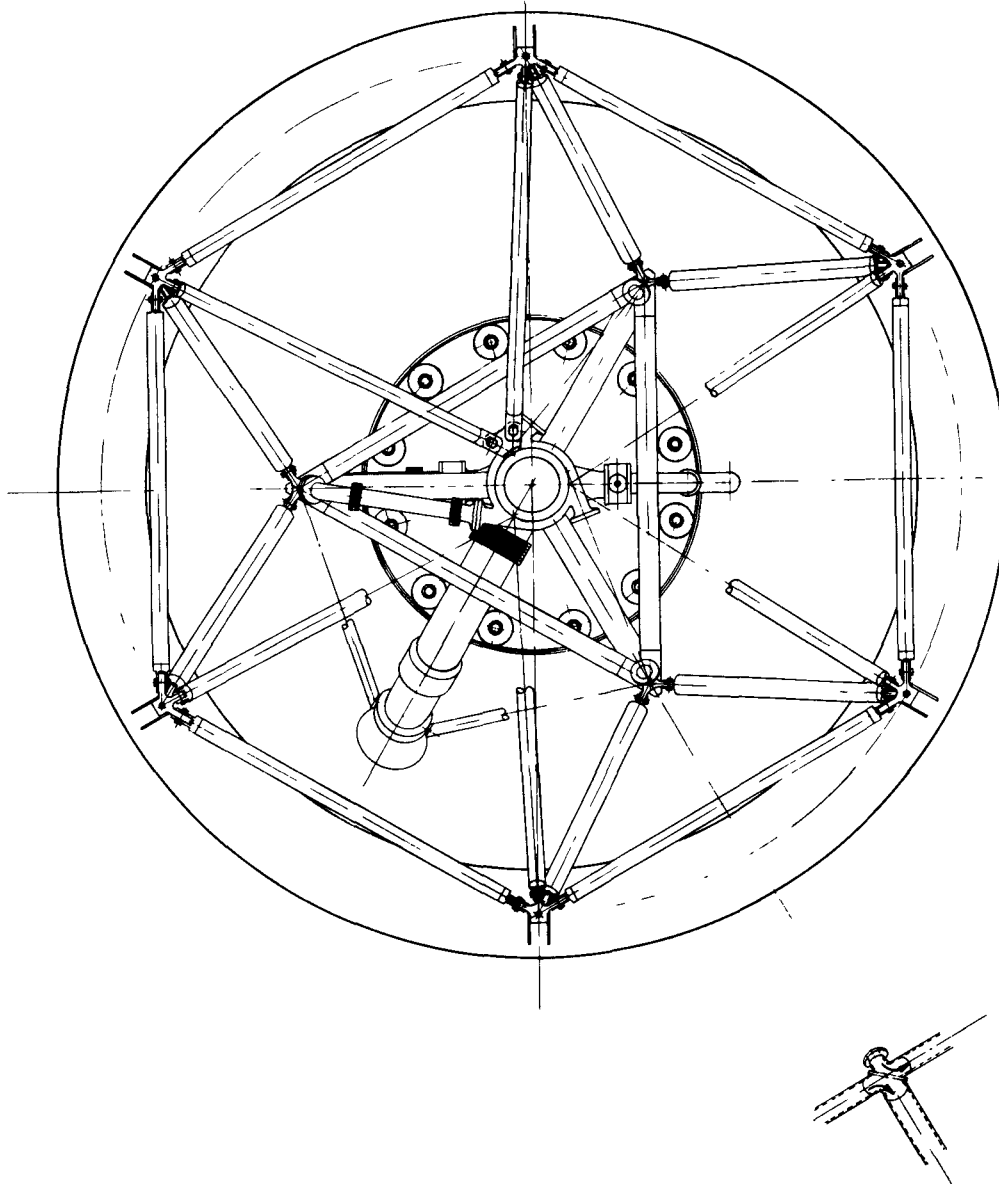


Figure 2. K-1 Engine Layout, End View

~~CONFIDENTIAL~~

---

## SHIELD SELECTION

A shield cannot be designed on the basis of radiation absorption properties alone. The shield should be light, compact, and strong so as not to require heavy additional supporting structure. It will absorb large amounts of radiation energy and must have adequate cooling. This requires a material with good heat transfer properties and high-temperature strength. It should not upset the neutron economy of the reactor or cause unacceptable power peaking. Shield materials must be evaluated with regard to attenuating both neutron and gamma fluxes, and care must be taken to avoid choosing a shield material on the basis of one type of radiation while neglecting the rest of the spectrum. Since consideration of component heating can be deferred, the foremost problem is that of propellant heating. Therefore, the absorption properties of the hydrogen propellant will tend to determine the shield material. Hydrogen is extremely effective in removing neutron kinetic energy through elastic collisions and captures, which makes effective neutron shielding mandatory. With regard to gamma attenuation, all non-hydrogenous materials are of about the same relative effectiveness, so the choice of shielding material will hinge primarily on its neutron absorption properties.

A wide variety of shield material was examined by Rocketdyne in order to specify the one or two most promising materials. One material, boronated graphite, offers most of the desirable properties already mentioned and is a good material to use in performing the preliminary optimization. The choice of boronated graphite for the system configuration analysis will not restrict the resulting system to use of boronated graphite. Other feasible shield materials are so similar to boronated graphite in their application and effect that the system selection will be unchanged by the use of a different material.

~~CONFIDENTIAL~~

---

## CONFIGURATION OPTIMIZATION

A study was made, based on propellant heating, to determine the optimum separation of the reactor from the tank and the optimum amount of shielding. The following relationships were considered:

1. Change in tank pressure (to prevent boiling) vs separation distance and shielding attenuation factor
2. Shield weight vs separation distance and attenuation factor
3. Tank weight vs tank pressure
4. Weight of residual gas in main propellant tank vs tank pressure
5. Interstage structure weight vs separation distance
6. Thrust structure weight vs separation distance and shielding attenuation factor

An analysis of the above relationships yields three curves representing the change in system weight vs reactor tank separation distance. Three curves are necessary to represent the three propellant tank flow models which appear possible in this design. These curves apply only to a pressure-stabilized tank in which the pressure required for stability is equal to or less than the pressure allowance for initial propellant vapor pressure, aerodynamic and solar heating, and NPSH. The following table summarizes the minimum system weights and corresponding separation distances and attenuation factors which are obtained from Fig. 3, 4, and 5.

**CONFIDENTIAL**

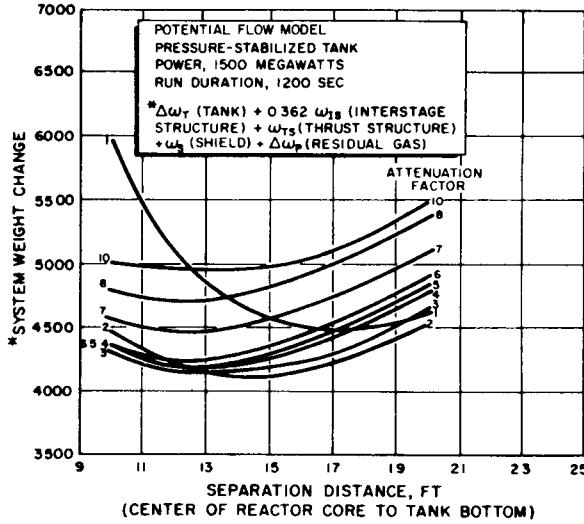


Figure 3. Change in System Weight vs Separation Distance (Potential Flow Model with 1500 Megawatts of Power)

Figure 4. Change in System Weight vs Separation Distance (Completely Mixed Flow Model with 1500 Megawatts of Power)

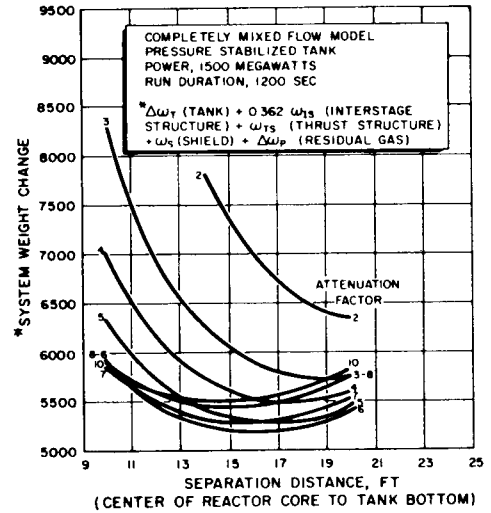
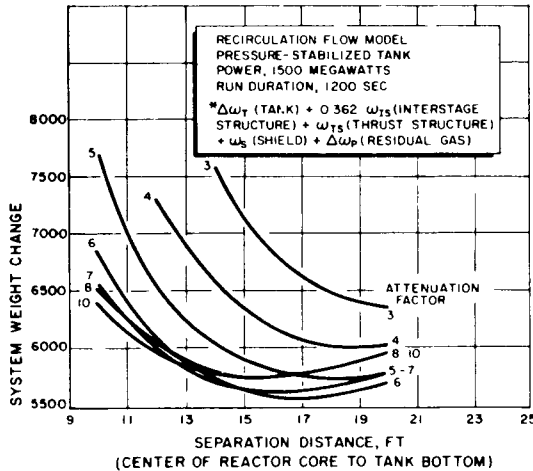


Figure 5. Change in System Weight vs Separation Distance (Recirculation Flow Model with 1500 Megawatts of Power)



~~CONFIDENTIAL~~

<u>Fig.</u>	<u>Flow Model</u>	<u>Power Level, Mw</u>	<u>Run Duration, sec</u>	<u>Separation Distance, ft</u>	<u>Attenuation factor</u>	<u>System Weight, lb</u>
3	Potential	1500	1200	14	2	4100
4	Completely mixed	1500	1200	16	6	5200
5	Recirculating	1500	1200	17	6	5500

Thus, a separation distance of 17 ft and a shielding attenuation factor of 6, using a boronated graphite shield, is indicated for the K-1 engine at 1500 megawatts. A separation distance of 14 ft is recommended because any reduction in propellant heating would tend to optimize the system at a lower separation distance than is indicated by the recirculating flow model. The resulting tank pressure rise is approximately 10 psi.

Figure 6 is a flux map describing the neutron and gamma fluxes in the engine system during 1500 Mw operation. Radiation in the vicinity of the feed system and propellant tank has been attenuated by a factor of 6 through the use of a 14-in. 20 percent-void boronated graphite shield.



**CONFIDENTIAL**

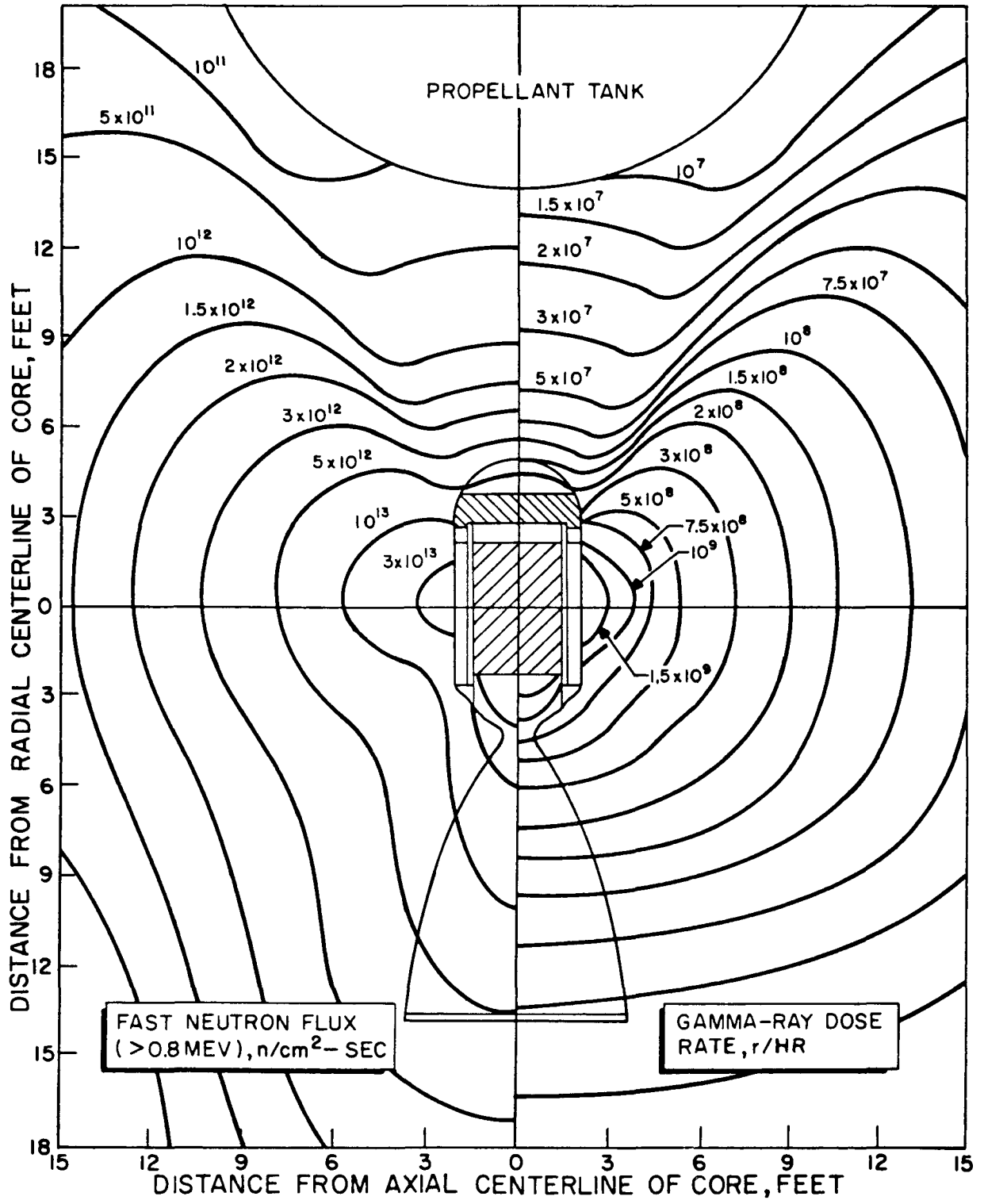


Figure 6. Isoflux and Isodose Curves for 1500 Megawatt K-1 Engine

**CONFIDENTIAL**

UNCLASSIFIED

page blank

12

UNCLASSIFIED

~~CONFIDENTIAL~~

---

## SUMMARY OF RADIATION EFFECTS ANALYSIS

### REQUIREMENTS

The requirements of the K-1 system demand reliable operation in an intense nuclear radiation field for 1200 sec. All parts of the system will endure high rates of internal heat generation, especially those near the reactor or those not protected by the shield. The high flux levels will tend to disrupt the operation of electrical equipment, while the integrated radiation dose is sufficient to cause changes in many organic materials. Not only must all parts of the system meet these operating requirements, but they must not become so radioactive as to impede disassembly and maintenance after developmental static tests.

### RADIATION HEATING IN TANKED PROPELLANT

An upper-stage nuclear vehicle is subject to five major mechanisms of propellant heating from the time tanking on the launch pad is completed. There will be heat transfer from the surrounding air as the vehicle goes through the launching procedure, and aerodynamic heating as the vehicle is accelerated through the atmosphere. During operation of the nuclear engine, the propellant will be heated by nuclear radiation and by heat transfer from the hot gas used to pressurize the propellant tank. As the nuclear vehicle is programmed to shut down and pass into a coast phase before restarting, solar radiation and "earthshine" will add more heat to the remaining propellant.

Of these five heating mechanisms, three are primarily dependent on the vehicle's tank insulation and the characteristics of its mission. They

~~CONFIDENTIAL~~

**CONFIDENTIAL**

---

do not influence the reactor-tank separation in this study. Heat transfer from hot pressurizing gas has been found to have a negligible effect on the reactor-tank separation. The remaining mechanism, nuclear radiation heating, is a strong function of reactor-tank separation distance and plays a major role in determining the optimum system configuration.

The important parameter for determining the separation is the temperature of the propellant flowing into the pump inlet, and this is strongly dependent on the flow pattern of propellant in the tank. The simplest model for propellant flow in the hydrogen tank, without radiation, is essentially nonviscous potential flow in which each particle of fluid moves evenly down the tank and into the pump. If the radiation heat generation were superimposed on this flow pattern, a steady state would soon develop in which radiation energy is removed at the same time rate at which it was being added. A plot of typical propellant exit temperatures as a function of engine operation time with this flow situation would follow the Potential Flow curve of Fig. 7. This can be considered to be an ideal case which cannot be achieved in practice because fluid in some streamlines receives more energy in its path to the tank exit than does other fluid.

Flow in the presence of strong radiation is not likely to be so favorable as the potential flow model would indicate. Figure 7 shows two other flow models which are more realistic. The two other flow models are termed Completely Mixed Flow and Recirculating Flow. In the former model, it is assumed that the energy deposited is uniformly distributed throughout the remaining propellant. Although this is an unrealistic model of real tank flow, it serves to show the large increases in propellant temperature that result from nonpotential flow.

**CONFIDENTIAL**

CONFIDENTIAL

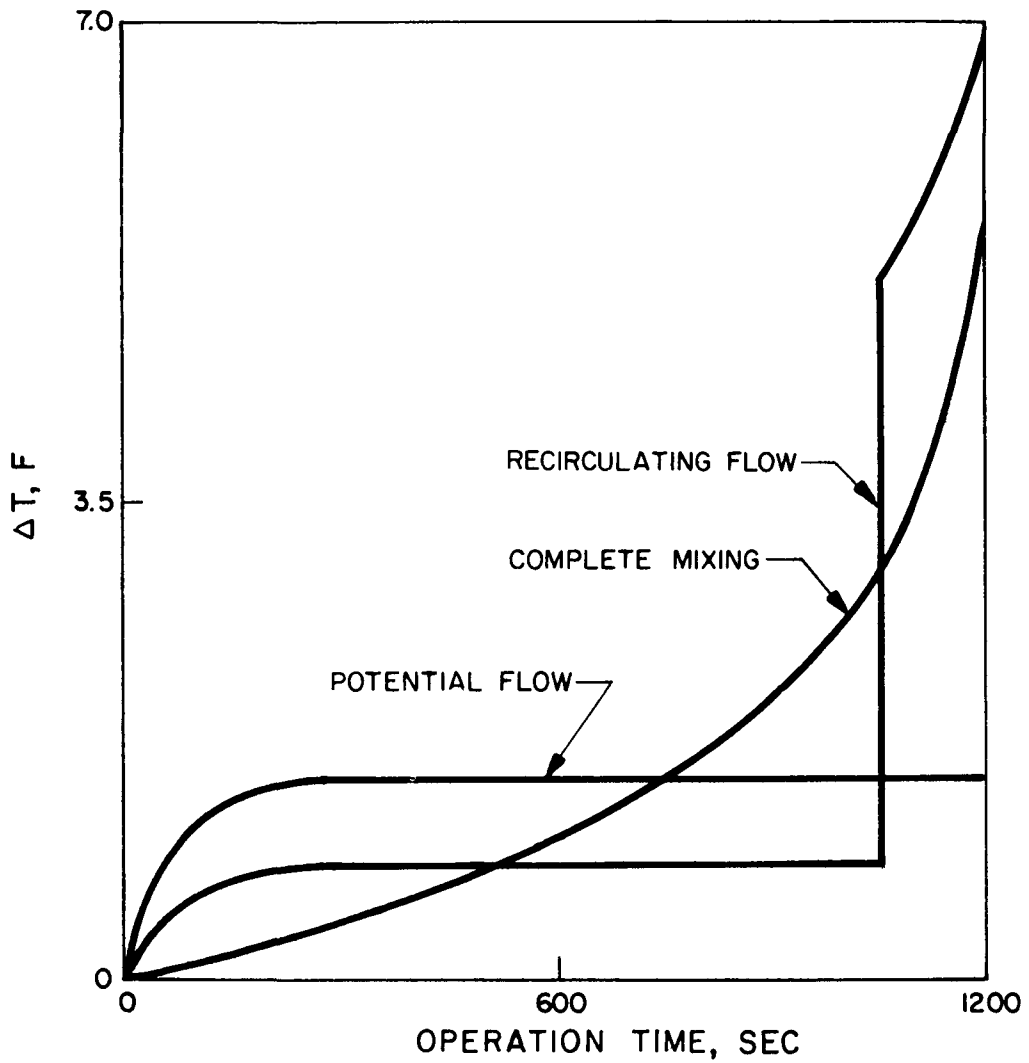


Figure 7. Typical Temperature Rise of Propellant Exit Flow as a Function of Engine Operation Time

CONFIDENTIAL

037281030

~~CONFIDENTIAL~~

Recirculating flow considers a realistic heat transfer mechanism within the propellant: that of convection currents. Convection currents were calculated which move up the tank walls and recirculate warm propellant to the top of the remaining fluid. The neutron flux causes most of the propellant heating in the first few inches of liquid hydrogen and is of prime importance in forming recirculation currents. The gamma heating, from both core gammas and capture gammas born in the first few inches of propellant, is distributed throughout several feet of fluid and is likely to be swept into the pump. The shape of the temperature curve therefore resembles the potential flow model early in the run, because the neutron flux energy is being convected upward and the rest of the propellant behaves as if it were in potential flow. When the fluid which recirculated at the beginning of the run again reaches the tank exit, the temperature of propellant entering the pump jumps sharply. Then a portion of this fluid is again recirculated and the process continues until the tank is empty.

It is not clear which of the three flow models best describes the conditions that will be realized in a real tank. It may be feasible to use baffles to reduce or prevent recirculation currents and bring the propellant exit temperature history closer to that of the potential flow model. This is discussed further in the Analysis section. In the absence of the results of such a research program, the problem of choosing the correct flow model remains. For the configuration analysis to have the widest possible range of applicability, both extremes plus the completely mixed model were considered.

Figures 8, 9, and 10 show the change in tank pressure required to prevent boiling vs shield attenuation factor and separation distance (core center to tank bottom) for the potential, completely mixed, and recirculating flow models at a power level of 1500 Mw and a run duration of 1200 sec.

~~CONFIDENTIAL~~

**CONFIDENTIAL**

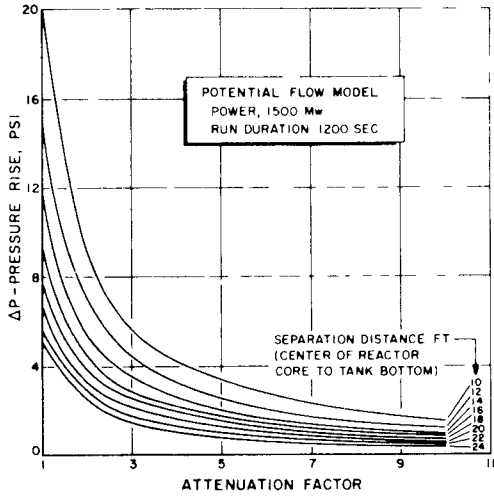


Figure 8 Pressure Rise (To Prevent Boiling) vs Attenuation Factor and Separation Distance (Potential Flow Model with Power at 1500 Mw)

Figure 9. Pressure Rise (To Prevent Boiling) vs Attenuation Factor and Separation Distance (Completely Mixed Flow Model with Power at 1500 Mw)

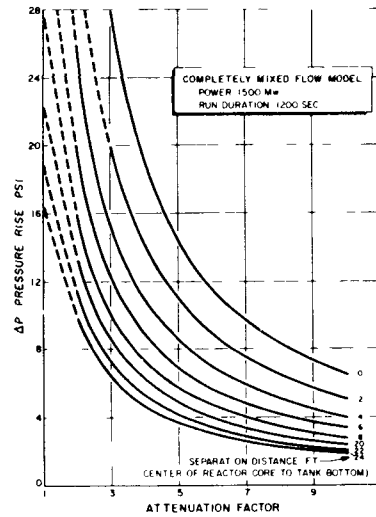
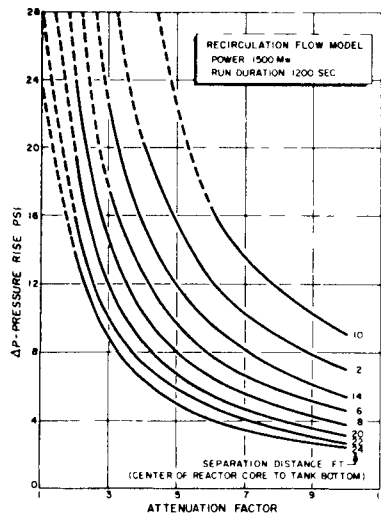


Figure 10. Pressure Rise (To Prevent Boiling) vs Attenuation Factor and Separation Distance (Recirculation Flow Model with Power at 1500 Mw)



~~CONFIDENTIAL~~

## RADIATION HEATING IN COMPONENTS

The heat generation effect of reactor radiation is shown graphically in Fig. 11. Lines of constant heat generation rate are shown on the left half of the diagram, and lines of constant adiabatic final temperature are shown on the right. Gamma heating from all important sources has been considered, including core gammas, capture gammas from the core support plate and from the tanked propellant, and capture gammas arising within the system components. Both halves of the figure were calculated assuming no self-shielding and no flux perturbations from components or structure, and are therefore the maximum possible values at each location within the system. The heat generation rate plot is roughly applicable to all nonhydrogenous materials, although it was calculated for iron-nickel alloys. However, the temperature rise plot applies only to iron-nickel alloys. It is based on the heat generation rates of the other plot, on a 1200-sec run at 1500 Mw, and on the specific heat of Inconel X. The values of temperature rise apply to a thin absorber, perfectly insulated, which assures that they represent the upper limit in any practical situation.

Figure 12 shows the heating rates for most metals at varying distances above the reactor core. The contributions of several radiation sources are shown on this plot as well as the sum of their effects. This curve serves to illustrate the relative importance of the secondary radiation sources exterior to the core as well as the attenuation of radiation with increasing distance from its source.

The following components of the engine system under consideration were analyzed with regard to their internal heat generation and heat removal problems. All are located externally to the reactor and pressure shell and were illustrated in Fig. 1.

~~CONFIDENTIAL~~



~~CONFIDENTIAL~~

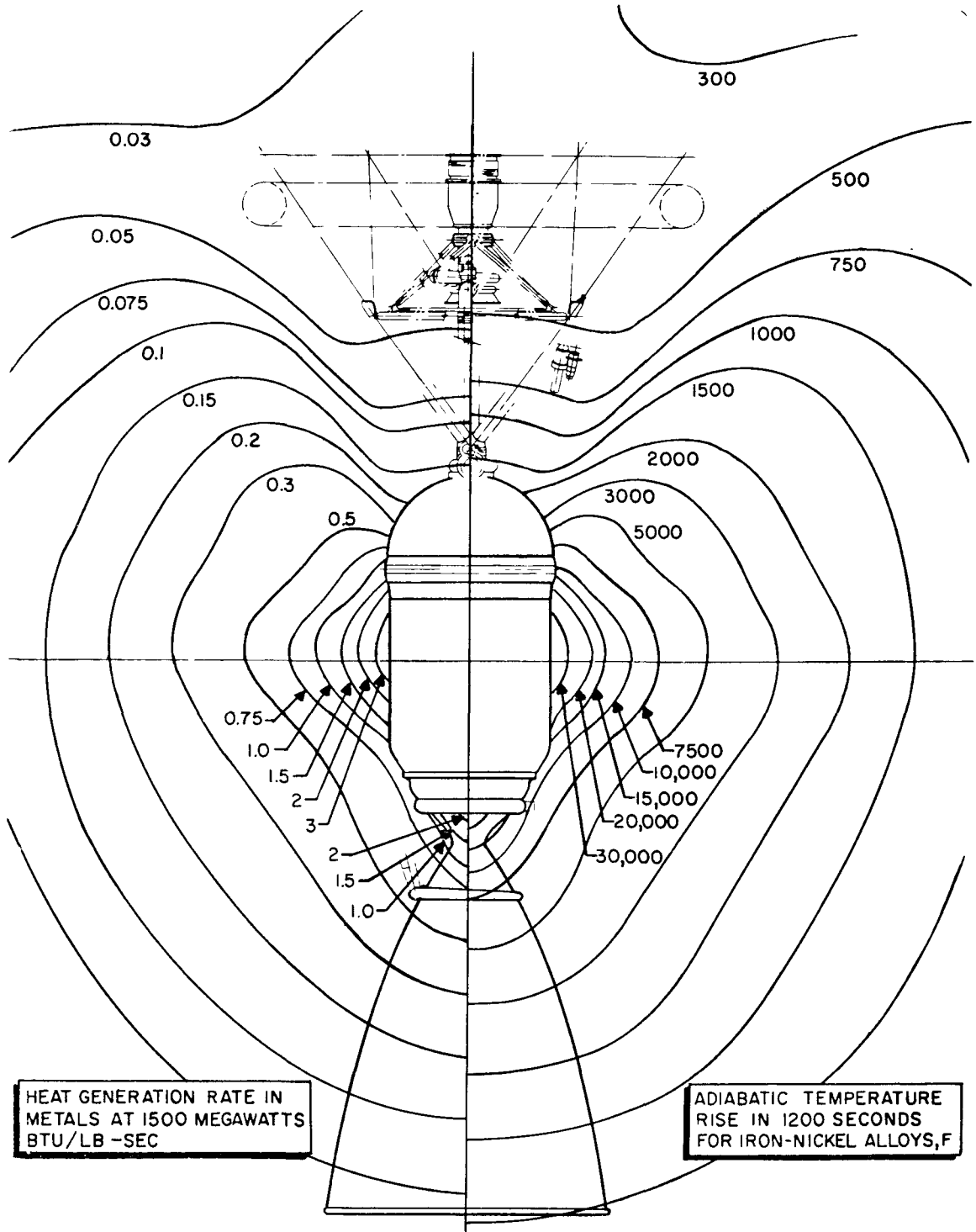


Figure 11. Engine Thermal Environment

**CONFIDENTIAL**

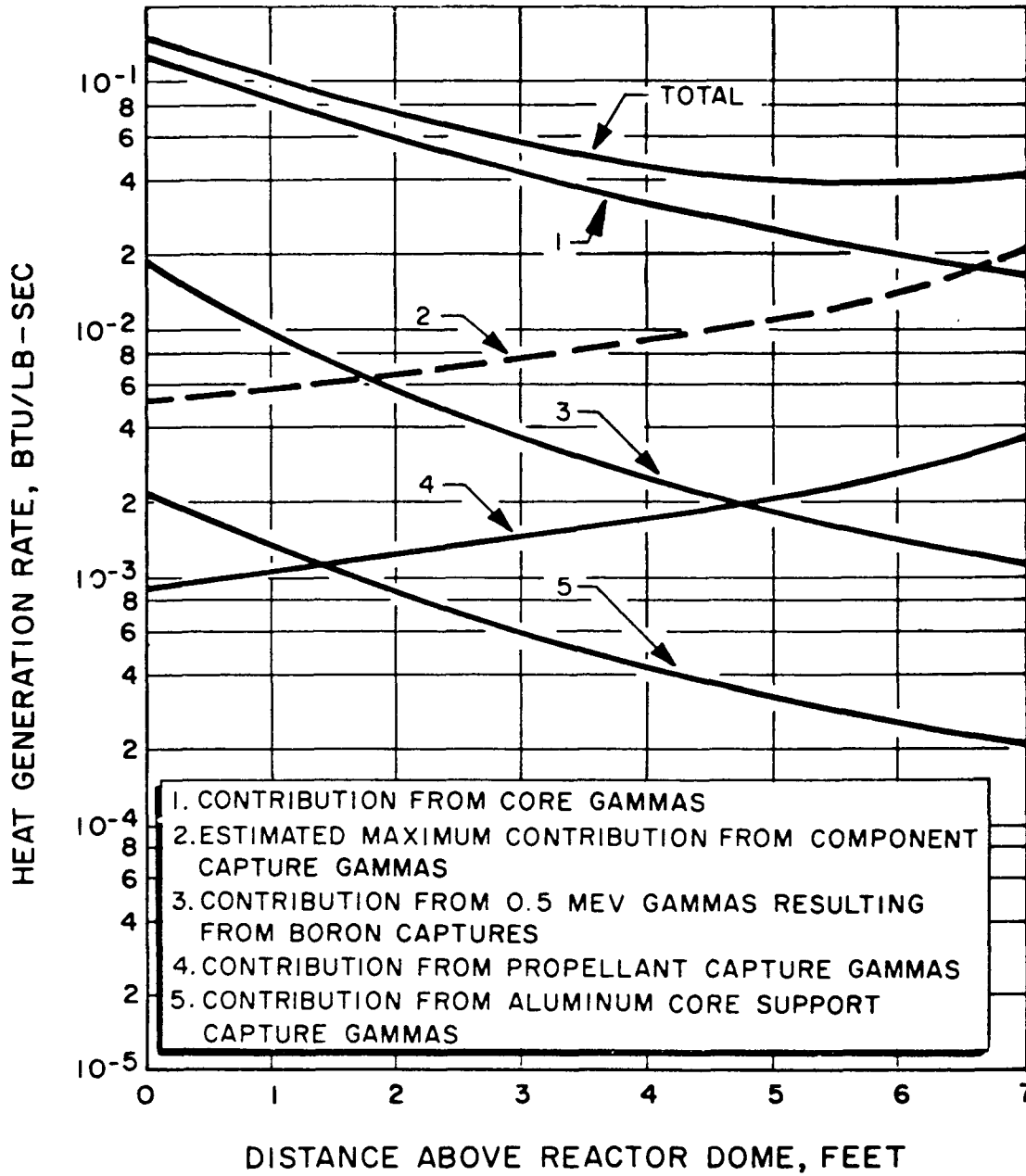


Figure 12. Heat Generation in Components Located Above Reactor Dome

~~CONFIDENTIAL~~

---

### Pneumatic Storage Tank

If the gas contained in the tank as well as the tank itself are assumed to be in thermal equilibrium, the surface temperature at the end of 1200 sec of 1500 Mw operation will be 825 R for the toroidal vessel. An initial temperature of 560 R is assumed.

### Thrust Structure

The structure closest to the reactor carries propellant from the feed pump and is thereby cooled. The forward thrust structure is not provided with such forced convection cooling but does, however, lose considerable heat by thermal radiation to space.

The hottest parts of the mount structure will be the pins used to join the pump and uncooled portions of the structure. These pins are essentially insulated and will not radiate their heat. Because the contact resistance of the pin-structure joint is difficult to predict, it must be assumed that no heat will be transferred to the thrust structure members. If the temperature of these components is approximately -150 F at reactor start-up, the final temperature of the pin will be 270 F and the hot end of the strut will be 180 F.

The clevis at the pump mount joints will be the hottest portion of the cooled thrust structure, but the presence of cold hydrogen in the struts will hold the maximum clevis temperature to approximately -370 F.

~~CONFIDENTIAL~~

---

### Development Test Pad Tank Support Strut

If atmospheric convection cooling is neglected, the tank support struts of the engine system test facility must be assumed to heat adiabatically. The temperature of the struts at the end of a 1200-sec engine run will be 270 F.

### Turbopump Mount Struts

These struts are similar to the uncooled thrust structure members in their environment, and undergo thermal radiation cooling. If they are initially at -150 F, their final temperature after 1200 sec will be 300 F.

### Turbopump

The Rocketdyne Mark 9 turbopump assembly which was used for this analysis is susceptible to radiation heating in the region of its turbine rotors. These parts operate at high design stresses and an increase in temperature of only a few degrees will cause a relatively large decrease in the design safety factors. Analysis indicates that if all heat generated in the rotors is transferred to the gas stream through the blades, the maximum temperature at the last stage wheel hub will be about 120 F above the turbine gas temperature. Any leakage of drive gas through the interstage seals will decrease this temperature difference.

### Turbine Exhaust Expansion Joints

The center-tie components of this joint are immersed in turbine exhaust gas which provides adequate forced convection cooling. The maximum temperature in the tie components will be about 5 F above the gas temperature.

~~CONFIDENTIAL~~

---

The expansion bellows is also cooled by the exhaust gas but the heat generated in the outer extremities of the convolutions must be conducted to the inner surfaces before being transferred to the gas stream. The maximum bellows temperature will therefore exceed exhaust gas temperature by about 14 F.

#### Main Propellant Valve

Cold hydrogen flowing through this valve will provide a heat sink for the heat generated in most of the valve components. It was found that the probable maximum temperatures during engine operation will not exceed 150 F in either the aluminum or steel valve parts.

#### Duct Support Brackets

Aluminum brackets are used to support the hydrogen ducts which lie along the pressure shell. One end is cooled by virtue of being welded to the pressure shell, and the bracket will not exceed 400 F.

#### Turbine Inlet Temperature Control Valve

This valve is located on top of the reactor dome and is internally cooled by the flow of liquid hydrogen. Maximum temperatures in its aluminum parts will remain within 50 F of the coolant temperature. Steel parts remote from the hydrogen will be as high as 300 F above coolant temperature.

~~CONFIDENTIAL~~

~~CONFIDENTIAL~~

---

### Turbine Throttle Valve

Turbine inlet gas flows through this valve during engine operation and removes radiation heat. In the zone containing the valve body, the maximum temperature will exceed the hot gas temperature by about 100 F. Temperatures will be lower in regions closer to the gas passage.

The zone containing the valve gear boxes will undergo a maximum temperature increase of 450 F. Forced cooling with gaseous hydrogen will reduce this maximum temperature.

### Gas Generator Expansion Joint Bellows

This component will be included if a turbine gas generator should be used in the system, but it is not shown in Fig. 1. The heat generation problems are similar to those of the turbine exhaust expansion joint, and the maximum bellows temperature will occur at the outer convolutions and will be about 19 F above the turbine gas temperature.

### Gimbal Bearing

The temperatures attained by the components of the gimbal bearing are critical because of the strict dimensional tolerances required. High temperatures and temperature gradients are not acceptable because of subsequent deformation which would impede reliable gimbal operation.

The temperature rise in the pilot bolt was found to be about 400 F and this temperature can be further reduced if a coolant flow passage were drilled through the bolt. Hydrogen coolant must be directed toward the central region of the gimbal block to prevent this component from reaching excessive

~~CONFIDENTIAL~~

~~CONFIDENTIAL~~

---

temperatures. Several coolant passages should be provided to maintain the gimbal bearing dome below 1000 F and these can also be used to direct additional coolant to the gimbal block. The bellows and volute will be adequately cooled by the hydrogen flow during engine operation.

#### Gimbal Actuator

The actuator and associated moving parts are located approximately 100 in. from the center of the core, while the actuator base assembly is attached to the reactor dome. Cooling of the actuator components and base assembly is facilitated by allowing a fraction of the actuator operating gas to leak through the system. The gas flows through the total length of the system and is dumped into the reactor dome. The maximum temperature of the uncooled actuator would reach 600 F at the end of the engine operation if 10 percent of the actuator flow were used for cooling, and the actuator body temperature would be held to 300 F.

#### Flexible Metal Hose

The flexible metal hose which carries pneumatic supply gas to the various actuators will reach temperatures which are a function of the outside metal braid wire and the braid wire emissivity, and are essentially independent of the hose diameter in the range considered. Depending on the emissivity assumed, the braid temperature will lie between 230 F and 460 F.

#### Nozzle Stiffening Bands

The stiffening bands oriented transverse to the nozzle wall tubes are cooled by the hydrogen flow within the nozzle, and the band temperatures will not exceed -100 F.

~~CONFIDENTIAL~~

---

### Exhaust Gas Instrumentation

Thermocouples in the nozzle throat section extend from the nozzle wall into the exhaust gas. Besides the heat load imposed by the exhaust, the transducer assemblies are subject to high radiation fluxes. Heat rejection by thermal radiation to the nozzle wall and conduction through the brazed mount will not prevent temperatures in excess of 4000 F after 1200-sec operation unless a cooled shroud is provided to enclose the transducer assemblies.

### Destruct System

A birdcage-shaped series of tubes containing shaped charges of high explosive is planned to completely encircle the reactor pressure shell. The tubes, containing a 1-in. diameter TNT charge, have a cross section resembling a disc with a 60-deg "pie slice" removed from it. If uncooled, the TNT would reach the autodetonation temperature in a very short time, but a manifold can be added to cool the explosive with either gaseous or liquid hydrogen. A flow of 0.20 lb/sec will limit the surface temperature of the explosive to 0 F at 1500 Mw reactor power.

### Radiation Shield

At full-power engine operation, the maximum thermal gradient in the shield is about 33 F. With full propellant flow through the shield, the gas-film temperature drop is about 120 F, causing a maximum material temperature of about 400 R. This is easily within the capability of the boronated graphite shield material.

~~CONFIDENTIAL~~



~~CONFIDENTIAL~~

---

## RADIATION DAMAGE

### Effects on Electrical Equipment

Transient radiation effects, which are rate-dependent and present only during reactor operation, are caused by ionization in the absorbing material. The high dose rates present during the short-duration reactor operation will have considerable effect on electrical equipment. Current leakage paths will be induced in insulators and spurious voltages will be caused in electronic equipment. Some specific examples of electrical equipment disruption are listed below.

Solenoid Valves and Servovalves. Coil assemblies may be shorted out by the breakdown of insulation, and the ionization of gases surrounding coils and wiring will introduce random noise into the control system.

Solid-State Electronics and Feedback Loops. Semiconductors are particularly susceptible to radiation because of the mechanism on which these devices depend for their operation. Free electrons produced by the ionizing radiation will introduce a preponderance of new charge carriers and thereby change the minority carrier into a majority carrier or create an avalanche of charge that blocks out the desired signal. Solid-state devices must be located in an area of low radiation intensity such as provided by the shield and by the propellant in the tank itself. Potentiometers employed in feedback loops may malfunction from false or erratic signals caused by radiation, and it may be necessary to provide these unit with individual shields.

~~CONFIDENTIAL~~

---

Temperature Measurement Devices. Thermocouples in the thrust chamber must withstand elevated temperatures and high gas velocities while maintaining adequate electrical stability in the high radiation fluxes. Structural integrity of the thermocouple probe can be obtained by supporting the probe insulation in a tungsten sheath and the best insulation at the present time appears to be beryllium oxide.

Turbine inlet gas temperature measurement can be accomplished with the same type of thermocouple used in the thrust chamber because the conditions of temperature and radiation at the turbine inlet are not so stringent.

It appears that the temperature of the cryogenic propellant can be measured with platinum resistance bulbs. If the instrumentation development program shows these devices to be seriously radiation-sensitive, it may be possible to substitute thermoelectric alloy thermocouples such as gold-cobalt-copper and copper-constantan.

A number of surface temperature measurements will be necessary to determine the operating temperatures of critical components. Thermocouples are the best choice of instrument for this application.

Pressure Measurement Devices. Pressure transducers are available which utilize several different principles for operation. Tests performed by Atomics International as part of the KEWB program indicate that strain gage-type transducers and quartz piezoelectric transducers are the most radiation resistant of the types tested.

**CONFIDENTIAL**

---

Flow Measurement Devices. Consideration of six different types of flow meters indicates that the turbine-type flow meter, used with a separate determination of density by measurement of temperature and pressure, is the superior device. This instrument is cooled by liquid hydrogen, is not affected by radiation-induced changes in mechanical properties, and its output is not sensitive to small changes in the magnetic and electrical properties of either the detector device or the transmission system.

Strain Measurements. While some problems exist in the application of resistance-type strain gages in the K-1 environment, these gages remain the logical choice. Difficulties may arise in attaching the gage to the component in which strain is to be measured. Ceramic adhesives appear the most promising, but they must be applied or cured at elevated temperatures. To avoid the long high-temperature curing cycles in shop or field applications, the gage may be attached in the laboratory to a thin metallic carrier of the same material as the test hardware. This assembly may then be spot welded to the test hardware during the assembly buildup.

Acceleration Measurements. Radiation tests by Atomics International indicate that quartz piezoelectric properties are unaffected by the radiation doses expected with the K-1 engine, but little information exists with which to evaluate the magnitude of dose-rate effects. These effects, along with radiation-induced interference in connecting cables, may be very difficult to compensate for because of the high internal impedance of the crystal and the high input impedance required at the preamplifier. These crystals are also temperature-sensitive and it may be necessary to provide cooling for them.

**CONFIDENTIAL**

~~CONFIDENTIAL~~

---

### Damage in Mechanical Components

Wherever possible, components containing organic parts should be examined for the possibility of substituting other materials or eliminating the organic parts altogether. Devices which may be susceptible to integrated-dose radiation damage are described below.

Bearings. Turbomachinery using liquid hydrogen as lubricant and coolant require a ball-retainer material which resists galling and is not affected by cryogenic temperatures. Glass-impregnated Teflon has been used successfully by Rocketdyne in the Mark 9 liquid hydrogen pump, but a substitute material such as carbon must be developed to meet the requirements of the K-1 engine system.

Seals. Seals of the Naflex type which have been developed by Rocketdyne will be suitable for use in all flanged joints of the K-1 engine system. The standard Naflex seal has a thin Teflon facing, but a soft metal foil has been successfully used in its place at temperatures from -320 F to 1200 F.

Explosive Devices. Reactor safety systems employing explosives to break up and disperse the reactor core in event of malfunction must be protected from overheating and integrated-dose radiation effects. The aromatic structure of TNT makes this explosive superior in radiation resistance, but a development program must be carried out to assure that this material will function properly in the K-1 environment.

~~CONFIDENTIAL~~

**CONFIDENTIAL**

---

Solid Lubricants. Solid-state lubricants are somewhat radiation sensitive but appear to retain their properties at doses exceeding those expected in the K-1 application. Methods of dry lubrication which should be evaluated are carbide coating, nitriding, sintered metal surfaces, and bonded graphite-MoS<sub>2</sub> surfaces

#### NEUTRON-INDUCED RADIOACTIVITY

Exposure of components and structural materials to neutrons escaping from the reactor during engine testing will result in an important source of long-lived radiation. Although the sum total of this induced radioactivity is inconsequential compared to the prompt radiation emitted during reactor operation, and also small compared to that emitted by fission products after shutdown, it can be large enough to present a considerable radiation hazard during maintenance operations.

Calculations of induced radioactivity assumed no self-absorption in the radioactive material, and a point-source geometry. The resulting activities for several components were calculated for a distance of 1 ft from each component at varying times after shutdown and are listed in Table 1 .

The decay of radioactivity with time for a number of alloys is shown in Fig. 13 . It is seen that the sum of induced activity falls rapidly during the first few days and then reaches a more constant value which is determined by the most dominant long-lived isotope. In the case of the turbopump, which contains Hastelloy C, cobalt is the source of the dominant activity after 10 days of cooldown. The dose rate from the turbopump at that time is sufficient to give a worker his full permissible weekly dose in about six minutes of close work. Even higher dose rates will actually be present because of radiation from other nearby parts of the engine system.

**CONFIDENTIAL**

**CONFIDENTIAL**

TABLE 1

COMPONENT ACTIVATION LEVELS

<u>Component</u>	<u>Dose Rate</u> 3 Days, R/hr at 1 foot	<u>Dose Rate</u> 10 Days, R/hr at 1 foot
Turbine	16	0.5
Thrust Nozzle	100	85
Forward Thrust Mount	1.0	0.5
Aft Thrust Mount	0.1	0.01
Reactor Assembly	$4 \times 10^5$	$2 \times 10^4$
Hot Gas Duct	5.0	1.0
Temperature Control Valve	0.03	0.02
Afterheat Coolant Valve	0.002	0.001
Main Propellant Valve	0.007	0.004
Gimbal Actuators	5.7	4.0
Roll Nozzle Assembly	0.2	0.1
Turbine Exhaust System	0.7	0.4

NOTE:

Components subjected to flow of gas from the reactor may accumulate fission products, and exhibit actual dose rates several orders of magnitude greater than those listed prior to decontamination.

~~CONFIDENTIAL~~

---

The disassembly and maintenance problems presented by induced activity may be lessened through close attention to material selection and operational procedures. Reactor-grade materials should be specified wherever possible and strong radiation sources should be removed from the system before maintenance work is begun. A boron-containing shield may also be used in certain components that must undergo extensive handling.

~~CONFIDENTIAL~~

~~CONFIDENTIAL~~

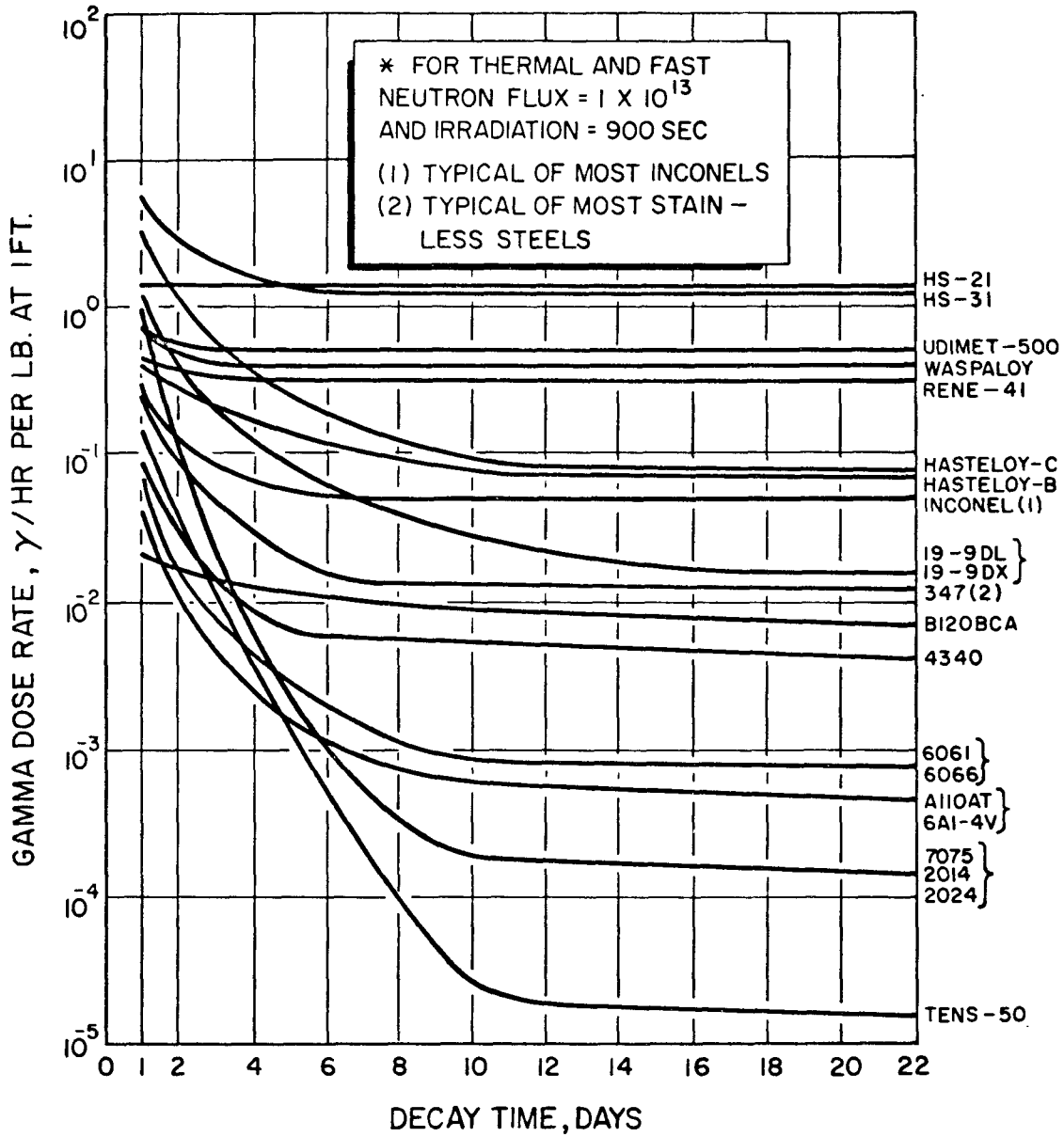


Figure 13 . Dose Rates Due to Activation of Some Common Metal Alloys



**CONFIDENTIAL**

---

RECOMMENDED DEVELOPMENT TEST PROGRAM

EXPERIMENTAL OBJECTIVES

Research experiments are essential for obtaining basic data to verify calculated results and will furnish an empirical basis for component radiation analysis. Development testing experiments will serve to prove out the fully engineered engine system and its components. The tests outlined here cover both types of experiment, although emphasis is placed on the final phase of component and system development which will utilize the radiation of the Kiwi-B reactor experiments at the Nevada Test Site.

AREAS OF EXPERIMENTAL INVESTIGATION

Reactor Leakage Flux

Considerable uncertainties exist in the calculation of radiation leakage fluxes. Therefore, instrumentation should be provided at all reactor experiments to record the magnitude and spectral distribution of neutron and gamma fluxes. Other instruments should be included to provide data on heat generation rates and temperature gradients in the components and materials of the engine system.

Shield Performance

The radiation shield controls heating within the tanked propellant as well as within the components of the engine system. The performance of the shield must be verified by testing it in an intense, highly directional radiation flux such as exists in the beam port of certain research reactors or in the leakage flux from the Kiwi-B experiments. A shield intended

~~CONFIDENTIAL~~

---

for testing in the Kiwi-B environment must be internally cooled and should be mounted as closely as possible to the reactor core. Heat generation rates and temperature gradients within the shield should be recorded, as well as data on heating of components and structure located behind the shield.

### Propellant Heating

Because of the importance of radiation-induced propellant heating, fluxes should be measured at various locations within a liquid hydrogen tank located close to the experimental reactor. Determination of convection currents and flow patterns within the propellant tank will require other means of investigation. Experiments during early stages of development must be performed under controllable, repeatable conditions in which the test system may be easily altered. One such early experiment might be performed with a tank of noncryogenic fluid heated by a nonnuclear energy source such as infrared lamps. Later tests might be performed in a research reactor and would utilize a mockup partial tank and liquid hydrogen flow system to duplicate the conditions of radiation and propellant flow which are expected in the nuclear engine system. Such an experiment could be performed in a pool-type reactor, and would have the advantage of allowing convenient access to the test system after it had been raised from the pool and the reactor covered with water.

A prototype tank, developed through these experimental programs, should be ready for testing with the rest of the engine system at the start of the nuclear engine system tests.

~~CONFIDENTIAL~~

**CONFIDENTIAL**

---

### Cavitation Studies

Low tank pressure is a desirable objective to achieve minimum tank weight and pressurant weight requirements, but radiation will make pressure increases necessary. Cavitation may occur in the pump inducer if pump inlet conditions do not meet the required levels of NPSH. Reactor leakage radiation will tend to heat propellant as it flows into the inducer, and the effect of heating on tank pressure has been analyzed in this report.

Other phenomena may also be theorized concerning changes in propellant phase due to deposited radiation energy. If the liquid hydrogen being pumped is in a metastable state, radiation may initiate transition to equilibrium, causing point pressure discontinuities from which cavitation may arise. Another concept is that the benefits arising from evaporative cooling, which would normally prevent cavitation in the inducer, may be counteracted because of radiation heat generation.

Experimental data can be obtained during Kiwi-B experiments by performing cavitation tests on an inducer-pump assembly on an adjacent test car or pad. This test would provide cavitation data as well as performance data on the feed system components used in the test. If test facility limitations prevent operation of an inducer test, useful data may be obtained through use of a cavitating venturi. Information from this test will show if a relationship exists between cavitation in the hydrogen propellant and the presence of strong radiation fluxes.

~~CONFIDENTIAL~~

---

### Component Tests

Those components which contain parts subject to radiation damage should be tested in existing test reactors where the advantages of convenient scheduling and repeatable conditions allow more control of testing than is possible with the Kiwi-B experiments. Initial attention would be concentrated on integrated-dose radiation damage in mechanical components and on dose-rate effects in electrical equipment. Test reactors such as Godiva and KEWB are the only present sources of radiation fluxes approaching that of a propulsion reactor, and they should be utilized as much as possible during early electrical system development.

Testing in the radiation of Kiwi-B is hampered by the presence of atmospheric convection cooling as well as air and ground scattered radiation. It is possible that certain components which will function satisfactorily in ground tests will overheat and fail in flight tests for lack of atmospheric cooling. However, the results of these studies show that the most serious heating problems exist in components which are forced to operate at high temperatures by the nature of their function. Such components include the turbine rotors and the hot gas throttle valve. Tests of these components in the Kiwi-B radiation will be valid, however, because they are not appreciably affected by atmospheric cooling.

Valuable data on induced radioactivity will be provided by the test of a mockup feed system in spite of the limited integrated neutron flux available. Induced activity may be scaled with reactor power and run duration to determine the effect of a full-power, full-duration engine run.

High-Speed Bearings. The critical importance of turbomachinery bearings from a system reliability standpoint make an intensive development program

~~CONFIDENTIAL~~

necessary to assure that these components will operate successfully in the K-1 radiation environment. Hydrogen-cooled bearings have, up to now, employed glass-reinforced Teflon ball retainers, but development of a substitute material may be necessary. Initial bearing development should include materials testing in testing reactors, and perhaps bearing tests should be conducted both in radiation and at cryogenic temperatures. If it is found that the effects of radiation and cryogenic temperature are not synergistic, the latter tests may be omitted.

Reactor Fragmentation Devices. High-explosive shaped charges and explosive projectiles have been proposed as safety systems with which to break the reactor core into subcritical fragments. It is imperative that the explosives be completely reliable throughout the operation of the nuclear engine. Environmental testing of these explosives will provide data on the changes in explosive efficiency, sensitivity, and brisance at the radiation doses and operating temperatures of the K-1 application.

Control Components. Individual parts of the control system which may be sensitive to radiation damage should be tested separately before the control subsystems are operated in the environment of an experimental propulsion reactor. When this preliminary development has been accomplished, functional tests may be performed in the environment of Kiwi-B. System development should include both calibration testing and functional testing in radiation.

Those control components which are presently available for testing should be incorporated into experiments which will check the functioning of their electrical equipment. Insulation breakdown under operating voltages and a high electrical noise level will indicate that further development is

~~CONFIDENTIAL~~

---

necessary. All components should also be tested for their resistance to radiation heating.

Flight Instrumentation. Early development of instrumentation should be conducted in testing reactors to prove the equipment's resistance to integrated-dose radiation damage as well as to rate-dependent ionization effects. Final proof of the adequacy of flight instrumentation will be obtained by testing in the Kiwi-B experiments. All instrumentation should be calibrated before and after exposure, and data obtained during reactor operation will be compared with data from reference instruments.

All instrumentation which supplies control information for system operation should be included in this development. These items include chamber temperature thermocouples, turbine inlet thermocouples, propellant temperature thermocouples, pressure transducers, flowmeters, strain gages, and accelerometers.

Integrated Feed System Tests. The final test of component and subsystem radiation resistance would be the operation of a complete feed system in the radiation of Kiwi-B. Although the test would be too short for accumulation of an appreciable integrated radiation dose, and atmospheric convection would furnish cooling which would not be present in a space environment, the information on rate-dependent radiation effects would be quite valuable. However, limitations of the existing test facility and the hazards associated with a turbopump failure under radiation testing make such a feed system test infeasible. Difficulties in testing a complete turbopump system may be greater than the test information which would be obtained.

Many of the feed system components which may be radiation sensitive can be tested separately in testing reactors or in early Kiwi-B tests, and

~~CONFIDENTIAL~~

---

it is believed that the pump will not be critically sensitive to radiation. However, the turbine appears to be a critical component from the standpoint of radiation heating. If a test of the turbine alone could be conducted during reactor operation, this data (combined with the results of radiation tests of other feed system components) will provide enough information to assure the success of a prototype engine system using the full feed system.

The turbine test should be conducted as part of a subsystem test which employs much of the engine system control equipment. Inlet gas can be obtained from the bleed manifold, and all associated piping and valves should be included. This test allows the reactor experiment to continue in case of turbine failure by means of valves which would direct the reactor bleed gas into an orificed duct which would vent to the atmosphere. Fire and blast danger is minimized by the absence of the large quantities of hydrogen needed for a pump test.

Considerable difficulties exist in absorbing the turbine power and therefore a locked rotor turbine test appears desirable. A locked rotor has the particular advantage of allowing temperature measurements over the entire turbine shaft assembly, and in this way operating temperatures in the radiation environment may be obtained and conclusions may be drawn about the probability of successful operation at design speeds.

In spite of the difficulties associated with a turbopump or turbine test in the Kiwi-B environment, a certain amount of testing of these systems under strong radiation must be accomplished before the feed system is entrusted to supply propellant to the first prototype engine system. Considerable expenditure of effort is justified for the purpose of providing assurance against unforeseen failure of the reactor-turbopump system.

DECLASSIFIED

page blank

DECLASSIFIED



~~CONFIDENTIAL~~

ANALYSIS

REACTOR RADIATION LEVELS

RADIATION SOURCES

Core Gamma-Ray Spectrum

To determine the radiation environment associated with the K-1 engine design it is necessary to know the magnitude and spectral distribution of the gamma-ray energy released from the reactor core. The sources of gamma radiation considered within the core are fission, decay of fission products, neutron captures in the fuel and other materials, and decay of capture products. Gamma rays from inelastic scattering in uranium and niobium are not considered because of their relatively low intensity and the complexity involved in their determination. The spectrum generated from each of the reactions considered is discussed below.

Prompt Fission Gamma Rays. The spectrum of gamma rays emitted within  $10^{-6}$  seconds of fission has been measured by Maienschein, et al. (Ref. 1) and by Skliarevskii, et al. (Ref. 2). The former authors cover photon energy ranges from 0.3 Mev to 7.3 Mev while the latter are concerned with photons of energies between 0.020 Mev and 0.26 Mev. Thus, the energy released within  $5 \times 10^{-8}$  seconds of fission and within the energy range from 0.020 Mev to 7.3 Mev is  $7.44 \pm 0.8$  Mev/f. In addition Maienschein has measured delayed gamma rays in the region between  $5 \times 10^{-8}$  seconds and  $10^{-6}$  seconds after fission. The intensity from this is reported to be  $5.7 \pm 0.3$  percent of the more prompt radiation or about 0.42 Mev/f. Thus the total energy released within  $10^{-6}$  seconds is about 7.9 Mev/f. The spectrum is shown in Fig. 14. A graphical integration of this spectrum over 1 Mev intervals gives the Mev per fission at average energies of 0.5 Mev, 1.5 Mev, 2.5 Mev, etc. These values are shown in Table 2.

~~CONFIDENTIAL~~

**CONFIDENTIAL**

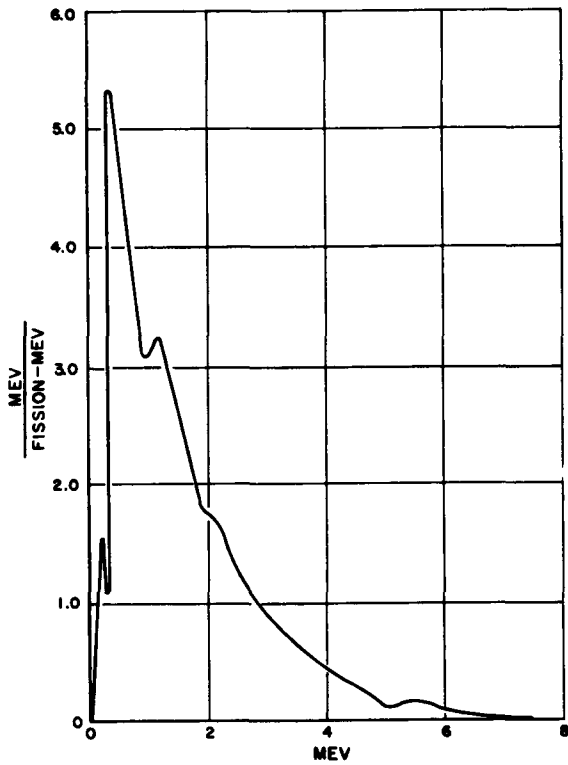


Figure 14. Spectrum of Gamma Rays  
Emitted Within  $10^{-6}$   
Seconds After Fission  
Normalized to 7.9 Mev  
per Fission

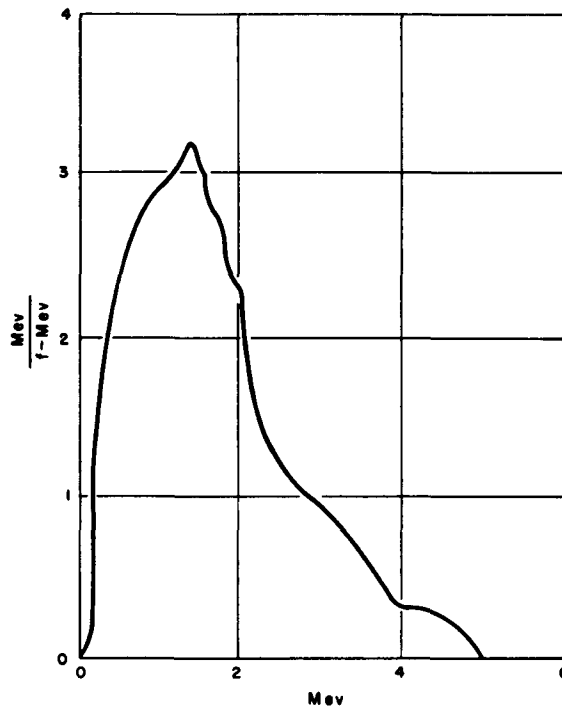


Figure 15. Spectrum of Gamma Rays  
Emitted by  $U^{235}$  Thermal  
Fission Products

TABLE 2

## CORE GAMMA-RAY SOURCES, MEV PER FISSION

Source	Mev										Total
	0.5	1.5	2.5	3.5	4.5	5.5	6.5	7.5	8.5	9.5	
Prompt Fission	3.06	2.49	1.28	0.59	0.26	0.16	0.060	..	..	..	7.90
Fission Product	1.00	2.10	1.10	0.58	0.23	0.13	..	..	..	..	5.14
U <sup>238</sup> Capture	0.09	0.08	0.04	0.01	0.01	..	..	..	..	..	0.23
Carbon Capture		2.5x10 <sup>-4</sup>	..	5.6x10 <sup>-4</sup>	1.8x10 <sup>-3</sup>	..	..	..	..	..	2.6x10 <sup>-3</sup>
Nb Capture	0.01	0.03	0.03	0.16	0.11	0.06	0.07	9.4x10 <sup>-3</sup>	6.9x10 <sup>-3</sup>	..	0.49
U <sup>235</sup> Capture	0.20	0.60	0.91	0.60	0.20	..	..	..	..	..	2.51
H <sub>2</sub> Capture	..	..	5x7x10 <sup>-4</sup>	..	..	..	..	..	..	..	5.7x10 <sup>-4</sup>
U <sup>239</sup> Decay	1.3x10 <sup>-3</sup>	..	..	..	..	..	..	..	..	..	1.3x10 <sup>-3</sup>
Total Mev/Fission	4.36	5.30	3.36	1.94	0.81	0.35	0.13	9.4x10 <sup>-3</sup>	6.9x10 <sup>-3</sup>	..	16.27
Mev/cc-sec x10 <sup>14</sup> at 1500 Mw	2.47	3.01	1.91	1.10	0.459	0.198	0.074	0.0053	0.0039	..	9.23

**CONFIDENTIAL**

Fission Product Gamma Rays. The fission product gamma-ray spectrum for infinite operation time and zero cooling time is shown in Fig. 15 . This figure was obtained by extrapolating the photon - intensity - time distributions of Maienschein (Ref. 1 ) from 1 second to zero, then integrating from zero to 1800 seconds. The contribution from 1800 seconds to  $5 \times 10^7$  seconds (there is essentially no change between  $5 \times 10^7$  seconds and infinity) was calculated separately using the data of Blomeke and Todd (Ref. 3 ). The sum, covering the energy range from 0.3 to 5.0 Mev, is 6.5 Mev/f. An estimate of the contribution from energies less than 0.3 Mev was obtained from the lowest energy group of Perkins and King (Ref. 4 ) which extends down to 0.1 Mev. This gives an additional increment of about 0.3 Mev/f, bringing the total to 6.8 Mev/f. The curve is arbitrarily normalized to 7.0 Mev/f. A graphical integration of the curve shown in Fig. 15 gives the Mev per fission at 1 Mev intervals for energies up to 5 Mev. The isotopes  $\text{Br}^{87}$  and  $\text{Rb}^{90}$ , emitting gamma rays of 5.4 Mev and 5.3 Mev, respectively, were not included in any of the mentioned references. Their contribution is included in the average energy group of 5.5 Mev. The total fission product energy release for infinite operation and zero cooling is 7.14 Mev/f.

To obtain comparable values for a finite operating period and zero cooling time, the following expression for the total fission product energy release can be used

$$E(T,t) = E(\infty, t) - E[\infty, (T + t)] , \quad (1)$$

where

$$E(T,t) = \text{Mev/f for operating time } T \text{ and cooling time } t,$$

$$E[\infty, (T + t)] = \text{Mev/f for infinite operation and cooling time } T + t.$$

**CONFIDENTIAL**

---

For a finite operating period of 900 seconds and zero cooling time Eq. (1) becomes

$$E(900,0) = E(\infty,0) - E(\infty,900)$$

The operating time of 900 seconds was chosen to obtain a mean value for the fission product energy release during a full duration test. In reality, the fission product energy release varies as a function of operating time, however, from about 200 to 1200 seconds it increases by only a small amount.

The value of  $E(\infty,0)$  is the 7.14 Mev/f discussed above. The value of  $E(\infty,900)$  was obtained from Perkins and King (Ref. 4). The spectra for  $E(\infty,0)$  and  $E(\infty,900)$ , and the resulting spectrum for  $E(900,0)$  are shown in the following table:

Average Photon Energy, Mev	Energy Release per Fission, Mev/f		
	$E(\infty,0)$	$E(\infty,900)$	$(900,0)$
0.5	1.96	0.96	1.00
1.5	2.77	0.67	2.10
2.5	1.44	0.34	1.10
3.5	0.61	0.03	0.56
4.5	0.23	- -	0.23
5.5	0.13	- -	0.13
Total	7.14	2.00	5.14

Thus, 5.14 Mev are released for each fission taking place at 900 seconds of reactor operation. This value was used in the core gamma-ray source strength.

CONFIDENTIAL

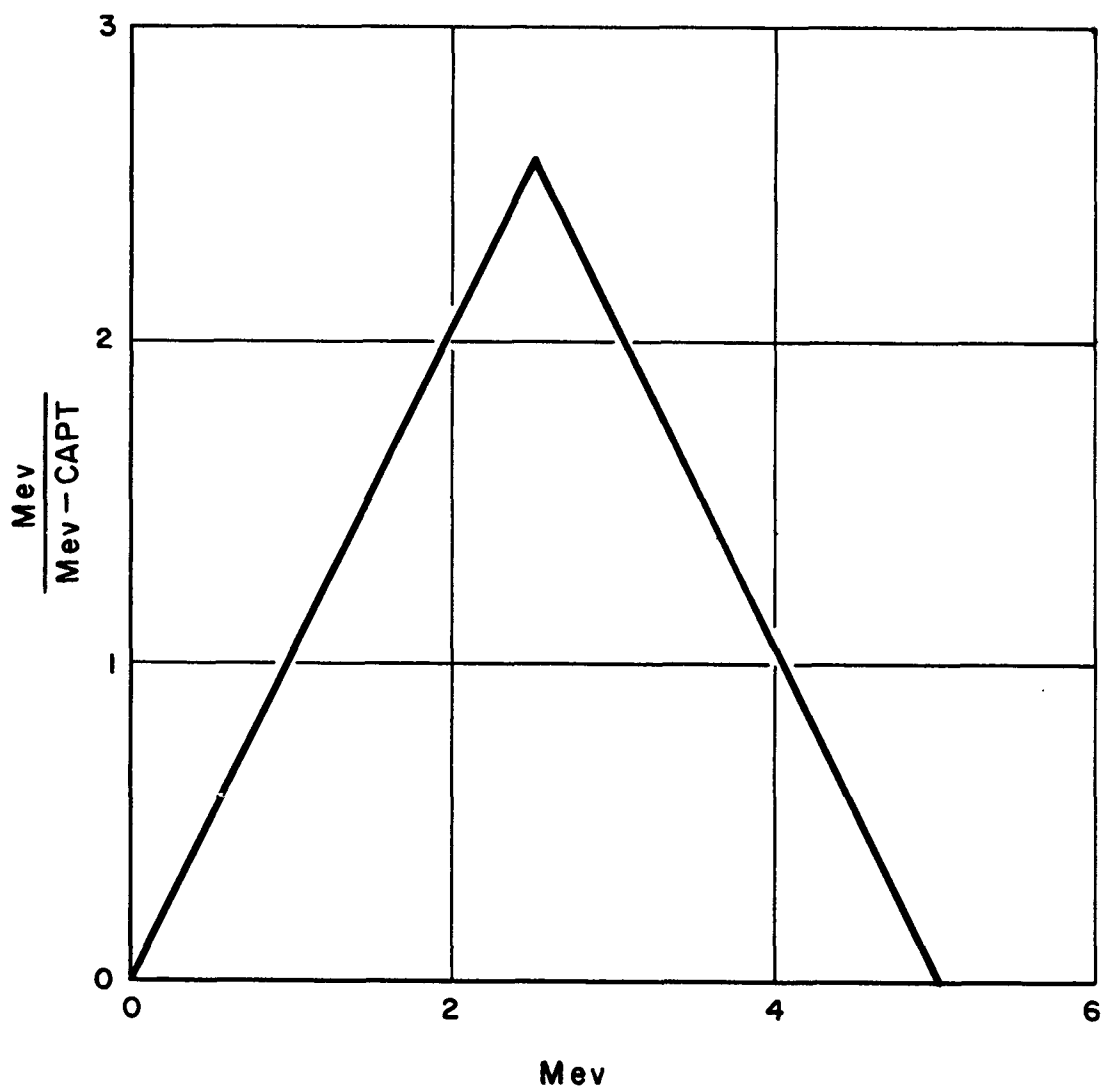
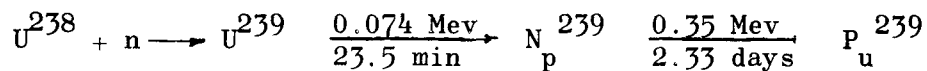


Figure 16. Capture Gamma-Ray Spectrum for  $U^{235}$ , Normalized to 6.42 Mev Per Capture

**CONFIDENTIAL**

Capture Gamma Rays. The number of captures in each element of the core per 100 neutrons born is given in the neutron economy table shown in Table 3. With the exception of  $U^{235}$ , the capture gamma-ray spectrum for each of these elements was obtained from Groshev et al. (Ref. 5) and Deloume (Ref. 6). The values are normalized to the binding energy for the particular element involved. The gamma-ray spectrum for  $U^{235}$  has not been measured. Groshev, et al. (Ref. 7) have measured the general shape of the  $(n, \gamma)$  spectra for even-even nuclei like  $U^{236}$ . They have shown that the continuous spectrum starts roughly at 1.5 Mev below the binding energy, increases to a maximum at about 2.5 Mev, and then decreases to zero. On this basis an approximate spectrum for  $U^{235}$   $(n, \gamma) U^{236}$  can be constructed and normalized to the binding energy of 6.42 Mev. Figure 16 indicates the shape of this proposed spectrum. Graphically integrating this curve over 1 Mev intervals gives the required energy breakdown. The values shown in Table 2 for the capture gamma sources are merely a product of the captures per fission and the Mev per capture.

Decay of  $U^{239}$ . The nonfission capture of a neutron by  $U^{238}$  leads to the following reaction:



From this it may be seen that at saturation ( $T \gg 2.33$  days) there are about 0.42 Mev per capture in the 0-1.0 Mev energy group. For a 900 second operation the above values are corrected as follows:

$$\begin{aligned}
 \text{Mev/cap} = & 0.074 \left[ 1 - e^{-\lambda_1 T} \right] + 0.35 \left[ \frac{1 - e^{-\lambda_2 T}}{\lambda_2} + \right. \\
 & \left. \frac{e^{-\lambda_2 T} - e^{-\lambda_1 T}}{\lambda_2 - \lambda_1} \right] \lambda_2
 \end{aligned} \tag{2}$$

**CONFIDENTIAL**

TABLE 3

NEUTRON ECONOMY TABLE

Core Source Neutrons		100.00
Core Reactions:		
Fission	U <sup>235</sup>	41.71
	U <sup>238</sup>	0.04
		41.75
Captures	U <sup>235</sup>	15.57
	U <sup>238</sup>	1.71
	C	0.01
	Nb	4.36
	H	0.01
		21.66
Leakage:		
Radial		26.01
Axial		10.58
		36.59
Total		100.00



~~CONFIDENTIAL~~

where

$$\begin{aligned}\lambda_1 &= \text{decay constant for } U^{239} \\ \lambda_2 &= \text{decay constant for } N_p^{239} \\ T &= \text{operating time, i.e. 900 seconds}\end{aligned}$$

Solving the above expression we get  $2.2 \times 10^{-4}$  Mev/capture due to the decay of  $U^{239}$  and  $N_p^{239}$ .

The capture gamma-ray spectrum for the reference core is summarized in Table 3.

#### Secondary Sources External to Core

There are several secondary sources of radiation which exist in the structure of the engine system surrounding the reactor core. They are created by the interaction of primary core radiations with nearby materials. Although they are small relative to the primary core fluxes, there are instances in which they are extremely important. If secondary radiation issues from a part of the engine not covered by shielding, the radiation-sensitive parts of the system will be subjected to an additional source of damaging flux. Many of these external radiation sources will persist long after the reactor is shut down; this will cause difficulties in post-test disassembly and handling. Other induced sources may tend to disrupt the neutron economy of the reactor core.

The major sources of radiation external to the reactor core are:

(1) neutron capture reactions, (2) neutron inelastic scattering, (3) gamma-ray Compton scattering and pair production, and (4) photoneutron effect (especially in beryllium).

~~CONFIDENTIAL~~

Neutron capture reactions result in several important effects. During engine operation, the  $(n, \gamma)$  capture reaction is of primary concern because the hard, penetrating, capture gammas are capable of contributing a significant amount of radiation to the existing environment. The gamma energy released in this reaction is dependent on the sum of the binding energy for an additional nucleon in the target nucleus and the kinetic energy of the incident neutron. This energy is released as gamma photons which may have energies as high as 9 Mev, as is the case with nickel. Although the energy can be released as a single photon, other decay schemes are more probable, and the result is a broad spectrum of gamma energies ranging from the soft continuum to energetic hard photons of several Mev. In general, medium and heavy target nuclei release the neutron capture energy promptly as they decay to their ground energy state. Capture-gamma fluxes must therefore be considered in the calculation of the total engine system radiation environment. This is accomplished with the following relationship:

$$S_{v,i} = E_{\gamma,i} \eta_i \sum_g \sum_{a,g} \phi_{n,g} \quad (3)$$

where

$S_{v,i}$  = gamma-ray source strength of ith gamma energy interval,  
Mev/cc-sec

$E_{\gamma,i}$  = average capture gamma-ray energy of ith interval, Mev

**CONFIDENTIAL**

- $\eta_i$  = number of gammas having energies in ith interval produced per neutron capture  
 $\sum_{a,g}$  = macroscopic neutron absorption cross section for neutrons in gth energy group  
 $\phi_{n,g}$  = neutron flux in gth energy group

The AIM-6 code (Ref. 8 ) was used to compute neutron fluxes. Macroscopic neutron cross sections for this calculation were obtained from the AIM-6 data library. The calculation was performed in the course of reactor leakage flux determination and shield analysis.

Although the majority of neutron captures result in prompt gamma emission, there are a number of target isotopes which decay with an appreciable half-life, and this fact gives rise to engine maintenance and disassembly problems after testing. This hazard is primarily a biological one, and is discussed in detail in a subsequent section of this report.

The relationship describing the buildup and decay of a radioactive isotope is as follows:

$$\frac{dN}{dt} = (1 - e^{-\lambda t_1}) e^{-\lambda t_2} \sum_g \sum_{a,g} \phi_{n,g} \quad (4)$$

where

- $\frac{dN}{dt}$  = decay rate of isotope, disintegration/sec  
 $\lambda$  = decay constant,  $\text{sec}^{-1}$   
 $t_1$  = reactor operating time, sec  
 $t_2$  = time from reactor shutdown, sec

~~CONFIDENTIAL~~

---

The term  $e^{-\lambda t_2}$  is unity at all times while the reactor is operating. Delayed radioactivity has little effect on engine system operation relative to the prompt capture effects.

Other important neutron capture reactions are those which result in the emission of particles other than gamma rays. A notable example is the  $(n, \alpha)$  reaction in  $B^{10}$ . This material is useful as a control rod material and a thermal neutron shield. The 2.38 Mev of kinetic energy released in the reaction is absorbed within the emitting material because of the very short range of the  $\alpha$  particle. A small amount of gamma energy (0.5 Mev) is also released by the decay of the metastable  $Li^7$  daughter nucleus. Reactions such as these are treated with a relationship of the same form as Eq. 3, with the additional assumption that all energy not released as gammas is deposited in the emitting material as heat.

Another neutron effect for consideration is inelastic scattering. In this reaction, the fast neutron transfers some of its kinetic energy to the target nucleus, thus raising it to a higher energy level. The nucleus subsequently decays to its ground state by emission of a gamma photon. Because certain threshold energies exist for the excitation of target nuclei, only that part of the fast flux above the threshold need be considered. There are cross sections for inelastic collisions which allow calculations to be made with Eq. 3, although the contribution of gammas from this source is usually negligible in relation to the core and capture gamma components. Rough calculations for the materials considered in the engine system show the effect to be unimportant. Therefore this effect is not a primary factor in the preliminary system calculations.

~~CONFIDENTIAL~~

~~CONFIDENTIAL~~

The effect of gamma rays in producing secondary radiation can be divided into two areas; electron interactions, and nuclear interactions. With electron interactions, the only effect of interest outside the target material is Compton scattering, in which the incident photon is scattered by an electron and continues through the material at a reduced energy and at an angle determined by the Klein-Nishina formula (Ref. 9 ). The energy of the electron is quickly absorbed within the material, and the scattered gamma is accounted for by the use of buildup factors. In nuclear interactions, either pair production or photoneutron emission may result. Pair production occurs when a gamma photon interacts with the target nucleus such that the gamma energy is transformed into an electron-positron pair, each with the same kinetic energy as dictated by conservation of momentum. The threshold energy for this reaction is that determined by the rest-mass energy-equivalent of the two particles, 1.02 Mev, and any additional energy appears as kinetic energy in the pair. This kinetic energy is quickly dissipated within the target material, and the positron annihilates another electron to form a pair of 0.51 Mev gammas, each equivalent to the rest mass of one of the annihilated particles.

The ejection of neutrons from target nuclei by gammas is an effect which is important in few materials. Beryllium, used extensively in the Kiwi reactors is one of these materials, therefore the photoneutron effect is significant in the engine system design. The effect of photoneutrons in adding to the external radiation flux is negligible compared to the primary leakage flux. The reactivity of the core will be slightly higher due to the additional neutrons born in beryllium, but is small enough to be ignored in a preliminary design. In reactor kinetics the photoneutron effect is a major criterion. Although the majority of photoneutrons are caused by prompt-fission gammas, there are sufficient delayed gammas to create a delayed photoneutron flux which forms an important addition to the normal delayed neutrons provided by neutron precursors.

~~CONFIDENTIAL~~

**CONFIDENTIAL**

---

The gammas released in fission product decay after reactor shutdown provide a small photoneutron flux which follows the decay curve of the fission products themselves. These neutrons are able to maintain a small fission rate in the reactor for the period the gamma flux is capable of producing them. While this fission rate is extremely small, and provides less power than the fission product afterheat, it does maintain a measurable neutron flux for several hours after shutdown. This makes reactor restart simpler and more rapid because there is no uncertainty about the rate of power increase in the core.

**CONFIDENTIAL**

---

### Core Neutron Flux Spectrum

As discussed in the previous section, it is generally found that capture-gamma radiation generated exterior to the reactor core is an important consideration in determining the amount and type of shielding required for a reactor system. To determine the magnitude and distribution of this source of radiation, it is necessary to know the thermal neutron flux distribution throughout the system. The degree of accuracy of this distribution will then be reflected in the subsequent capture-gamma ray analysis. For an engine system of the type being considered here, the heat generated in the propellant by kinetic energy loss of fast neutrons must also be evaluated. This consideration requires a detailed determination of the fast neutron flux distribution exterior to the core.

Thermal-Neutron Flux. The first step in determining the thermal-neutron flux distribution in the engine system is to evaluate the fast-neutron flux distribution using the removal theory (Ref. 10, 11, and 12). This calculation is performed with either the GRACE-I (Ref. 13) or the GRACE-II (Ref. 14) code as described in another section. A sixteen-group neutron diffusion code, AIM-6 (Ref. 8) is used to calculate a fast- and thermal-neutron flux distribution for the system. It is then assumed that, in the hydrogenous regions, the correct attenuation and magnitude of the fast-neutron flux is given by the removal theory (Ref. 10), and the equilibrium ratio between fast and thermal flux is computed correctly by diffusion theory. Thus, as equilibrium is approached, the thermal-neutron flux is obtained by multiplying the fast-neutron removal flux by the ratio of fast to thermal flux obtained from AIM-6. In the nonhydrogenous regions of the system the thermal-neutron flux distribution is assumed to be as predicted by diffusion theory. This method has been shown to be reasonably accurate for systems of this type (Ref. 11 and 12).

**CONFIDENTIAL**

~~CONFIDENTIAL~~

Fast-Neutron Removal Flux. The use of the removal theory (Ref. 10) to calculate the fast-flux distribution first requires the specification of a neutron attenuation kernel which describes the attenuation of fast neutrons in a hydrogenous medium from a point isotropic fission source. The fast-neutron flux distribution is then obtained by integrating this kernel over the source volume. Thus, the fast flux distribution is given by:

$$\phi_f = \int_V \frac{N(\ell) S_n}{4 \pi \ell^2} dV, \quad (4)$$

- where:  $\phi_f$  = fast neutron flux, n/cm<sup>2</sup> - sec  
 $N(\ell)$  = fast flux attenuation kernel  
 $\ell$  = distance from the differential source volume to the detector, cm  
 $S_n$  = fission neutron density, n/cm<sup>2</sup>-sec

The attenuation kernel chosen for use in Eq. 4 was represented by the expression:

$$N(\ell) = \frac{\nu_{eff}}{2.43} \sum_{n=1}^3 \frac{1}{F_n} \exp \left[ - \sum_i \left[ \sigma_{H,n} N_i(H) + \sum_k \sigma_k N_i(k) \right] r_i \right] \quad (5)$$

where:

- $\nu_{eff}$  = a constant representing an effective number of fast neutrons produced per fission  
 $F_n$  = constants obtained by fitting the fast neutron removal kernel to moments data



~~CONFIDENTIAL~~

TABLE 4

MICROSCOPIC REMOVAL CROSS SECTIONS

Element	Removal Cross Section, barns
H	$\sigma_{H,1} = 1.56$  $\sigma_{H,2} = 1.04$  $\sigma_{H,3} = 0.70$
B <sub>e</sub>	1.07
C	0.81
B	0.92
A <sub>1</sub>	1.31
F <sub>e</sub>	1.98
N <sub>i</sub>	1.89
Z <sub>r</sub>	2.35
W	2.51
U	3.60

Kernel Constants

$$v_{\text{eff}} = 1.8, F_1 = 1, F_2 = 6, F_3 = 300$$

**CONFIDENTIAL**

---

$\sigma_{H, n}$  = fitted removal cross sections for hydrogen, barns

$\sigma_k$  = removal cross section for element k, barns

$N_i(k)$  = number density of the kth element in the ith  
shield region, atoms/cm<sup>2</sup>

A kernel of this form was chosen so the integration could be performed using one of the existing GRACE codes (Ref. 13 and 14), both of which are readily adaptable to an exponential kernel of this type. Values of  $\nu_{eff}$ ,  $F_n$ , and  $\sigma_{H, n}$  were obtained by fitting Eq. 5 to moments method data for H, H<sub>2</sub>O, C, CH, and CH<sub>2</sub> (Ref. 15). The fast neutron fluxes in these materials were obtained by numerically integrating, above 0.8 Mev, the differential energy spectra data obtained from the moments method calculations. The values of the fitted constants along with the removal cross sections (Ref. 16) for the other materials used in this study are given in Table 4. The results obtained by using these values in evaluating Eq. 5 were found to be in close agreement with moments calculations in the materials mentioned.

#### DESCRIPTION OF COMPUTER PROGRAMS USED IN ATTENUATION CALCULATIONS

Two codes, GRACE I and GRACE II, have been used extensively throughout this analysis for calculating radiation attenuation and heating effects. A detailed description of these codes follows.

#### GRACE-I Code

GRACE I (Ref. 13) is a multigroup, multiregion, gamma-ray attenuation code written in FORTRAN for the IBM 709. The code was designed primarily

**CONFIDENTIAL**

for computing gamma-ray heating and gamma-ray dose rates in multiregion finite or semi-infinite slab shields; however, it can also be used to calculate fast neutron fluxes and dose rates by substituting removal cross sections for the gamma-ray attenuation coefficients.

The basic equations used to compute the flux distribution in a multi-region slab shield were taken from a compilation of formulas given by Foderaro and Obenshain (Ref. 17). Approximations to the exponential integral functions,  $E_1(x)$ , for positive and negative values of the argument in the range  $10^{-40} < |x| < 110$  were taken from a compilation by Gannon (Ref. 18 ). A brief description of the equations follows.

Using the notation shown in Fig. 17 , the gamma-ray flux at the apex of a shielded truncated-cone source of uniform source intensity is given by

$$\phi_\gamma = \frac{S_v(0)}{2\mu_s} \sum_{n=1}^2 \frac{A_n}{1+\alpha_n} \left[ E_2(b_{1n}) - E_2(b_{2n}) - \frac{E_2(b_{1n} \sec \theta)}{\sec \theta} + \frac{E_2(b_{2n} \sec \theta)}{\sec \theta} \right] \quad (6)$$

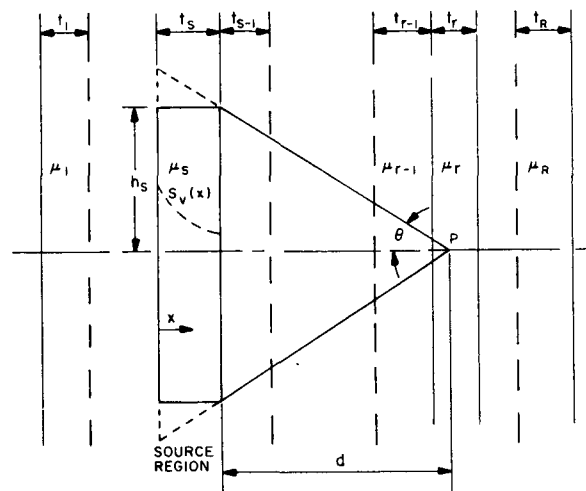


Figure 17. Shield Geometry for GRACE-I Code

**CONFIDENTIAL**

where:

$\phi_\gamma$  = gamma-ray energy flux, Mev/cm<sup>2</sup>-sec

$S_v(0) = \sum_a \phi_{th}(0) E_\gamma \eta$  = gamma-ray source strength of volume distributed source, Mev/cm<sup>3</sup>-sec

$\sum_a$  = macroscopic thermal neutron absorption cross section, cm<sup>-1</sup>

$\phi_{th}(0)$  = incident thermal neutron flux, n/cm<sup>2</sup>-sec

$E_\gamma$  = capture gamma-ray energy, Mev

$\eta$  = number of gamma rays of energy  $E_\gamma$  produced per thermal neutron capture

$\mu_s$  = linear absorption coefficient of source material, cm<sup>-1</sup>

$A_n, \alpha_n$  = coefficients used in double exponential representation of the point isotropic buildup factor

$$E_n(b) = b^{n-1} \int_b^\infty t^{-n} e^{-t} dt, n \geq 0$$

$$b = \sum_r \mu_r t_r$$

$\mu_r$  = linear absorption coefficient of r<sup>th</sup> shield region, cm<sup>-1</sup>

$t_r$  = thickness of r<sup>th</sup> shield region, cm

$$b_{ln} = b(1 + \alpha_n)$$

**CONFIDENTIAL**

---

$$b_{2n} = (b + \mu_s t_s)(1 + \alpha_n)$$

$t_s$  = thickness of source region, cm

$$\theta = \tan^{-1}(h_s/d)$$

$h_s$  = source radius, cm

$d$  = distance from detector to edge of source region, cm

In the expression for the flux (Eq. 6), as in those which follow, the buildup factor has been represented by a double exponential expression of the form

$$B(\mu r) = \sum_{n=1}^2 A_n e^{-\alpha_n \mu r} \quad (7)$$

where:

$$A_2 = 1 - A_1$$

For an exponential distribution of the source intensity, i.e.,

$$S_v(x) = S_v(0) e^{-Kx} \quad (8)$$

the flux at the apex of the cone becomes

~~CONFIDENTIAL~~

$$\phi_{\gamma} = \frac{S_v(0)}{2\mu_s} \exp \left[ \frac{\kappa}{\mu_s} (b + \mu_s t_s) \right] \sum_{n=1}^2 \frac{A_n}{1+\alpha_n} \left[ F_1(b_{2n}, a_n) - \right. \\
 \left. F_1(b_{1n}, a_n) - \frac{F_1(b_{2n} \sec \theta, a_n/\sec \theta)}{\sec \theta} + \frac{F_1(b_{1n} \sec \theta, a_n/\sec \theta)}{\sec \theta} \right] \quad (9)$$

where:

$$\kappa = \frac{1}{t_s} \ln \frac{\phi_{th}(t_s)}{\phi_{th}(0)} = \text{inverse relaxation length of source distribution, cm}^{-1}$$

$$F_1(\tau, a) = \int_0^{\tau} e^{ab} E_1(b) db \\
 a_n = -\kappa / \left[ \mu_s (1 + \alpha_n) \right]$$

Note, that since  $\sec \theta$  is infinite for  $\theta = \pi/2$ , the gamma-ray flux from an infinite slab source may be obtained by setting the last two terms in Eq. 6 and 9 equal to zero.

The gamma-ray flux at a point within a semi-infinite slab source of uniform source intensity is given by

$$\phi_{\gamma} = \frac{S_v(0)}{2\mu_s} \sum_{n=1}^2 \frac{A_n}{1+\alpha_n} \left\{ 2 - E_2 \left[ \mu_s d(1+\alpha_n) \right] - \right. \\
 \left. E_2 \left[ \mu_s (t_s - d)(1+\alpha_n) \right] \right\} \quad (10)$$

**CONFIDENTIAL**

For an exponential source distribution the flux becomes

$$\phi_{\gamma} = \frac{S_v(0)}{2\mu_s} e^{-\kappa t_s} \sum_{n=1}^2 \frac{A_n}{1+\alpha_n} \left\{ F_1 \left[ \mu_s d(1+\alpha_n), a_n \right] + \right.$$

$$\left. F_1 \left[ \mu_s (t_s - d)(1+\alpha_n), a_n \right] \right\} \tag{11}$$

Note that the flux within a truncated cone is not defined.

The function  $F_1(\tau, a)$  is evaluated by use of the following expressions (Ref. 17):

$$F_1(\tau, a) = \frac{1}{a} \left\{ e^{a\tau} E_1(\tau) - E_1[\tau(1-a)] - \ln|a-1| \right\}, \quad a \neq 0 \text{ or } 1, \tau \neq 0$$

$$= e^{\tau} E_1(\tau) + \ln(\tau) + 0.577216, \quad a = 1, \tau = 0$$

$$= 1 - E_2(\tau), \quad a \text{ or } \tau = 0.$$

For the numerical calculation of  $E_2(x)$  the two equations

$$E_2(x) = e^{-x} - x E_1(x) \text{ and } E_2(0) = 1.0$$

are employed.

Equations 6, 9, 10 and 11 are used to compute the gamma-ray flux distributions from slab and truncated-cone sources in multiregion slab shields.

~~CONFIDENTIAL~~

The flux distributions obtained are converted to dose rates or heat generation rates by use of the relation

$$D = \left[ \left( \frac{\mu_e}{\rho} \right) C_1 + \frac{C_2}{k} \right] \phi_\gamma, \quad (12)$$

where:

D = gamma-ray dose rate or heat generation rate

$\mu_e$  = energy absorption coefficient,  $\text{cm}^{-1}$

$\rho$  = material density,  $\text{gm/cc}$

k = conversion factor from gamma-ray energy flux to dose rate

$C_1 = 0$  for dose rate calculations

$C_2 = 0$  for heat generation rate calculations

For each shield region either a uniform or an exponential source distribution may be specified. Furthermore, by specification of a radius,  $h_s$ , for a given source region, the truncated-cone calculation is automatically performed when the detector is located outside the source region. Since the detector must be located at the apex of the cone, the cone angle,  $\theta$ , for a given source radius  $h_s$ , is defined by

$$\theta = \tan^{-1} \frac{h_s}{d}, \quad (13)$$

where d is the distance from the source to the detector. Note that the cone angle for a given source region varies with detector position in the shield. For those positions where  $h_s/d$  is greater than 5, i.e., within



~~CONFIDENTIAL~~

---

or relatively close to the source region, or when  $h_g$  is set equal to zero, only the semi-infinite slab calculation is performed. Since the value of  $h_g$  is specified by source region, any source geometry which can be approximated by a series of disc or truncated-cone sources may be handled by the code.

One of the important features of the GRACE-I code is the method used to specify the buildup factor. In computing the flux distribution at a particular location in the shield from a given source region, a single-material buildup factor is used. However, this buildup factor may be specified in two ways depending upon the specific shield arrangement being investigated. In the first, a single buildup factor is assigned to each region in which the flux distribution is desired. This buildup factor is then used to calculate the flux distribution in that region from every source region in the shield. In the second, a set of buildup factors is assigned to each region, each member of the set corresponding to a different source region. The flux distribution is then computed using the buildup factor associated with each source. In this way, the code attempts to alleviate some of the problems which arise when a shield consists of materials of widely varying atomic number.

#### GRACE-II Code

The GRACE-II code (Ref. 14) was also written in FORTRAN for the IBM 709. However, this code computes the total dose rate or heat generation rate in a multiregion shield along the radial centerline of either a spherical or cylindrical source volume. The source, containing up to 20 gamma-ray energy groups, may be located in either the central region of the system or in the first concentric shell surrounding it. Dose rates or heat generation rates are calculated at detector points within the source volume,

~~CONFIDENTIAL~~

~~CONFIDENTIAL~~

or in as many as 20 concentric or semi-infinite slab regions located outside the source volume. The source and shield geometries are shown in Fig. 18 and 19. A brief discussion of the equations follows.

The gamma-ray flux at any position, P, in a shield (Fig. 19) because of a volume distributed source in the shield, can be described by the expression

$$\phi_{\gamma} = \int_V \frac{B(\mu \ell) S_v e^{-\mu \ell}}{4 \pi \ell^2} dv \quad (14)$$

where  $B(\mu \ell)$  is the point isotropic buildup factor and  $\mu \ell$  represents the total penetration distance from the differential volume element to the detector. Using the notation of Fig. 18 and 19, and substituting  $r = \ell$  and  $dv = 2 \pi r^2 \sin \theta dr d\theta$  into Eq. , the flux distribution from a spherical volume or shell source becomes

$$\phi_{\gamma} (\text{sphere}) = 1/2 \int_0^{\theta_0} \sin \theta d\theta \int_{L_1}^{L_2} B(b) S_v e^{-b} dr \quad (15)$$

Similarly, substituting  $r = \ell \cos \psi$  and  $dv = \ell^2 d\psi d\theta dr$  into Eq. 14, the flux distribution from a cylindrical volume or shell source becomes

$$\phi_{\gamma} (\text{cylinder}) = \frac{1}{\pi} \int_0^{\theta_0} d\theta \int_{L_1}^{L_2} dr \int_0^{\psi_0} B(b \sec \psi) S_v e^{-b \sec \psi} d\psi \quad (16)$$

**CONFIDENTIAL**

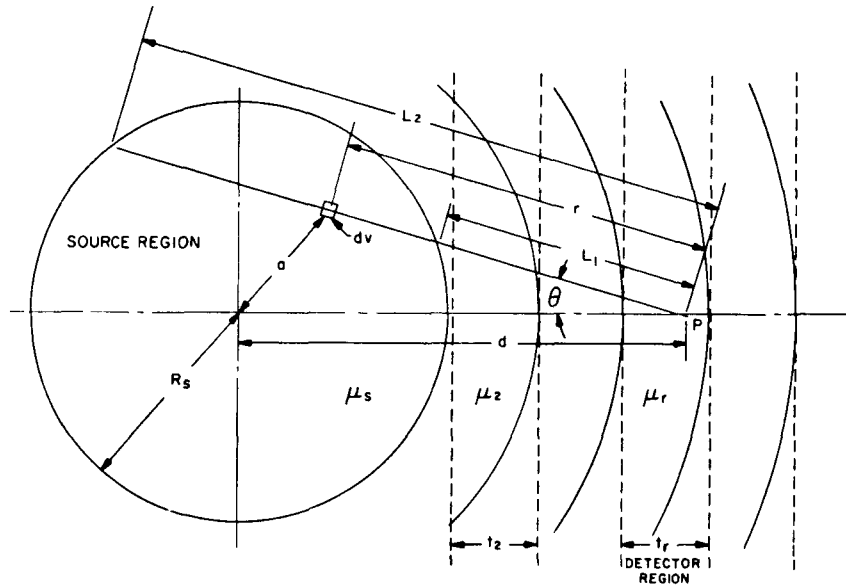


Figure 18. Source and Shield Geometry for GRACE-II Code

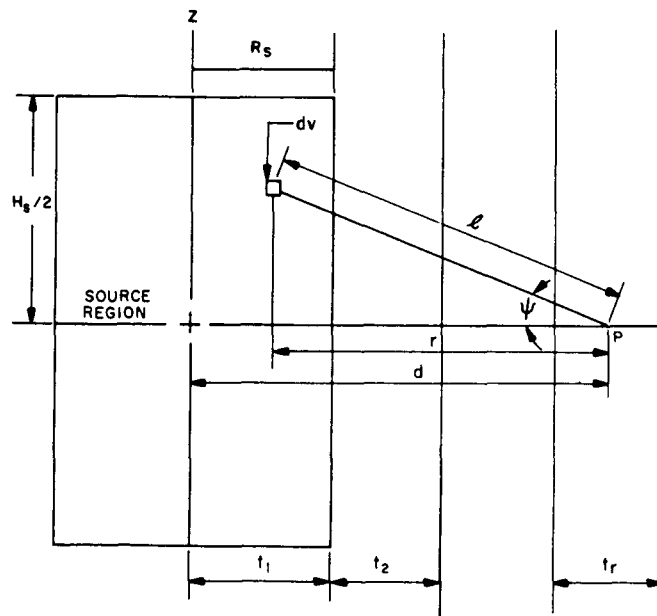


Figure 19. Cylindrical Geometry for GRACE-II Code

**CONFIDENTIAL**

where  $\psi_0 = \tan^{-1}(h_s/2r)$ . For computational purposes  $\psi_0$  is set equal to  $\pi/2$  when  $h_s/2r > 10$ . The values for the limits on the  $\theta$  and  $r$  integrations and the value of  $b$  in Eq. 15 and 16 depend upon the region in which the source is located and upon the detector position. Furthermore, the value of  $b$  depends on whether the shield regions outside the source volume are represented by concentric shells or semi-infinite slabs.

As in the GRACE-I code, the buildup factor,  $B$ , is represented by a double exponential expression of the form

$$B(\mu\rho) = A_1 e^{-\alpha_1 \mu\rho} + (1-A_1) e^{-\alpha_2 \mu\rho} \quad (17)$$

where  $A_1$ ,  $\alpha_1$ , and  $\alpha_2$  are the energy dependent material constants. Although a single-material buildup factor is used in calculating the flux distribution in any region of the shield, a different buildup factor may be assigned to each region in which the dose rate or heat generation rate is being computed.

The distribution of the source strength,  $S_v$ , in the source volume may be uniform or variable in either or both the radial and axial (in the cylindrical case) directions. The variation in the radial direction is given by either an exponential or a polynomial of the fourth degree. In the axial direction, only the polynomial variation is allowed. Thus the source strength (including a term for the axial variation in the cylindrical case) may be described by either

$$S_v = S_v(0) e^{-\kappa(R_s - a)} \sum_{n=0}^4 A_n z^n, \quad (18)$$

**CONFIDENTIAL**

---

or

$$S_v = S_v(0) \sum_{n=0}^L R_n (R_s - a)^n \sum_{n=0}^L A_n z^n \quad (19)$$

where  $a$  is the radial distance from the center of the source to the differential volume element (Fig. 18),  $\kappa$  is the inverse relaxation length of the source, and  $A_n$  and  $R_n$  are the axial and radial polynomial coefficients, respectively. The polynomial coefficients are obtained using weighting factors in conjunction with a least-squares subroutine which has been built into the code.

Equations 15 and 16 are solved numerically using Simpson's Rule. The order of the integration is as indicated. The flux distributions obtained are then converted to dose rates or heat generation rates in the same manner as for GRACE I (see Eq. 12).

~~CONFIDENTIAL~~

---

### Basic Gamma-Ray Data

A 10-group energy separation has been used for the majority of the gamma-ray attenuation calculations described in this study. The basic gamma-ray data for these calculations are given in Table 5. Only data for those materials considered in this study are presented. A brief description of these data follows.

Total Gamma-Ray Attenuation Coefficients. The product of these numbers and the material density give the total gamma-ray cross section. These data were compiled from Ref.19.

Energy Absorption Coefficients. Only a fraction of the events represented by the total attenuation cross section actually remove the gamma-ray. In particular, Compton scattering can cause a change in the direction and the energy of a photon without absorbing it. The energy-absorption coefficient is a measure of the fraction of the gamma-ray energy which is converted from radiant energy into heat. Thus, the product of the gamma-ray flux and the energy absorption coefficient gives the heat generation rate in the material. The energy absorption coefficients shown in Table 5 were also taken from Ref. 19.

Buildup Factor Constants. Because not all gamma interactions are absorptive, and some scattered radiation may ultimately penetrate a shield, a numerical correction is commonly used in attenuation calculations. The uncollided flux is calculated using total cross sections, and then multiplied by the appropriate buildup factor to give a more realistic value

~~CONFIDENTIAL~~

---

for the transmitted flux. Buildup factors have been determined theoretically by the method of moments (Ref. 20). The buildup factor is a function of distance into the shield, measured in mean free paths, as well as the particular material and gamma-ray energy. Table 5 gives the constants for a double-exponential analytical fit to dose and energy-absorption buildup-factor data. Buildup-factor data are not available for all materials; however, graphite buildup factors can be used for hydrogen, beryllium, and air, aluminum buildup factors for ordinary concrete, and iron buildup factors for Inconel, steel, and zirconium hydride with little resulting error. The data shown were taken from Ref. 17 and 21.

Capture Gamma-Rays. The prompt capture gamma-ray spectra from thermal neutron capture were taken from Ref. 5 and 6. These data have been normalized to the neutron binding energy for the nucleus involved.

TABLE 5

## BASIC GAMMA-RAY DATA\*

(Gamma-Ray Energy, Mev)

Material	0.5	1.5	2.5	3.5	4.5	5.5	6.5	7.5	8.5	9.5
<u>Hydrogen</u>										
$\mu/\rho$	0.1730	0.1030	0.0775	0.0630	0.0535	0.0475	0.0425	0.0390	0.0360	0.0335
$\mu e/\rho$	0.0596	0.0512	0.0450	0.0377	0.0340	0.0310	0.0282	0.0263	0.0248	0.0234
MEV/Capture	2.23									
<u>Beryllium</u>										
$\mu/\rho$	0.0773	0.0459	0.0348	0.0287	0.0250	0.0223	0.0203	0.0188	0.0176	0.0162
$\mu e/\rho$	0.0266	0.0218	0.0203	0.0172	0.0157	0.0148	0.0138	0.0132	0.0125	0.0120
MEV/Capture	1.70				5.12					
<u>Graphite</u>										
$\mu/\rho$	0.0870	0.0576	0.0393	0.0327	0.0285	0.0258	0.0237	0.0221	0.0209	0.0199
$\mu e/\rho$	0.0298	0.0257	0.0225	0.0194	0.0186	0.0174	0.0164	0.0156	0.0150	0.0146
MEV/Capture	0.50		1.10		3.46					
Ad	7.00	7.80	5.60	4.80	4.20	3.80	3.40	3.10	2.90	2.76
$\alpha 1d$	-0.260	-0.0879	-0.0680	-0.0580	-0.0532	-0.0530	-0.0483	-0.0460	-0.0440	-0.0420
$\alpha 2d$	0.0730		0.1018	0.1122	0.1190	0.1220	0.1250	0.1265	0.1284	0.1300

CONFIDENTIAL

R-3007


  
**ROCKWELL**  
 A DIVISION OF NORTH AMERICAN AVIATION INC  
**CONFIDENTIAL**



TABLE 5  
(Cont.)

Ad	10.00	7.53	5.71	4.40	3.70	3.28	2.92	2.60	2.35	2.10
$\alpha_{1d}$	-0.0940	-0.0794	-0.0720	-0.0725	-0.0755	-0.0788	-0.0800	-0.0830	-0.0865	-0.0905
$\alpha_{2d}$	0.0184	0.0365	0.0530	0.0629	0.0659	0.0658	0.0640	0.0614	0.0540	0.0430
Ae	15.90	8.40	5.32	3.90	3.10	2.60	2.30	2.00	1.75	1.60
$\alpha_{1e}$	-0.0950	-0.0805	-0.0755	-0.0808	-0.0835	-0.0850	-0.0862	-0.0880	-0.0900	-0.0935
$\alpha_{2e}$	0.0365	0.0615	0.0810	0.0930	0.0990	0.1010	0.0995	0.0940	0.0830	0.0630
<u>Tungsten</u>										
$\mu/\rho$	0.1260	0.0493	0.0416	0.0402	0.0406	0.0414	0.0423	0.0433	0.0440	0.0458
$\mu_e/\rho$	0.0800	0.0312	0.0277	0.0300	0.0335	0.0345	0.0365	0.0382	0.0400	0.0418
MEV/Capture	0.89	1.50	1.50	1.28	0.77	0.58	0.33	0.33		
Ad	3.10	3.10	2.80	2.40	1.80	1.35	1.10	0.80	0.60	0.60
$\alpha_{1d}$	-0.058	-0.058	-0.078	-0.099	-0.132	-0.159	-0.181	-0.199	-0.210	-0.214
$\alpha_{2d}$	0.185	0.185	0.164	0.101	0.045	0.003	0.009	0.035	0.072	0.118
<u>Zirconium</u>										
<u>Hydride</u> $\mu/\rho$	0.0840	0.0460	0.0372	0.0346	0.0340	0.0336	0.0338	0.0340	0.0343	0.0350
$\mu_e/\rho$	0.0340	0.0229	0.0220	0.0240	0.0255	0.0264	0.0275	0.0285	0.0295	0.0306
MEV/Capture		0.12	1.85	0.60	0.41	0.25	0.27	0.04	0.03	

TABLE 5  
(Cont.)

Ae	11.00	8.80	6.40	5.35	4.50	4.00	3.60	3.21	3.00	2.80
$\alpha_{1e}$	-0.134	-0.0800	-0.0632	-0.0540	-0.0498	-0.0460	-0.0439	-0.0420	-0.0415	-0.0398
$\alpha_{2e}$		0.0662	0.0950	0.1078	0.1158	0.1218	0.1230	0.1298	0.1310	0.1320
<u>Aluminum</u>										
$\mu/\rho$	0.0840	0.0500	0.0382	0.0328	0.0296	0.0274	0.0258	0.0248	0.0240	0.0234
$\mu_{e/\rho}$	0.0290	0.0248	0.0238	0.0216	0.0197	0.0192	0.0190	0.0186	0.0179	0.0167
MEV/Capture	0.14	1.78	0.85	1.14	1.82	0.48	0.63	2.65		
Ad	12.50	6.45	4.98	4.10	3.60	3.30	2.80	2.42	2.20	2.20
$\alpha_{1d}$	-0.1130	-0.0915	-0.0780	-0.0700	-0.0645	-0.0640	-0.0635	-0.0624	-0.0615	-0.0605
$\alpha_{2d}$	0.0060	0.0730	0.1062	0.1230	0.1370	0.1480	0.1540	0.1530	0.1460	0.1348
Ae	12.00	6.75	5.10	4.20	3.52	3.02	2.77	2.68	2.54	2.27
$\alpha_{1e}$	-0.1390	-0.0942	-0.0780	-0.0707	-0.0653	-0.0640	-0.0619	-0.0600	-0.0588	-0.0596
$\alpha_{2e}$	-0.0800	0.0660	0.1039	0.1226	0.1369	0.1488	0.1525	0.1246	0.1151	0.1300
<u>Inconel or Steel</u>										
$\mu/\rho$	0.0825	0.0486	0.0382	0.0340	0.0320	0.0309	0.0302	0.0298	0.0298	0.0299
$\mu_{e/\rho}$	0.0295	0.0239	0.0208	0.0172	0.0158	0.0142	0.0127	0.0118	0.0110	0.0107
MEV/Capture				0.17	0.37	0.63	1.20	1.50	4.61	0.17

TABLE 5  
(Cont.)

Ordinary Concrete											
$\mu/p$	0.0875	0.0522	0.0408	0.0340	0.0304	0.0280	0.0265	0.0251	0.0242	0.0235	
$\mu_e/p$	0.0302	0.0260	0.0236	0.0212	0.0200	0.0192	0.0185	0.0180	0.0176	0.0174	
MEV/Capture	0.12	0.58	1.27	0.96	1.51	0.74	0.74	0.71	0.04	0.03	
Air											
$\mu/p$	0.0870	0.0516	0.0394	0.0329	0.0289	0.0263	0.0243	0.0228	0.0217	0.0208	

\*Dose buildup factor constants are subscripted with a "d" and energy absorption buildup factor constants are subscripted with an "e"

R-3007

CONFIDENTIAL

ROCKETDYNE  
A DIVISION OF NORTH AMERICAN AVIATION INC  
CONFIDENTIAL

**CONFIDENTIAL**

---

The AIM-6 Neutron Diffusion Code

The one-dimension multigroup diffusion theory approximation to the Boltzmann equation in plane, cylindrical, or spherical geometry is solved by AIM-6. The code handles up to 18 lethargy groups, 101 space points, 20 material regions and allows for downscatter to as many as five groups. Microscopic cross sections (16 and 18 group) are available, and are derived from IASL internal document N-2-753 and LAMS -2255, respectively. Any combination of three homogeneous, and one inhomogeneous boundary conditions, is available at either the interior or exterior boundary.

The principal features of the code are:

1. Calculation of fluxes and eigenvalues
2. Fixed source distribution problems
3. Criticality calculations on the transverse buckling, homogeneous poison, and critical radius
4. Search on the critical concentration of one or two elements
5. Location of a poison boundary, and a fuel boundary
6. Calculation of adjoint fluxes
7. Changes to library at time of execution
8. Calculation of group-dependent extrapolation distances
9. Data edit giving peak-to-average-power, percent fissions and absorption, and mass by per element per region, median fission efflux, and absorption energy for core and by mesh point, leakage and absorption rates per region, integrated fluxes per group per region, etc.

Several AIM-6 decks are available for special purposes.

**CONFIDENTIAL**

---

## SHIELD MATERIAL SELECTION

### SHIELD PHILOSOPHY

A shield designed for use in a nuclear rocket engine system is very different from the sort employed in conventional ground-based nuclear reactors. Its primary purpose is to absorb heat-producing radiation from the reactor with little concern for reducing escaping fluxes to biologically permissible levels. The rocket engine shield must be narrowly directional to conserve weight, therefore providing protection only to those parts of the rocket vehicle which require it. It must be relatively compact, and have a cooling system capable of absorbing the tremendous quantities of radiation energy generated within it during operation of the engine.

Shielding is necessary because the rocket engine system cannot be designed to operate efficiently in the powerful unattenuated heat-generating radiations of a propulsion reactor. The two areas of the engine system most in need of protection are components and structure located close to the reactor, and propellant in the vehicle's tanks.

Some leeway for the accommodation of nuclear heating exists in the design of components and structure: cooling can be provided for the individual parts, or local shielding can be added in special cases, but the propellant heating problem does not lend itself to such a variety of solutions. The temperature rise due to radiation in propellant entering the feed pump is a function only of radiation flux levels, reactor-tank separation distance, and propellant flow patterns within the tank. In consideration of these facts, it appears that propellant heating is the more inflexible problem, and that both shield material and shield design should therefore be based on it. This shield will also provide considerable protection to

**CONFIDENTIAL**

~~CONFIDENTIAL~~

---

components and structure, while still allowing the designer to use all the weight-saving artifices and techniques possible to assure the functioning of all equipment in the radiation field.

An optimum shield material or composite of materials must offer the best possible combination of neutron and gamma attenuation with respect to both the reactor radiation spectrum, and the relative contribution of each type of radiation to propellant heating. For this reason a propellant heating attenuation factor which allows a useful comparison between different types of shields has been devised. This factor is defined as the ratio of the unshielded integrated heat generated in an infinite column of fluid to that in the same fluid with the addition of a shield. Such a definition takes into account the primary gamma radiation from the core, any neutron capture gammas from shield, the rapid absorption of fast neutron kinetic energy in hydrogen, and the isotropic nature of the hydrogen capture gamma. Almost half the capture gamma energy escapes from the tank because the neutron flux is attenuated in the first few inches of propellant. This definition also serves as a general guide to the reduction of heat generation in components and structures.

The strong directionality of radiation escaping from the reactor means that a shield need only be large enough to fill the solid angle subtended by the propellant tank relative to the reactor. Since shield thickness is only a function of the attenuation factor required, it is clear that the minimum shield weight will be obtained when the shield is mounted as close as possible to the source of radiation. This means that the shield should be located inside the reactor pressure shell. Cooling can then be provided by the full flow of high-pressure propellant, and a separate pressure vessel is not required. There are some disadvantages to this location. The high heat fluxes, temperature gradients, and thermal stresses created by such close proximity to the reactor will demand a shield material with good heat transfer properties and adequate strength at high temperatures. The shield

~~CONFIDENTIAL~~

**CONFIDENTIAL**

---

should have no other undesirable effects, such as altering the power profile in the reactor core due to a change in neutron economy near its upper surface. All of the shield materials considered will be evaluated with regard to these requirements.

#### SHIELD MATERIALS

The range of possible shield materials can be divided into a few broad classes. Neutron attenuation favors the choice of light nuclei, and thus hydrogen deserves consideration either in its liquid form or as a hydride with other materials. Light elements such as lithium, beryllium, and carbon form another group. A final class of shield materials would encompass the dense, heavy metals such as iron, tungsten, and uranium. Those of the latter group cannot be used alone because their high thermal-neutron capture cross sections would cause large secondary gamma fluxes and lower the efficiency of the shield. It is desirable to "load" them with boron which removes thermal neutrons through the  $(n, \alpha)$  reaction in  $B^{10}$ . Capture reactions within the propellant are similarly reduced.

Attenuation properties of the 12 most promising shield materials have been calculated and are listed in Table 6. They are compared against a reference material (graphite) for convenience in evaluation. The tabulated values show the relative weight and thickness of each material as compared to a graphite shield of the same attenuation factor.

The values in this table demonstrate the relative merits of several of the most promising materials. The gamma attenuation numbers are based on the linear mass attenuation coefficients of the respective materials for a gamma energy of 2 Mev, the approximate mean energy of gamma radiation escaping the shield. Neutron attenuation values have been obtained through the use of fast neutron removal cross sections because it is the fast spectrum which is most important in propellant heating. These numbers are very valuable for comparing the attributes of a wide variety of different shield materials, but of course they do not take the place of a detailed analysis for evaluating the total effect of the shield on the engine system.


  
**CONFIDENTIAL**

TABLE 6

EQUIVALENT WEIGHTS AND THICKNESSES OF POSSIBLE SHIELD  
MATERIALS AS COMPARED TO BORONATED GRAPHITE

Shield Materials	Density, gm/cc	Required Weight of Shield Material Per Unit Weight of Boronated Graphite		Required Thickness of Shield Material Per Unit Thickness of Boronated Graphite	
		For Equivalent Fast Neutron Attenuation	For Equivalent 2.0 Mev Gamma Attenuation	For Equivalent Fast Neutron Attenuation	For Equivalent 2.0 Mev Gamma Attenuation
H	0.069	0.065	0.51	1.60	12.45
LiH	0.82	0.26	1.00	0.55	2.08
C	1.70	1.00	1.00	1.00	1.00
Be	1.85	0.57	1.13	0.52	1.04
B <sub>4</sub> C	2.51	0.80	1.06	0.54	0.72
ZrH <sub>1.8</sub>	5.60	1.49	0.94	0.46	0.29
Zr	6.50	2.62	0.96	0.69	0.26
Steel	7.80	1.91	1.03	0.42	0.23
W	19.30	4.96	1.02	0.44	0.089
U	18.90	4.49	0.92	0.40	0.083
Be + Steel	3.72	0.36 Be + 0.70 Fe	0.36 Be + 0.70 Fe	0.33 Be + 0.15 Fe	0.33 Be + 0.15 Fe
Be + U	3.50	0.51 Be + 0.51 U	0.51 Be + 0.51 U	0.47 Be + 0.046 U	0.47 Be + 0.046 U



**CONFIDENTIAL**

---

As shown in Table 6, liquid hydrogen is by far the best shield material on the basis of shield material weight alone. Its atomic weight of 1 makes it theoretically possible to remove all of a neutron's kinetic energy in one elastic collision. Its charge-to-mass ratio is approximately double that of any other material and makes it the best possible gamma shield on a per-unit-mass basis. These desirable atomic and nuclear properties are outweighed by the problems of utilizing liquid hydrogen for use as a single material shield. For example, a hydrogen shield to provide an attenuation factor of 6, the value resulting from the configuration analysis discussed in the next section, would have to be 11 ft thick. This would necessitate relocation of the turbomachinery from its central location and addition of a quantity of complex high-pressure ducting.

Hydrogen's greatest disadvantage is in the removal of energy absorbed by the liquid shield; the only means of removing heat at low pressures is through boiling. An attempt to run full propellant flow through a low-pressure hydrogen shield and into the feed pump would present even more undesirable pump inlet conditions than an unshielded configuration. If  $5/6$  of the radiation energy entering a 40-degree solid angle at 1500 megawatts was used to vaporize hydrogen, the total boiloff during a 1200-second run would be 2500 pounds, assuming the shield were continuously replenished. This loss is more than twice the weight of a boronated graphite shield designed for the same purpose. The shield boiloff is not hot enough to be considered as a tank pressurant; even if part of the flow were passed through a heat exchanger and heated to 560 R, there would still be 2140 pounds more than is needed for tank pressurization. The only propellant bleed in the entire system which approaches the mass flowrate of shield boiloff is the turbine cold gas bleed, but this must be at the nozzle inlet pressure or above. A high-pressure liquid hydrogen shield would not allow heat removal through boiling because the fluid would be supercritical, and the pressure vessel needed to contain it would be prohibitively heavy.

~~CONFIDENTIAL~~

Clearly, liquid hydrogen is not feasible for use by itself as a radiation shield. However, this does not rule it out for use in a composite shield employing another material to supply the majority of the attenuation. This possibility is discussed in a subsequent portion of this section.

Other shield materials in Table 6 incorporate hydrogen as a hydride, and possess some of hydrogen's excellent neutron attenuation properties with the additional advantage of high density. They will make efficient, compact shields with good attenuation of both neutron and gamma fluxes. Table 6 would indicate that lithium hydride is the better of the two hydrides listed, but it must be ruled out because of its tendency to dissociate at high temperatures and in strong radiation fields. It might find use as an auxiliary neutron shield in combination with another material. Zirconium hydride may be employed as a single-material shield with no serious problems.

Of the nonhydrogenous materials, only carbon and zirconium (Table 4), do not have troublesome high capture cross sections for thermal neutrons. Consequently, the high-cross-section materials cannot be used without some means of disposing of thermal neutrons before they are captured and create a secondary source of hard gammas. The best way of accomplishing this is to employ boron either as an alloy, as a mixture, or as boral (boron-aluminum) plates. Most of the thermal neutrons will then be removed in the  $(n, \alpha)$  reaction in  $B^{10}$ , which deposits more energy in the shield but prevents it from reaching the rest of the vehicle. It is advisable to use boron loading in any shield that tends to reduce neutron fluxes to thermal energies, because this will substantially reduce capture-gamma reactions in the hydrogen propellant. The amount of boron loading required to reduce capture-gamma fluxes to an order of magnitude less than the attenuated primary fluxes is only a percent or two by weight.

~~CONFIDENTIAL~~

~~CONFIDENTIAL~~

Carbon, beryllium, and boron carbide ( $B_4C$ ) stand out among the non-hydrogenous shield materials as combining good neutron attenuation properties with fair gamma attenuation. However, because of the low thermal conductivity of boron carbide (about one fourth that of graphite) only carbon and beryllium have adequate physical and mechanical properties to permit their use in a compact shield mounted within the pressure shell. Although beryllium is preferable to carbon for neutron attenuation, this advantage is offset by carbon's superior gamma attenuation. Therefore, since carbon and beryllium are so similar in their densities and total attenuation properties, other factors must be considered in choosing between them. The most important of these is cost; a beryllium shield to provide an attenuation of 6 would cost approximately \$150,000 for the material alone. Graphite (with the previously mentioned boron loading) is therefore the most promising of the single-material shields, although beryllium should be reconsidered for use as an auxiliary neutron attenuator in a composite shield.

To choose a composite shield, the materials must provide better radiation attenuation in combination than could be provided individually. Although it may not be appreciably lighter than one of the better single-material shields such as graphite, a more compact shield may be obtained. The desirability of locating the shield within the pressure shell again disqualifies liquid hydrogen and lithium hydride, although the hydrogen coolant passing through the shield will provide a small amount of additional attenuation. Beryllium remains as the logical choice for the neutron attenuating component of a composite shield. The gamma attenuating component could be any of the relatively heavy elements listed in Table 6, because they have similar gamma attenuating properties and are dense enough so the difference in thickness of the resultant shields would be unimportant. Iron (steel) has markedly superior neutron attenuation properties, is easier and less expensive to fabricate, and therefore is the best choice.

**CONFIDENTIAL**

---

The optimum proportions of iron and beryllium in the composite shield are determined by the resultant heating effect of the attenuated flux in tanked propellant. Theoretically, the optimum composition would be that in which the same reduction in heat generation is obtained from the addition of a small additional amount of either material. Although the calculations necessary to precisely determine the ideal composition are lengthy, an approximation which is sufficiently close for the purposes of this analysis can be obtained. In view of the similar gamma attenuating properties of the two materials, iron would be the material chosen on the basis of gamma absorption alone because of its high density and low cost. Beryllium, on the other hand, is by far the superior neutron shield and is employed primarily for this purpose. Then, an approximation to the ideal composition can be obtained by simply adding to an existing iron shield an amount of beryllium necessary to reduce the neutron-caused propellant heating to some arbitrary fraction of the gamma effect. If the proportion of beryllium chosen is small relative to the iron fraction, the error in the required weight of beryllium will be quite small relative to the total weight of the shield. It is assured that the iron-beryllium shield chosen for comparison with the other possible materials is representative of the best possible combination of the two constituents. For this analysis, the proportions of beryllium and iron in the resulting composite would attenuate gammas and neutrons in the same ratio as would graphite. This composition contains 34 percent beryllium by weight; an amount that is probably several percent more than the true optimum for approximate attenuation factors of 6, but which will cause very little error in the resultant over-all shield weight because of the similar gamma shielding properties of the two components.

~~CONFIDENTIAL~~

The list of possible shield materials has been reduced to the three most promising types: zirconium hydride, graphite, and iron-beryllium. All three will employ boron loading to capture thermalized neutrons as was previously explained. It is now necessary to perform detailed propellant heating calculations with each of these shields to demonstrate the superiority of one type. Table 7 outlines the various shields which will be analyzed with respect to their effects on propellant heating.

TABLE 7  
SHIELD MATERIALS AND COMPOSITIONS USED

Shield	Composition			
	Density, gm/cc	Element	Number Density, Atoms/cc x 10 <sup>-24</sup>	Thickness Considered, in.
Zirconium Hydride (ZrH <sub>1.8</sub> ) Containing 1 w/o Boron	5.6	H B Zr	0.0654 0.00312 0.0363	3 and 5
Graphite Containing 1 w/o Boron	1.7	B C	0.000945 0.0854	9.88 and 16.47
Borated Steel followed by Beryllium con- taining 2 w/o Boron	3.72	<u>Steel</u>		
		B	0.00434	1.41 Steel + 3.11 Be
		Fe	0.0665	
		Ni	0.0160	
<u>Beryllium</u>				
B	0.001029	2.35 Steel + 5.18 Be		
Be	0.1239			

An attempt has been made to choose these examples so the results will show the relative merits of the three shield types in the range of attenuation indicated by the optimization analysis. It is likely that the attenuation properties of the three will be very similar, therefore other criteria must be considered in the final material selection. The carbon shield may be too thick for convenient mounting, while the zirconium hydride shield may suffer from its relatively low thermal conductivity and

**CONFIDENTIAL**

---

need for protective cladding. The extremely high cost of beryllium will be a factor against the iron-beryllium shield, other things being equal. All of these considerations which are factors in the design of the reactor-reflector-pressure-shell assembly are weighed and evaluated in the next section.

Optimum Shield Material and Design. The primary criterion used for shield evaluation to this point has been the attenuation factor obtainable with minimum shield weight. Thus it has been assumed that the important radiation effect on propellant is the integrated energy deposition; no importance was attached to the relative amounts of propellant heating supplied by neutrons and gammas. This assumption is acceptable for the preliminary analysis and design, but it must be discarded when the nature of tank internal flow patterns is used as a determining factor.

If the propellant flowed evenly out of the tank and into the feed pump (the potential flow model described in this report) then the integrated energy deposition concept would be valid. But potential flow does not appear likely in view of the large amounts of radiation energy absorbed by the propellant, especially in regions near the tank bottom. A large proportion of the total absorbed radiation energy is deposited in the first few inches of propellant above the tank bottom and will cause convection currents within the tank. Because the fast neutrons are the primary cause of this localized heat generation, there may be considerable advantage in shielding fast neutrons preferentially.

Several of the previously mentioned shield materials are suitable for use in a composite shield to reduce fast neutron fluxes preferentially. Beryllium was employed for this purpose in the iron-beryllium shield, and additional beryllium would reduce the neutron-to-gamma ratio still further.

**CONFIDENTIAL**  
DECLASSIFIED

**CONFIDENTIAL**

---

An auxiliary neutron absorber positioned above the primary shield, is subject to far less internal heating and can be made of a material such as lithium hydride which would otherwise be unsuitable for use as a single-material shield. Only small weights of additional absorber would be needed to cut the fast neutron heat generation at points within the propellant to valves less than those due to gammas. Even high pressure hydrogen cannot be discounted, since only a few inches may be sufficient to achieve the desired attenuation.

Large system weight reductions will be realized if the propellant flow pattern resembles the potential flow model. Weight savings will result from the reduction of tank pressure and shield requirements, and the entire engine system will become lighter and more compact. Preferential neutron radiation absorption represents a feasible method of preventing propellant recirculation currents, but other possibilities exist through the utilization of internal tank baffles. Such baffles are described in the next section of this report. Because such great advantages lie in obtaining a desirable mode of tank flow, it should be the object of intensive research and development.

UNCLASSIFIED

page blank

UNCLASSIFIED



**CONFIDENTIAL**

---

RADIATION PROBLEM AREAS AND MEANS OF SOLUTION

PROPELLANT HEATING

Nuclear Heat Generation in Propellant

The objectives of the analysis described in this section are (1) to describe the calculations performed to determine propellant heating rates resulting from radiation escaping the reactor vessel, and (2) to utilize the results of a parameter study on the effectiveness of several shield materials from the standpoint of minimum shield weight.

Heat generation rates in propellant with and without shielding were calculated. Results of these calculations were made for the shield materials and thicknesses are shown in Table 7. The analysis was performed for a separation distance of 14 feet; however, propellant heating at different separation distances can be determined by applying an inverse square correction to the results. Total heat generation rates for the shields considered are summarized in Fig. 20 for a reactor power level of 1500 megawatts.

The fast and thermal neutron flux distribution in the propellant tank was determined using the methods described previously. The fast neutron flux was calculated with the GRACE I code. To account for the axial power distribution in the core, the core region was divided into 6 axial subregions of exponentially varying power distribution. The radial power distribution for the core was assumed constant. The ratio of fast to thermal flux in the propellant was calculated with the AIM-6 code. In obtaining this ratio, the fast flux was defined as the total flux above 0.8 Mev, and the

**CONFIDENTIAL**

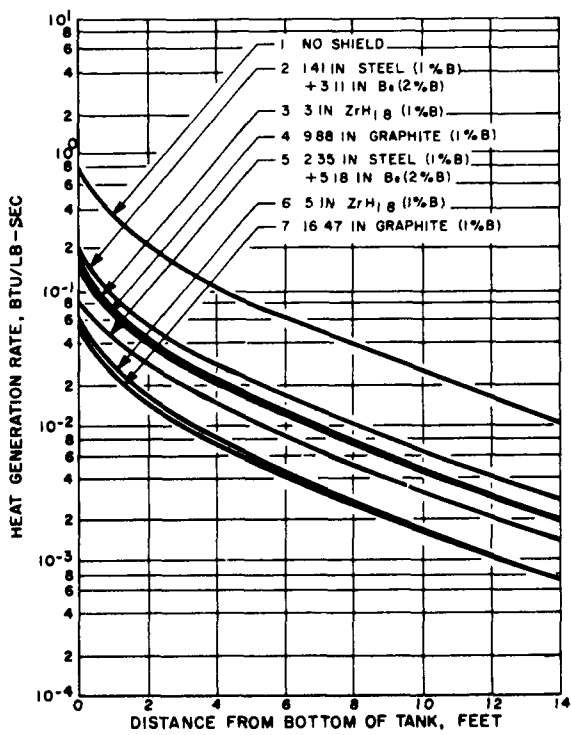


Figure 20. Summary of Propellant Heating Curves

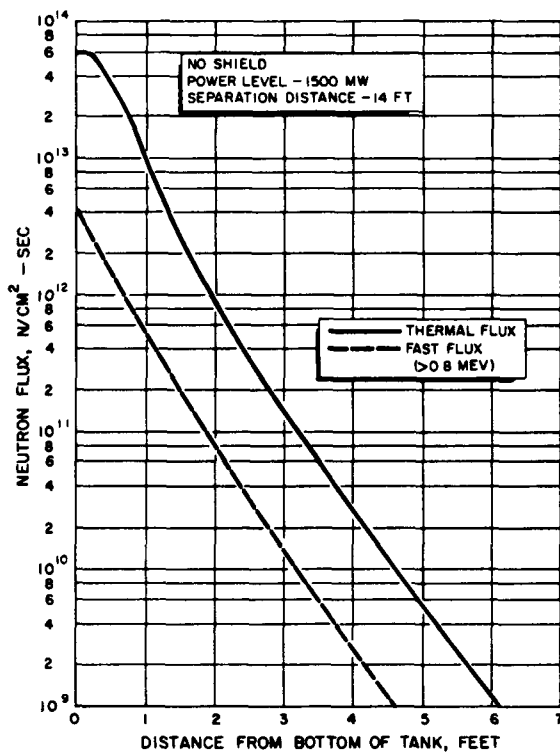


Figure 21. Neutron Flux Distribution in Propellant

~~CONFIDENTIAL~~

---

thermal flux as the total thermal absorption rate divided by the  $2200 \text{ cm}^{-1}$  value of the macroscopic absorption cross section. This definition of the thermal flux provides a convenient method for determining the capture gamma-ray source strength in the propellant without having to account for the large changes which take place in the thermal neutron spectrum with increasing penetration into the tank. Although this approach is not absolutely correct, it is believed to be sufficiently accurate for this analysis because, as will be shown later, the propellant capture gammas are not the prime contributor to propellant heating for a shielded system. Furthermore, some conservatism exists in the predicted thermal flux distributions. This conservatism is a consequence of assuming the propellant to be composed of normal hydrogen, i.e., 75 percent ortho-hydrogen and 25 percent parahydrogen. In reality the propellant is composed of 95 percent parahydrogen, a result of the cryogenic temperature of the fluid. Since the transport cross section for parahydrogen is considerably less than the corresponding value for orthohydrogen, the neutron leakage in the propellant should be greater than calculated, and therefore the predicted thermal flux distributions should decrease. Thus, the contribution to propellant heating from hydrogen capture gammas has been overestimated.

The fast and thermal neutron flux distributions in the propellant tank are shown in Fig. 21, 22, and 23. To evaluate the effectiveness of the boron in the shield materials, the thermal neutron flux in the propellant with and without 1 weight percent boron in a 3-inch zirconium hydride shield was calculated (Fig. 22). For this particular case the

**CONFIDENTIAL**

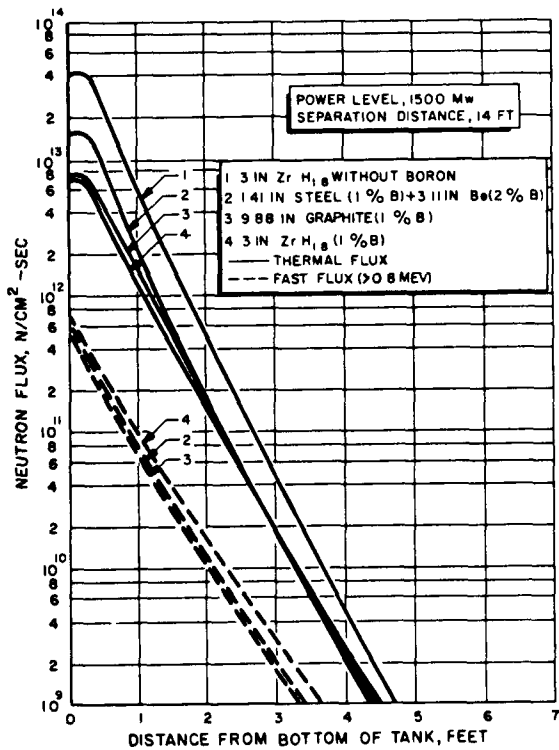


Figure 22. Neutron Flux Distributions in Propellant

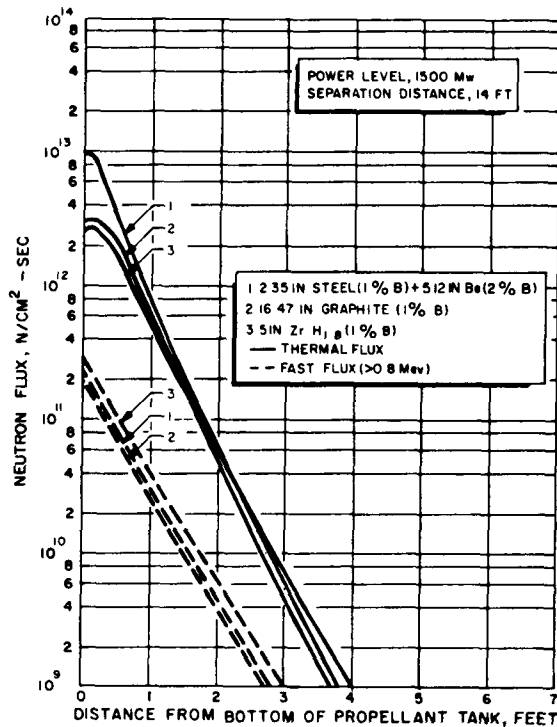


Figure 23. Neutron Flux Distributions in Propellant

**CONFIDENTIAL**

---

boron reduces the thermal neutron flux in the propellant; hence, the gamma-ray source strength is reduced by a factor 3 to 6. Thus, with no boron in the shield, the increase in the total heat generation rate is in excess of 50 percent. And, it was concluded that boronation of the shields is required for maximum shield effectiveness.

Determining accurately total heat generation rate in the propellant because of kinetic energy loss by fast neutrons is an extremely difficult problem. However, with a number of simplifying assumptions a reasonable estimate of its magnitude and distribution can be made. The assumptions utilized for this calculation were:

1. The magnitude of the fast neutron current at any position in the propellant is equal to the magnitude of the fast neutron flux ( $> 0.8$  Mev) at that point.
2. The average fast neutron energy is 2.0 Mev.
3. Each neutron removed from the fast neutron current by elastic scattering with hydrogen loses all its kinetic energy at the point of removal.

Thus, the heat generation rate in the propellant resulting from the absorption of 2.0 Mev of kinetic energy for each neutron removed from the fast neutron current, is:

$$\begin{aligned}
 H(x) &= 6.9 \times 10^{-14} \times 2.0 \times \frac{1}{\rho} \left[ \nabla \phi_f(x) \right] & (20) \\
 &\cong 1.38 \times 10^{-13} \frac{\sum_r}{\rho} \phi_f(x) \text{ Btu/lb-sec,}
 \end{aligned}$$

**CONFIDENTIAL**

where  $6.9 \times 10^{-14}$  is the conversion from Mev/gm to Btu/lb. Thus, for a propellant density of 0.067 gm/cc and a fast neutron removal cross section,  $\sum_r$ , of  $0.0651 \text{ cm}^{-1}$

$$H(x) = 1.3 \times 10^{-13} \phi_f(x) \text{ Btu/lb-sec}$$

The core gamma contribution to the propellant heat generation rate was calculated using the GRACE I code. The axial power distribution in the core was included in the same manner as described for the fast neutron flux calculation. The core gamma-ray spectrum was represented by the 10-group spectrum given in Table 5 .

The contribution to propellant heating from hydrogen captures in the tank was also calculated with GRACE I. The tank diameter was assumed to be 260 inches. The source distribution was obtained by multiplying the thermal flux distribution in the tank by the 2200 m/sec macroscopic absorption cross section for the propellant and by the 2.23 Mev gamma-ray energy produced per hydrogen capture.

Using a boronated shield material it was found that capture gamma rays produced in other materials in the system would be negligible.

The heat generation rates in the propellant for the different shield materials considered are shown in Fig. 24 through 30. The results are summarized in Fig. 20 . It was found from these results that, regardless of the shield material and thickness considered, the total heat generation rate in the tank at 1500 megawatts as a function of distance above the bottom of the tank can be approximated by:

$$H(x) = 95.0 \frac{e^{-\beta t}}{d_s^2} \left[ e^{-1.59x} + 0.338e^{-0.46x} + 0.378e^{-0.219x} \right] \text{ Btu/lb-sec,} \quad (21)$$

**CONFIDENTIAL**

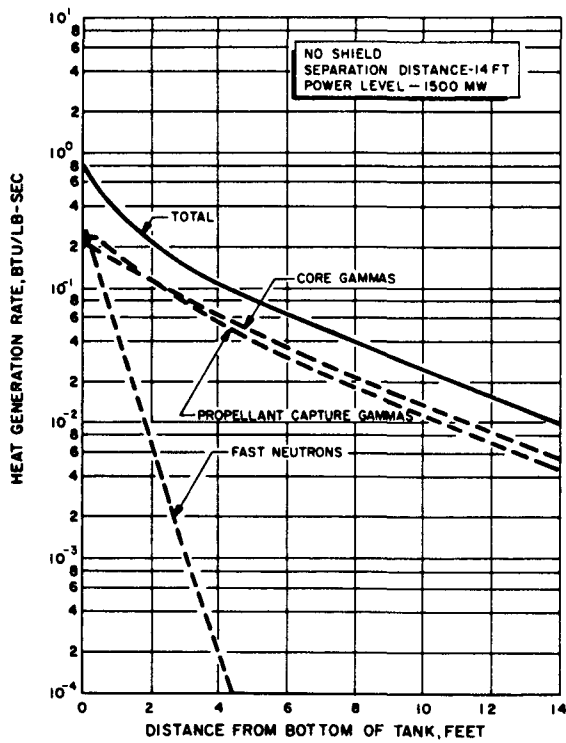


Figure 24 . Heat Generation Rate in Propellant

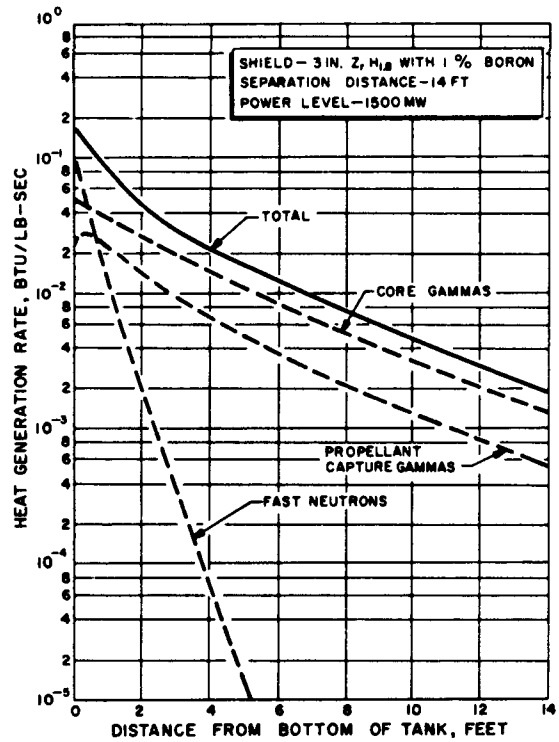


Figure 25 . Heat Generation Rate in Propellant

**CONFIDENTIAL**

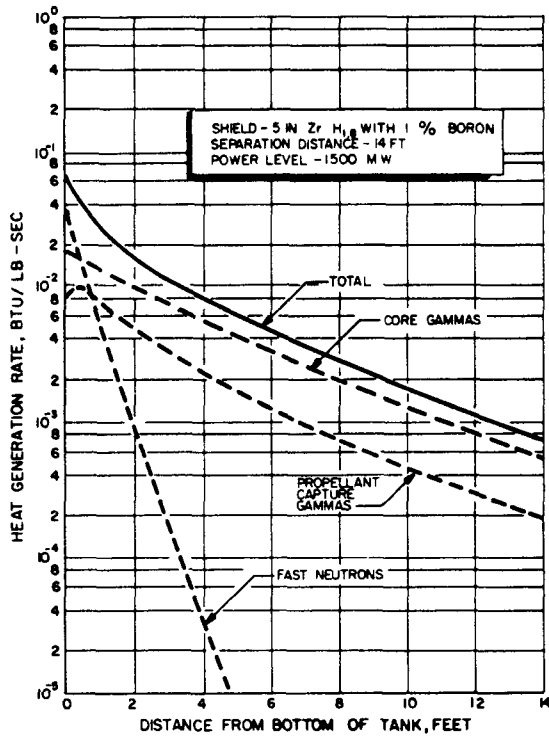


Figure 26. Heat Generation Rate in Propellant



**CONFIDENTIAL**

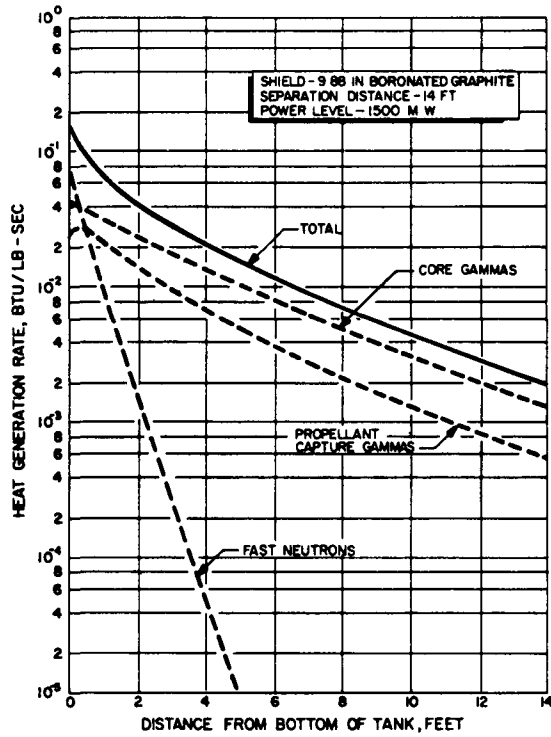


Figure 27. Heat Generation Rate in Propellant

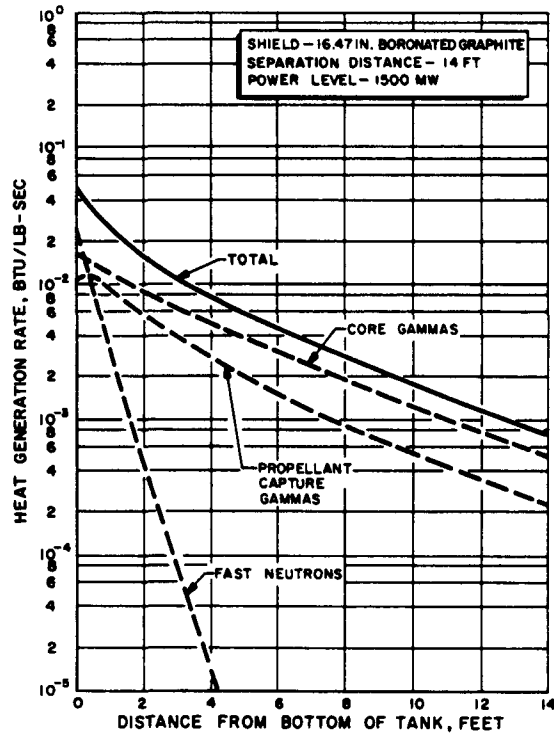


Figure 28 Heat Generation Rate in Propellant

**CONFIDENTIAL**

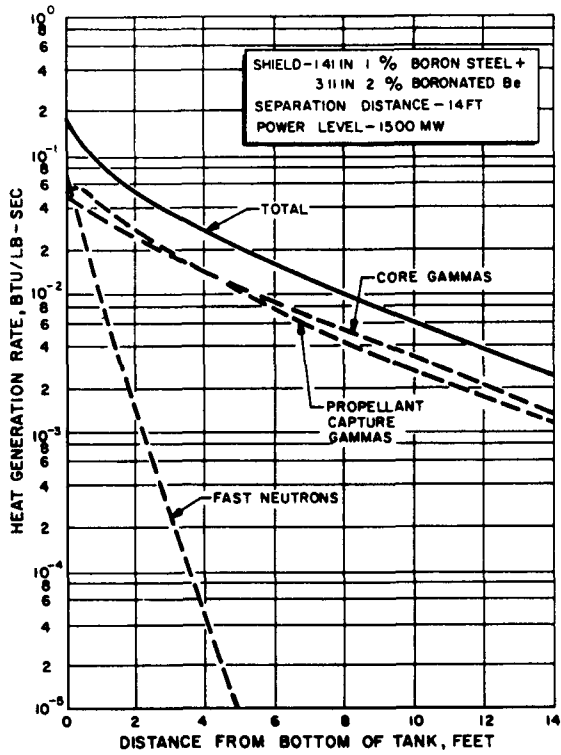


Figure 29. Heat Generation Rate in Propellant

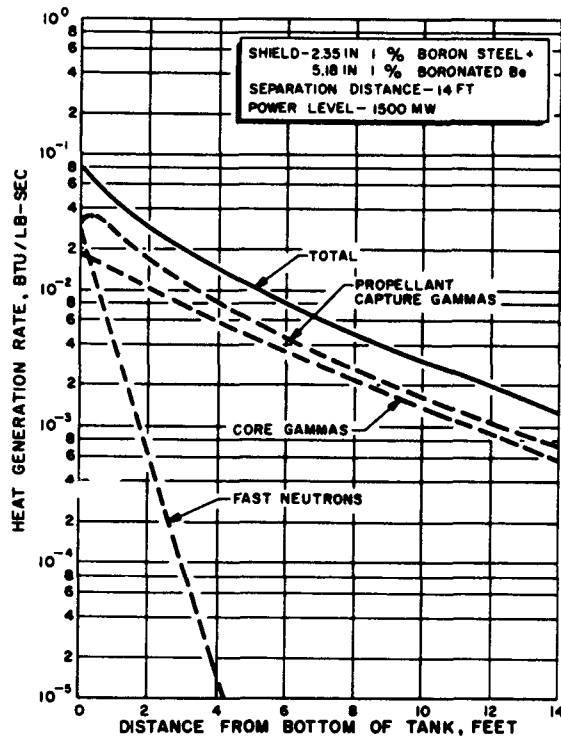


Figure 30. Heat Generation Rate in Propellant

**CONFIDENTIAL**

where:

- $H(x)$  = heat generation rate at 1500 megawatts, Btu/lb-sec,
- $d_s$  = separation distance, feet,
- $x$  = distance into propellant from bottom of tank, feet,
- $t$  = shield thickness, inches
- $\beta$  = attenuation coefficient for the shield material considered,  $\text{inch}^{-1}$ .

The values of  $\beta$  for each shield material are:

<u>Material</u>	<u><math>\beta</math>, in.<sup>-1</sup></u>
Zirconium hydride	0.519
Boronated graphite	0.1622
Boronated steel and beryllium	0.288

The total amount of heat deposited in the propellant per square foot of tank bottom is

$$H_T = \rho \int_0^{\infty} H(x) dx = \frac{1270}{d_s^2} = e^{-\beta t} \text{ Btu/ft}^2\text{-sec.} \quad (22)$$

The attenuation factor for a given shield is defined as  $f(t) = e^{-\beta t}$ . This factor is shown graphically in Fig. 31 for each of the three shields considered as a function of  $\bar{\rho} t$ , i.e., the average shield density times the shield thickness. From this figure, it is readily seen that a boronated graphite shield is slightly better than a boronated zirconium hydride shield, and that both of these shield materials are considerably better than a shield composed of boron steel and boronated beryllium.

CONFIDENTIAL

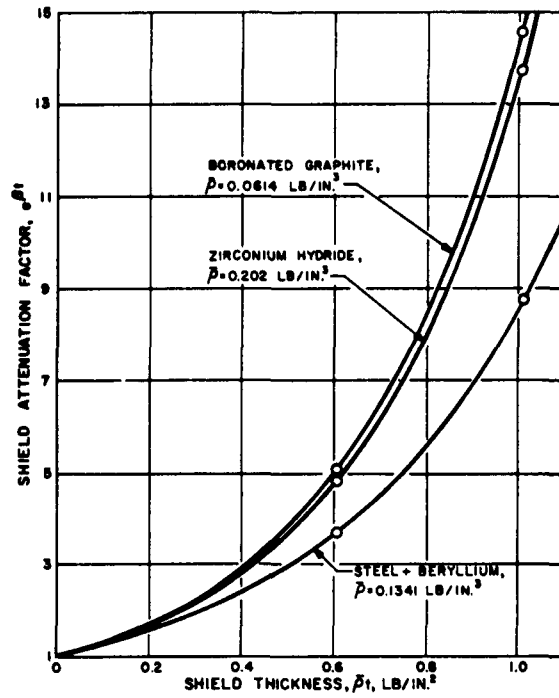


Figure 31. Shield Attenuation Factor vs Shield Thickness

**CONFIDENTIAL**

---

Propellant Flow and Convection Currents

Liquid hydrogen contained in the propellant tank may be heated by several mechanisms. These include:

1. Nuclear radiation absorption during nuclear rocket engine firing
2. Heat transfer by convection and thermal radiation from the ground atmosphere before flight
3. Aerodynamic convection heating while in flight in the earth's atmosphere
4. Solar radiation, particularly during the coast phase of the flight
5. Heat transfer from hot tank pressurizing gas to cold propellant

This section is restricted to consideration of the effect of nuclear radiation heating discussed previously.

The magnitude of the liquid hydrogen temperature rise, due to nuclear radiation heating as it discharges from the tank, depends on the type of liquid motion in the tank. Three possible flow models are considered here: (1) potential (or nonviscous) flow with buoyant forces and thermal conduction neglected, (2) completely mixed flow in which the temperature of the fluid leaving the tank at any instant is equal to the uniform fluid temperature within the tank, (3) recirculation flow in which the nuclear radiation absorbed near the bottom of the tank sets up a natural convection current which carries heated propellant up the inside walls of the tank to the top of the fluid level where it forms a stratified layer.

The recirculation-flow model results in the largest propellant temperature rise as complete tank drainage is approached. This model is also the most realistic of the three models in a simple tank because of the relatively

~~CONFIDENTIAL~~

---

low bulk propellant velocity in the tank except near the bottom of the tank axis, and the great tendency of liquid hydrogen to form natural convection currents due to its relatively high coefficient of thermal expansion and its low kinematic viscosity. However, as discussed below, it may be possible with a properly designed tank baffle to prevent the formation of a natural convection current and, thereby, approach the potential-flow model.

Potential-Flow Model. A typical propellant tank is shown in Fig. 32. The assumption of irrotational, potential (or ideal, nonviscous), incompressible, steady-state flow with no vortex motion throughout the tank, leads to the following differential equations (Ref. 22) in cylindrical coordinates for describing the velocity distribution.

Continuity.

$$\frac{\partial v_r}{\partial r} + \frac{v_r}{r} + \frac{\partial v_z}{\partial z} = 0 \quad (23)$$

Momentum (Equations of Motion).

radial direction

$$v_r \frac{\partial v_r}{\partial r} + v_z \frac{\partial v_r}{\partial z} = -\frac{g_c}{\rho} \frac{\partial p}{\partial r} \quad (24)$$

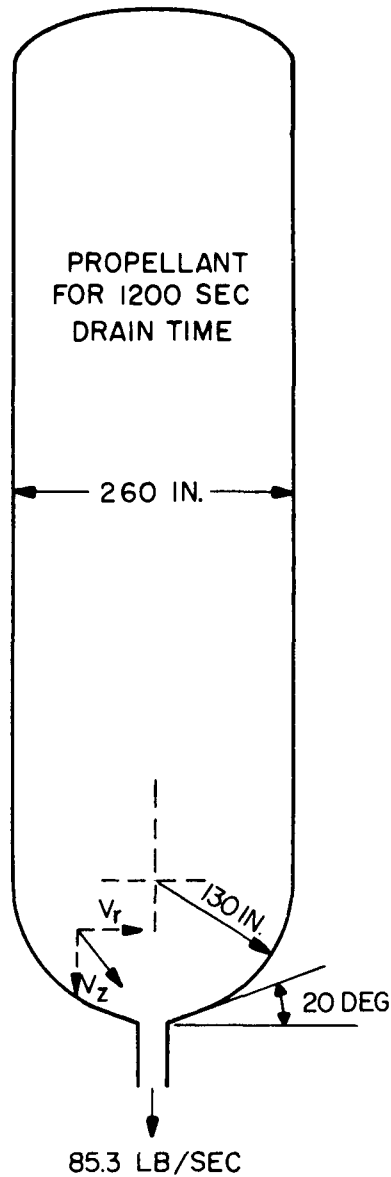


Figure 32. Propellant Tank Example 1500 Megawatt Reactor

**CONFIDENTIAL**

vertical direction

$$v_r \frac{\partial v_z}{\partial r} + v_z \frac{\partial v_z}{\partial z} = - \frac{g_c}{\rho} \frac{\partial p}{\partial z} + g \quad (25)$$

where

- $g$  = Acceleration due to gravity (may vary from approximately 0.5 to 1.5 times normal value at sea level for a nuclear rocket engine), ft/sec<sup>2</sup>
- $g_c$  = Conversion factor 32.17 lbm-ft/lbf-sec<sup>2</sup>
- $p$  = Pressure, lbf/sq ft
- $r$  = Distance in radial direction, ft
- $v_r$  = Velocity in radial direction, ft/sec
- $v_z$  = Velocity downward in vertical direction, ft/sec
- $z$  = Distance downward in vertical direction, ft/sec

The solution of Eqs.23 to 25 is subject to the boundary conditions of the flow. For the tank shape shown in Fig. 32, these conditions present considerable difficulty in obtaining an analytical solution in closed form. Therefore, the equations were solved graphically by means of a two-dimensional electrical field plot using conducting paper. This necessitated the assumption that the velocity ratio (velocity at any radius,  $r$ , divided by the mean velocity at that vertical distance,  $z$ ) for the actual situation is the same as that for the two-dimensional case. However, the maximum error due to the use of the two-dimensional field plot was estimated from Ref. 23 to be only about five percent. The results of the calculations for the tank shown in Fig. 32 and a hydrogen flowrate of 85.3 lb/sec are shown in Fig. 33 and 34. These



~~CONFIDENTIAL~~

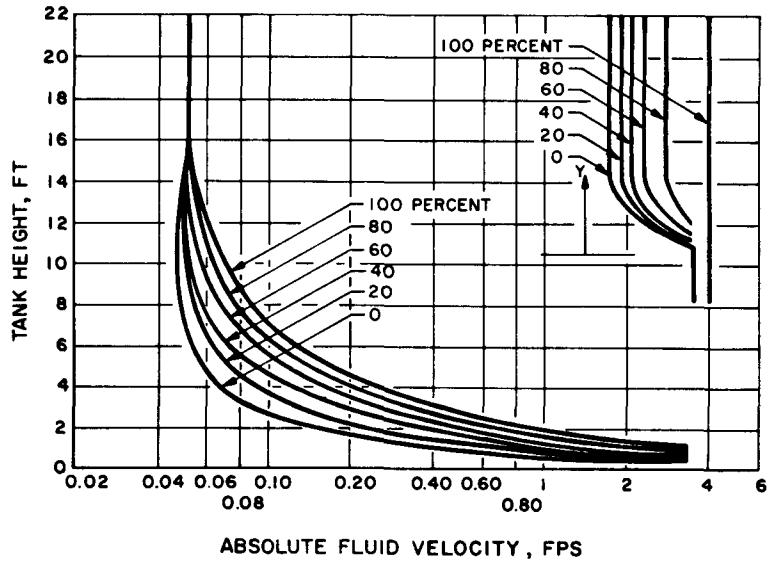


Figure 33. Potential Flow Velocity Distribution

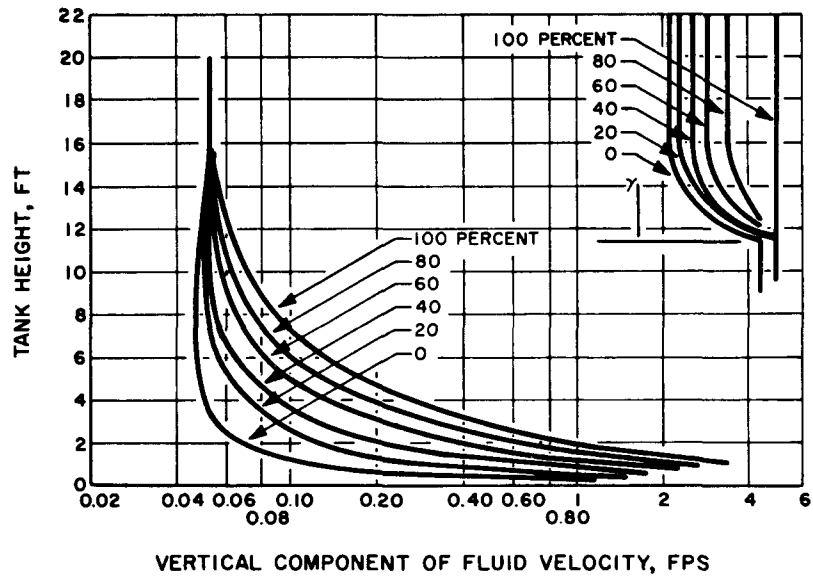


Figure 34. Potential Flow Velocity Distribution  
(Vertical Component)

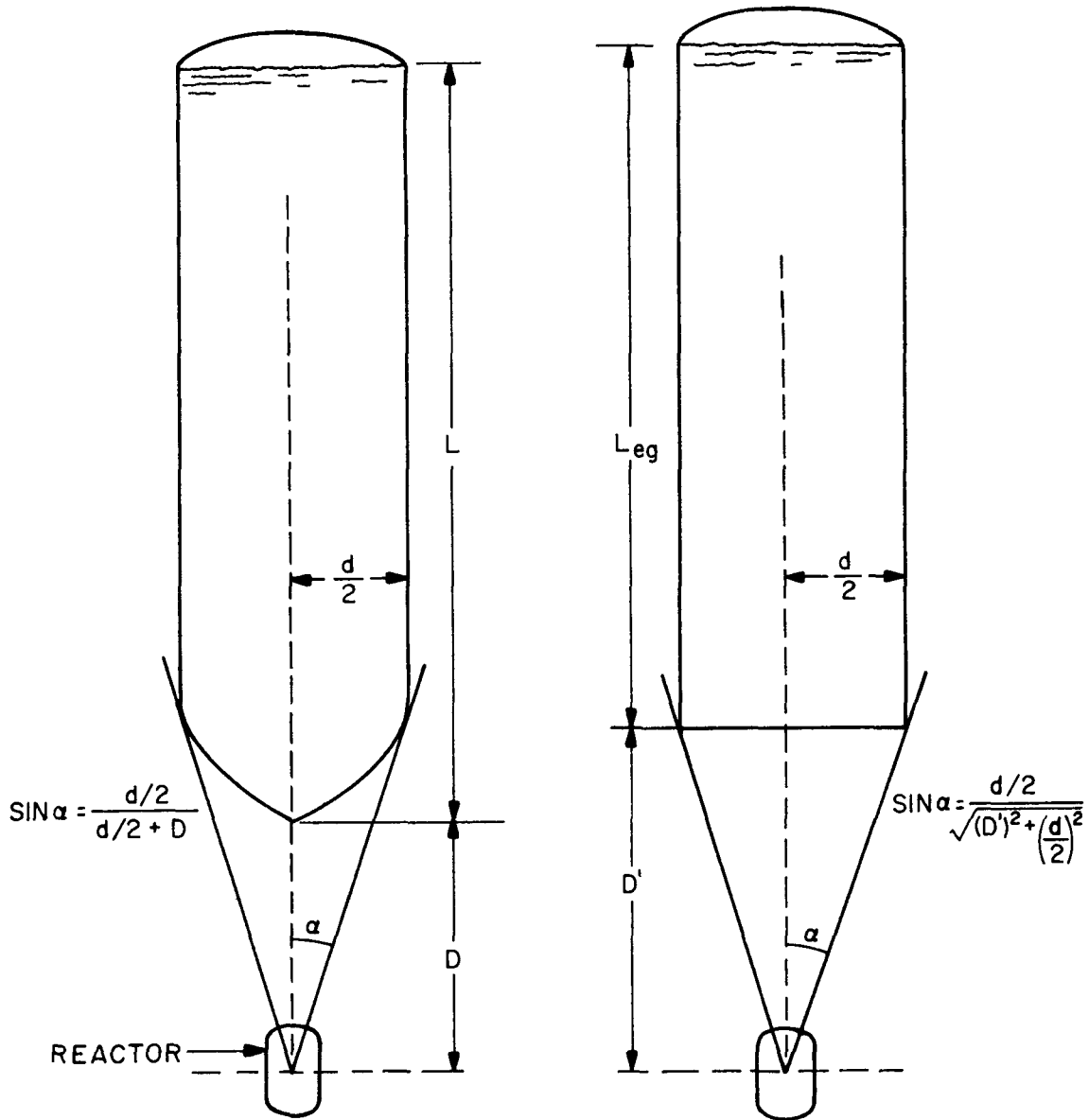
**CONFIDENTIAL**

curves are valid only when the fluid level is above the bottom of the cylindrical section of the tank. In Fig. 33, the absolute fluid velocity is plotted against tank height with a parameter of stream surface location. For example, the 60-percent stream surface refers to the surface of a stream tube outside of which 60 percent of the flow occurs. Therefore, the tank centerline is 100 percent, and the tank wall zero percent. Figure 34 presents the vertical component of the fluid velocity plotted against tank height with a parameter of stream surface location. As can be seen from Fig. 33, the velocity at a given tank height varies considerably over the cross section. For example, at an elevation of 2 feet, the centerline velocity is 0.85 ft/sec, while the wall velocity is only 0.132 ft/sec with a vertical component of only 0.064 ft/sec. As will be discussed in the portion on the recirculation-flow model, the tendency toward relatively low velocities at the tank wall permits upward-flowing natural convection currents to form due to nuclear radiation heating.

To calculate the propellant temperature rise due to nuclear radiation heating during tank discharge for the potential-flow model, a modification of the short method of Graves and Streetman (Ref. 24) may be used. The modification consists of transforming the tank bottom shape shown in Fig. 32 to a square-bottom configuration shown in Fig. 35. Then, neglecting leakage of nuclear radiation out of the tank, the temperature rise of the propellant is given by a heat balance:

$$\dot{m}C_p dT = -\rho S H(x) dx = - \frac{4\pi D^2 (1 - \cos \alpha) \rho H(x) dx}{2} \quad (26)$$

**CONFIDENTIAL**



EQUATING EXPRESSIONS FOR  $\sin \alpha$ , GET  $(D')^2 = dD + D^2$

$$\frac{1 - \cos \alpha}{2} \approx \frac{d^2}{16 (D')^2} = \frac{d^2}{16 (dD + D^2)}$$

Figure 35. Transformation to a Flat-Bottom Tank

**CONFIDENTIAL**

where

- $C_p$  = Propellant specific heat, Btu/lb-R
- $D$  = Separation distance from the center of the reactor core to the bottom of the tank, feet
- $H(x)$  = Heat generation rate, Btu/lb-sec
- $L$  = Initial height of propellant in tank, feet
- $\dot{m}$  = Propellant discharge rate from tank, lb/sec
- $S$  = Cross-sectional area of propellant tank, sq ft
- $T$  = Temperature, degrees R
- $x$  = Depth of penetration of nuclear radiation into propellant, feet
- $\alpha$  = Half angle (Fig. 35)

The maximum temperature rise, which occurs when the last bit of propellant drains from the tank, is therefore,

$$\Delta T_{\max} \cong \frac{4\pi D^2 (1 - \cos \alpha) \rho}{2 \dot{m} C_p} \int_0^L H(x) dx \quad (27)$$

But by the transformation shown in Fig. 23

$$\frac{1 - \cos \alpha}{2} \cong \frac{d^2}{16 (d D + D^2)} \quad (28)$$

~~CONFIDENTIAL~~

where

$d$  = diameter of cylindrical section of propellant tank, feet

Therefore Eq. 27 may be written as

$$\Delta T_{\max} \cong \frac{\pi D^2 d^2 \rho}{4(d D + D^2) \dot{m} C_p} \int_0^L H(x) dx \quad (29)$$

The equation presented for the heating rate in the section Nuclear Heat Generation in Propellant may be written for 1500 megawatts as

$$H(x) = \frac{95}{D^2 A} \left[ e^{-1.59 x} + 0.338 e^{-0.46 x} + 0.378 e^{-0.219 x} \right] \quad (30)$$

where

$$A = \frac{1}{e^{-\beta s}} = \text{Attenuation factor}$$

If Eq. 30 is substituted in Eq. 29 and the resulting integral is evaluated, the result is

$$\Delta T_{\max} \cong \frac{95 \pi d^2 \rho}{4(d D + D^2) \dot{m} C_p A} \left[ \frac{1}{1.59} (1 - e^{-1.59 L}) + \frac{0.338}{0.46} (1 - e^{-0.46 L}) + \frac{0.378}{0.219} (1 - e^{-0.219 L}) \right] \quad (31)$$

**CONFIDENTIAL**

---

For a given separation distance,  $D$ , and attenuation factor,  $A$ , Eq. 31 may be used to determine the maximum propellant temperature rise,  $\Delta T_{\max}$ , for potential flow. The exponentials involving  $L$  vanish for values of initial propellant height,  $L$ , greater than about 30 feet.

Equation 31 gives the maximum temperature rise of the propellant. It is the temperature rise of that portion of the propellant which is initially at the top surface and, has a residence time in the tank approaching the full-drain time period. To calculate the temperature rise as a function of time, the factor,  $L$ , in Eq. 31 may be replaced by

$$L \left( \frac{t}{t_L} \right)$$

where

$t$  = time from start of draining, seconds

$t_L$  = time to completely drain tank with initial level at  $L$ , seconds

The derivation of Eq. 31 neglects the effect of heat transfer in the vertical or axial direction. This is justified by the following theoretical consideration. Since the fluid is assumed to be in streamline flow, any heat transfer will take place by thermal conduction. Thus, an additional term for conduction may be added to Eq. 26 for the heat balance giving

$$\dot{m} C_p dT = - \rho S H_{(x)} dx + kS \frac{d^2 T}{dx^2} dx \quad (32)$$

~~CONFIDENTIAL~~

where

$k$  = propellant thermal conductivity, Btu/hr-ft-R

Equation 32 may be rearranged to

$$\frac{dT}{dx} + \frac{\rho SH(x)}{\dot{m} C_p} - \left( \frac{kS}{\dot{m} C_p} \right) \frac{d^2 T}{dx^2} = 0 \quad (33)$$

The order of magnitude of the conduction term may now be compared. This is most conveniently done at the bottom of the tank where the temperature gradient and thus, the tendency for thermal conduction to take place, is greatest. If thermal conduction is important then the third term must be of the same order of magnitude as the first and second terms. Thus,

$$\frac{d^2 T}{dx^2} \text{ must be of the order of } \frac{\rho H(x)}{k}$$

For liquid hydrogen

$$\rho \cong 4.3 \text{ lbm/cu ft}$$

$$k \cong 0.00002 \text{ Btu/ft-F-sec}$$

A typical value for  $H(x)$  at the bottom of the tank would be

$$H(x) = 0.2 \text{ Btu/lbm-sec}$$

~~CONFIDENTIAL~~

Therefore,

$$\frac{d^2T}{dx^2} \text{ must be of the order } \frac{(4.3)(0.2)}{(0.00002)} = 43,000 \frac{F}{sq ft}$$

in order for thermal conduction to be important. This is not the case, however, because without thermal conduction, it can be seen from Eq. 33 that

$$\frac{dT}{dx} = -\frac{\rho SH(x)}{\dot{m} C_p} = -\frac{\rho S (95)}{\dot{m} C_p D^2 A} \left[ e^{-1.59 x} + 0.338 e^{-0.46 x} + 0.378 e^{-0.219 x} \right]$$

Therefore, taking the derivative,

$$\left( \frac{d^2T}{dx^2} \right)_{x=0} = \frac{\rho S(95)}{\dot{m} C_p D^2 A} \left[ 1.59 + (0.46)(0.338) + (0.219)(0.378) \right]$$

Using values of

- $\rho = 4.3 \text{ lbm/cu ft}$
- $S = 40 \text{ sq ft}$
- $\dot{m} = 85.3 \text{ lbm/sec}$
- $C_p = 2.5 \text{ Btu/lbm-R}$
- $D = 10 \text{ feet}$
- $A = 4$



**CONFIDENTIAL**

we obtain,

$$\left( \frac{d^2 T}{dx^2} \right)_{x=0} = 0.279 \frac{F}{\text{sq ft}}$$

This is a very small value compared to 43,000. If thermal conduction were important, the value of 0.279 would even be lower. Therefore, it must be concluded that thermal conduction in the axial direction can be neglected.

Completely-Mixed-Flow Model. During the tank drainage period of the completely-mixed-flow model, the propellant in the tank is completely mixed. Thus, although the magnitude of the nuclear radiation absorption decreases exponentially with depth into the propellant as seen in Eq. 30 the mixing action instantaneously distributes the heat uniformly throughout the propellant. The temperature of the propellant leaving the tank at any instant is equal to the mixed temperature of the propellant in the tank.

$$\int_{T_0}^T W C_p dT \cong \int_0^t \int_0^{x(t)} \frac{\pi D^2 d^2 \rho H(x)}{4(dD + D^2)} dx dt \quad (34)$$

where

$W$  = weight of propellant in tank at time,  $t$ , lbm

**CONFIDENTIAL**

The maximum temperature rise is therefore, for a 1500 megawatt reactor

$$\Delta T \cong \frac{95 \pi d^2 \rho}{4(dD + D^2) C_p A} \int_0^{t_L} \int_0^{x(t)} \frac{(e^{-1.59x} + 0.338e^{-0.46x} + 0.378e^{-0.219x})}{W} dx dt \quad (35)$$

Both the weight of propellant in the tank,  $W$ , and the elevation of propellant in the tank at any instant,  $x(t)$ , are related to the time by the expressions

$$W = W_0 \left(1 - \frac{t}{t_L}\right) \quad (36)$$

$$x(t) = L \left(1 - \frac{t}{t_L}\right) \quad (37)$$

Substitution of Eq. 36 and 37 into Eq. 35 gives

$$\Delta T \cong \frac{95 d^2 \pi \rho}{4(dD + D^2) C_p A} \int_0^t \int_0^{L(1 - \frac{t}{t_L})} \frac{(e^{-1.59x} + 0.338e^{-0.46x} + 0.378e^{-0.219x})}{W_0 \left(1 - \frac{t}{t_L}\right)} dx dt \quad (38)$$

To facilitate the integration, it is worthwhile to make the following transformation of variable in Eq. 38.

$$t_1 = 1 - \frac{t}{t_L}$$

~~CONFIDENTIAL~~

Then, integration of Eq. 38 with respect to x gives

$$\Delta T \cong \frac{95 d^2 \pi \rho}{4(dD + D^2) C_p \text{Am}}$$

$$\int_1^{1 - \frac{t}{t_L}} \frac{1}{t_1} \left[ \frac{1}{1.59} \left( e^{-1.59 Lt_1} - 1 \right) + \frac{0.338}{0.46} \left( e^{-0.46 Lt_1} - 1 \right) + \frac{0.378}{0.219} \left( e^{-0.219 Lt_1} - 1 \right) \right] dt_1 \quad (39)$$

The following additional transformations are made on Eq. 39 to obtain a readily integrated form

$$\begin{aligned}
 t_2 &= 1.59 Lt_1 \\
 t_3 &= 0.46 Lt_1 \\
 t_4 &= 0.219 Lt_1
 \end{aligned}$$

In addition, the upper limit of time is taken at  $t_L$  which corresponds to the maximum  $\Delta T$ . Then, Eq. 39 becomes

$$\Delta T_{\max} \cong \frac{95 d^2 \pi \rho}{4(dD + D^2) C_p \text{Am}} \left[ \frac{1}{1.59} \left( \int_{1.59L}^0 \frac{e^{-t_2}}{t_2} dt_2 - \int_{1.59L}^0 \frac{dt_2}{t_2} \right) + \right.$$

**CONFIDENTIAL**

$$\frac{0.338}{0.46} \left( \int_{0.46L}^0 \frac{e^{-t_3}}{t_3} - \int_{0.46L}^0 \frac{dt_3}{t_3} \right) + \frac{0.378}{0.219} \left( \int_{0.219L}^0 \frac{e^{-t_4}}{t_4} dt_4 - \int_{0.219L}^0 \frac{dt_4}{t_4} \right) \quad (40)$$

Equation 40 contains three pairs of improper, indeterminate, integral expressions of the general form

$$\int_y^0 \frac{e^{-z}}{z} dz - \int_y^0 \frac{dz}{z} = \infty - \infty \quad (41)$$

These integrals are finite, however, and may be evaluated by writing Eq. 41 in the equivalent form

$$\int_y^\infty \frac{e^{-z}}{z} dz + \int_\infty^1 \frac{e^{-z}}{z} dz + \int_1^0 \frac{e^{-z}}{z} dz - \int_y^1 \frac{dz}{z} - \int_1^0 \frac{dz}{z} \quad (42)$$

Now

$$\int_1^0 \frac{e^{-z}}{z} dz - \int_1^0 \frac{dz}{z} = \int_0^1 \frac{dz}{z} - \int_0^1 \frac{e^{-z}}{z} dz =$$

$$\ln z - \ln z + z - \frac{z^2}{2 \cdot 2!} + \frac{z^3}{3 \cdot 3!} - \dots + \left[ \frac{(-1)^n z^n}{n \cdot n!} \right]_0^1 = 0.797 \quad (43)$$

**CONFIDENTIAL**

Thus, the log terms cancel and the remaining series is rapidly convergent.

Therefore, Eq. 40 becomes

$$\begin{aligned}
 \Delta T_{\max} \cong & \frac{95 d^2 \pi \rho}{4(dD + D^2) C_p A_m} \left[ \frac{1}{1.59} \left( \int_{1.59L}^{\infty} \frac{e^{-t_2}}{t_2} dt_2 - \right. \right. \\
 & \int_1^{\infty} \frac{e^{-t_2}}{t_2} dt_2 + \ln(1.59L) \Big) + \frac{0.338}{0.46} \left( \int_{0.46L}^{\infty} \frac{e^{-t_3}}{t_3} dt_3 - \int_1^{\infty} \frac{e^{-t_2}}{t_2} dt_3 + \right. \\
 & \ln(0.46L) \Big) + \frac{0.378}{0.219} \left( \int_{0.219L}^{\infty} \frac{e^{-t_4}}{t_4} dt_4 - \int_1^{\infty} \frac{e^{-t_4}}{t_4} dt_4 + \right. \\
 & \left. \left. \ln(0.219L) \right) + 3.089 (0.797) \right] \quad (44)
 \end{aligned}$$

For a given separation distance, D, and attenuation factor, A, Eq. 44 may be used to determine the maximum propellant temperature rise,  $\Delta T_{\max}$ , for completely mixed flow. The integrals in Eq. 44 may be evaluated using the curves in Ref. 25. For a value of initial propellant height, L, greater than about 30 feet, the three integrals involving L as part of the lower limit tend to vanish.

~~CONFIDENTIAL~~

Equation 39 may be developed, as follows, into a form suitable for calculating the temperature rise for completely mixed flow as a function of time. In this case, the same transformations as used above lead to the equation

$$\begin{aligned}
 \Delta T \cong & \frac{95 d^2 \pi \rho}{4(dD + D^2) C_p A_m} \left[ \frac{1}{1.59} \int_{1.59L}^{1.59L \left(1 - \frac{t}{t_L}\right)} \left( \frac{e^{-z}}{z} - \frac{1}{z} \right) dz + \right. \\
 & \left. \frac{0.338}{0.46} \int_{0.46L}^{0.46L \left(1 - \frac{t}{t_L}\right)} \left( \frac{e^{-z}}{z} - \frac{1}{z} \right) dz + \frac{0.378}{0.219} \int_{0.219L}^{0.219 \left(1 - \frac{t}{t_L}\right)} \left( \frac{e^{-z}}{z} - \frac{1}{z} \right) dz \right] \quad (45)
 \end{aligned}$$

where  $z$  = variable of the transformation.

The integrals in Eq. 45 are not improper and, therefore, do not present the difficulty of evaluation that was discussed in connection with Eq. 40. Reference 25 may be used again to evaluate the exponential integral noting that

$$\int_a^b \frac{e^{-z}}{z} dz = \int_a^\infty \frac{e^{-z}}{z} dz - \int_b^\infty \frac{e^{-z}}{z} dz$$

It should be mentioned that the above model of completely mixed flow is identical to the solution of a potential-flow (non-mixed) model where the thermal conductivity of the propellant is infinite. Of course, such is far from the actual situation with liquid hydrogen, as we have seen.

~~CONFIDENTIAL~~

---

Recirculation-Flow Model. The basis for the development of the recirculation-flow model is the recent experience reported in the literature (Ref. 26) concerning stratification in cryogenic propellant tanks caused by aerodynamic heating. Here, the fluid adjacent to the warm tank wall is heated, causing it to rise to the top of the tank by natural convection where it remains essentially as a stratified layer at a higher temperature than the main bulk of propellant below. As discussed above, the relatively low thermal conductivity of cryogenic liquids prevents any appreciable heat exchange by conduction between the layers.

In a similar manner, natural convection currents can be established in the propellant tank by nuclear radiation heating (mainly the leakage neutron contribution which is largely localized to the first several inches of propellant depth at the bottom of the tank) provided that the upward buoyant force of the natural convection current tending to form is high enough to overcome the downward inertia force of the flowing propellant.

The usual criterion for natural convection, in the absence of boiling, is the dimensionless Grashof number,  $N_{Gr}$  which is defined by the equation

$$N_{Gr} = \frac{L^3 \rho^2 g \beta (\Delta t)}{\mu^2} = \frac{(\text{inertia force}) (\text{bouyant force})}{(\text{viscous force})^2} \quad (46)$$

~~CONFIDENTIAL~~

where

$L$  = Some characteristic dimension, feet

$\beta$  = Coefficient of thermal expansion for the fluid,  $R^{-1}$

$\Delta t$  = Temperature differential between fluid next to the warm wall and the bulk of the fluid, R

$\mu$  = Fluid viscosity, lbm/ft-hr

Under conditions of a zero free-stream or bulk fluid velocity, the usual range of Grashof number for a fluid with a Prandtl number of about one is (Ref. 27 ) shown below.

Flow Regime	$N_{Gr}$	
	Vertical Plate	Horizontal Plate
Laminar free convection	$10^4$ to $10^9$	$10^5$ to $2 \times 10^7$
Turbulent free convection	$10^9$ to $10^{12}$	$2 \times 10^7$ to $3 \times 10^{10}$

For liquid hydrogen at a temperature of 40 R,

$$\rho = 4.24 \text{ lbm/cu ft}$$

$$\mu = 0.029 \text{ lbm/ft-hr}$$

$$\beta = 0.0106 \text{ R}^{-1}$$

Also,

$g = 4.17 \times 10^8 \text{ ft}^2/\text{hr}$ . This value, that of gravitational acceleration on the earth's surface, was chosen as typical of that during flight of a missile using the K-1 engine.



**CONFIDENTIAL**

And if L and  $\Delta t$  are taken as

$$L = 1 \text{ foot}$$

$$\Delta t = 1 \text{ deg, R}$$

then, the Grashof number is

$$N_{Gr} = \frac{(1)^3 (4.24)^2 (4.17 \times 10^8) (0.0106) (1)}{(0.029)^2} = 9.46 \times 10^{10}$$

This value is in the turbulent free convection region. In this region, some idea as to the order of magnitude of the velocity in the free convection zone may be obtained from Ref. 28. The following equation is given for the maximum velocity in the boundary layer on a vertical, flat, heated plate:

$$U_{max} = 0.636 \frac{\mu}{\rho L} (N_{Gr})^{1/2} \left[ 1 + 0.494 (N_{Pr})^{2/3} \right]^{-1/2} \quad (47)$$

Using the values of  $\mu$ ,  $\rho$ , L and  $N_{Gr}$  given above and a Prandtl number,  $N_{Pr}$ , of 1.05, the maximum velocity is

$$U_{max} = \frac{(0.636)(0.029)(9.46 \times 10^{10})^{1/2}}{4.24 (1)} \left[ 1 + 0.494 (1.05)^{2/3} \right]^{-1/2}$$

$$= 1080 \text{ ft/hr}$$

$$= 0.3 \text{ ft/sec}$$

~~CONFIDENTIAL~~

As can be seen from Fig. 33, this velocity is considerably larger than the potential flow velocity near the wall at distances greater than about two feet above the tank bottom.

The above considerations are strictly applicable only when the free-stream velocity approaches zero. When the free-stream velocity is finite, an analysis of the boundary layer equations in dimensionless form as given by Eckert and Drake (Ref. 29) shows that the criterion for the influence of natural convection is

$$\frac{N_{Gr}}{(N_{Re})^2} = \frac{Lg \beta (\Delta t)}{v_z^2} = \frac{\text{(buoyant force)}}{\text{(inertia force)}} \quad (48)$$

where

$N_{Re}$  = Reynolds number

$v_z$  = Downward free-stream velocity, ft/sec

Using the values cited above and a value of 0.054 ft/sec for  $v_z$  (which corresponds to the propellant flow velocity in the cylindrical section of the tank), Eq. 48 gives

$$\frac{N_{Gr}}{(N_{Re})^2} = \frac{(1)(32.2)(0.0106)(1)}{(0.054)^2} = 117$$

This is a rather high value. As pointed out by Acrivos (Ref. 30), for upward, external flow over a flat, heated, vertical plate, free convection predominates (if  $N_{Pr} \approx 1$ ) at values of  $N_{Gr}/(N_{Re})^2$  above about 2. If the

**CONFIDENTIAL**

---

same result is assumed to apply for downward, external flow, then, except in the region very close to the discharge point of the propellant tank, it appears that the bouyancy force is large enough to indicate that a turbulent, natural convection layer will tend to form next to the tank wall near the bottom of the tank and carry heated propellant to the top of the tank. This view is also supported by the rather large Grashof number for liquid hydrogen and the resulting relatively large maximum velocity of the natural convection boundary layer.

Based on the above evidence that a natural convection layer will tend to form next to the propellant tank wall, a recirculation-flow model may be developed as follows. As with the potential-flow and completely-mixed-flow models, the transformation shown in Fig. 35 for converting to a square-bottom tank is again used. It is then assumed that all the nuclear radiation absorbed in the first foot of depth,  $x$ , (from Eq. 21) is effective in promoting the natural convection layer. At a depth of one foot there is a relatively sharp break in the heat-generation-rate equation. This layer flows radially out along the inclined tank bottom and subsequently up the wall of the tank. The remaining nuclear radiation is absorbed in the downward flowing propellant above the 1-foot depth. This main region of propellant flow is of the potential-flow type. It is assumed there is no thermal interaction between the upward-flowing natural convection layer and the downward-moving, main potential flow. This is shown in Fig. 36. Depending on the rate of circulation by natural convection, a stratified layer builds up above the, as yet, uncirculated propellant. After a certain time period the bottom of the stratified layer reaches the bottom of the tank and a second circulation can begin. For example, if the net propellant discharge rate is 100 lbm/sec and the circulation rate is 20 lbm/sec, then by the time the tank is 5/6 empty, the bottom of the first stratified layer will reach the bottom of the tank.

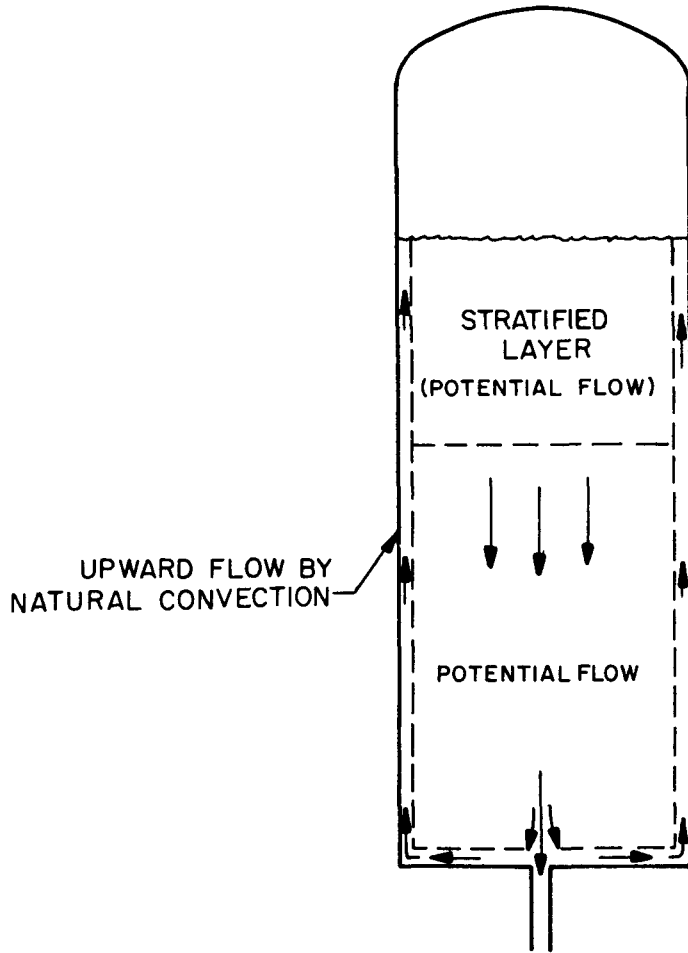


Figure 36. Recirculation Flow Model

~~CONFIDENTIAL~~

When the propellant level in the tank drops to the point where propellant remaining in the tank fills only the bottom head, it is assumed that interaction between the natural convection flow and the main downward bulk flow becomes appreciable and a completely mixed flow then takes place until the tank is empty.

The calculation of the maximum propellant temperature rise for the recirculation-flow model consists of adding together the various contributions according to the equation

$$\Delta T_{\max} = \Delta T_1 + \Delta T_2 + \Delta T_3 \quad (49)$$

where

$\Delta T_1$  = temperature rise of the discharging propellant due to nuclear radiation absorption in the potential flow (effective from 1 foot on out) from time zero until the stratified (or circulated layer) reaches the bottom of the propellant tank

$\Delta T_2$  = Additional temperature rise due to nuclear radiation absorption in the natural convection layer and in the downward flowing stratified layer (in potential flow) until the remaining propellant just fills the bottom head

$\Delta T_3$  = Additional temperature rise due to nuclear radiation absorption in the completely mixed flow while the bottom tank head is draining

**CONFIDENTIAL**

The first step is to calculate the time,  $t_H$ , required for the propellant level to reach the top of the bottom head and the corresponding equivalent head height for a flat-bottom tank with the same head volume. For the tank geometry shown in Fig. 32, the result is 1066 seconds (based on  $t_L = 1200$  seconds) and 7.23 feet (based on a propellant flow-rate of 85.3 lbm/sec).

The next step is to estimate the circulation rate in the natural convection layer. By a material balance at the end of one complete circulation

$$W = Rt = R \left( \frac{W_o}{R + \dot{m}} \right) \quad (50)$$

where

$R$  = circulation rate, lbm/sec

$t$  = time, sec

At the end of two complete circulations,

$$W = \frac{\left( \frac{R W_o}{R + \dot{m}} \right) R}{R + \dot{m}} = W_o \left( \frac{R}{R + M} \right) \quad (51)$$

Successive application of Eq. 50 to "n" circulations leads to the equation

$$W = \frac{W_o}{\left( 1 + \frac{\dot{m}}{R} \right)^n} \quad (52)$$

**CONFIDENTIAL**

The circulation rate is assumed to be the same for each circulation. By a heat balance on the natural convection layer

$$q = RC_p \Delta T \quad (53)$$

where

- $q$  = Nuclear heat absorbed in first foot of penetration, Btu/sec
- $\Delta T$  = Net temperature rise of propellant in passing through the natural convection zone during one circulation

The heat absorption rate is obtained by the application of Eq. 29 and 30 Thus, for a 1-foot penetration

$$q = \frac{95 \pi d^2 \rho}{4(dD + D^2) A} \int_0^1 (e^{-1.59x} + 0.338e^{-0.46x} + 0.378e^{-0.219x}) dx \quad (54)$$

Integration of Eq. 55 leads to

$$q = \frac{95 \pi d^2 \rho (1.110)}{4(dD + D^2) A} \quad (55)$$

The temperature rise,  $\Delta T$ , may be approximated by considering turbulent, natural convection. It is assumed that the available relations for natural convection heat transfer from a hot wall apply to the case of natural convection due to a heat source within the fluid. Some evidence that this may be a fair approximation is given by Randall and Sesonske (Ref. 31). According to McAdams, for either vertical or horizontal (facing up) hot plates, the heat transfer coefficient for turbulent, natural convection is

$$h \approx 0.135 \frac{k}{L} \left[ (N_{Gr}) (N_{Pr}) \right]^{1/3} \quad (56)$$

**CONFIDENTIAL**

where

$h$  = heat transfer coefficient, Btu/hr-ft<sup>2</sup>-R

$N_{Gr}$  is given by Eq. 46

It should be noted that Eq. 56 is independent of the length dimension,  $L$ , because  $L^3$  appears in the numerator of the Grashof number. In addition

$$\frac{q'}{S} = h \Delta T = \text{a function of } (\Delta t) \quad (57)$$

where

$\Delta t$  = temperature drop across the natural convection layer, R

$q'$  = heat absorbed, Btu/sec =  $q/3600$

Figure 37 is a plot of  $q/S$  vs  $\Delta t$  as calculated from Eq. 56 and 57

Now,  $\Delta T$  in Eq. 53 is the average bulk temperature rise in the natural convection layer. It can be determined from the velocity and temperature distributions given by Eckert and Jackson (Ref. 28 ) as follows:

$$\mu = \mu_1 \left(\frac{y}{\delta}\right)^{1/7} \left(1 - \frac{y}{\delta}\right)^4 \quad (58)$$

$$\Delta t_y = \Delta t \left[1 - \left(\frac{y}{\delta}\right)^{1/7}\right] \quad (59)$$



~~CONFIDENTIAL~~

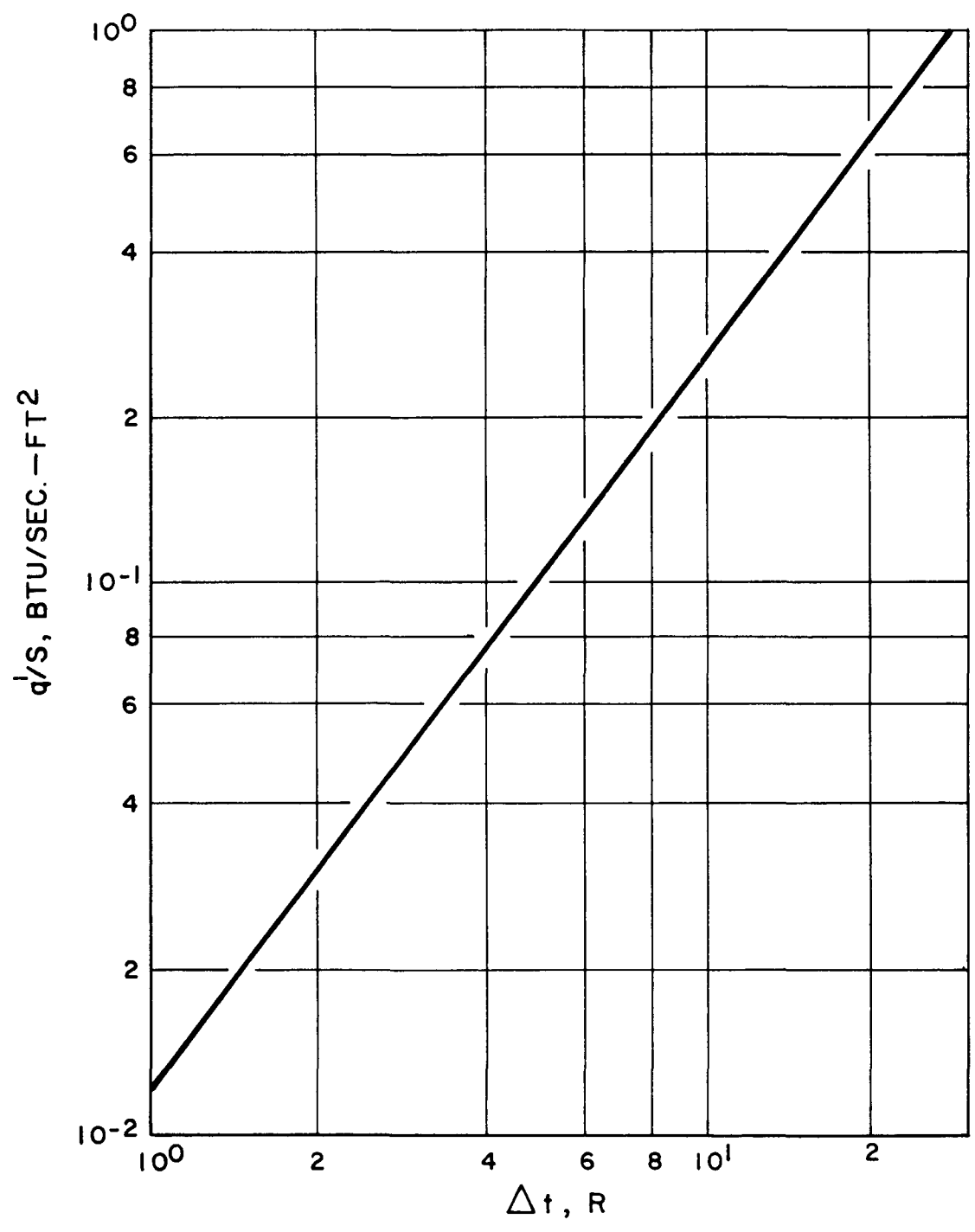


Figure 37. Heat Transfer by Turbulent Free Convection to Liquid Hydrogen

**CONFIDENTIAL**

where

$u_1$  = constant

$\delta$  = Boundary layer thickness, feet

$y$  = Distance from wall, feet

$$\Delta T = \Delta t_{\text{ave}} = \frac{\int_0^{\delta} \Delta t_y u \, dy}{\int_0^{\delta} u \, dy}$$

$$\Delta T = \frac{\Delta t \int_0^{\delta} \left[ \left( \frac{y}{\delta} \right)^{1/7} \left( 1 - \frac{y}{\delta} \right)^4 \right] \left[ 1 - \left( \frac{y}{\delta} \right)^{1/7} \right] dy}{\int_0^{\delta} \left[ \left( \frac{y}{\delta} \right)^{1/7} \left( 1 - \frac{y}{\delta} \right)^4 \right] dy} \quad (60)$$

Integration of Eq. 60 gives

$$\Delta T = 0.25 \Delta t \quad (61)$$

Thus, for a given separation distance,  $D$ , and attenuation factor,  $A$ , the circulation rate,  $R$ , can be calculated from Eq. 53, 55, 56, 61, and Fig. 37.

With the circulation rate,  $R$ , known, the quantity  $\Delta T$ , in Eq. 49 can be calculated from Eq. 29 where  $\dot{m}$  is replaced by  $(\dot{m} + R)$  and the lower limit of zero is replaced by one to give

$$\Delta T_1 \cong \frac{\pi D^2 d^2 \rho}{4(dD + D^2) (\dot{m} + R) C_p} \int_1^L H(x) \, dx \quad (62)$$

~~CONFIDENTIAL~~

where  $H_{(x)}$  is given by Eq. 30 for 1500 megawatts

Integration of Eq. 62 gives

$$\Delta T_1 \cong \frac{95 \pi d^2 \rho}{4(dD + D^2) (\dot{m} + R) C_p A} \left[ \frac{1}{1.59} (e^{-1.59} - e^{-1.59L}) + \frac{0.338}{0.46} (e^{-0.46} - e^{-0.46L}) + \frac{0.378}{0.219} (e^{-0.219} - e^{0.219L}) \right] \quad (63)$$

In Eq. 41, the exponentials involving L vanish for values of initial propellant height, L, greater than about 30 feet. By a modification somewhat similar to that discussed for Eq. 31, Eq. 63 can be used to calculate the propellant discharge temperature as a function of time until the stratified layer reaches the tank bottom.

The quantity  $\Delta T_2$  in Eq. 49 depends on the number of circulations, n. With the circulation rate, R, known, n can be calculated from Eq. 52 which can be rearranged to

$$n = \frac{\ln \left( \frac{t_L}{t_L - t_H} \right)}{\ln \left( 1 + \frac{\dot{m}}{R} \right)} \quad (64)$$

As mentioned previously, for the propellant tank shown in Fig. 32.

$$\begin{aligned} t_L &= 1200 \text{ sec} \\ t_H &= 1066 \text{ sec} \\ \dot{m} &= 85.3 \text{ lb/sec} \end{aligned}$$

~~CONFIDENTIAL~~

and the value of  $n$  is calculated to be approximately equal to one over a wide range of separation distance and attenuation factor. For only one circulation, the quantity  $\Delta T_2$  is most conveniently determined by noting that the propellant is assumed to become completely mixed just as the propellant level drops to the point where the bottom head is filled. Then, if the heat appearing in the discharged propellant up until the time,  $t_H$ , is  $Q_1$ , Btu, and the total heat absorbed by the propellant (both that discharged and that remaining in the tank) is  $Q_H$ , Btu, then  $\Delta T_2$  is given by

$$\Delta T_2 = \frac{Q_H - Q_1}{W C_p} \quad (65)$$

where

$$W = \text{propellant contained in the bottom head} = 85.3 (1200-1066) = 11,440 \text{ lbm}$$

The heat,  $Q_H$ , may be calculated from a heat balance

$$Q_H = \frac{D^2 \pi d^2 \rho}{4(dD + D^2)} \int_0^{t_H} \int_0^c H(x) dx dt \quad (66)$$

where

$$x = L \left( 1 - \frac{t}{t_L} \right)$$

**CONFIDENTIAL**

Substitution of Eq. 30 for  $H(x)$  and subsequent integration gives

$$\begin{aligned}
 Q_H = & \frac{95 \pi d^2 \rho}{4(dD + D^2) A} \left\{ 3.089 t_H + \right. \\
 & \frac{t_L}{L} \left[ \frac{\left( e^{-1.59L} - e^{-1.59L} \left( 1 - \frac{t_H}{t_L} \right) \right)}{(1.59)^2} + \frac{\left( e^{-0.46L} - e^{-0.46L} \left( 1 - \frac{t_H}{t_L} \right) \right)}{(0.46)^2} + \right. \\
 & \left. \left. \frac{\left( e^{-0.219L} - e^{-0.219L} \left( 1 - \frac{t_H}{t_L} \right) \right)}{(0.219)^2} \right] \right\} \quad (67)
 \end{aligned}$$

The quantity  $Q_1$  is given by

$$Q_1 = \frac{D^2 \pi d^2 \rho \dot{m}}{4(dD + D^2) (\dot{m} + R)} \int_{\frac{t_H}{L}}^{t_H} \int_1^L \left( 1 - \frac{t}{t_H} \right) H(x) dx dt \quad (68)$$

An integration similar to that for Eq. 66 gives

$$\begin{aligned}
 Q_1 = & \left( \frac{\dot{m}}{\dot{m} + R} \right) \frac{95 \pi d^2 \rho}{4(dD + D^2) A} \left\{ \left( t_H - \frac{t_H}{L} \right) \left[ \frac{e^{-1.59}}{1.59} + \frac{0.338}{0.46} e^{-0.46} + \right. \right. \\
 & \left. \left. \frac{0.378}{0.219} e^{-0.219} \right] + \frac{t_H}{L} \left[ \frac{\left( 1 - e^{-1.59(L-1)} \right)}{(1.59)^2} + \frac{0.338 \left( 1 - e^{-0.46(L-1)} \right)}{(0.46)^2} + \right. \right. \\
 & \left. \left. \frac{0.378 \left( 1 - e^{-0.219(L-1)} \right)}{(0.219)^2} \right] \right\} \quad (69)
 \end{aligned}$$

**CONFIDENTIAL**

---

Thus, from Eq. 65, 67, and 69,  $\Delta T_2$  can be calculated. For only one circulation, this  $\Delta T_2$  occurs as a sharp, instantaneous rise at  $t = t_H$ .

The last quantity,  $\Delta T_3$ , for the additional temperature rise occurring at the completion of draining of the bottom head, is calculated from Eq. 44 with  $L = 7.23$  ft. To calculate the additional temperature rise during this completely-mixed-flow period of the recirculation-flow model as a function of time, Eq. 45 may be used with  $L = 7.23$  ft,  $t_L = 134$  sec and with  $t$  replaced by  $1200 - t$ .

With values for  $\Delta T_1$ ,  $\Delta T_2$ , and  $\Delta T_3$ , the total maximum temperature rise for recirculation flow may be obtained from Eq. 49. A temperature rise vs time plot may also be calculated as outlined above.

Comparison of Models. Figure 38 presents a typical plot of temperature rise vs time for a propellant tank similar to that shown in Fig. 32 with a separation distance of 12 feet, an attenuation factor of 4, a propellant rate of 104 lbm/sec and a drain time of 900 sec. Curves for all three flow models are shown. The maximum temperature rises for the three models are

<u>Model</u>	<u><math>\Delta T</math> max, R</u>
Potential Flow	1.08
Completely Mixed Flow	4.0
Recirculation Flow	5.45

Based on the tendency of liquid hydrogen to form a natural convection layer next to the tank wall, the recirculation-flow model is perhaps the most realistic model if a baffle (as discussed below) is not used to prevent the formation of a natural convection current. The recirculation-flow model calculations presented here are based on only one

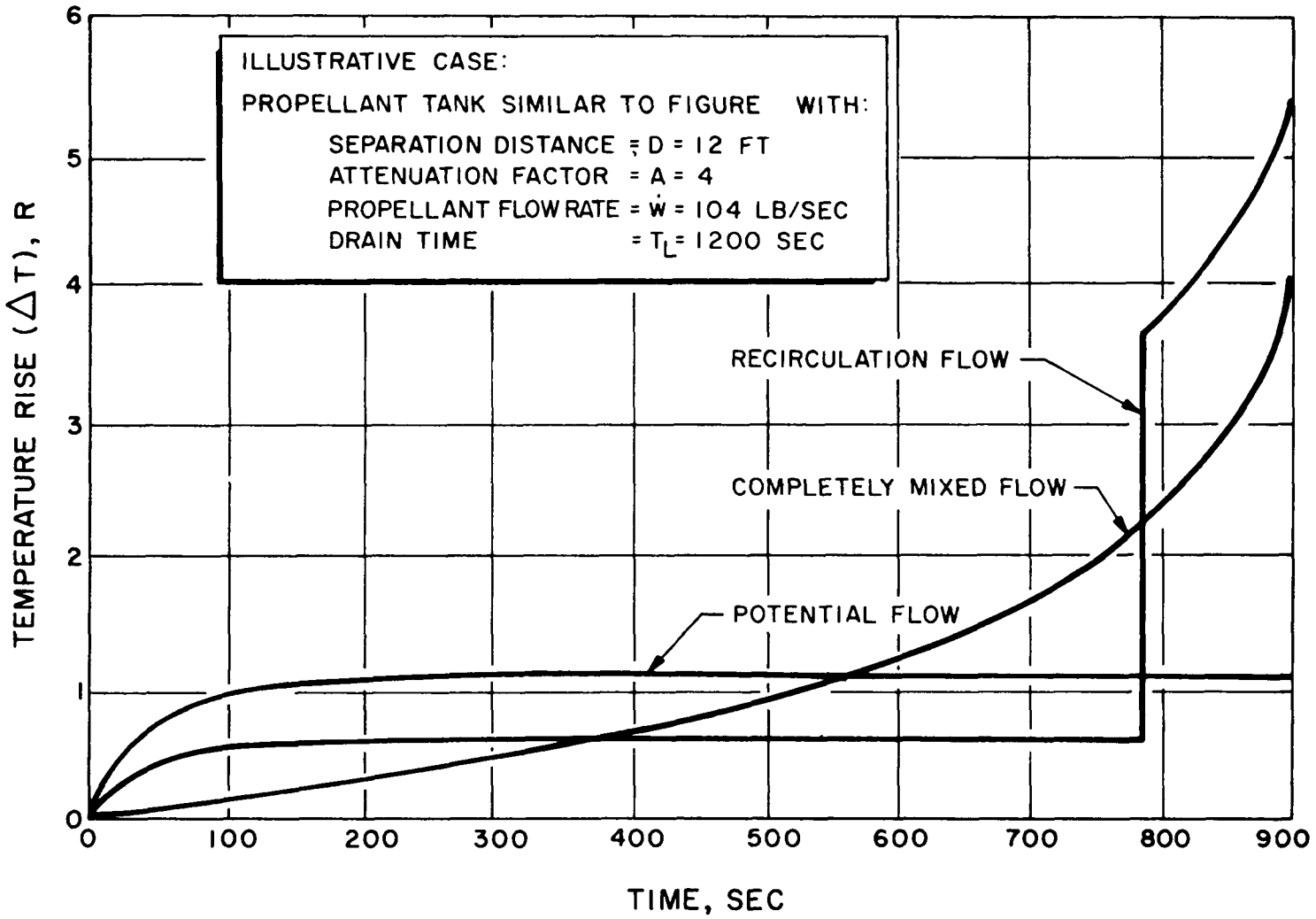


Figure 38. Comparison of Propellant Heating Models

**CONFIDENTIAL**

---

circulation. For more than one circulation, the  $\Delta T_{\max}$  for recirculation flow will be reduced and will tend to approach the completely-mixed-flow model. If some method of baffling can be devised to prevent the upward flow of the natural convection layer, then the motion in the tank should approach the potential-flow model. This would be highly desirable.

Tank Baffling. The relatively large propellant temperature rise for the recirculation-flow model as compared to that for the potential-flow model suggests the possibility of providing a tank baffle to prevent the formation of the natural convection current. As discussed above, the upward natural convection current forms in the region near the tank bottom where the nuclear radiation absorption is high and the downward propellant stream velocity is low. If the downward propellant stream velocity in this region can be greatly increased, natural convection will be suppressed.

A baffle design which accomplishes this objective is shown in Fig. 39 for a spherical-bottom tank. As the downward flowing propellant approaches the discharge, it is blocked from entering the discharge pipe and is thereby forced to flow, at considerably increased velocity, upward through a channel until the angle of tangency shown is reached. Then the propellant turns and flows downward through an adjacent channel which follows along the tank bottom. The velocity and pressure drop in the channel depend on the separation of the baffles. Figure 40 shows the propellant velocity as a function of angle from the vertical. For a baffle separation of 4 inches, the propellant velocity in the channels is 1-ft/sec or greater with a pressure drop of only 0.012 psi. This velocity is somewhat greater than the anticipated natural convection velocity.



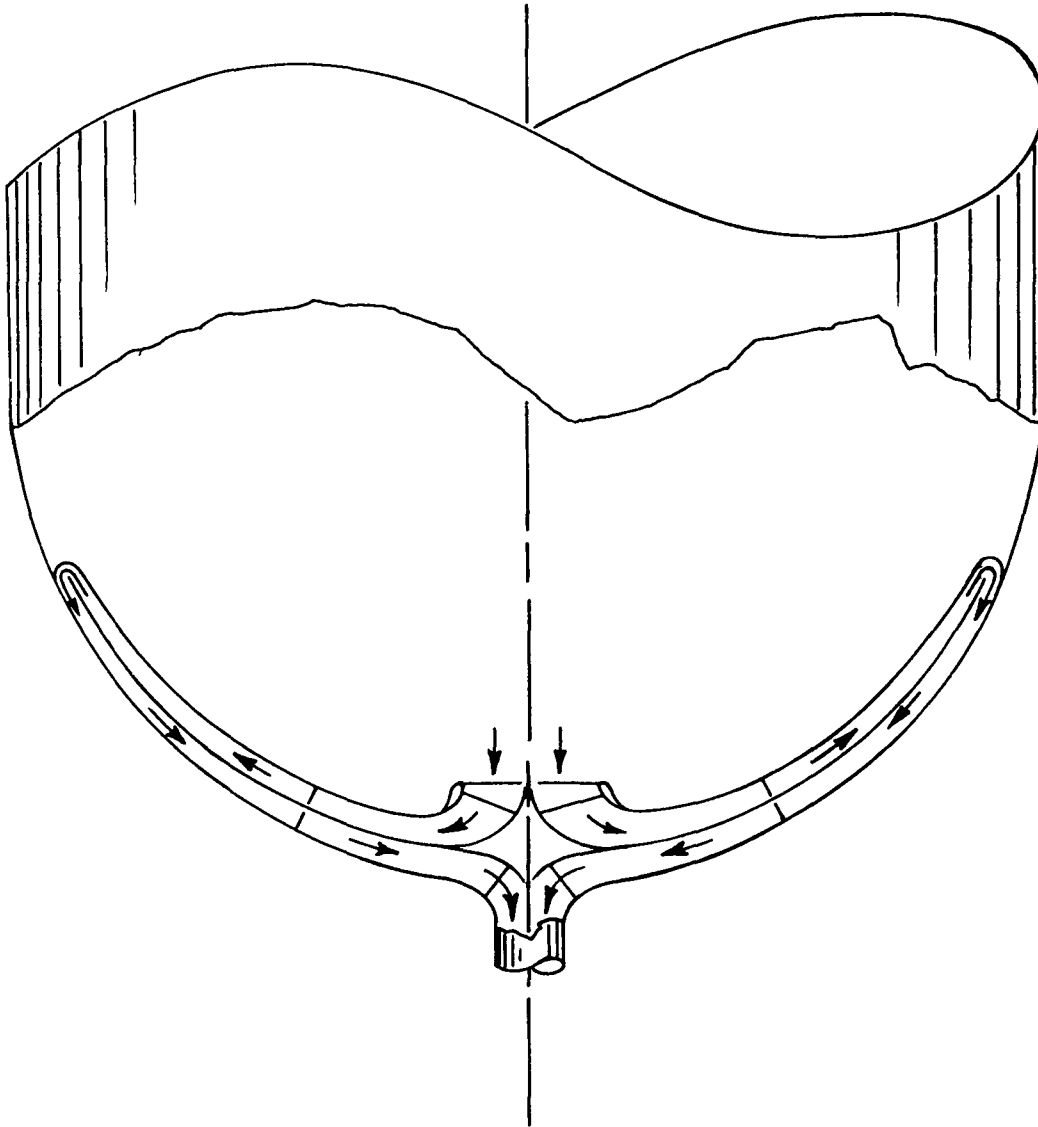


Figure 39. Tank Baffle to Eliminate Recirculation Currents Caused by Radiation Heating

~~CONFIDENTIAL~~

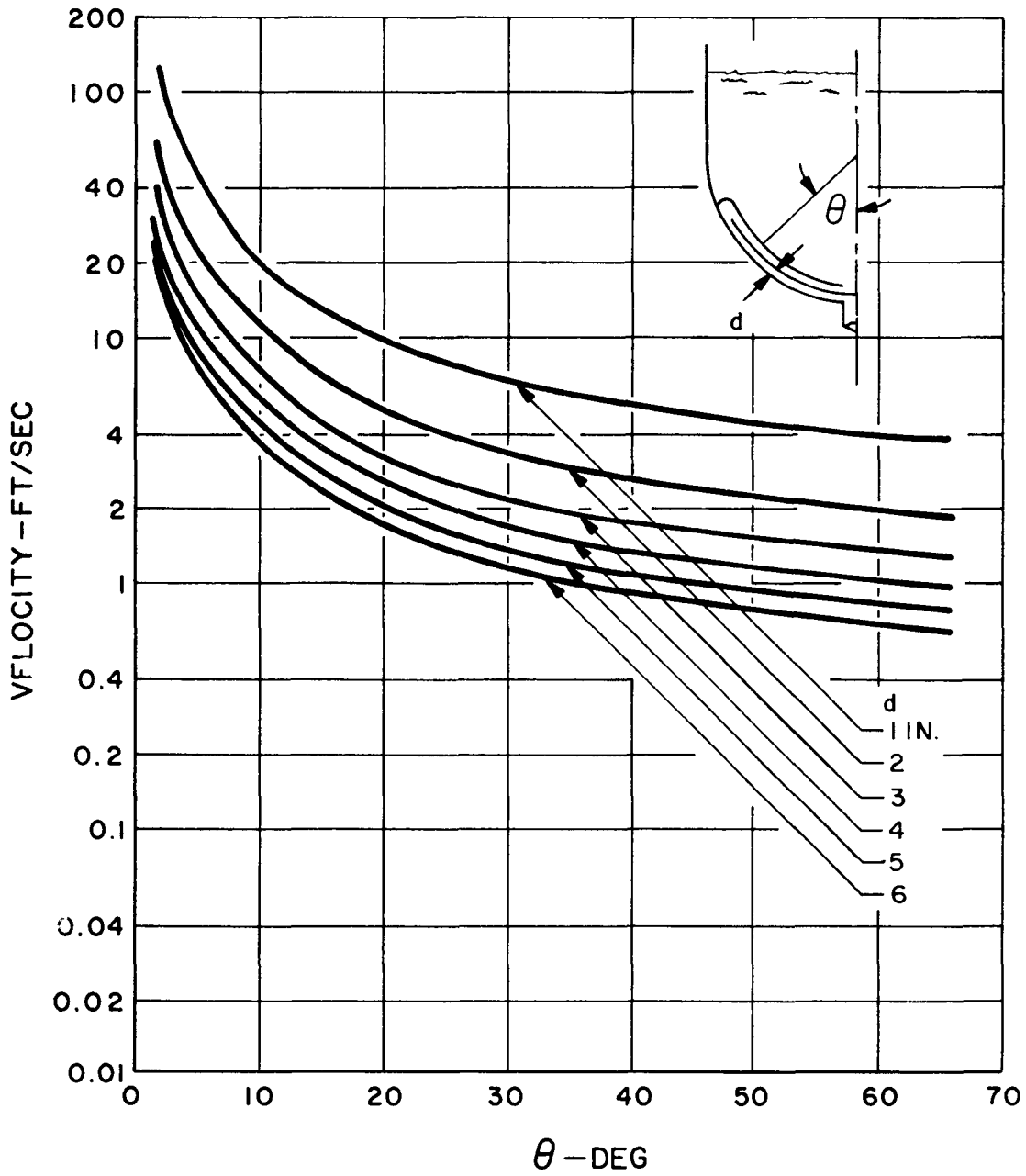


Figure 40. Baffle Velocity Profile

~~CONFIDENTIAL~~

---

Furthermore, the criterion for the influence of natural convection in the presence of a finite free stream velocity is

$$\frac{N_{Gr}}{(NR_e)^2} = \frac{(1) (32.2) (0.0106) (1)}{(1)^2} = 0.34$$

This value is less than 2 and, as discussed above, it appears that under these conditions the natural convection currents would be suppressed.

Although a constant baffle separation distance was used in the above analysis, a tapered separation could also be used. This would provide a more uniformly high velocity than that shown in Fig. 40.

### Conclusions

The relatively large spread of the values for the temperature rise as calculated for the three models indicates that the propellant heating problem requires careful consideration. The use of a baffle to obtain high propellant velocities so as to suppress natural convection near the tank bottom offers a means to approach the potential-flow model and its corresponding relatively low temperature rise. Further theoretical studies and experimental research are required to gain further insight into the nature of the fluid motion within the tank during draining.

~~CONFIDENTIAL~~

---

## REACTOR, TANK SEPARATION BASED ON PROPELLANT HEATING

During operation of the K-1 engine, nuclear radiation will heat the propellant while it is still in the main tank. This heating reduces the NPSH that is available to the engine feed system for a given tank pressure, or at a fixed NPSH can considerably increase the required tank pressure. Use of heavy reactor shielding and large separation distances between the tank and reactor would lessen this problem but may give a large reduction in payload. Therefore, a study was made to determine the optimum separation of the reactor from the tank and the optimum amount of shielding, based on propellant heating. The following variables were considered:

1. Change in tank pressure (to prevent boiling) vs separation distance and shielding attenuation factor.
2. Shield weight vs separation distance and attenuation factor
3. Tank weight vs tank pressure
4. Weight of residual gas in main propellant tank vs tank pressure
5. Interstage structure weight vs separation distance
6. Thrust structure weight vs separation distance and shielding attenuation factor

These variables will be discussed in the above order and applied to the restartable K-1 engine based on a total thrust period of 1200 seconds.

### Propellant Heating

The important parameter for determining the separation is the temperature of the propellant flowing into the pump inlet, and this is strongly de-

~~CONFIDENTIAL~~

~~CONFIDENTIAL~~

pendent on the flow pattern of propellant in the tank. The simplest model for propellant flow in the hydrogen tank, without radiation, is essentially nonviscous potential flow in which each particle of fluid moves evenly down the tank and into the pump. If the radiation heat generation were superimposed on this flow pattern, a steady state would soon develop in which radiation energy is removed at the same time rate at which it was being added. A plot of typical propellant exit temperatures as a function of engine operation time with this flow situation would follow the Potential Flow curve of Fig. 38 . This can be considered to be an ideal case which cannot be achieved in practice because fluid in some streamlines receives more energy in its path to the tank exit than does other fluid.

Flow in the presence of strong radiation may not be as favorable as the potential flow model would indicate. Figure 38 shows two other flow models which are more realistic. It should be noted that while the three models are different, the area under their  $\Delta T$  curves from engine start to burnout must be the same. The energy absorbed at any time is a function only of the amount of propellant remaining; thus, a tank which empties at a constant rate will absorb the same total amount of energy with any internal flow pattern.

It is not clear which of the three flow models best describes the conditions that will be realized in a real tank. It may be feasible to use baffles to reduce or prevent recirculation currents and bring the propellant exit temperature history closer to that of the potential flow model. Figure 39 shows a possible arrangement that may prevent recirculation currents and thereby approach the potential flow model. A preliminary calculation indicates that a payload increase (or reduction in system component weight) of 700 pounds could result from this baffling arrangement. Reliable answers to these and other propellant heating problems will require a broad program of analysis and research utilizing model propellant tanks having close dynamic similitude with the actual nuclear vehicle.

~~CONFIDENTIAL~~

~~CONFIDENTIAL~~

In the absence of such a research program, the problem of choosing the correct flow model remains. On the one hand, the best possible conditions are given by the potential flow model. At the other extreme is recirculating flow, which is a good approximation of the most undesirable flow patterns which are likely to occur. For the following configuration analysis to have the widest possible range of applicability, both extremes plus the completely mixed model will be considered. The conclusions from these parallel studies will then be evaluated to determine how much effect the uncertainty in propellant flow behavior has on the minimum-weight engine system configuration.

Figures 41, 42, and 43 show the change in tank pressure required to prevent boiling vs shield attenuation factor and separation distance (core center to tank bottom) for the potential, completely mixed, and recirculating flow models as a power level of 1500 megawatts and a run duration of 1200 seconds.

The radiation environment is a factor in determining the optimum engine system configuration. Reactor-tank separation distance is one independent variable, and the factor by which a shield reduces the heat-producing radiation is another. Heat generation problems in individual components cannot be evaluated until the general configuration of the engine system is specified.

#### Shield Weight

A wide variety of shield material was examined by Rocketdyne in order to specify the one or two most promising materials. One material, boronated graphite, offers most of the desirable properties already mentioned and is a good material to use in performing the preliminary optimization.

~~CONFIDENTIAL~~

**CONFIDENTIAL**

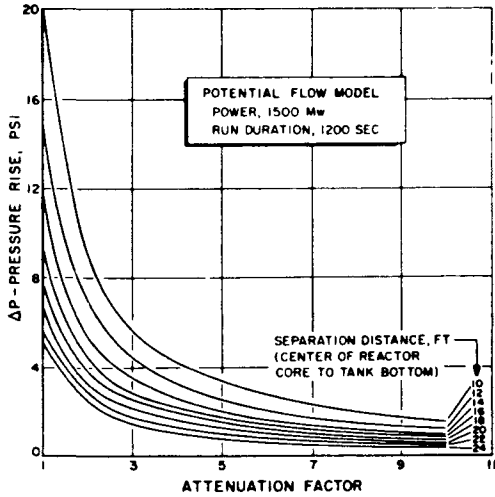


Figure 41. Pressure Rise (To Prevent Boiling) vs Attenuation Factor and Separation Distance (Potential Flow Model with Power at 1500 Mw)

Figure 42. Pressure Rise (To Prevent Boiling) vs Attenuation Factor and Separation Distance (Completely Mixed Flow Model with Power at 1500 Mw)

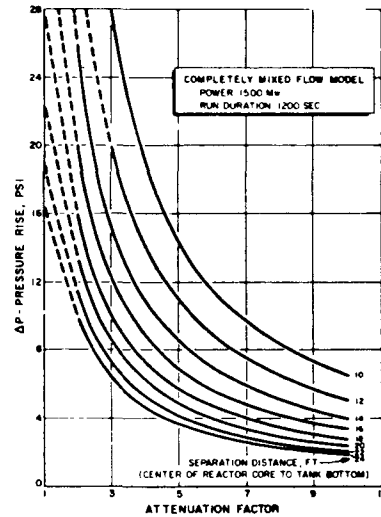
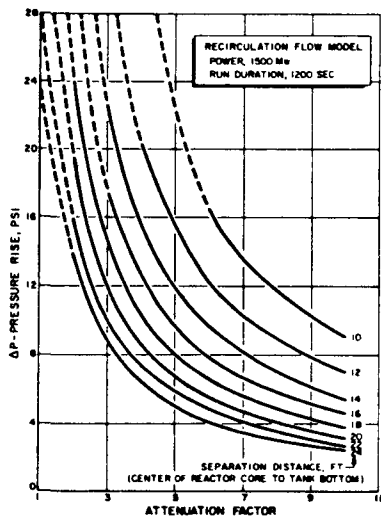


Figure 43. Pressure Rise (To Prevent Boiling) vs Attenuation Factor and Separation Distance (Recirculation Flow Model with Power at 1500 Mw)



~~CONFIDENTIAL~~

---

Graphite has excellent moderating properties. The addition of boron provides a means of absorbing the moderated neutron flux through the  $(n, \alpha)$  reaction which leaves its energy in the shield and does not create secondary gammas in the process. Graphite also has a relatively high mass attenuation coefficient in the range of most prevalent gamma energies ( $\sim 2$  Mev). Graphite possesses good strength and thermal conductivity at high temperatures, is not susceptible to radiation damage, and is easy and inexpensive to fabricate. The choice of boronated graphite for the system configuration analysis will not restrict the resulting system to use of boronated graphite. Other feasible shield materials are so similar to boronated graphite in their application and effect that the system selection will be unchanged by the use of a different material. The results of the propellant internal heat generation calculations were reduced and simplified to an empirical formula (Eq. 21) for use in this optimization analysis.

Another necessary relationship is the manner in which shield weight varies with reactor tank separation distance. Shield diameter increases as the tank is brought closer because of the increasing solid angle which the tank and shield subtend relative to the reactor. Since shield thickness is constant for a given attenuation, the shield weight decreases as it is moved closer to the reactor. Therefore, an optimum system would incorporate the shield close to the reactor core, preferably within the reactor pressure shell. This allows the shield to be cooled by the full propellant flow, and eliminates the separate pressure vessel and associated controls needed for an auxiliary cooling system. The reference shield of boronated graphite can provide radiation attenuation factors up to approximately 15 without having to extend the pressure shell unreasonably.

~~CONFIDENTIAL~~



~~CONFIDENTIAL~~

The variation of shield weight with reactor-tank separation distance for various values of attenuation factor is shown in Fig. 44 . Separation distance is defined as the length between the reactor center and the bottom of a hemispherical-end propellant tank. Attenuation factor is defined as pertaining to the reduction of heat generation in propellant only. A given shield would have a slightly different attenuator factor for radiation heating in metals. In calculating Fig. 44 a simple geometrical approximation was made which assumed a constant-thickness slab shield. The reflector was assumed to effectively shield any radiation from the sides of the reactor core. This preliminary calculation is subject to errors arising from the simplified geometry and the assumed flat radial core power distribution with no side leakage, but it is adequate for preliminary optimization.

Tank and Residual Gas Weight vs Tank Pressure

Figures 45 and 46 contain information used in optimizing reactor-tank separation and shield attenuation for tank weight, and weight of residual gas vs tank pressure, respectively.

Interstage Structure Weight vs Separation Distance

To estimate the change of interstage structure weight as a function of engine-tank separation distance, a study was made of vehicle axial and bending loads for a Saturn upper-stage nuclear vehicle. The following assumptions were made for this study:

1. Tank diameter is 260 inches
2. Pressure stabilized tank
3. The interstage structure is of truss-core sandwich construction.

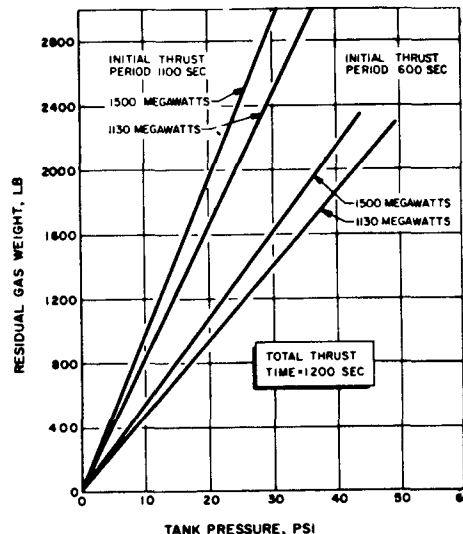


Figure 45 . Residual Gas Weight and Propellant Depletion vs Tank Pressure

**CONFIDENTIAL**

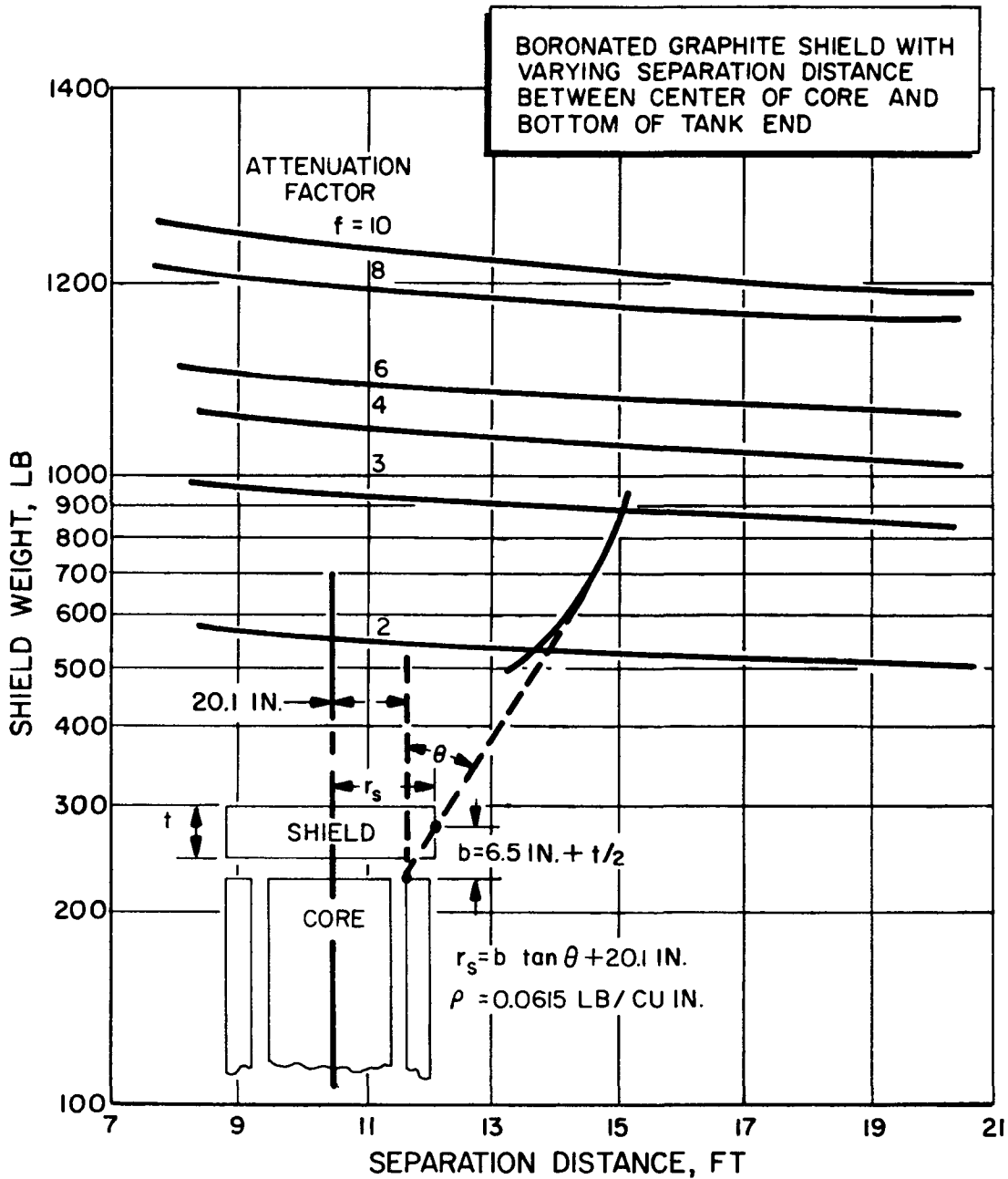


Figure 44 . Shield Weight vs Separation Distance

**CONFIDENTIAL**

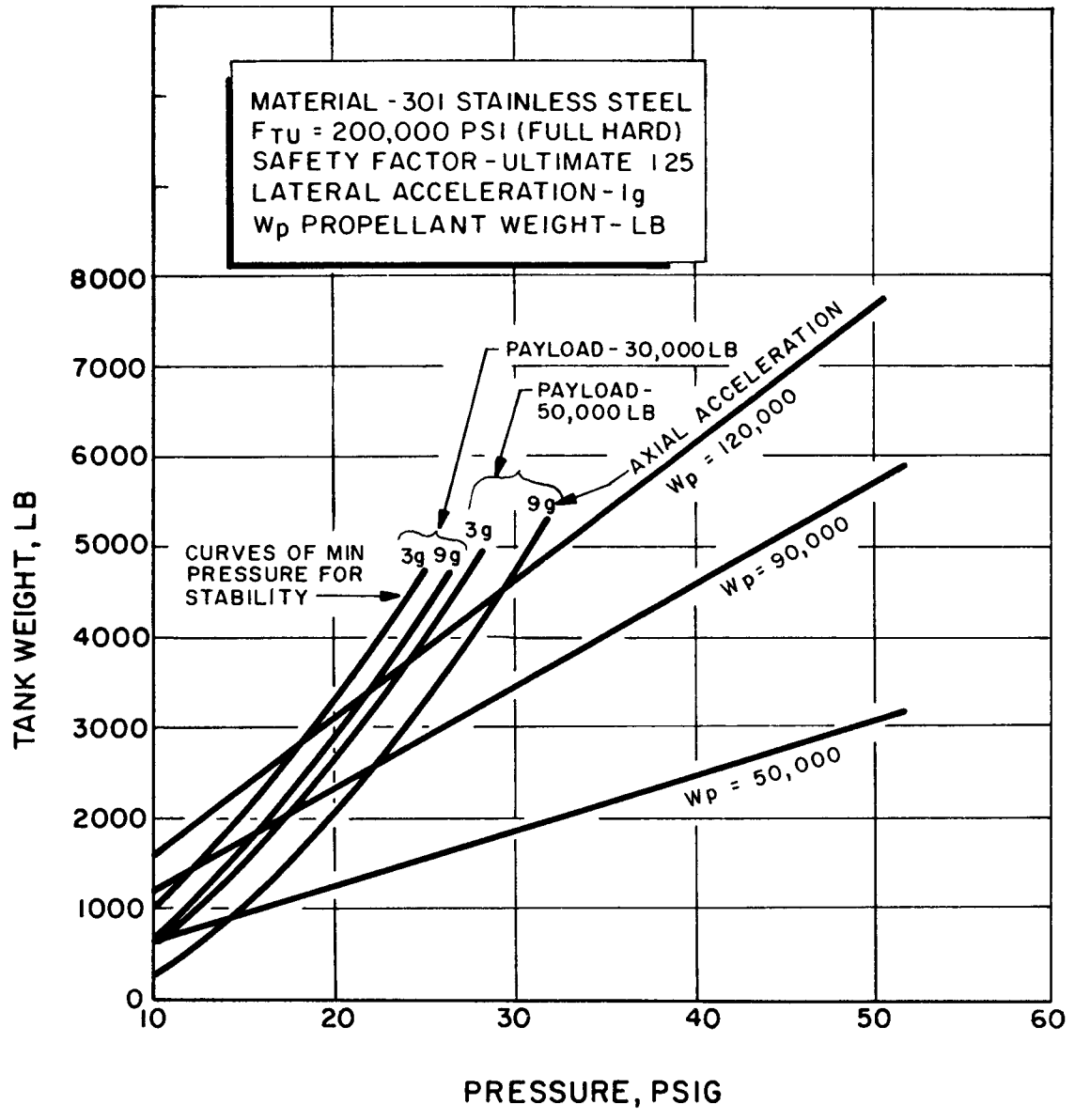


Figure 46 . Tank Weight vs Tank Pressure

**CONFIDENTIAL**

---

4. The skin temperatures encountered permit use of aluminum for interstage structure material.
5. Gross takeoff weight of Saturn S-I stage is 709,500 lb.
6. Gross weight of Saturn S-II stage is 325,650 lb.
7. Gross weight of nuclear third stage is approximately 160,000 lb.
8. Payload weight is 40,380 lb concentrated at nose cone base.

Figure 47 shows the geometry and loading diagram of the reference vehicle, and includes the air load distribution under maximum dynamic pressure conditions, the accompanying vehicle stabilizing force, and the resulting inertia loads. The resulting shear and bending moments are shown in Fig. 48 . The sandwich panel selection for the interstage structure was made on the basis that both general and local instability failure modes occur at the same unit loading. The critical stress for general instability was determined from Fig. 49 . The critical crippling stress for the elements comprising the sandwich panels was obtained from Fig. 50 . The resulting interstage structure weight is shown in Fig. 51 as a function of its length.

Thrust Structure Weight vs Separation  
Distance and Attenuation Factor

In order to determine the effect of engine thrust structure on separation distance between the tank bottom and center of reactor core, a study was made to determine the weight of the thrust structure as a function of separation distance and shield attenuation factor. Figure 52 presents the results of this study.

The basic thrust structure consists of an aft-cooled and a forward uncooled space frame. Cooling of the aft section with liquid hydrogen is necessary because of the radiation heatflux encountered near the reactor. Figure 53 shows a simplified layout of the basic engine thrust structure.

**CONFIDENTIAL**

**CONFIDENTIAL**

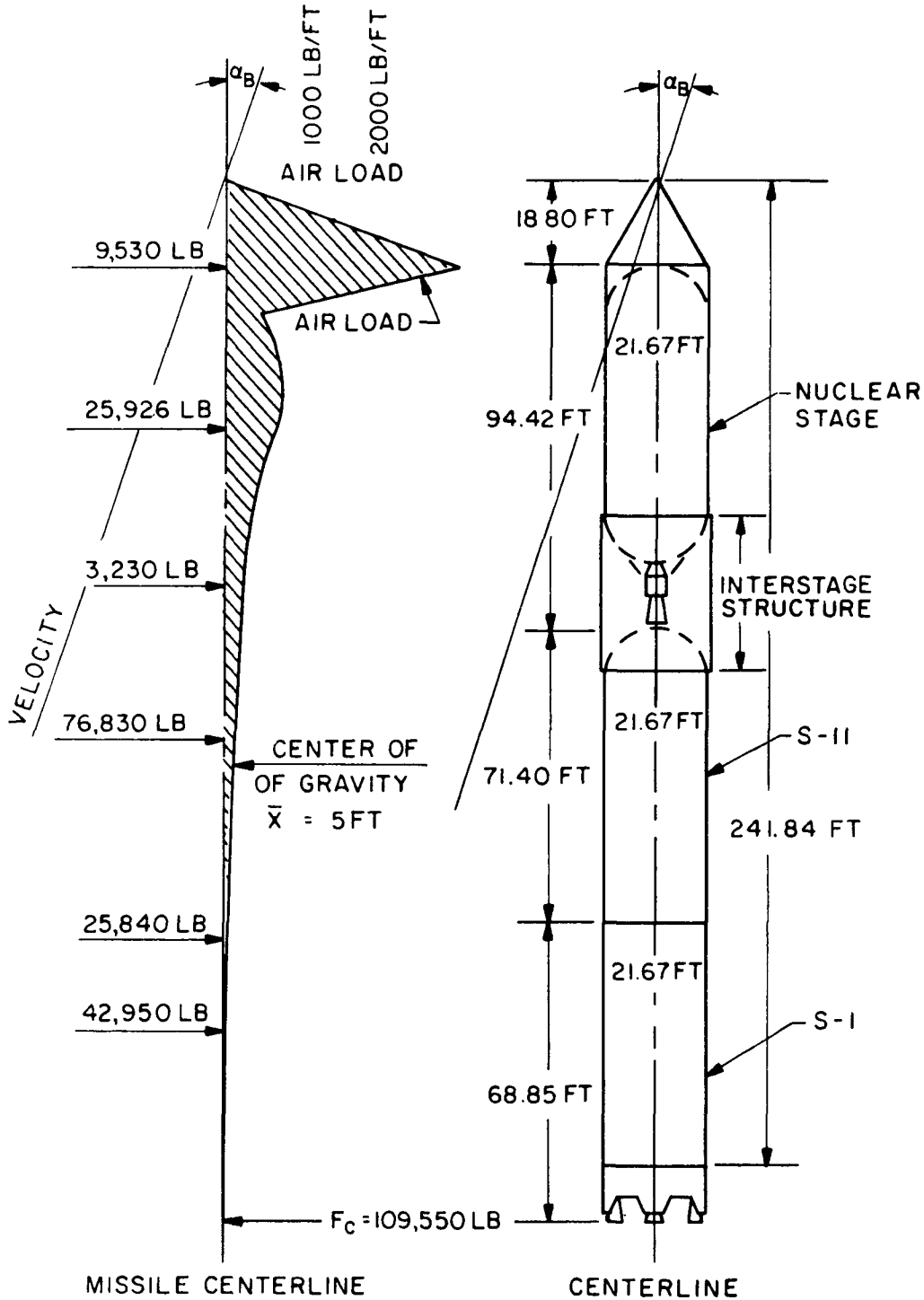


Figure 47 . Load Diagram Reference Vehicle

CONFIDENTIAL

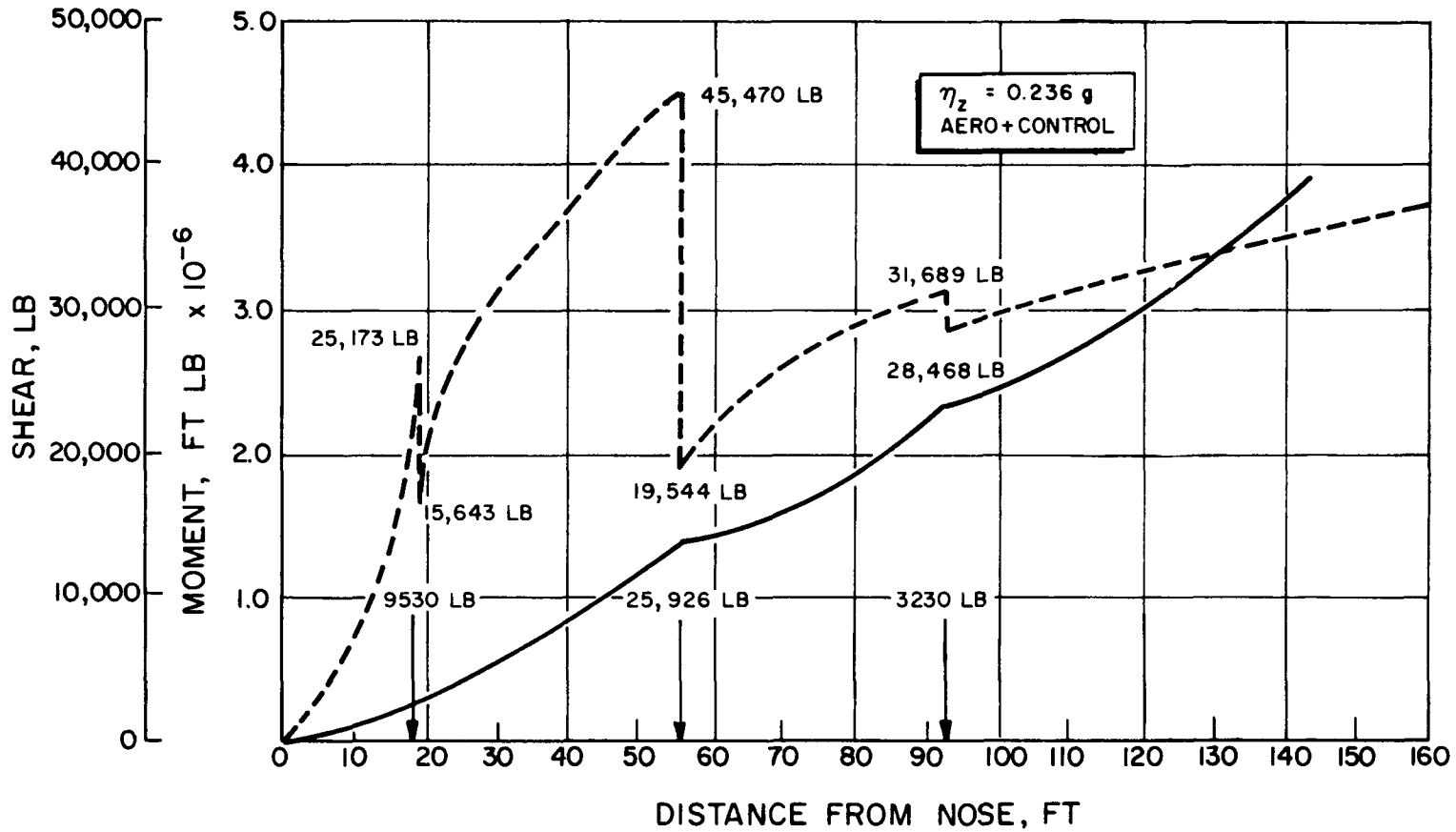


Figure 48 . Shear and Moment Resulting from Aerodynamic Pressure, Control Force, and Inertia Loading

**CONFIDENTIAL**  
**ROCKETDYNE**  
 A DIVISION OF NORTH AMERICAN AVIATION INC

~~CONFIDENTIAL~~

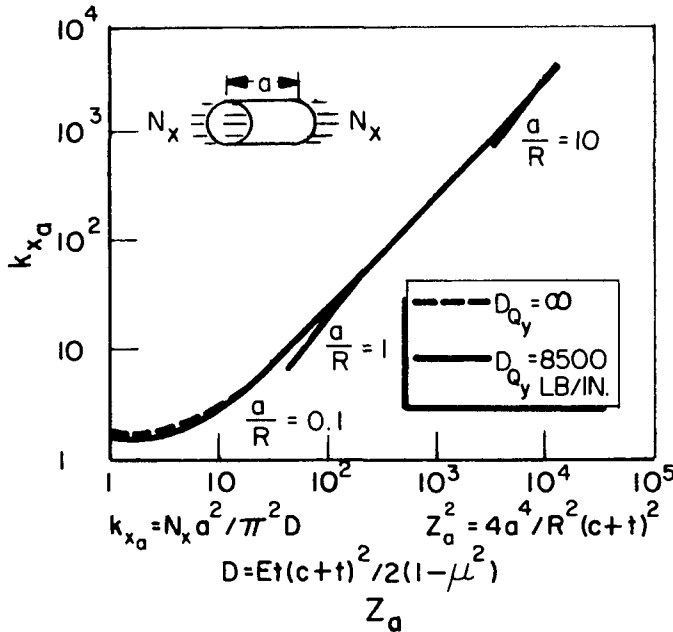


Figure 49. Critical Axial Compression Coefficients for Simply-Supported Sandwich Cylinders With Corrugated Core Oriented in the Axial Direction

NOMENCLATURE

- a Length in axial direction
- b Length in circumferential direction
- c Core depth
- D Membrane flexural rigidity of the facings  
 $= Et(c+t)^2 / 2(1-\mu^2)$  for isotropic core sandwich  
 $= Et(c+t)^2 / 2$  for corrugated core sandwich
- $D_q$  Core shear stiffness  $= G_c c$
- E Young's modulus of the facings
- G Core shear modulus
- $K_{x_a}^c$   $K_{x_b}$  Axial compression load coefficients:  
 $N_x a^2 / \pi^2 D, N_x b^2 / \pi^2 D$ , respectively
- R Radius of curvature to midplane of sandwich
- $r_a, r_b$  Sandwich stiffness parameters:  
 $\pi^2 D / D_q a^2, \pi^2 D / D_q b^2$ , respectively
- t Thickness of each facing
- x Axial coordinate, as subscript denotes direction
- $y_a^2, y_b^2$  Circumferential coordinate, as subscript denotes direction
- $Z_a^2, Z_b^2$  Curvature parameters:  
 $4a^4 / R^2 (c+t)^2, 4b^4 / R^2 (c+t)^2$ , respectively

**CONFIDENTIAL**

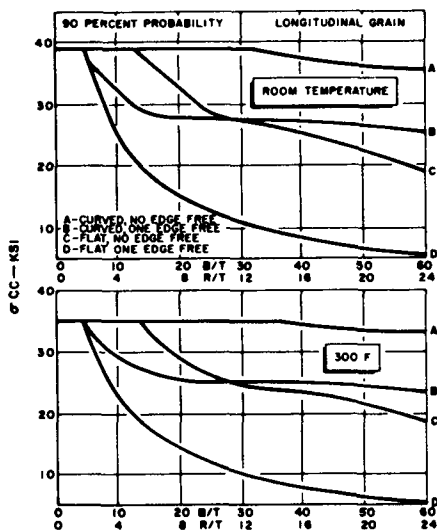


Figure 50. Ultimate Element Crippling Curves Alclad 2024-T3, T4 Aluminum Alloy Sheet

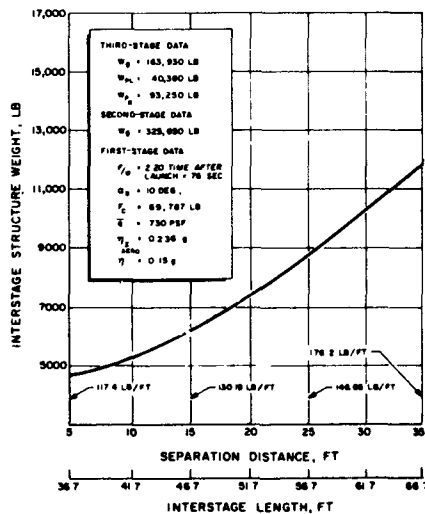


Figure 51. Interstage Structure Weight vs Length

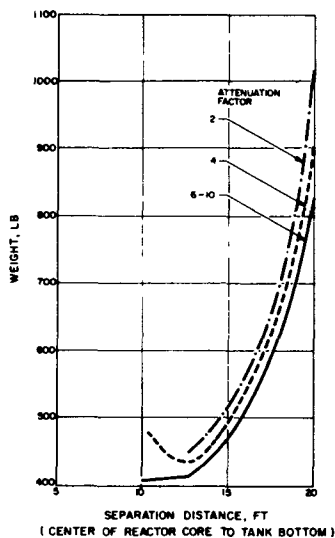


Figure 52. Engine Mount Weight vs Separation Distance

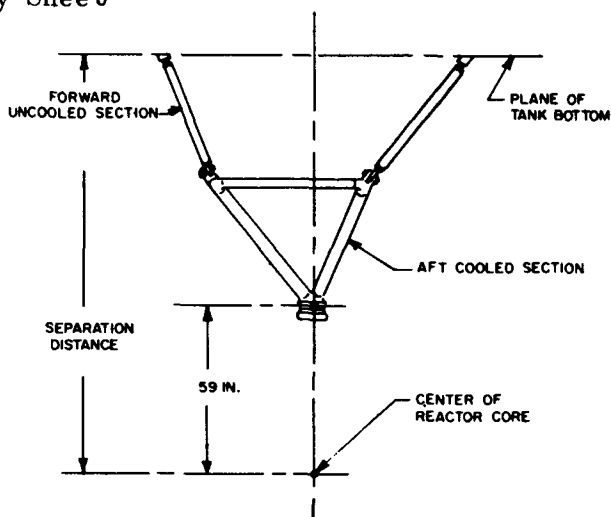


Figure 53. General Thrust Structure Mount Arrangement



**CONFIDENTIAL**

---

The following assumptions were made in determining the weight of the engine thrust structure:

1. The aft section is made of stainless-steel tubing cooled with liquid hydrogen.
2. The forward section is made of pin-connected Inconel X tubing.
3. The diameter of the vehicle attach points is constant.
4. The maximum allowable temperature in the uncooled Inconel X tubing is 1500 F.

For the purpose of this study the aft-cooled section of the thrust structure was varied from approximately 2 to 3-1/2 ft. The uncooled forward-thrust structure section was varied to make up the total length of thrust structure being considered.

The temperature rise in the uncooled section because of nuclear radiation was computed at the point of connection between the uncooled and cooled sections. With an attenuation factor of 2, and below a separation distance of 13 ft, the maximum allowable temperature of the uncooled material was exceeded.

Change in System Weight vs Separation Distance of  
Reactor Core Center to Tank Bottom

The variable weights previously discussed are used as follows to determine the separation between the center of the reactor core and the tank bottom.

**CONFIDENTIAL**

---

Utilizing the tank weight curve and the propellant weight for a 1200-sec run duration yields the tank weight per unit of tank pressure. Multiplying this factor by a particular  $\Delta p$  (to prevent boiling) value taken from Fig. 41 through 43 yields the change in residual pressurizing gas weights for a given attenuation factor and separation distance.

Figure 52 gives the change in thrust structure weight vs separation distance and attenuation factor for 1500 megawatts. The weight of the interstage structure shown in Fig. 53 for 1500 megawatts power level is multiplied by an exchange factor to give the equivalent interstage weight effect on the third-stage payload. This factor is approximately 0.362 for a 2.6-day lunar mission. For other missions investigated, this factor does not change significantly; therefore, the reactor-tank separation and the shielding attenuation factor will remain approximately the same.

Summarizing the above curves with shield weight (Fig. 44 ) yields the change in system weight vs separation distance (Fig. 54 through 56 ) for the three tank flows models investigated. These curves apply only to a pressure-stabilized tank in which the pressure required for stability is equal to or less than the pressure allowance for initial propellant vapor pressure, aerodynamic and solar heating, and NPSH.

### Conclusions

The following Table 8 summarizes the minimum system weight and the corresponding separation distance and attenuation factor for Fig. 54 through 56 .

**CONFIDENTIAL**

**CONFIDENTIAL**

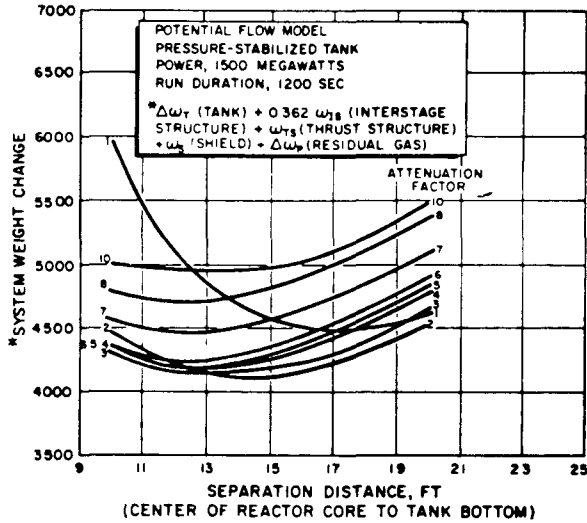


Figure 54 . Change in System Weight vs Separation Distance (Potential Flow Model with 1500 Megawatts of Power)

Figure 55. Change in System Weight vs Separation Distance (Completely Mixed Flow Model with 1500 Megawatts of Power)

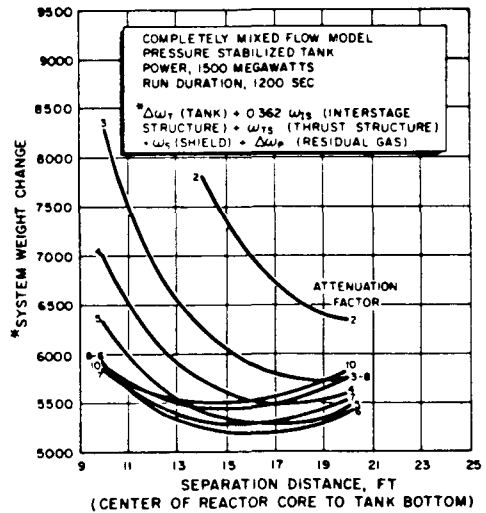
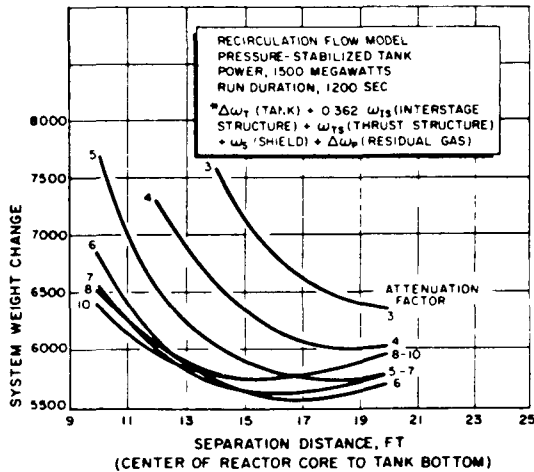


Figure 56. Change in System Weight vs Separation Distance (Recirculation Flow Model with 1500 Megawatts of Power)



~~CONFIDENTIAL~~

TABLE 8  
 SYSTEM WEIGHT, SEPARATION DISTANCE,  
 AND ATTENUATION FACTOR

<u>Fig.</u>	<u>Flow Model</u>	<u>Power Level, Mw</u>	<u>Run Duration, sec</u>	<u>Separation Distance, ft</u>	<u>Attenuation factor</u>	<u>System Weight, lb</u>
54	Potential	1500	1200	14	2	4100
55	Completely mixed	1500	1200	16	6	5200
56	Recirculating	1500	1200	17	6	5500

Thus, a separation distance of 17 feet and a shielding attenuation factor of 6, using a boronated graphite shield, is indicated for the K-1 engine at 1500 megawatts. A separation distance of 14 feet is recommended because any reduction in propellant heating would tend to optimize the system at a lower separation distance than is indicated by the recirculating flow model. The resulting tank pressure rise is approximately 10 psi.

The flux map (Fig. 57) shows the intensity of gamma and fast neutron radiation in the region of the engine system during 1500 megawatt operation. Heat generation and electrical disruption are proportional to the gamma fluxes on this plot, while heating in hydrogen is more a function of the fast neutron flux. Figure 58 shows the heating rates (Btu/lb-sec) for most metals at varying distances above the core. The latter curve illustrates the magnitude of the radiation heating problem as well as the radiation attenuation with distance.

CONFIDENTIAL

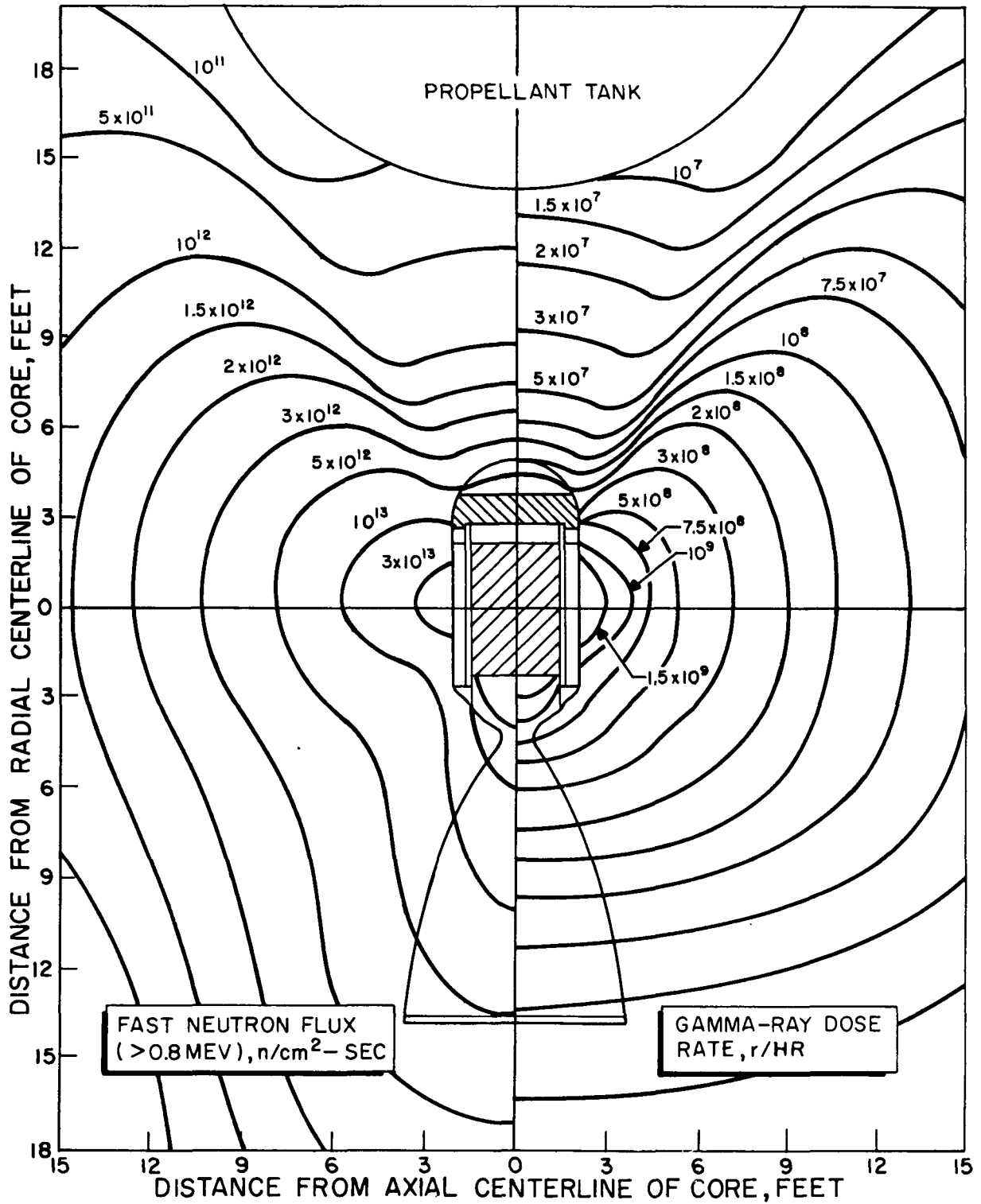


Figure 57 . Isoflux and Isodose Curves for 1500 Megawatt K-1 Engine

~~CONFIDENTIAL~~

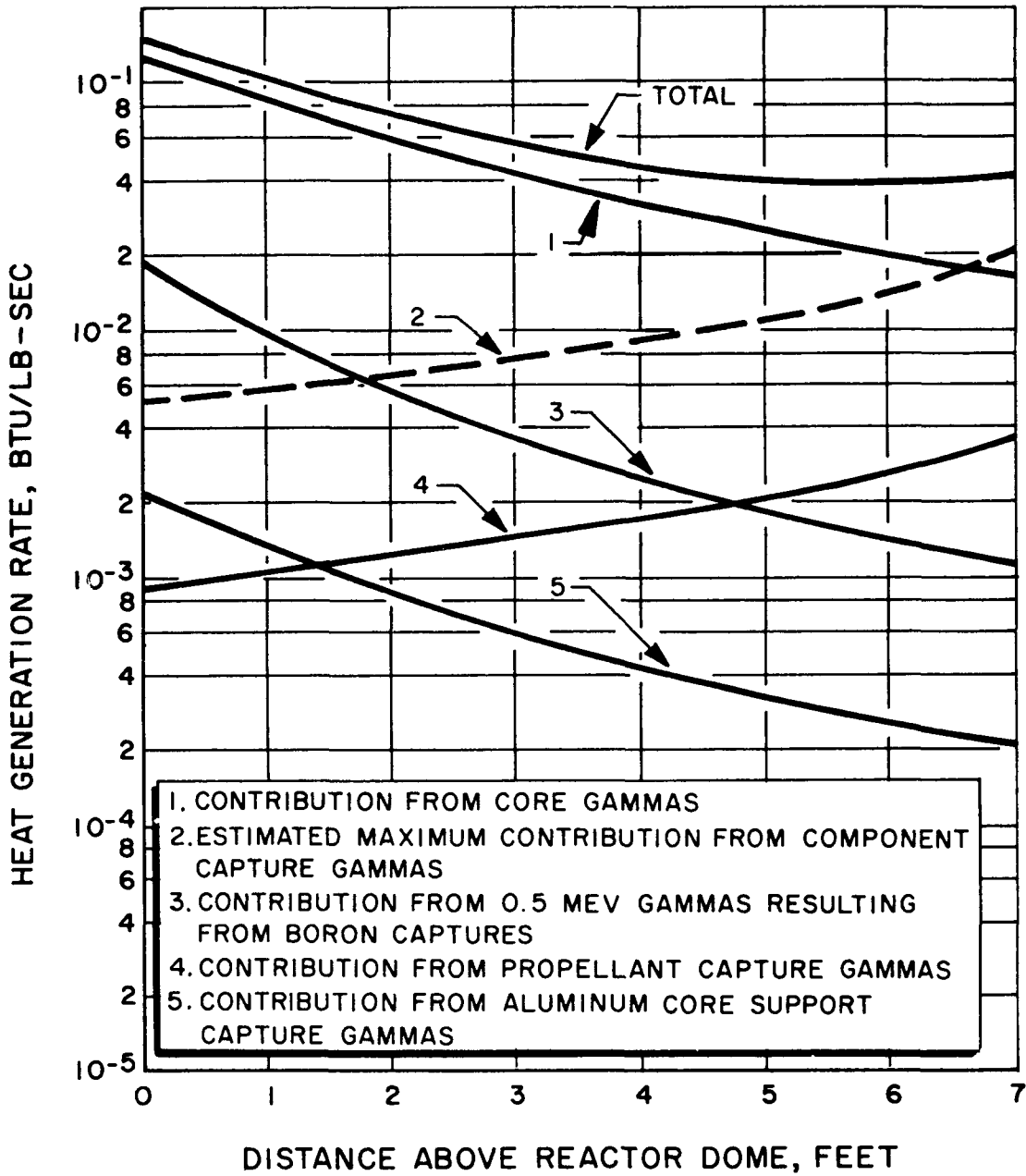


Figure 58. Heat Generation in Components Located Above Reactor Dome

~~CONFIDENTIAL~~

## COMPONENT HEATING

The core gamma flux generates heat directly in components and structure and therefore lends itself to straightforward calculation, but the neutron flux generates heat through the capture gamma reaction. Each region of the engine system is a secondary gamma source which must be considered separately. The neutron flux also produces some heat directly through elastic and inelastic collisions, but this effect is so small in non-hydrogenous materials that it is disregarded.

Above the pressure dome, two of the neutron capture secondary gamma sources can be considered to be part of the primary core flux because they issue from within the reactor pressure shell. They are the capture gammas from the aluminum-core support plate and the 0.5 Mev gammas resulting from the decay of the  $\text{Li}^7$  isotope formed by the  $(n, \alpha)$  reaction in  $\text{B}^{10}$  in the shield. A strong secondary source is also created in the propellant tank from the 2.23 Mev hydrogen capture gammas, and this radiation must be considered separately because it reaches components from a different direction. Neutron captures also occur within the components themselves, and the resulting gammas add to the heat generation in that component as well as in other nearby components. Thus, there are five distinct radiation sources which must be considered in the analysis of each component located between the pressure dome and the propellant tank:

1. Core gammas
2. Captures in aluminum support plate
3.  $\text{Li}^7$  gammas from neutron capture in  $\text{B}^{10}$
4. Capture in tanked propellant
5. Captures within components themselves

~~CONFIDENTIAL~~

---

The engine design for which these sources were calculated is that described in the summary. The 260-inch diameter tank was assumed to be flat-bottomed for simplicity, and the shield employed was 13 inches of boronated graphite with 20 percent void and 1 percent of natural boron.

The internal heat generation from the above sources is shown in Fig. 58 for a thin (no self-shielding) slab of Inconel located at varying distances from the reactor. Units of this curve are Btu/lb-sec, and their similar gamma absorption properties make this curve apply to aluminum and steel as well. It should be noted that the heating from hydrogen capture gammas becomes greater as the component is moved nearer the tank, while the other contributions decrease approximately with the inverse square of their distance from the reactor.

To find the heat generation at points within thicker components, the self-shielding factors of Fig. 60 are used in conjunction with Fig. 58. The factors are plotted as functions of  $t$ , the thickness of material between the point of interest and the surface upon which the radiation is incident. Two curves are plotted to account for the difference in absorption properties between aluminum and iron-nickel alloys. If the component of interest is shielded by other materials, the product of two or more self-shielding factors can be used to adjust the original thick slab heat generation.

Calculation of the gamma heating caused by neutron captures within the components themselves is made very difficult by the neutron captures in one component tending to affect the heat generation in another. In general, the capture rate will be proportional to the thermal neutron flux, and this is highest near the propellant tank where backscatter of thermal neutrons is significant. The capture rates can be calculated at this point, and

~~CONFIDENTIAL~~



~~CONFIDENTIAL~~

---

they can be estimated at other points by rough calculation. If the heating contribution from this source can be shown to be insignificant for the components of interest, then the problem of heating from captures within the components themselves can be safely neglected.

The dashed curve on Fig. 58 shows that this is indeed the case for all components located in the high-flux region close to the reactor. Conservative assumptions have ensured that the values on this estimated curve are higher than will be realized in practice. The capture rate at the tank face was calculated using the neutron flux at that point, and a thick slab of steel was used for calculating the volume-distributed source. Geometric attenuation then reduces the heat generation rate near the reactor from this source to values that are small relative to the other sources.

Values on these curves are typical, and may have  $\pm 30$  percent error. Components that are only partly shielded or which have odd geometries require separate analysis, but the curves can be used for preliminary design. Critical areas in the final design should be checked with a Monte Carlo analysis.

The heat generation rate below the core along the axial centerline of the nozzle is shown in Fig. 59. In this case, only the gamma rays escaping from the core make a significant contribution to the heating. Self-shielding effects in the nozzle region are not important because of the small thicknesses of the materials located in this region.

Component failures from radiation heating are caused by decreased strength at high temperatures, thermal stresses, and thermal expansion of parts whose dimensions are critical. Space environment will not provide the atmospheric convection cooling of ground tests, and radiative cooling will be small except at prohibitively high temperatures. Therefore, resistance

~~CONFIDENTIAL~~

**CONFIDENTIAL**

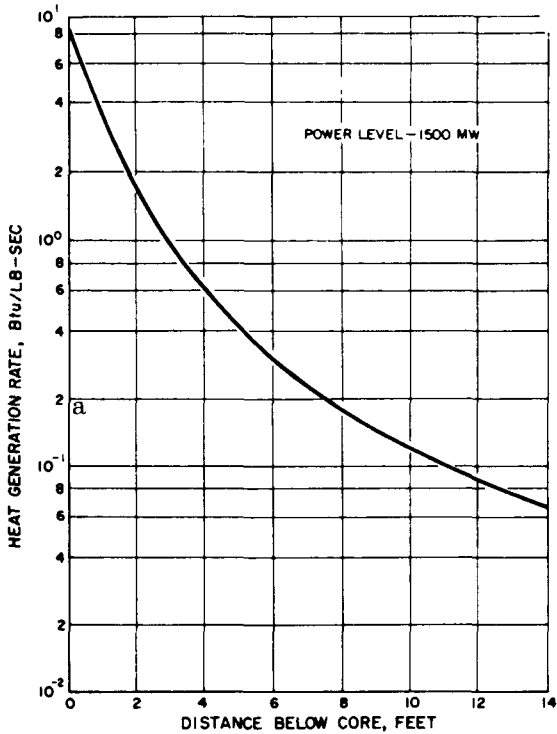


Figure 59 . Heat Generation Rate Along Axial Centerline Below Core

to nuclear radiation heating must be inherent in the design of each component. The designer may reduce heating rates in components by locating them farther from the reactor or in the "shadow" of another component. The designer may (1) provide thermal capacitance by including heat sinks and paths of heat conduction, or (2) cool the components with propellant flow.

Since the physical location of the various components is primarily dictated by convenience, plumbing restraints, or component geometrical restraints, most of the components must endure whatever radiation dose rate is present in their assigned

location (Fig. 1). Figure 58 indicates that some rates will be excessive for structural materials in many locations in the absence of heat sinks. In this figure the heat generation effect of reactor radiation is shown graphically. Lines of constant heat generation rate are shown on the left half of the diagram, and lines of constant, adiabatic final temperature are shown on the right. Gamma heating from all important sources has been considered, including core gammas, capture gammas from the core support plate and from the tanked propellant, and capture gammas arising within the system components. Both halves of the figure were calculated assuming no self-shielding and no flux perturbations from components or structure, and are therefore the maximum possible values at each location within the system. The heat generation rate plot is roughly applicable to all nonhydrogenous

**CONFIDENTIAL**

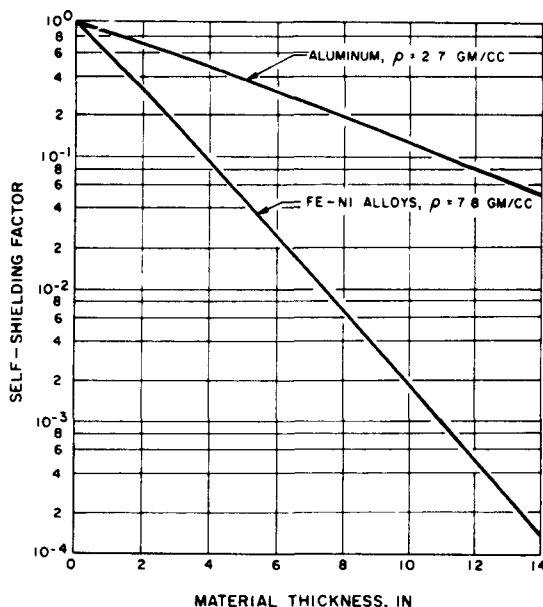


Figure 60 . Component Self-Shielding Factors

materials, although it was calculated for iron-nickel alloys. However, the temperature rise plot applies only to iron-nickel alloys. It is based on the heat generation rates of the other plot, on a 1200-second run at 1500 megawatts, and on the specific heat of Inconel X. The values of temperature rise apply to a thin absorber, perfectly insulated, which assures that they represent the upper limit in any practical situation.

As has been shown, the propellant tank must be provided with a large amount of radiation shielding. This same shield will reduce the radiation dose rates for many of the components. Figure 61 indicates the decrease in temperature rise in the region above the core due to the shielding effects.

Although a radiation shield will undoubtedly be provided, many of the components will still undergo excessive temperature rise rates during the

~~CONFIDENTIAL~~

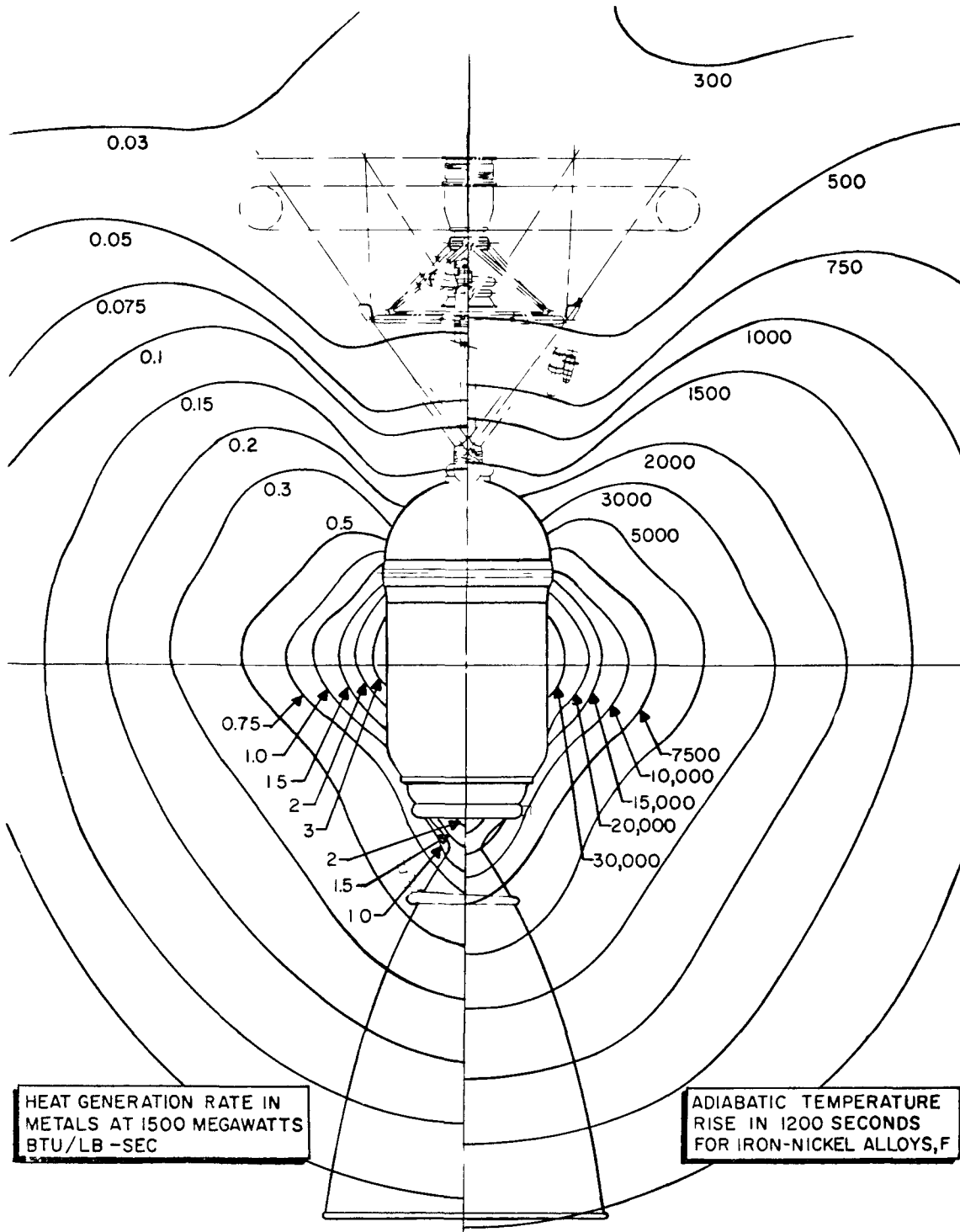


Figure 61 . Engine Thermal Environment

**CONFIDENTIAL**

---

1200 sec operating time. Rather than increase the shield necessary to limit the maximum temperature in these components, it is convenient to provide heat sinks of one form or another. The hydrogen propellant can be used to advantage to carry off much of the heat generated in the components. Enclosed parts of the lower thrust structure, for instance, would reach a temperature on the order of 1500 F without some means of enhancing the transfer of heat. Utilization of the thrust structure to transport the hydrogen propellant from the pump to the gimbal bearing offers a convenient method of cooling the structure members. Likewise the gimbal bearing and other components are sufficiently cooled as will be shown in following paragraphs.

In some cases thermal radiation to space provides adequate heat transfer to sufficiently limit a component's maximum temperature. Figure 62 indicates the effects of thermal radiation and shows the temperature which a part ( $C_p = 0.39$  Btu/lb-F,  $\rho = 0.1$  lb/in.<sup>3</sup>) will attain in 900 sec as a function of its emissivity, density, specific heat, and surface-to-volume ratio. This figure combines the effects of the heat capacity of the part and the effects of thermal radiation to space. It assumes uniform heat generation throughout the part (equivalent to infinite thermal conductivity) and an initial temperature of 40 F.

In order to account for the effects of radiation attenuation through a thick metal part and the subsequent nonuniform heating of a part with finite thermal conduction, Fig. 63 was constructed. This provides a correction factor for the ultimate temperature predicted in Fig. 62. The result is the temperature of the edge of a "thick" (1/4-in.) metal part nearest to the radiation source. As can be seen in the figure, the correction factor is a function of part material and its thickness in the direction of the radiation current. This figure is the result of a digital computer evaluation involving a theoretical equation for the case of

~~CONFIDENTIAL~~

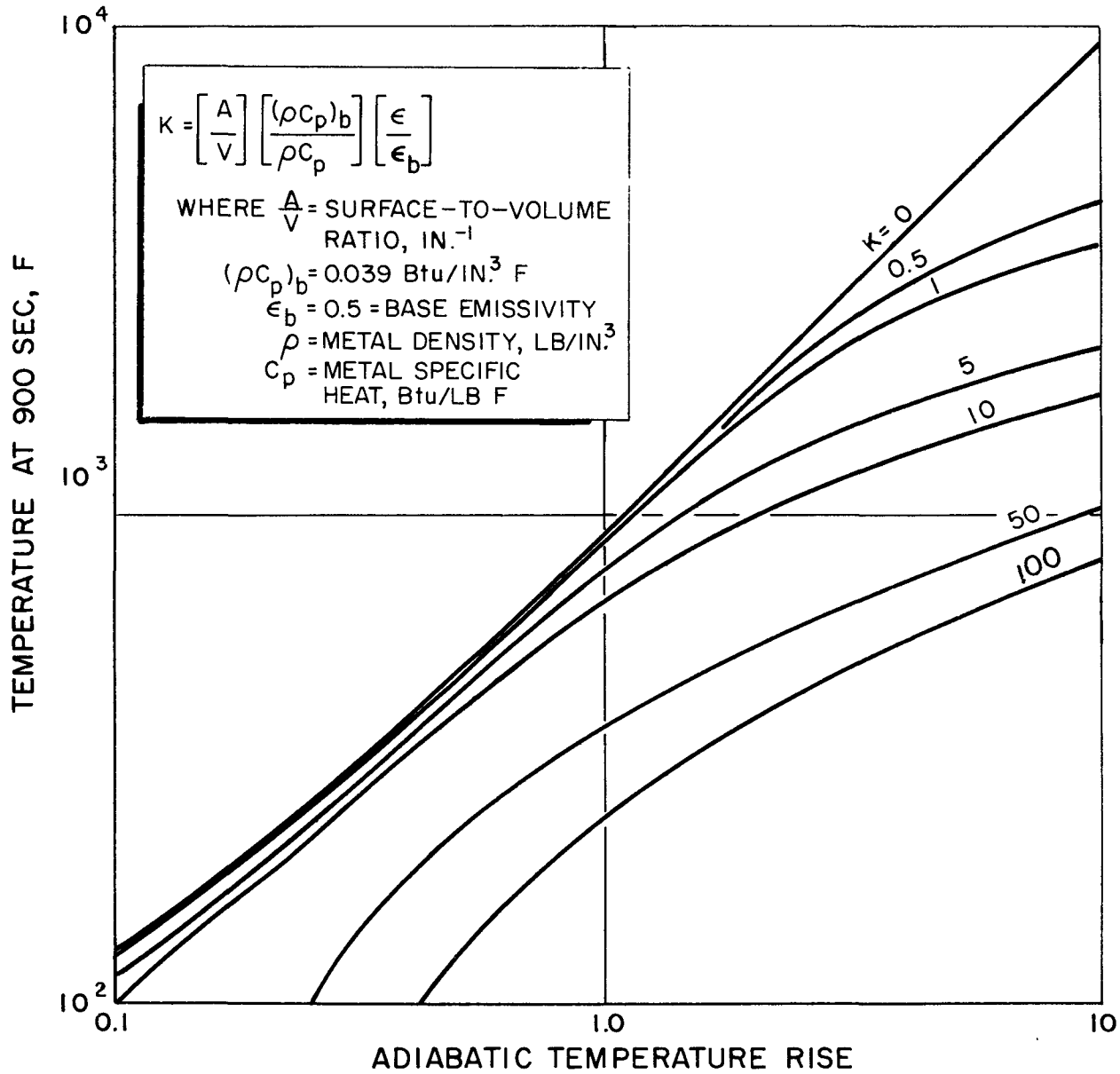


Figure 62. Effects of Thermal Radiation on End Temperature

**CONFIDENTIAL**

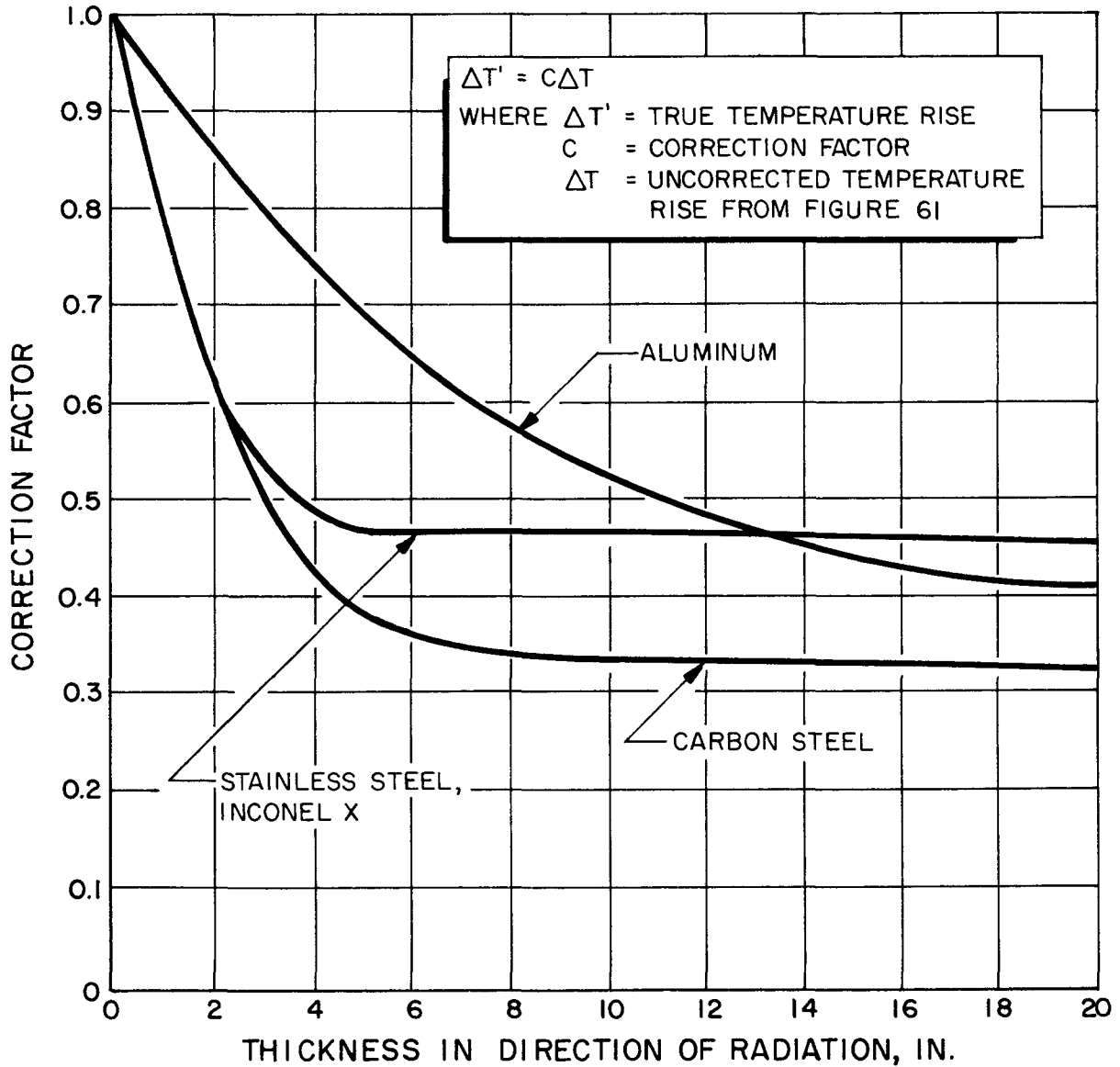


Figure 63. Correction Factor for Self-Attenuation and Thermal Conduction

~~CONFIDENTIAL~~

nonuniform heat generation in an insulated metal slab with the heat generation rate varying exponentially with distance. Figure 63 must be used with caution since variations will occur due to radiation scattering, intersection of radiation with the sides of the object due to nonpoint source geometry or component alignment, and proximity of object to the reactor. However, for use with objects two core diameters or more from the core center the figure can be used as presented.

#### COMPONENTS IN THE FLIGHT SYSTEM

The following are components in the flight-type system which were analyzed with regard to their internal heat generation and heat removal problems. All are located external to the reactor pressure shell as in Fig. 1; the components therein are treated separately.

#### Pneumatic Storage Tank

The tank well and contained gas are assumed to be in thermal equilibrium and the material convection coefficient between well and gas can be approximated by  $h \cong 16 \Delta T^{1/3}$

$$\text{Heat lost by thermal radiation} = \sigma \epsilon A_s T^4$$

$$\text{Heat input from solar radiation} = Q_s a A_p$$

$$\text{Heat input by nuclear radiation} = W_T Q_T + W_G Q_G$$

$$\text{Heat storage in the gas} = q = W_G C_{VG} \frac{dT_G}{d\theta} \approx W_G C_{VG} \frac{dT}{d\theta} \text{ if } T_G = T_T = T$$

$$\text{Heat storage in the metal} = q = W_T C_T \frac{dT}{d\theta}$$

The heat balance =

$$q \text{ in} = q \text{ out} + q \text{ stored}$$



**CONFIDENTIAL**

---

$$= (W_{\theta} C_{VG} + W_T C_T) \frac{dT}{d\theta} + \sigma \epsilon A_s T^4 = Q_s a A_p + W_T Q_T + W_G Q_G$$

where

- $A_p$  = projected surface area towards sun (ft<sup>2</sup>)
- $A_s$  = total surface area (ft<sup>2</sup>)
- $a$  = absorptivity
- $C$  = specific heat (V = constant volume) (G = Gas)
- $Q_s$  = solar heat input = (Btu/hr ft<sup>2</sup>)
- $Q$  = nuclear heat input (T = metal, G = gas)
- $T$  = temperature (R)
- $W$  = weight (lb)
- $\sigma$  = Stephan-Boltzman constant
- $\epsilon$  = emissivity
- $\theta$  = time (hr)

- Torus weight, lb = 850
- Torus pressure, psi = 3000
- Torus surface area, ft<sup>2</sup> = 117
- Torus projected area, ft<sup>2</sup> = 24
- Torus stored gas weight, lb = 36

~~CONFIDENTIAL~~

and emissivity of the titanium walls is 0.3 to 0.5, then the surface temperature at the end of 1200 sec operation of the 1500 Mw reactor will be:

$$\text{torus surface temperature} = 825 \text{ R}$$

An initial temperature of 560 R is assumed.

### Thrust Structure

The front thrust structure is not provided with forced convection cooling. It does, however, lose considerable heat by means of thermal radiation to space. With the hot end of the Inconel structure members situated about 110-in. from the core center the heating rate (Fig. 61 ) is about 0.035 F/sec or a final adiabatic temperature change of 420 in 1200 sec. These members have a surface to volume ratio ( $A/V$ ) of 8 indicating a reduction in the final temperature of about 90 F or a total temperature change at the hot end of the tubular members of 330 F.

The hottest parts of the front or uncooled thrust structure will be the pins used to join the turbopump mount structures. Since this pin is essentially insulated it will not radiate its heat. Also, since contact resistances to heat flow are difficult to predict, in this case a conservative assumption is that no heat will be transferred to the thrust structure members. It can then be assumed that the pin will undergo a temperature rise of up to 420 F. If the initial temperature of these components is approximately -150 F at time of reactor start-up, the final temperature of the "hot" end of the strut will be 180 F and the pin will reach about 270 F.

~~CONFIDENTIAL~~

~~CONFIDENTIAL~~

---

The high-temperature portion of the cooled thrust structure will be the clevis at the pump mount joints. By virtue of the cold hydrogen flowing through the tubes and the fairly short heat transfer distance (1.5 in.), the maximum temperature of the joint clevis will be approximately -370 F.

#### Development Test Pad Tank Support Struts

No thorough analysis has been performed on the free convection cooling of the development site tank support struts. However, the adiabatic temperature rise rate in these struts (aluminum at 25 ft from the core) will be approximately 0.17 F/sec, causing a 210 F temperature rise and a final temperature of about 270 F. Free convection air currents will reduce this.

#### Turbopump Mount Struts

Analysis of the six uncooled 1-3/4 in. OD by 0.107 in. wall Inconel X struts 3-1/2 ft (closest portion) from the reactor dome was performed. In this region the heat generation rate is approximately 0.05 Btu/lb-sec. The maximum adiabatic temperature rise is reduced approximately 15 percent due to thermal radiation having a "hot end" rise of 500 F. With an initial temperature of -150 F to -200 F the final 1200-sec maximum temperature will be 300 F to 350 F.

#### Turbopump

The most sensitive components in the Rocketdyne Mark 9 turbopump assembly are in the region of the turbine wheels. The wheels and blades all operate at fairly high design stresses. Therefore, an increase in temperature of even a few degrees will represent a relatively large decrease in the design safety factors.

~~CONFIDENTIAL~~

---

The two Inconel X turbine wheels are the most critical items. They are 3 in. thick from shaft inner surface to blade root and average  $3/4$  in. deep. The wheels are cooled by conduction to the blades and to the shaft, by exhaust gases across the rear face of the sixth-stage wheel, and by leakage gas from the blade region across the other faces.

The heat generation rate on the rear face of the sixth stage is approximately 0.033 Btu/lb-sec. The first stage will be shielded by the other wheels and will be subject to an average heating rate of about 0.002 Btu/lb-sec.

Since there are large uncertainties in the amount of gas flow which will leak through the blade seals to cool the wheels, the first-stage analysis was performed without considering this as a heat sink. It was assumed instead that the first-stage wheel would reach equilibrium by transferring its heat to the blades. It was further assumed that the sixth-stage wheel would be cooled by forced convection of the exhaust gas over its entire rear face.

The analysis indicates that the heat generated in the first-stage wheel will cause the wheel temperature to rise only 20 F. This will be negligible relative to the inlet gas temperature.

The temperature drop due to conduction across the sixth-stage wheel will amount to about 15 F if all of the heat generated within this wheel is assumed to be conducted to the rear face and then to the exhaust gas. Some of the constants of the heat transfer coefficient are uncertain without

~~CONFIDENTIAL~~

~~CONFIDENTIAL~~

---

some empirical data. However, exclusion calculations have shown that the wheel surface temperature should be limited to within 100 F to 150 F above the final exhaust gas temperature. As with the first-stage wheel, interstage seal leakage will further reduce this temperature.

#### Turbine Exhaust Expansion Joint

This joint is an internally tied bellows located in a region where radiation flux causes a heat generation rate of about 0.05 Btu/lb-sec. The component is fabricated of Inconel X throughout.

The center tie components are immersed in the exhaust gas which provides adequate forced convection cooling. The maximum temperature in the tie components is on the order of 5 F above the gas temperature.

The bellows is also cooled by the exhaust gas. A conservative analysis was performed on the bellows regarding the heat transfer across the surface film. Since the flow patterns and velocities within the convolutions are unknown it was assumed that the total heat transfer area was 0.2 in. of the bottom of each convolution. This amounts to about 20 percent of the total exposed surface area. The heat generated in the outer extremities of the convolutions thus must be conducted to the inner surfaces before being transferred to the exhaust gas. This conduction path plus the film resistance produces a temperature drop of about 14 F. The maximum temperature of the bellows will then exceed the exhaust gas by about 14 F. Convection currents within the convolutions will probably reduce this somewhat.

~~CONFIDENTIAL~~

**CONFIDENTIAL**

---

### Main Propellant Valve

The main propellant valve is to be located beside the gimbal bearing. It is constructed primarily of aluminum except for the piston, bolts, washers, etc., which are steel. The incident heat generation rate at this location is 0.15 Btu/lb-sec. Cold hydrogen flowing through the valve will act as a heat sink for most of the valve components.

An analysis of the valve assembly indicates that the maximum possible temperature increase attainable after 1200 sec of heating will be 750 F in the aluminum parts and 1120 F in the steel parts. With an initial temperature of -360 F this would result in maximum temperatures of 390 F in the aluminum and 760 F in the steel. However, because of self-shielding effects and thermal conduction in the components it was found that the probable maximum temperature with hydrogen flowing would be closer to about 150 F in both aluminum and steel parts.

### Duct Support Brackets

Aluminum brackets 0.02 in. thick are assumed to be used to support the hydrogen ducts mounted beside the pressure shell. Since these brackets will be in a rather high radiation flux (a heat generation rate of 4.0 to 4.5 Btu/lb-sec), the length will have to be limited and at least one end will have to be cooled. Welding the bracket to the pressure shell, the surface of which will be maintained at about 300 R, will satisfy the latter requirement.

Assuming a maximum temperature of 400 F for the extreme end of the bracket and assuming no heat transfer to or from the duct so all heat generated within the bracket flows to the pressure shell, a simple conduction solution with internal sources indicates that the maximum bracket length must not exceed 2.4 in. which appears to be a mechanically useful length.

**CONFIDENTIAL**

---

### Temperature Control Valve

The temperature control valve is located on top of the reactor dome about 5 ft from the core center. Heat generation rate at this location is about 0.15 Btu/lb-sec. The working fluid is liquid hydrogen at 50 R.

The material used will be primarily aluminum; some parts such as the piston and liner will use Inconel X. An alternate design may use aluminum for the piston material with steel piston rings.

Maximum temperatures in the aluminum parts will remain within 50 F of the coolant temperature; the steel parts remote from the hydrogen will run somewhat higher. If the use of steel is limited to the piston and liner, the maximum temperature will be within 300 F of the fluid temperature.

### Turbine Throttle Valve

The turbine throttle valve is located about 4 ft above the reactor dome. Turbine inlet gas at 1200 F flows through it during reactor operation. It is constructed primarily of Inconel X.

The temperature analysis was done by dividing the valve into two heat transfer zones separated by a "thermal barrier". In the zone containing the valve body through which the hot gas flows, the maximum temperature will be about 1300 F. This will occur approximately 1-in. from the periphery of the hot gas passage in the valve body and in the shaft. Temperatures will be lower in regions closer to the gas passage as well as outside of the 1-in. region, dropping to about 600 F at the thermal barrier.

The zone containing the gear boxes will undergo a maximum temperature rise of about 450 F. An initial temperature of -250 F will allow a maximum

~~CONFIDENTIAL~~

---

temperature in this region of 200 F. Forced cooling with gaseous hydrogen at 100 R will reduce the maximum temperatures to as low as 100 F.

#### Gas Generator Expansion Joint Bellows

This component will be included if a turbine gas generator is used in the engine system. The analysis is similar to that for the turbine exhaust expansion joint. Location and geometry differences cause a maximum temperature at the outer extremities of the bellows slightly higher than for the turbine exhaust bellows. This temperature is about 19 F higher than the gas temperature, or about 1419 F.

#### Gimbal Bearing

The temperature levels attained by the components of the gimbal bearing are critical because of the strict dimensional tolerances required. Although the Inconel X parts (pilot bolt, bearing and gimbal block) would still have useful strength at temperatures above 800 F, such a temperature is not acceptable since large thermal gradients and subsequent stresses would impede reliable gimbal operation.

Analysis of the pilot bolt indicates that the shielding effects of the gimbal block and cooling of the ends of the bolt with liquid hydrogen at 50 R will limit the maximum bolt temperature rise to about 400 F, producing a maximum temperature of about 0 F. This temperature can be further reduced if a coolant flow passage is drilled axially through the bolt.

Hydrogen coolant must be directed toward the central region of the gimbal block below the pilot bolt to maintain the gimbal block near room temperature. This component could reach 900 F in some places without such cooling.



**CONFIDENTIAL**

---

To maintain the upper region of the dome below 1000 F, several coolant flow passages should be provided. These passages can also direct additional coolant to the top of the gimbal block.

The bellows and the volute will be adequately cooled by the hydrogen flow. Their temperatures will be about -300 F and -400 F, respectively.

#### Gimbal Actuator

The gimbal actuator is composed primarily of Inconel X and steel. It is operated by a Lear pneumatic actuator using 0.08 lb/sec of hydrogen at 100 F and 1000 psia. The Lear actuator and associated moving parts are located approximately 100 in. from the core center while the base assembly is attached to the reactor dome. The highest temperatures will appear in the base assembly.

To facilitate cooling of the actuator components, including the base assembly, a fraction of the operating gas is allowed to leak through the system. This gas, bled from the supply duct in the upper regions of the actuator, flows through the total length of the system and is dumped into the reactor dome. In the absence of this coolant, and disregarding thermal radiation, the actuator base assembly would reach temperatures in excess of 1500 F from the heat generation rate of about 1.3 Btu/lb-sec in this region. The temperature limit in the base assembly with the coolant gas is of course a function of the flowrate and will vary from about 500 F with 100 percent of the total actuator flowrate used as coolant to about 640 F with 50 percent, 800 F with 25 percent, and 980 F with 10 percent.

The temperatures in the actuator will be substantially lower because of distance attenuation. The uncooled maximum temperature would be about 600 F. With 10 percent of the actuator hydrogen flowrate bled off, the actuator

**CONFIDENTIAL**

---

temperature will be about 300 F. Actual design of the cooling passages in the actuator will of course influence this temperature.

Flexible Metal Hose

The flexible metal hose which carries the 100 F pneumatic supply gas to the various actuators was analyzed for radiation heating. The model used for analysis was the Flexonics Co. Rex-Flex RF-51 with a single braid covering. It was assumed that the center portions of the hose would be maintained at near the 100 F gas temperature.

The outside metal braid temperature is a function of the braid wire emissivity and heat generation rate and is essentially independent of the hose diameter in the 0.218-in. to 0.500-in. range considered. Calculations of equilibrium temperatures resulting from the 0.15 Btu/lb-sec and thermal radiation to space and the inner tube, which is assumed to have an outside surface temperature of 200 F, result in the following maximum wire braid temperatures for a range of emissivities:

<u>Emissivity</u>	<u>Max Braid Temperature (F)</u>
1.0	230
0.5	330
0.25	460

These values appear to bracket reasonable values for emissivity and indicate noncritical temperature levels for the wire braid.

~~CONFIDENTIAL~~

---

Exhaust Gas Instrumentation

Thermocouples are used to measure the propellant temperature in the nozzle throat section. The thermocouple hot junction is subjected to 4500 F gas, and its leads are enclosed in a 0.25-in. OD tungsten tube. This tube extends through the nozzle wall where it is brazed to a stainless steel tube.

Besides the heat load imposed by the hot exhaust gases, the transducer assemblies are subjected to nuclear radiation heating of about 0.72 Btu/lb-sec. The only possible heat rejection other than by thermal radiation is to the nozzle wall which is composed on Inconel X tubes with 50 to 100 R hydrogen flowing through them. However, high contact resistance can be expected between the transducer and the wall.

With thermal radiation providing the major heat sink, the assembly will achieve a temperature in excess of 4000 F in 1200 sec of operation. Since this is too high for anything but the tungsten parts, a cooled shroud obviously must be provided to enclose the transducer assemblies.

Destruct System

An external destruct system designed to open the pressure shell and expose the reactor core for further demolition has been designed. It consists of a birdcage-shaped series of tubes completely encircling the reactor pressure shell. These tubes house a 1-in. diameter linear shaped charge of TNT. The cross section of the charge resembles a disk with a 60 degree "pie slice" cut from it. This pie slice is replaced with a similar one of aluminum, located to leave a 1/8-in. gap between it and the charge for cooling purposes.

~~CONFIDENTIAL~~

---

The system is mounted within a few inches of the pressure shell in a radiation flux, causing an average heat generation rate of about 2.5 Btu/lb-sec. Uncooled, the TNT would reach its autodetonation temperature in a very few minutes.

Heat transfer analysis has shown that if the surface of the charge is cooled the centerline temperature in steady state will be approximately 380 F higher than the surface. Since limiting the maximum temperature to 400 F is desirable, the surface temperature should be no higher than 0 F.

There are two potential sources of cold hydrogen for this cooling purpose. One method is to tap the liquid hydrogen off the main propellant feed line, direct it to the destruct system and exhaust it to the nozzle coolant discharge area. Flow required would be 0.12 lb/sec. Pressure loss through a 1/8-in. annulus would be about 0.01 psi. The second method would be to tap gaseous hydrogen from the nozzle coolant discharge and exhaust it to the reactor inlet area. With this method the required flow to maintain 0-deg surface temperature would be about 0.20 lb/sec with a pressure loss of 0.20 psi. In both cases the flowrates specified would sufficiently cool the steel outer tube.

#### Shield Heating

In a previous section it was shown that, of the three shield materials considered, the boronated graphite shield and the boronated zirconium hydride shield are the most effective from the standpoint of minimum shield weight. One of the considerations in determining which of these materials will provide the best shield design is the magnitude and distribution of the heat generation rates in these shields. This information is necessary to establish the shield cooling requirements and is used in the engine design.

**CONFIDENTIAL**

Heat generation rates were calculated for 3- and 5-inch zirconium hydride shields and for 9.88- and 16.47-inch boronated graphite shields. The results are shown on Fig. 64 through 67. The core gamma contribution was calculated in a manner analogous to the calculation performed for the propellant. The heat produced by the  $B^{10} (n, \alpha) Li^7$  reaction was calculated with the aid of the AIM-6 diffusion code. The capture rate in boron as a function of distance into the shield was obtained from the 16 group output of the AIM-6 code. Since the total energy released per boron capture is 2.88 Mev (2.40 Mev kinetic energy and 0.48 Mev gamma energy), the heat generation rate resulting from boron captures is

$$H(t) = 6.9 \times 10^{-14} \times 8.6 \times \frac{1}{\rho} \sum_{g=1}^{16} a_{,g} \phi_g(t) \text{ Btu/sec-lb,}$$

where

$H(t)$  = heat generation rate, Btu/lb-sec

$t$  = distance from the bottom of the shield

$\rho$  = shield density, gm/cc

$\sum a_{,g}$  = macroscopic absorption cross section for boron in group  $g$ ,  $\text{cm}^{-1}$

$\phi_g(t)$  = spatial distribution of the flux in group  $g$ ,  $\text{n/cm}^2\text{-sec}$

The energy release resulting from neutron capture in materials other than boron outside the core are negligible contributors to the shield heating. Furthermore, the contribution from fast neutron heating can be neglected.

**CONFIDENTIAL**

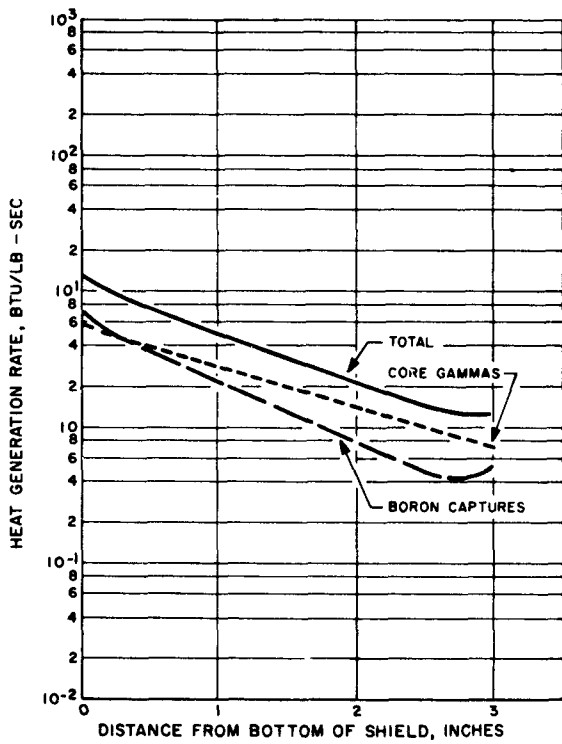


Figure 64 . Heat Generation in 3-Inch Zr H<sub>1.8</sub> One-Weight-Percent Boron Shield. Power Level, 1500 Mw

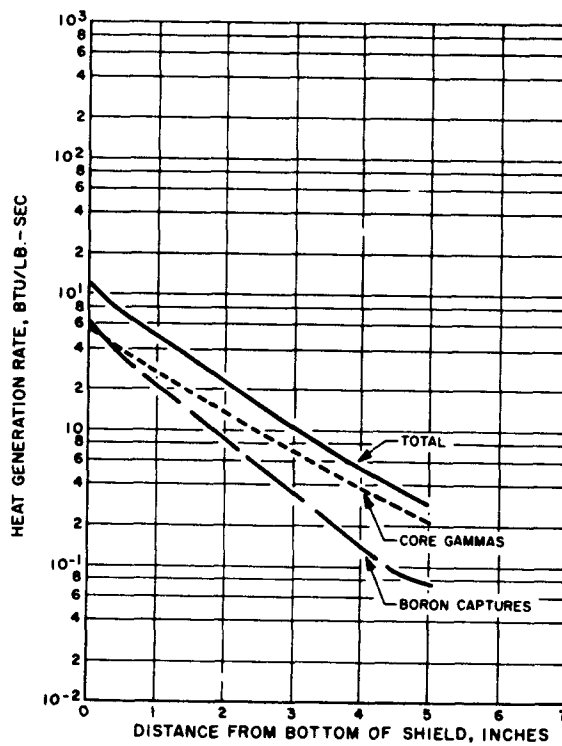


Figure 65 . Heat Generation in 5-Inch Zr H<sub>1.8</sub> One-Weight-Percent Boron Shield. Power Level, 1500 Mw

4

~~CONFIDENTIAL~~

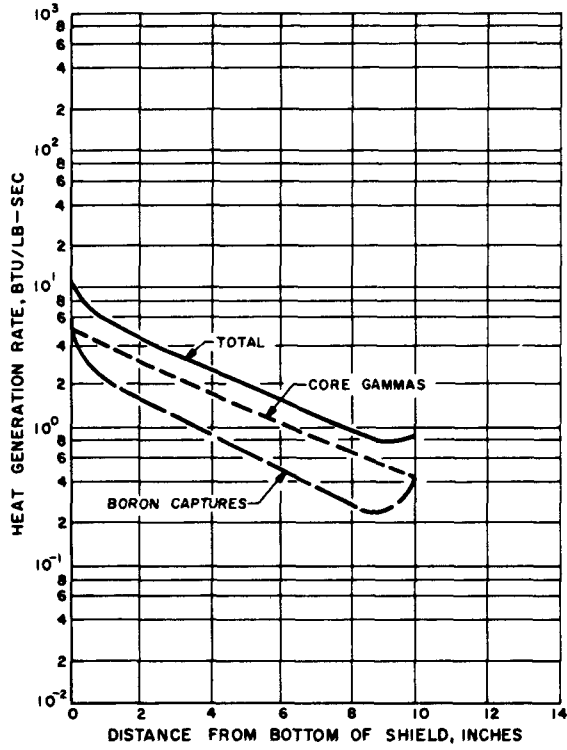


Figure 66. Heat Generation in 9.88-inch Boronated Graphite Shield. Power Level - 1500 Mw

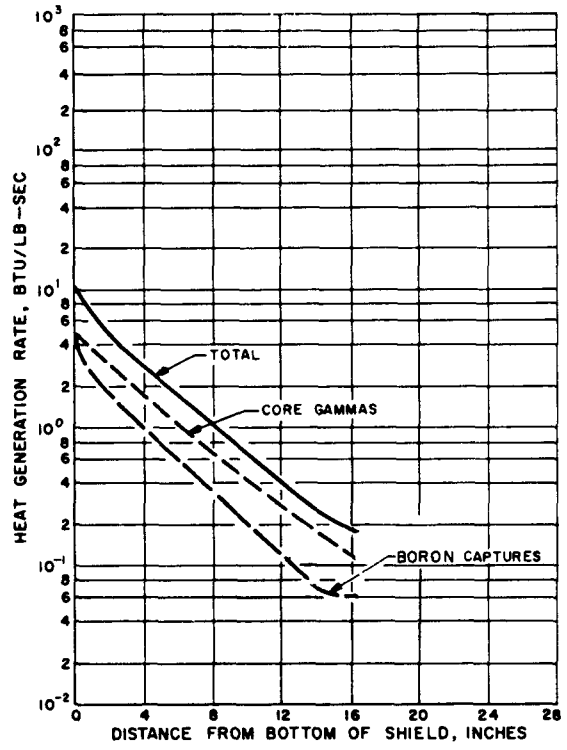


Figure 67. Heat Generation in 16.47-inch Boronated Graphite Shield. Power Level - 1500 Mw

~~CONFIDENTIAL~~

The shield chosen for heating analysis consists of graphite with 1 percent natural boron. It is assumed to be positioned  $1/2$  in. above the active core and is 13 in. thick. Coolant holes penetrate the shield directly over the core and are chevron-shaped in elevation to prevent radiation streaming. Each leg of a chevron forms a 20-deg angle with the core axis. The coolant holes comprise 20 percent of the total shield volume.

The heat generation in a 9.9-in. shield is shown in Fig. 66 as a function of location. With a graphite thermal conductivity of 130 Btu/hr/ft/F at 400 R, and a hydraulic diameter of  $1/2$  in. in the coolant holes which are spaced on a 1.1-in. pitch, the maximum thermal gradient in the shield material is about 33 F. With about 80 lb/sec of 250 R gaseous hydrogen flowing, the film temperature drop is about 120 F, causing a maximum material temperature of about 400 R. These temperatures and gradients are easily within the capabilities of the material in this application.

#### Nozzle Stiffening Bands

The stiffening bands oriented transverse to the nozzle wall tubes are brazed to these tubes every 0.244 in. with a 0.003-in. thick braze 0.1 in. wide. The bands are assumed to be Inconel X and are 0.040 in. thick with the maximum conduction path about 0.78 in. long. The band closest to the core is placed 20 in. downstream of the nozzle throat and is subjected to a radiation heat generation rate of 0.3 Btu/lb-sec.

Heat transfer analysis indicates that the nozzle coolant (-300 F in the tubes) will limit the band maximum temperature to about -100 F.



~~CONFIDENTIAL~~

---

RADIATION LEVELS FROM RADIOACTIVITY  
INDUCED IN MATERIALS AND COMPONENTS

Exposure of components and structural materials in the static test area to neutrons escaping from the reactor during a test will result in an important source of radiation. Most materials subjected to a neutron flux become radioactive by the transmutation of some stable atoms into one or more unstable types. With thermal neutrons, the usual reaction is a neutron capture by the target nucleus followed by the immediate ejection of a gamma ray ( $n, \gamma$ ). Fast neutrons can cause a wider variety of reactions such as ( $n, 2n$ ), ( $n, p$ ) and ( $n, \alpha$ ). Although the sum total of this additional radioactivity is insignificant compared to the prompt fission radiation emitted during reactor operation and also small compared to that emitted by fission products after reactor shutdown, it can be large enough to present a considerable radiation hazard in itself under certain conditions.

Considering only the gamma radiation emitted during decay of the induced radioactivity, the following general expression is applicable:

$$D_R = 2.33 \times 10^{-2} \frac{M}{r^2} \sum_m f_m \left[ \sum_n \phi_{th} \frac{\sigma_n F_n A_n}{W_n} (1 - e^{-\lambda_n t_1}) e^{-\lambda_n t_2} \right] \quad (71)$$

where:

- $D_R$  = Radiation level from irradiated object (r/hr) (assuming no self-absorption in the material and point source geometry)
- $M$  = Weight of object (pounds)
- $r$  = Distance from object (feet)

**CONFIDENTIAL**

- $m$  = Element  
 $f_m$  = Weight fraction of element  $m$  in object (fraction)  
 $n$  = Reaction  
 $\phi_{th}$  = Thermal neutron flux level at object position for  $(n, \gamma)$  reaction  
 $\phi_f$  = Fast neutron flux level for  $(n, \alpha)$ ,  $(n, p)$  and  $(n, 2n)$  reactions ( $n/cm^2/sec$ )  
 $\sigma_n$  = Activation cross section of reaction,  $n$  (barns)  
 $F_n$  = Isotopic abundance of target isotope of reaction,  $n$ , (fraction)  
 $A_n = \sum J_i K(E)_i$  where  
      $i$  = Energy  $E$  of photon emitted from product isotope  
      $J_i$  = Number of photons of energy  $E$  emitted per disintegration for reaction  $n$   
      $K(B)_i =$  Conversion factor  $\left( \frac{r/hr}{\text{photon}/cm^2\text{-sec}} \right)$   
 $W_n$  = Atomic weight of target isotope of reaction,  $n$ , (grams)  
 $\lambda_n$  = Disintegration constant associated with product isotope ( $\text{seconds}^{-1}$ )  
 $t_1$  = Irradiation time or reactor operating time (seconds)  
 $t_2$  = Decay time or time after shutdown (seconds)

The assumption of a point source geometry in the radiation level calculations will result in an overestimate of the dose rate at distances that are small compared to the largest physical dimensions of the source. If a high degree of accuracy is needed in a particular case, the specific source geometry and distance must be treated in a more complicated manner.

~~CONFIDENTIAL~~

The assumption of no self-absorption in the source material will also result in an appreciable overestimate of the dose rates when massive sources are involved. No general rule can be given, but for large objects (i.e., several hundred pounds) the reduction by self-absorption approaches a value of about 10. As with the source geometry factor, particular cases have to be treated in detail if greater accuracy is desired.

Table 9 lists the constituent elements and impurities in the alloys under consideration in this investigation. The weight fraction of each element and impurity in the alloys was obtained from this table and used as the fixed parameter,  $f_m$ , in Eq. 71.

Table 10 lists the most important neutron-induced reactions and product isotopes expected from the elements in the alloys listed in Table 9. The basic nuclear reaction and product data for the various radioisotopes are also presented in this table. The following were obtained from the table and used as fixed parameters in Eq. 71.

- $\sigma$  (activation cross section)
- $F_n$  (isotopic abundance of target element)
- $W_n$  (atomic weight of target isotope)
- $J$  (number of photons of energy  $E$  per disintegration)
- $K$  (conversion factor to change flux to  $r/hr$ )
- $\lambda$  (disintegration constant or  $0.693/\text{half-life}$ )

Table 11 shows the specific radiation levels ( $r/hr/lb$ ) from one pound of a basic element for selected times after shutdown. Table 12 gives the same data for some reactor-grade materials. The tabulated values for each element were calculated from Eq. 71 using the following assumed conditions:

TABLE 9  
COMPOSITION OF ALLOYS (IN PERCENT)

ALLOY	INCO 713	INCO 718	INCONEL	INCONEL X	HASTELLOY B	HASTELLOY C	K MONEL	TRW-1800	NICKEL A	INCO 713 (R.G.)	INCO 718 (R.G.)	INCONEL (R.G.)	INCONEL X (R.G.)	HASTELLOY B (R.G.)	HASTELLOY C (R.G.)	K MONEL (R.G.)	RENE 41	WASPALLOY	UDIMET 500	HS-21	HS-31	AI10AT	6 Al-4V	B 120 BCA
ALLOY CLASSIFIED ELEMENT	Ni	Ni	Ni	Ni	Ni	Ni	Ni	Ni	Ni	Ni	Ni	Ni	Ni	Ni	Ni	Ni	Ni-Co	Ni-Co	Ni-Co	Ni-Co	Ni-Co	Ti	Ti	Ti
H																						0.003-0.02	0.015*	250 ppm
Be																								
B	0.005/0.020									0.005/0.020							0.003-0.01	0.005	0.003-0.01	0.007*				
C	0.08/0.20	0.10*	0.15*	0.08*	0.05*	0.08*	0.25*	0.07/0.12	0.06	0.08/0.30	0.10*	0.15*	0.08*	0.05*	0.08*	0.25*	0.12*	0.1*	0.1*	0.2-0.3	0.45-0.55	0.15*	0.08*	0.05*
N																						0.07*	0.05*	0.08*
Mg																								
Al	5.5/6.5	0.2/1.0		0.4/1.0			2/4	5.75/6.5		5.5/6.5	0.2/1.0		0.4/1.0			2-4	1.4-1.8	1.9-1.5	2.5-3.25			4-6	5.5-6.5	3
Si	0.5*	0.75*	0.50*	0.50*	1.0*	1.0*	1.0*		0.05	0.5*	0.75*	0.50*	0.50*	1.0*	1.0*	1.0*	0.5*	0.75*	0.30*	0.1*	0.1*			
P					0.04*	0.04*								0.04*	0.04*									
S	0.015*	0.03*	0.015*	0.01*	0.03*	0.03*			0.005	0.015*	0.03*	0.015*	0.01*	0.03*	0.03*		0.015*	0.03*	0.015*		0.04*			
Ti	0.35/0.90	0.3/1.3		2.25/2.75			0.25/1.0	0.3/1.0		0.35/0.90	0.3/1.3		2.25/2.75			0.25-1.0	3-3.3	2.2-2.8	2.5-3.25			BAL.	BAL.	BAL.
V					0.20/0.60	0.35*								0.20-0.60	0.35*								3.5-4.5	13.5
Cr	11/14	17/21	14/17	14/17	1.0*	14.5/16.5		12/14		11/14	17/21	14/17	14/17	1.0*	14.5-16.5		18-20	18-21	16-20	25-29	24.5-26.5			11
Mn	0.2*	0.5*	1.0*	1.0*	1.0*	1.0*	1.5*		0.25	0.2*	0.5*	1.0*	1.0*	1.0*	1.0*	1.5*	0.1*	1.0*	0.20*	0.1*	0.1*	0.3*		
Fe	2.5*	BAL.	6/10	5/9	4/7	4/7	2.0*		0.15	2.5*	BAL.	6/10	5/9	4-7	4-7	2.0*	5*	2*	2*	3*	2*	0.5*	0.25*	
Co	1.0*	1.0*	1.0*	1.0*	2.5*	2.5*	1.0	1.0*	1.0*	0.1	0.1	0.1	0.1	0.1*	0.1*	0.1*	10-12	12-15	16-20	BAL.	BAL.			
Ni	BAL.	50/55	72 <sup>□</sup>	70 <sup>□</sup>	BAL.	BAL.	63/70	BAL.	99.45	BAL.	50/55	72 <sup>□</sup>	70 <sup>□</sup>	BAL.	BAL.	63/70	BAL.	BAL.	BAL.	1.75-3.75	9.5-11.5			
Cu		0.75*	0.50*	0.50*			BAL.		0.05		0.75*	0.50*	0.50*			BAL.		0.5*	0.1*					
Zn																								
Zr	0.05/0.2							0.03/0.1		0.05/0.2								0.005						
Cb(Nb)																								
Cb+Ta	1.5/2.5	4.75/5.75		0.7/1.2							4.75/5.75		0.7/1.2											
Mo	3.5/5.5	2.8/3.3			36	15/17				3.5/5.5	2.8/3.3			36	15-17		9-10.5	2.5-4.5	3-5	5-6				
Cd																								
Sn																						2-3		
Sb																								
Ta	0.1* Cb+Ta	0.1* Cb+Ta		0.1* Cb+Ta						0.1*	0.1*		0.1*											
W						3/4.5		8/10																

\* MAXIMUM □ MINIMUM

TABLE 9  
(Continued)

ALLOY	A286	321	310	347	348	29-20	440-C	19-9DL	19-9DX	16-25-6	4340	4150	6061	6066	7075	2014	2024	TENS-50	7079	Be-Cu	Cu (OXYGEN FREE)	Cr-Cu
ALLOY CLASSIFICATION ELEMENT	SS	SS	SS	SS	SS	SS	SS	SS	SS	SS	STEEL	STEEL	Al	Al	Al	Al	Al	Al	Al	Cu	Cu	Cu
H																						
Be																		0.1-0.3		2.0		
B																						
C	0.08*	0.08*	0.25*	0.10*	0.08*	0.07*	0.95-1.20	0.28-0.35	0.28-0.35	0.12*	0.38-0.43	0.30										
N										0.1-0.2												
Mg													0.8-1.2	0.8-1.4	2.1-2.9	0.2-0.8	1.2-1.8	0.4-0.6				
Al													BAL.	BAL.	BAL.	BAL.	BAL.	BAL.				
Si	0.4-1.0	1.0*	1.5*	1.0*	1.0*	1.0*	1.0*	0.3-0.8	0.3-0.8	0.3-0.8	0.2-0.35		0.4-0.8	0.9-1.8	0.5*	0.5-1.2	0.5*	7.6-8.6				
P	0.04*	0.04*	0.04*	0.04*		0.03*	0.04*	0.04*	0.04*	0.04*	0.04*											
S	0.03*	0.03*	0.03*	0.03*		0.015*	0.03*	0.03*	0.03*	0.03*	0.04*											
Ti	1.9-3.3	0.4			0.8 <sup>□</sup>			0.1-0.35	0.4-0.75				0.15*	0.20*	0.2*	0.15*		0.1-0.2				
V	0.1-0.5																					
Cr	13.5-16	17-19	24-26	17-19	17-19	19-21	16-18	18-21	18-21	15-17.5	0.7-0.9	1.0	0.15-0.35	0.4*	0.18-0.4	0.10*	0.10*					0.5
Mn	1-2	2.0*	2.0*	2.0*	2.0*	1.0*	1.0*	0.75-1.50	0.75-1.50	2*	0.65-0.85	0.50	0.15*	0.6-1.1	0.3*	0.4-1.2	0.3-0.9					
Fe	BAL.	BAL.	BAL.	BAL.	BAL.	BAL.	BAL.	BAL.	BAL.	BAL.	BAL.	BAL.	0.7*	0.5*	0.7*	1.0*	0.5*	0.4*				
Co																				0.3		
Ni	24-27	8-11	19-22	9-12	9-13	28-32	0.75*	8-11	8-11	24-27	1.65-2.0											
Cu						3-4		0.5*	0.5*	0.5*			0.15-0.40	0.7-1.2	1.2-2.0	3.9-5.0	3.8-4.9			97.7	99.92	99.5
Zn													0.25*	0.25*	5.1-6.1	0.25*	0.25*					
Zr																						
Cb(Nb)					0.8 <sup>□</sup>																	
Cb+Ta						1.0*		0.25-0.60														
Mo	1.0-1.5					2-3	0.4-0.6	1-1.75	1.25-2	5.5-7	0.2-0.3	0.2										
Cd																						
Sn																						
Sb																						
Ta					0.1*																	
W								1-1.75	1-1.75													

TABLE 10  
NUCLEAR REACTIONS AND PRODUCT ISOTOPE DATA

TARGET, REACTION, % PRODUCT	F	$\sigma^*$	HALF-LIFE (AS NOTED)	$\lambda$	E	J	K
	TARGET ABUNDANCE FRACTION	CROSS SECTION BARNs		SEC <sup>-1</sup>	GAMMA ENERGY MeV	$\gamma$ PHOTONS DISINTEGRATION	r/hr photon/km <sup>2</sup> sec
Mg <sup>26</sup> (n, $\gamma$ )Mg <sup>27</sup>	0.113	0.027	10.2 m	$1.13 \times 10^{-3}$	0.84 1.01	0.7 0.3	$1.67 \times 10^{-6}$ $1.95 \times 10^{-6}$
Mg <sup>24</sup> (n,p)Na <sup>24</sup>	0.786	0.0013 (4.95)	15.0 h	$1.28 \times 10^{-5}$	1.38 2.75	1.0 1.0	$2.47 \times 10^{-6}$ $4.05 \times 10^{-6}$
Al <sup>27</sup> (n, $\gamma$ )Al <sup>28</sup>	1.00	0.21	23 m	$5.02 \times 10^{-3}$	1.78	1.0	$2.96 \times 10^{-6}$
Al <sup>27</sup> (n, $\alpha$ )Na <sup>24</sup>	1.00	0.0006 (3.3)	15.0 h	$1.28 \times 10^{-5}$	1.38 2.75	1.0 1.0	$2.47 \times 10^{-6}$ $4.05 \times 10^{-6}$
Al <sup>27</sup> (n,p)Mg <sup>27</sup>	1.00	0.0034 (1.9)	10.2 m	$1.13 \times 10^{-3}$	0.84 1.01	0.7 0.3	$1.67 \times 10^{-6}$ $1.95 \times 10^{-6}$
Ti <sup>50</sup> (n, $\gamma$ )Ti <sup>51</sup>	0.053	0.14	6.0 m	$1.92 \times 10^{-3}$	0.3	0.95	$6.1 \times 10^{-7}$
Ti <sup>46</sup> (n,p)Sc <sup>46</sup>	0.08	0.0041 (1.61)	85.0 d	$9.44 \times 10^{-8}$	0.89 1.12	1.0 1.0	$1.74 \times 10^{-6}$ $2.10 \times 10^{-6}$
Ti <sup>47</sup> (n,p)Sc <sup>47</sup>	0.0775	0.00021 (-0.09)	3.4 d	$2.36 \times 10^{-6}$	0.16	0.74	$2.86 \times 10^{-7}$
Ti <sup>48</sup> (n,p)Sc <sup>48</sup>	0.734	0.00077 (3.25)	44.0 h	$4.37 \times 10^{-6}$	1.33 0.98 1.00	1.0 1.0 1.0	$2.41 \times 10^{-6}$ $1.98 \times 10^{-6}$ $1.93 \times 10^{-6}$
V <sup>51</sup> (n, $\alpha$ )Sc <sup>48</sup>	0.9975	0.00008 (2.14)	44.0 h	$4.37 \times 10^{-6}$	1.33 0.98 1.0	1.0 1.0 1.0	$2.41 \times 10^{-6}$ $1.90 \times 10^{-6}$ $1.93 \times 10^{-6}$
Cr <sup>50</sup> (n, $\gamma$ )Cr <sup>51</sup>	0.044	13.5	27.8 d	$2.89 \times 10^{-7}$	0.32	0.10	$1.35 \times 10^{-6}$
Mn <sup>55</sup> (n, $\gamma$ )Mn <sup>56</sup>	1.0	13.4	2.59 h	$7.43 \times 10^{-5}$	0.84 1.81 2.13	1.0 0.25 0.15	$1.67 \times 10^{-6}$ $3.05 \times 10^{-6}$ $3.38 \times 10^{-6}$
Fe <sup>58</sup> (n, $\gamma$ )Fe <sup>59</sup>	0.0033	0.98	46 d	$1.74 \times 10^{-7}$	1.1 1.3	0.5 0.5	$2.07 \times 10^{-6}$ $2.37 \times 10^{-6}$
Fe <sup>54</sup> (n,p)Mn <sup>54</sup>	0.0584	0.0534 (-0.16)	291 d	$2.76 \times 10^{-8}$	0.84	1.0	$1.67 \times 10^{-6}$
Fe <sup>54</sup> (n, $\alpha$ )Cr <sup>51</sup>	0.0584	0.0037 (-0.86)	27.8 d	$2.89 \times 10^{-7}$	0.32	0.1	$6.5 \times 10^{-7}$
Fe <sup>56</sup> (n,p)Mn <sup>56</sup>	0.916	0.00087 (2.94)	2.59 h	$7.43 \times 10^{-5}$	0.84 1.81 2.13	1.0 0.25 0.15	$1.67 \times 10^{-6}$ $3.05 \times 10^{-6}$ $3.38 \times 10^{-6}$
Co <sup>59</sup> (n, $\gamma$ )Co <sup>60</sup>	1.00	36.3	5.3 y	$4.15 \times 10^{-9}$	1.17 1.33	1.0 1.0	$2.19 \times 10^{-6}$ $2.14 \times 10^{-6}$
Co <sup>59</sup> (n,p)Fe <sup>59</sup>	1.00	0.00025 (0.79)	46 d	$1.74 \times 10^{-7}$	1.10 1.30	0.5 0.5	$2.07 \times 10^{-6}$ $2.37 \times 10^{-6}$
Co <sup>59</sup> (n, $\alpha$ )Mn <sup>56</sup>	1.00	0.00014 (-0.44)	2.59 h	$7.43 \times 10^{-5}$	0.84 1.81 2.13	1.00 0.25 0.15	$1.67 \times 10^{-6}$ $3.05 \times 10^{-6}$ $3.38 \times 10^{-6}$
Ni <sup>64</sup> (n, $\gamma$ )Ni <sup>65</sup>	0.01	1.6	2.56 h	$7.51 \times 10^{-5}$	1.12 1.49	0.14 0.29	$2.1 \times 10^{-6}$ $2.64 \times 10^{-6}$
Ni <sup>58</sup> (n,p)Co <sup>58</sup>	0.678	0.027 (-0.64)	72 d	$1.12 \times 10^{-7}$	0.81	1.00	$1.62 \times 10^{-6}$
Ni <sup>60</sup> (n,p)Co <sup>60</sup>	0.62	0.002 (2.07)	5.3 y	$4.15 \times 10^{-9}$	1.17 1.33	1.00 1.00	$2.19 \times 10^{-6}$ $2.41 \times 10^{-6}$
Ni <sup>62</sup> (n, $\alpha$ )Fe <sup>59</sup>	0.366	0.000013 (0.884)	46 d	$1.74 \times 10^{-7}$	1.10 1.30	0.50 0.50	$2.07 \times 10^{-6}$ $2.37 \times 10^{-6}$
Cu <sup>63</sup> (n, $\gamma$ )Cu <sup>64</sup>	0.69	4.3	12.8 h	$1.5 \times 10^{-5}$	0.51	0.37	$1.05 \times 10^{-6}$
Cu <sup>63</sup> (n, $\alpha$ )Co <sup>60</sup>	0.69	0.00014 (-0.44)	5.3 y	$4.15 \times 10^{-9}$	1.17 1.33	1.00 1.00	$2.19 \times 10^{-6}$ $2.41 \times 10^{-6}$
Cu <sup>65</sup> (n,p)Ni <sup>65</sup>	0.31	0.0032 (2.3)	2.56 h	$7.51 \times 10^{-5}$	1.12 1.49	0.14 0.29	$2.10 \times 10^{-6}$ $2.64 \times 10^{-6}$

\*(Number in parentheses is the threshold energy in Mev)

CONFIDENTIAL

CONFIDENTIAL

ROCKETDYNE  
A Division of North American Aviation, Inc.

CONFIDENTIAL

TABLE 10  
(Continued)

TARGET, REACTION, % PRODUCT	F TARGET ABUNDANCE FRACTION	$\sigma^*$ CROSS SECTION BARNs	HALF-LIFE (AS NOTED)	$\lambda$ SEC <sup>-1</sup>	E GAMMA ENERGY MeV	J PHOTONS DISINTEG.	K r/hr photon/cm <sup>2</sup> -sec
Zn <sup>64</sup> (n, $\gamma$ )Zn <sup>65</sup>	0.489	0.44	250 d	$3.21 \times 10^{-8}$	1.12	0.45	$2.10 \times 10^{-6}$
Zn <sup>68</sup> (n, $\gamma$ )Zn <sup>69m</sup>	0.186	0.097	14 h	$1.37 \times 10^{-5}$	0.44	1.0	$9.2 \times 10^{-7}$
Zn <sup>68</sup> (n, $\alpha$ )Ni <sup>65</sup>	0.186	0.00002 (-0.93)	2.56 h	$7.51 \times 10^{-5}$	1.49	0.25	$5.45 \times 10^{-6}$
					1.12	0.18	$3.16 \times 10^{-6}$
					0.37	0.04	$2.52 \times 10^{-7}$
Zn <sup>64</sup> (n,p)Cu <sup>64</sup>	0.489	0.0365 (-0.22)	12.8 h	$1.5 \times 10^{-5}$	0.51	0.37	$1.05 \times 10^{-6}$
Zn <sup>67</sup> (n,p)Cu <sup>67</sup>	0.041	0.0561 (-0.214)	61 h	$3.15 \times 10^{-6}$	0.19	0.29	$3.55 \times 10^{-7}$
					0.09	0.665	$1.42 \times 10^{-7}$
Zn <sup>94</sup> (n, $\gamma$ )Zn <sup>95</sup> Nb <sup>95</sup>	0.174	0.09	65 d (65-35d)	$1.24 \times 10^{-7}$	0.75	1.00	$1.5 \times 10^{-6}$
					0.77	0.99	$1.53 \times 10^{-6}$
					0.23	0.01	$4.45 \times 10^{-7}$
Zr <sup>96</sup> (n, $\gamma$ )Zr <sup>97</sup>	0.028	0.10	17 h	$1.13 \times 10^{-5}$	0.75	1.00	$1.5 \times 10^{-6}$
					0.67	1.00	$1.38 \times 10^{-6}$
Mo <sup>92</sup> (n, $\gamma$ )Mo <sup>93m</sup>	0.157	<0.006	6.7 h	$2.87 \times 10^{-5}$	0.26	1.00	$5.1 \times 10^{-7}$
					0.68	1.00	$1.38 \times 10^{-6}$
					1.48	1.00	$2.60 \times 10^{-6}$
Mo <sup>98</sup> (n, $\gamma$ )Mo <sup>99</sup>	0.238	0.45	67 h	$2.87 \times 10^{-6}$	0.14	0.10	$2.45 \times 10^{-7}$
					0.18	0.90	$3.34 \times 10^{-7}$
					0.37	small	$7.6 \times 10^{-7}$
					0.74	0.10	$1.49 \times 10^{-6}$
					0.78	0.10	$1.56 \times 10^{-6}$
Mo <sup>100</sup> (n, $\gamma$ )Mo <sup>101</sup>	0.95	0.20	15 m	$7.7 \times 10^{-4}$	0.08	0.94	$1.31 \times 10^{-7}$
					0.40	1.90	$8.25 \times 10^{-7}$
					1.5	0.15	$2.65 \times 10^{-6}$
Mo <sup>92</sup> (n,p)Nb <sup>92</sup>	0.159	0.0013 (-0.416)	10 d	$8.01 \times 10^{-7}$	0.93	0.98	$1.8 \times 10^{-6}$
					1.83	0.03	$3.05 \times 10^{-6}$
Mo <sup>92</sup> (n, $\alpha$ )Zr <sup>89</sup>	0.159	0.00017 (-3.00)	79 h	$2.44 \times 10^{-6}$	0.91	1.0	$1.78 \times 10^{-6}$
Mo <sup>95</sup> (n,p)Nb <sup>95</sup>	0.157	0.0001 (0.150)	35 d	$2.3 \times 10^{-7}$	0.77	0.99	$1.53 \times 10^{-6}$
Cd <sup>106</sup> (n, $\gamma$ )Cd <sup>107</sup>	0.012	1.0	6.7 h	$2.87 \times 10^{-5}$	0.09	0.99	$1.42 \times 10^{-7}$
Cd <sup>114</sup> (n, $\gamma$ )Cd <sup>115m</sup>	0.288	0.14	43 d	$1.87 \times 10^{-7}$	1.30	0.02	$2.38 \times 10^{-6}$
					0.95	0.94	$1.84 \times 10^{-6}$
					0.48	0.12	$9.9 \times 10^{-7}$
Cd <sup>114</sup> (n, $\gamma$ )Cd <sup>115</sup>	0.0288	1.1	58 h	$3.32 \times 10^{-6}$	0.34	0.58	$6.95 \times 10^{-7}$
					0.36	0.42	$7.35 \times 10^{-7}$
					0.52	0.42	$1.07 \times 10^{-6}$
Cd <sup>116</sup> (n, $\gamma$ )Cd <sup>117</sup>	0.076	1.5	2.9 h	$6.63 \times 10^{-5}$	1.2	1.00	$2.23 \times 10^{-6}$
Sb <sup>121</sup> (n, $\gamma$ )Sb <sup>122</sup>	0.572	6.8	2.8 d	$2.87 \times 10^{-6}$	0.56	0.70	$1.16 \times 10^{-6}$
Sb <sup>122</sup> (n, $\gamma$ )Sb <sup>124</sup>	0.428	2.5	60 d	$1.34 \times 10^{-7}$	0.600	1.00	$1.22 \times 10^{-6}$
					1.70	0.43	$2.90 \times 10^{-6}$
					2.09	0.06	$3.33 \times 10^{-6}$
					0.75	0.30	$1.50 \times 10^{-6}$
Ta <sup>181</sup> (n, $\gamma$ )Ta <sup>182</sup>	1.0	19	111 d	$7.23 \times 10^{-8}$	0.66	0.31	$1.35 \times 10^{-6}$
					1.22	0.91	$2.25 \times 10^{-6}$
					0.20	0.60	$3.78 \times 10^{-7}$
W <sup>180</sup> (n, $\gamma$ )W <sup>181</sup>	0.0014	10	140 d	$5.73 \times 10^{-8}$	0.14	0.0029	$2.44 \times 10^{-7}$
W <sup>186</sup> (n, $\gamma$ )W <sup>187</sup>	0.287	34	24 h	$8.03 \times 10^{-6}$	0.69	0.80	$1.40 \times 10^{-6}$

\*(Number in parentheses is the threshold energy in Mev)

TABLE 11  
 SPECIFIC RADIATION LEVELS FROM ELEMENTS PER UNIT FLUX  
 (FAST AND THERMAL)

ELEMENT & REACTION	RADIATION LEVEL 1 FT. FROM 1 LB. OF THE ELEMENT/UNIT EFFECTIVE FLUX					
	NO DECAY r/hr	1 DAY r/hr	5 DAYS r/hr	10 DAYS r/hr	15 DAYS r/hr	30 DAYS r/hr
ALUMINUM THERMAL	$5.3 \times 10^{-10}$	—	—	—	—	—
FAST	$3.33 \times 10^{-12}$	$1.25 \times 10^{-14}$	$1.5 \times 10^{-16}$	$6 \times 10^{-19}$	—	—
MAGNESIUM THERMAL	$3.06 \times 10^{-12}$	—	—	—	—	—
FAST	$7.35 \times 10^{-15}$	$2.4 \times 10^{-15}$	$2.7 \times 10^{-17}$	$1 \times 10^{-19}$	—	—
TITANIUM THERMAL	—	—	—	—	—	—
FAST	$7.24 \times 10^{-16}$	$5.05 \times 10^{-16}$	$1.52 \times 10^{-16}$	$6.55 \times 10^{-17}$	$5.00 \times 10^{-17}$	$4.2 \times 10^{-17}$
CHROMIUM THERMAL	$9.73 \times 10^{-15}$	$9.7 \times 10^{-15}$	$8.4 \times 10^{-15}$	$7.4 \times 10^{-15}$	$6.5 \times 10^{-15}$	$4.5 \times 10^{-15}$
FAST	—	—	—	—	—	—
VANADIUM THERMAL	—	—	—	—	—	—
FAST	$8.9 \times 10^{-16}$	$6.1 \times 10^{-16}$	$1.35 \times 10^{-16}$	$2.05 \times 10^{-17}$	$3.0 \times 10^{-18}$	$1.2 \times 10^{-20}$
MANGANESE THERMAL	$1.13 \times 10^{-9}$	$1.5 \times 10^{-12}$	—	—	—	—
FAST	—	—	—	—	—	—
IRON THERMAL	$4.51 \times 10^{-16}$	$4.4 \times 10^{-16}$	$4.1 \times 10^{-16}$	$3.8 \times 10^{-16}$	$3.6 \times 10^{-16}$	$2.9 \times 10^{-16}$
FAST	$6.29 \times 10^{-14}$	$1.95 \times 10^{-16}$	$5.41 \times 10^{-17}$	$5.4 \times 10^{-17}$	$5.31 \times 10^{-17}$	$5.25 \times 10^{-17}$
COBALT THERMAL	$2.46 \times 10^{-13}$	$2.46 \times 10^{-13}$	$2.46 \times 10^{-13}$	$2.46 \times 10^{-13}$	$2.46 \times 10^{-13}$	$2.46 \times 10^{-13}$
FAST	$1.05 \times 10^{-14}$	$5.4 \times 10^{-17}$	$3.2 \times 10^{-17}$	$2.9 \times 10^{-17}$	$2.7 \times 10^{-17}$	$2.1 \times 10^{-17}$
NICKEL THERMAL	$4.04 \times 10^{-13}$	$4.0 \times 10^{-16}$	—	—	—	—
FAST	$5.91 \times 10^{-14}$	$1.12 \times 10^{-14}$	$1.14 \times 10^{-15}$	$1.09 \times 10^{-15}$	$1.03 \times 10^{-15}$	$9.05 \times 10^{-16}$
COPPER THERMAL	$5.68 \times 10^{-12}$	$1.6 \times 10^{-12}$	$9.0 \times 10^{-15}$	$1.4 \times 10^{-17}$	$2 \times 10^{-20}$	—
FAST	$2.58 \times 10^{-14}$	$1.0 \times 10^{-16}$	$6.14 \times 10^{-19}$	$6.14 \times 10^{-19}$	$6.14 \times 10^{-19}$	$6.14 \times 10^{-19}$
ZINC THERMAL	$7.19 \times 10^{-14}$	$2.4 \times 10^{-15}$	$2.33 \times 10^{-15}$	$2.1 \times 10^{-15}$	$2.1 \times 10^{-15}$	$2.1 \times 10^{-15}$
FAST	$3.41 \times 10^{-14}$	$1.04 \times 10^{-14}$	$1.65 \times 10^{-16}$	$2.9 \times 10^{-17}$	$7.5 \times 10^{-18}$	$1.2 \times 10^{-19}$
ZIRCONIUM THERMAL	$2.04 \times 10^{-14}$	$1.46 \times 10^{-14}$	$6.85 \times 10^{-15}$	$6.81 \times 10^{-15}$	$6.80 \times 10^{-15}$	$6.80 \times 10^{-15}$
FAST	—	—	—	—	—	—
MOLYBDENUM THERMAL	$4.7 \times 10^{-12}$	$3.53 \times 10^{-14}$	$1.2 \times 10^{-14}$	$3.5 \times 10^{-15}$	$1 \times 10^{-15}$	$2.4 \times 10^{-17}$
FAST	$7.12 \times 10^{-17}$	$6.9 \times 10^{-17}$	$5.11 \times 10^{-17}$	$3.6 \times 10^{-17}$	$2.49 \times 10^{-17}$	$9.05 \times 10^{-18}$
CADMIUM THERMAL	$3.2 \times 10^{-12}$	$1.9 \times 10^{-13}$	$5.74 \times 10^{-14}$	$1.52 \times 10^{-14}$	$5.1 \times 10^{-15}$	$1.65 \times 10^{-15}$
FAST	—	—	—	—	—	—
ANTIMONY THERMAL	$1.63 \times 10^{-12}$	$1.27 \times 10^{-12}$	$5.2 \times 10^{-13}$	$1.96 \times 10^{-13}$	$1.0 \times 10^{-13}$	$5.69 \times 10^{-14}$
FAST	—	—	—	—	—	—
TANTALUM THERMAL	$4.26 \times 10^{-13}$	$4.25 \times 10^{-13}$	$4.1 \times 10^{-13}$	$4.0 \times 10^{-13}$	$3.8 \times 10^{-13}$	$3.5 \times 10^{-13}$
FAST	—	—	—	—	—	—
TUNGSTEN THERMAL	$9.89 \times 10^{-12}$	$5 \times 10^{-12}$	$3.2 \times 10^{-13}$	$1.0 \times 10^{-14}$	$3.2 \times 10^{-16}$	$7.0 \times 10^{-20}$
FAST	—	—	—	—	—	—



TABLE 12

SPECIFIC RADIATION LEVELS FROM REGULAR  
AND REACTOR GRADE (R.G.) ALLOYS  
(A COMPARISON)

ALLOY	RADIATION LEVEL 1 FT. FROM 1 LB. ALLOY, UNIT FLUX (r/hr)					
	NO DECAY	1 DAY	5 DAYS	10 DAYS	15 DAYS	30 DAYS
INCO 713						
THERMAL	$3.73 \times 10^{-11}$	$1.01 \times 10^{-14}$	$5.35 \times 10^{-15}$	$4.71 \times 10^{-15}$	$4.4 \times 10^{-15}$	$3.99 \times 10^{-15}$
FAST	$2.57 \times 10^{-13}$	$8.71 \times 10^{-15}$	$7.67 \times 10^{-16}$	$7.24 \times 10^{-16}$	$6.83 \times 10^{-16}$	$5.99 \times 10^{-16}$
INCO 713 R.G.						
THERMAL	$3.73 \times 10^{-11}$	$7.27 \times 10^{-15}$	$3.5 \times 10^{-15}$	$1.9 \times 10^{-15}$	$1.61 \times 10^{-15}$	$1.25 \times 10^{-15}$
FAST	$2.57 \times 10^{-13}$	$8.71 \times 10^{-15}$	$7.67 \times 10^{-16}$	$7.24 \times 10^{-16}$	$6.83 \times 10^{-16}$	$5.99 \times 10^{-16}$
INCO 718						
THERMAL	$5.91 \times 10^{-11}$	$2.78 \times 10^{-14}$	$7.1 \times 10^{-15}$	$6.48 \times 10^{-15}$	$6.09 \times 10^{-15}$	$5.46 \times 10^{-15}$
FAST	$7.2 \times 10^{-14}$	$8.15 \times 10^{-15}$	$6.37 \times 10^{-16}$	$6.07 \times 10^{-16}$	$5.72 \times 10^{-16}$	$5.0 \times 10^{-16}$
INCO 718 R.G.						
THERMAL	$5.91 \times 10^{-11}$	$2.36 \times 10^{-14}$	$2.93 \times 10^{-15}$	$2.36 \times 10^{-15}$	$2.06 \times 10^{-15}$	$1.58 \times 10^{-15}$
FAST	$7.2 \times 10^{-14}$	$8.15 \times 10^{-15}$	$6.37 \times 10^{-16}$	$6.07 \times 10^{-16}$	$5.72 \times 10^{-16}$	$5.0 \times 10^{-16}$
INCONEL						
THERMAL	$1.16 \times 10^{-11}$	$2.74 \times 10^{-14}$	$3.98 \times 10^{-15}$	$3.76 \times 10^{-15}$	$3.60 \times 10^{-15}$	$3.26 \times 10^{-15}$
FAST	$4.91 \times 10^{-14}$	$8.08 \times 10^{-15}$	$8.27 \times 10^{-16}$	$7.91 \times 10^{-16}$	$7.47 \times 10^{-16}$	$6.56 \times 10^{-16}$
INCONEL R.G.						
THERMAL	$1.16 \times 10^{-11}$	$2.52 \times 10^{-14}$	$1.76 \times 10^{-15}$	$1.55 \times 10^{-15}$	$1.39 \times 10^{-15}$	$1.05 \times 10^{-15}$
FAST	$4.90 \times 10^{-14}$	$8.08 \times 10^{-15}$	$8.27 \times 10^{-16}$	$7.91 \times 10^{-16}$	$7.47 \times 10^{-16}$	$6.56 \times 10^{-16}$
INCONEL X						
THERMAL	$1.69 \times 10^{-11}$	$1.99 \times 10^{-14}$	$4.46 \times 10^{-15}$	$4.23 \times 10^{-15}$	$4.05 \times 10^{-15}$	$3.67 \times 10^{-15}$
FAST	$8.06 \times 10^{-14}$	$8.01 \times 10^{-15}$	$8.1 \times 10^{-16}$	$7.71 \times 10^{-16}$	$7.27 \times 10^{-16}$	$6.40 \times 10^{-16}$
INCONEL X R.G.						
THERMAL	$1.69 \times 10^{-11}$	$1.77 \times 10^{-14}$	$2.25 \times 10^{-15}$	$2.02 \times 10^{-15}$	$1.84 \times 10^{-15}$	$1.46 \times 10^{-15}$
FAST	$8.05 \times 10^{-14}$	$8.01 \times 10^{-15}$	$8.1 \times 10^{-16}$	$7.71 \times 10^{-16}$	$7.27 \times 10^{-16}$	$6.40 \times 10^{-16}$
HASTELLOY B						
THERMAL	$2.45 \times 10^{-11}$	$4.92 \times 10^{-14}$	$1.06 \times 10^{-14}$	$7.51 \times 10^{-15}$	$6.60 \times 10^{-15}$	$6.22 \times 10^{-15}$
FAST	$3.47 \times 10^{-14}$	$5.73 \times 10^{-15}$	$8.03 \times 10^{-16}$	$5.70 \times 10^{-16}$	$5.35 \times 10^{-16}$	$4.66 \times 10^{-16}$
HASTELLOY B R.G.						
THERMAL	$2.45 \times 10^{-11}$	$4.33 \times 10^{-14}$	$4.68 \times 10^{-15}$	$1.61 \times 10^{-15}$	$7.0 \times 10^{-16}$	$3.2 \times 10^{-16}$
FAST	$3.44 \times 10^{-14}$	$5.73 \times 10^{-15}$	$8.02 \times 10^{-16}$	$5.69 \times 10^{-16}$	$5.34 \times 10^{-16}$	$4.65 \times 10^{-16}$
HASTELLOY C						
THERMAL	$2.42 \times 10^{-11}$	$9.33 \times 10^{-13}$	$2.66 \times 10^{-14}$	$8.62 \times 10^{-15}$	$7.51 \times 10^{-15}$	$6.96 \times 10^{-15}$
FAST	$3.26 \times 10^{-14}$	$5.32 \times 10^{-15}$	$5.53 \times 10^{-16}$	$5.26 \times 10^{-16}$	$4.95 \times 10^{-16}$	$4.33 \times 10^{-16}$
HASTELLOY C R.G.						
THERMAL	$2.42 \times 10^{-11}$	$9.27 \times 10^{-13}$	$2.07 \times 10^{-14}$	$2.72 \times 10^{-15}$	$1.61 \times 10^{-15}$	$1.06 \times 10^{-15}$
FAST	$3.24 \times 10^{-14}$	$5.32 \times 10^{-15}$	$5.52 \times 10^{-16}$	$5.25 \times 10^{-16}$	$4.94 \times 10^{-16}$	$4.32 \times 10^{-16}$
K MONEL						
THERMAL	$3.96 \times 10^{-11}$	$3.49 \times 10^{-13}$	$4.29 \times 10^{-15}$	$2.47 \times 10^{-15}$	$2.46 \times 10^{-15}$	$2.46 \times 10^{-15}$
FAST	$1.81 \times 10^{-13}$	$8.63 \times 10^{-15}$	$1.05 \times 10^{-15}$	$1.01 \times 10^{-15}$	$9.69 \times 10^{-16}$	$8.82 \times 10^{-16}$
K MONEL R.G.						
THERMAL	$3.96 \times 10^{-11}$	$3.47 \times 10^{-13}$	$2.08 \times 10^{-15}$	$2.57 \times 10^{-16}$	$2.53 \times 10^{-16}$	$2.46 \times 10^{-16}$
FAST	$1.81 \times 10^{-13}$	$8.63 \times 10^{-15}$	$1.05 \times 10^{-15}$	$1.01 \times 10^{-15}$	$9.69 \times 10^{-16}$	$8.82 \times 10^{-16}$

CONFIDENTIAL

ROCKETDYNE

ROCKETDYNE

A DIVISION OF NORTH AMERICAN AVIATION, INC.

CONFIDENTIAL

**CONFIDENTIAL**

- $t_1$  = 900 sec (reactor operating time or irradiation time)
- $t_2$  = 0, 5, 10, 15, 30 days (time after shutdown)
- $r$  = 1 foot (exposure distance)
- $\phi$  = 1 (thermal neutron flux level) and/or 1 (effective fast neutron flux level)

The technique of analyzing induced radioactivity in an actual component is demonstrated by the following illustrative example. It is desired to know what levels of radiation are induced in the turbopump assembly, what materials are responsible for the majority of this activity, and the time required for the intense short-lived radiations to fall below the level due to isotopes with long halflives. The neutron flux at the turbopump consists of direct reactor leakage flux and neutron backscatter from the propellant tank. The thermal portion of neutron flux induces about ten times as much activity as does the fast flux, so the latter may be neglected in preliminary calculations. Because the primary thermal flux from the reactor is almost all absorbed in the boron-containing shield, the thermalized backscatter from the propellant is dominant. This flux falls from  $4.6 \times 10^{12}$  to  $1.5 \times 10^{12}$  nv (thermal) in the distance from tank to reactor dome, and it is an adequate approximation to assume an average value of  $3.0 \times 10^{12}$  nv (thermal) throughout the engine system.

The amount of each kind of material used in the turbopump is then tabulated as in Table 13 . Where many of the materials are very similar and are used in small quantities (such as the carbon steels) they can be safely lumped into a single item. If a large bulk of material is

~~CONFIDENTIAL~~

TABLE 13

TURBOPUMP MATERIALS LIST

Alloy	Weight, Pounds	Equivalent, Pounds*
310 stainless steel	118.3	30
K-Monel	98.2	30
Hastelloy C	58.5	20
Inco 718	33.0	10
A-286	8.4	
Inco 713	5.8	
321 stainless steel	4.6	4
Stellite 21	3.8	
Al 2024	2.1	
Inconel	1.8	
440 C stainless steel	1.5	
4130 stainless steel	0.9	
4340 stainless steel	0.9	
Inconel X	0.6	
410	0.4	
416	0.3	
302	0.3	
52100	0.2	
Carbon	0.1	

\*Reduced Weight Because of Self-Shielding Effect

**CONFIDENTIAL**

---

encountered, its weight must be adjusted by a factor to obtain an equivalent weight which takes into account internal self-attenuation of the induced radiation. A factor of roughly 0.3 has been used in this example for massive parts, but experimental evidence will be required to substantiate these calculations. The curves of Fig. 68 can now be used to obtain the induced activity in each material (after adjusting the numbers for the difference in integrated flux). The resulting activity for each material is calculated for a distance of 1 foot from the turbopump at varying times after shutdown, and is shown in Fig. 69. The activity in several major components is shown in Table 14.

It is seen from Fig. 69 that the sum of induced radioactivity falls rapidly during the first few days, and then reaches a more constant value which is determined by the most dominant long-lived isotope. In the case of the turbopump, cobalt in the Hastelloy C is the source of the dominant activity after 10 days of cooldown. The dose rate at that time is sufficient to give a worker his full weekly dose in only 6 minutes of work close to the turbopump. Even higher dose rates will be present if radiation from other parts of the engine system is added.

The disassembly and maintenance problems presented by the presence of induced activity may be lessened through close attention to material selection and operational procedures. Reactor-grade materials should be specified wherever possible and strong radiation sources should be removed from the system before maintenance work is begun. A boron-containing shield may also be used in certain components that must undergo extensive handling.

**CONFIDENTIAL**

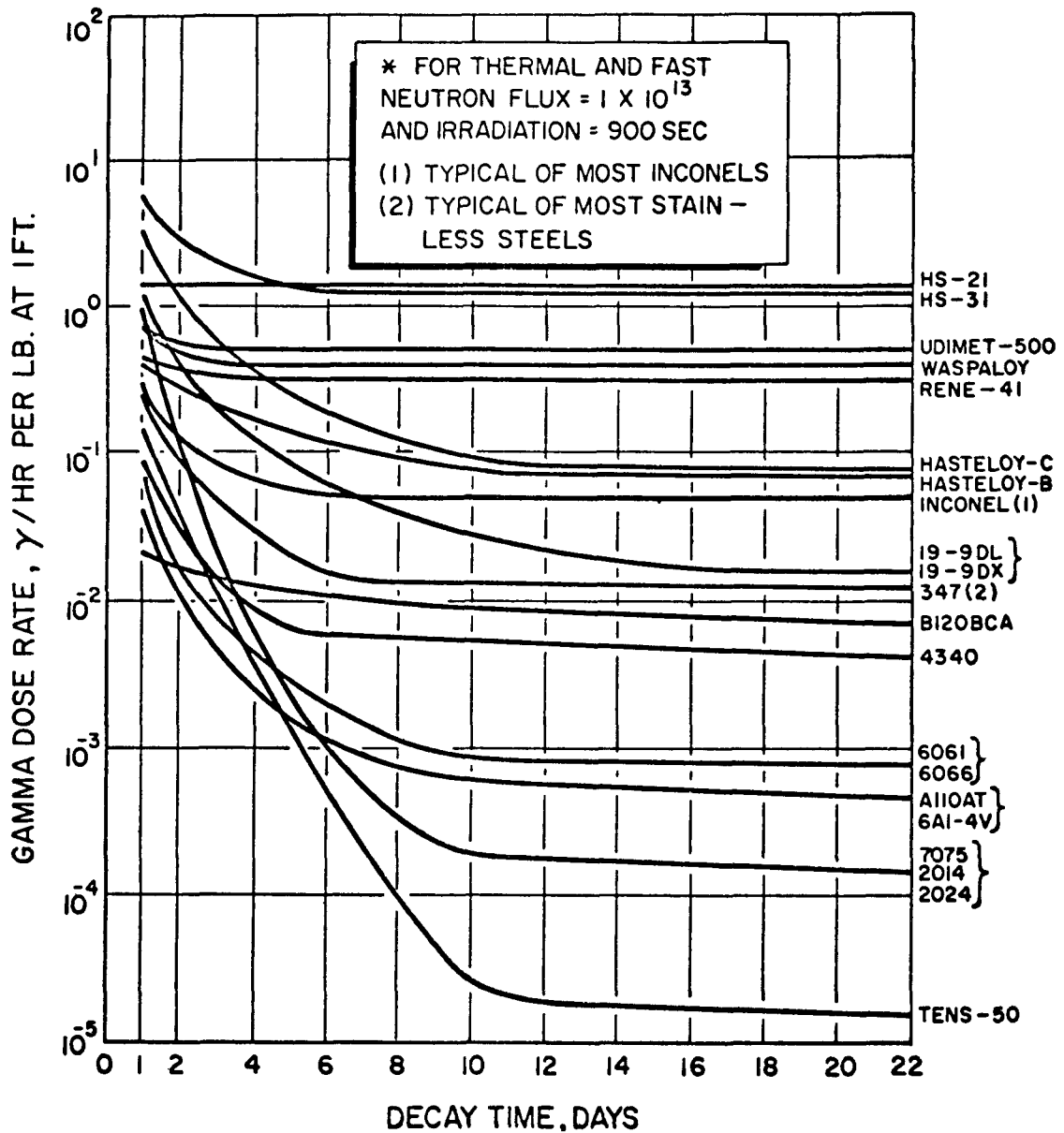


Figure 68. Dose Rates Due to Activation of Some Common Metal Alloys

~~CONFIDENTIAL~~

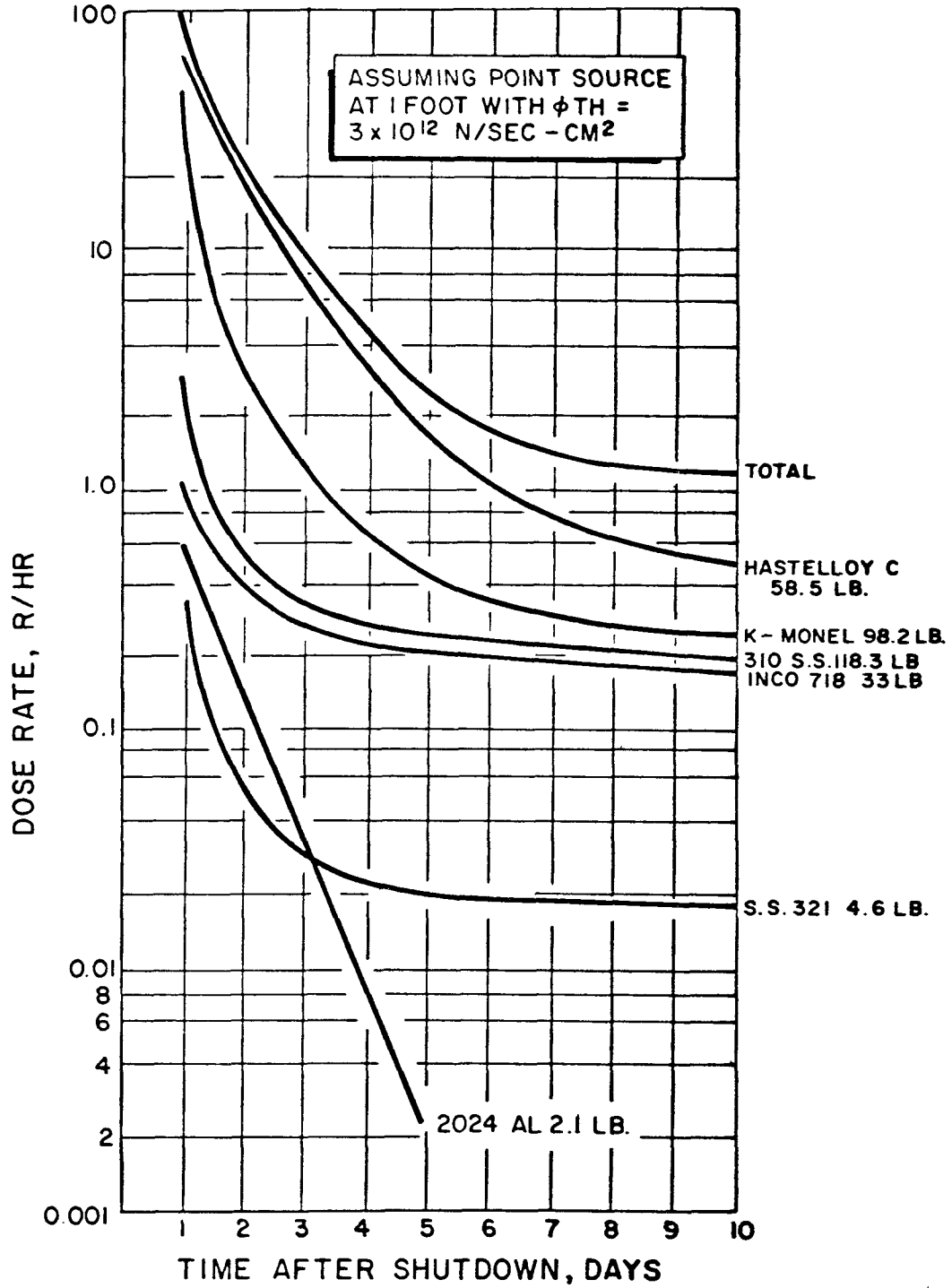


Figure 69. Turbopump Activity After Shutdown

**CONFIDENTIAL**

---

TABLE 14

COMPONENT ACTIVATION LEVELS

<u>Component</u>	<u>Dose Rate 3 Days, R/hr at 1 foot</u>	<u>Dose Rate 10 Days, R/hr at 1 foot</u>
Turbine	16	0.5
Thrust Nozzle	100	85
Forward Thrust Mount	1.0	0.5
Aft Thrust Mount	0.1	0.01
Reactor Assembly	$4 \times 10^5$	$2 \times 10^4$
Hot Gas Duct	5.0	1.0
Temperature Control Valve	0.03	0.02
Afterheat Coolant Valve	0.002	0.001
Main Propellant Valve	0.007	0.004
Gimbal Actuators	5.7	4.0
Roll Nozzle Assembly	0.2	0.1
Turbine Exhaust System	0.7	0.4

**NOTE:**

Components subjected to flow of gas from the reactor may accumulate fission products, and exhibit actual dose rates, several orders of magnitude greater than those listed prior to decontamination.

**CONFIDENTIAL**

---

## RADIATION DAMAGE

### Effects on Electrical Equipment

The predominant mechanism of nuclear radiation attenuation is ionization which creates difficulties in operating electrical equipment. Two distinct phases of damage occur: the rate-dependent transient effects which are only present during reactor operation, and the permanent effects which accumulate as a function of the integrated radiation dose.

Calculations based on the K-1 preliminary design indicate that only a few sensitive components will receive an integrated dose sufficient to appreciably alter their physical properties. But the high dose rates present during the short-duration reactor operation will have serious effects on electrical equipment, introducing current leakage paths in insulation and causing spurious voltages in conductors.

The means of preventing electrical breakdown due to the ionizing effects of radiation lie in shielding, radiation-resistant insulating materials, and the use of low-voltage, low-impedance circuitry in all instrumentation and control. Some specific examples of electrical equipment disruption and preventive measures are listed below.

### Solenoid Valves and Servovalves

These components are subject to failure through the shorting of coil assemblies by the breakdown of insulation in the nuclear radiation. There may also be spurious voltages induced by ionization of gases surrounding coils and wiring which will introduce a degree of random noise into the control system. It is expected that coil insulation will be made of a



**CONFIDENTIAL**

---

ceramic material, possibly a mineral oxide or, in the case of aluminum, an anodized insulation. The high rates of heat generation associated with the intense radiation necessitates this type of material. However, ceramic materials are subject to considerably greater electrical breakdown in radiation than organics because of the nature of their ionic bond. The free electrons created by ionization in conventional organic insulating materials have much less mobility within the insulator, and therefore present a greater degree of resistance to leakage currents than do ceramic insulations. But, by careful design of adequate insulation and the use of low-impedance circuit design, the signal-to-noise ratio will be maintained at a useful level and the device will function satisfactorily.

#### Solid-State Electronics and Feedback Loops

Solid-state electronics are particularly susceptible to transient radiation damage effects as well as permanent integrated dose effects because of the mechanism on which semiconductor devices depend for their operation. Free electrons produced by an ionizing radiation field tend to introduce a preponderance of new charge carriers into the junction region of the semiconductor, thereby changing a minority carrier into a majority carrier or creating an avalanche of charge that blocks out the desired signal. Because of the severity of this effect, solid-state devices must be located in an area of low radiation intensity such as provided by the propellant shield and by the propellant itself. These devices need not be located in close proximity to the reactor, and therefore are best placed near the top of the propellant tank. Solid-state amplifiers are employed as components in control feedback loops which also utilize a position-indicating potentiometer which is subject to malfunction from false or erratic signals caused by induced currents and high electronic noise level. The potentiometers should be fabricated from high-resistance nickel-chromium-alloy wire to

**~~CONFIDENTIAL~~**

---

reduce the effects of temperature, and the circuitry should again be of low impedance design to increase the signal-to-noise ratio. It may be necessary to protect the position-indicating units with individual shields or cooling to maintain their temperature at a reasonable level.

#### Motor-Driven Valves

The K-1 engine system will utilize valves which contain geared-down direct current motors for actuation. The motors are subject to the same type of failure as the solenoids and potentiometers previously mentioned. Adequate electrical insulation and heat protection can be supplied through the use of ceramic insulating materials and careful attention to insulation design.

#### Chamber Temperature Thermocouples

The design of the high-temperature thermocouples is by far the most difficult task which must be undertaken in the temperature measurement system. The major design requirements can be classified in three areas: (1) selection of the thermoelectric materials which will develop an adequate output and maintain their thermal electric integrity over the entire temperature and nuclear environment range, (2) designing the thermocouple probe to maintain sufficient mechanical strength at the elevated temperature to withstand the gas velocities, and (3) maintaining adequate electrical insulation at the elevated temperatures and high nuclear radiation ionization rate.

Investigation of high-temperature thermoelectric materials revealed two promising combinations. They are rhenium-tungsten and tungsten-26 percent

~~CONFIDENTIAL~~

---

rhodium-tungsten. A plot of the outputs of these two combinations over their reported operating ranges is given in Fig. 70. The electromotive force-temperature relationship for the rhodium-tungsten combination was stopped at 4000 F since considerable electromotive force scattering has been reported above this temperature. The sensitivity of the tungsten-26 percent rhodium-tungsten combination is approximately  $7 \mu\text{v}/\text{deg}$  at 4000 F (the primary control point), while the sensitivity of the rhodium-tungsten combination is approximately  $2.6 \mu\text{v}/\text{deg}$  at the same temperature. For this reason, the tungsten-26 percent-rhodium-tungsten is preferred for this application.

It is assumed that a reliable welded thermocouple junction can be achieved. In the high-temperature thermocouple studies conducted at IASL, as part of the Kiwi program, reliable welded junctions have not been achieved because of the recrystallization of the tungsten; hence mechanical junctions have been used. Due to the improvement in time constant and the reduction in thermal radiation and nuclear heating errors which can be achieved, welded junctions must be given further study. This is particularly true in light of the successes which have been reported in welding other combinations of metals with some of the newer welding techniques such as electron-beam welding.

The structural integrity of the probe can be obtained by supporting the thermocouple probe insulation in a tungsten sheath. The best choice for insulation at the present time appears to be beryllium oxide. Since the resistivity of beryllium oxide decreases rapidly at the elevated temperature, investigation of other insulating materials must be continued.

~~CONFIDENTIAL~~

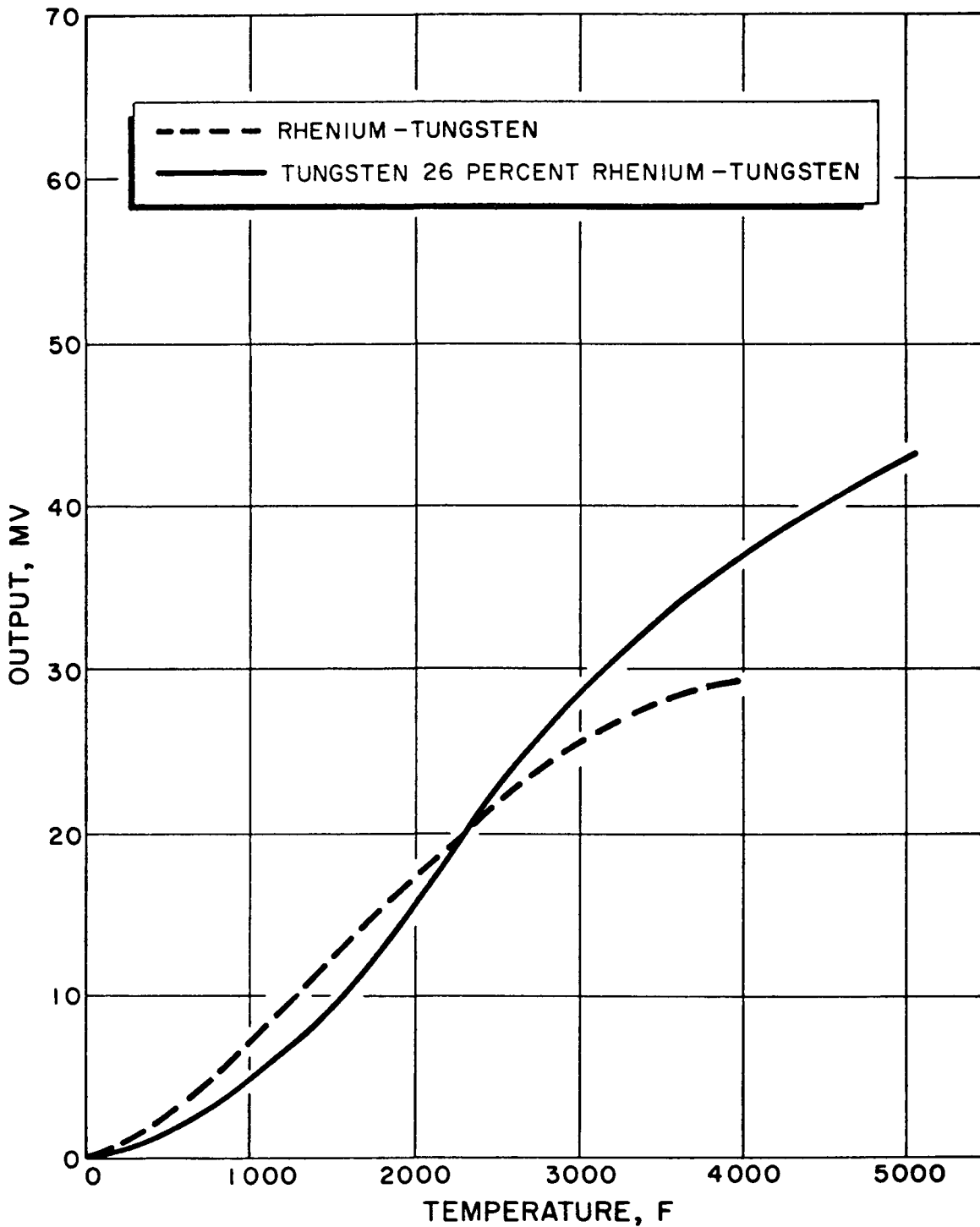


Figure 70 . Temperature-EMF Relationship for Two High-Temperature Thermocouple Combinations, (Reference Junction at 32 F)

**CONFIDENTIAL**

---

Turbine Inlet Thermocouples

While the thermocouple for turbine inlet gas temperature measurement could be the same as for the chamber temperature measurement, other alloys, which are more readily available and less expensive, will give higher sensitivities and more dependable service in this temperature range. Figure 71 shows the temperature-electromotive force relationship for chromel-constantan which is an excellent choice for this measurement since it has the highest sensitivity of the readily available alloys, is stable in a hydrogen atmosphere over the temperature range and is not subject to atmospheric corrosion.

Magnesium oxide is an excellent insulator for this thermocouple provided it is of high purity and is protected from moisture. Use of alloys which are easier to form for the sheath material also will be possible.

Cryogenic Temperature Measurement Devices

Platinum resistance bulbs have given excellent results in measuring cryogenic temperatures on all past programs at Rocketdyne. They have been successfully employed in measuring the pump inlet and outlet temperatures on the Rover program and the fuel temperatures on the J-2 program. On both of these programs the propellant is liquid hydrogen. However, none of the service has been in the nuclear environment expected in the K-1 program. Little information is available in literature regarding the nuclear effects on platinum at cryogenic temperatures. At ambient temperatures, little effect has been reported for integrated fluxes below  $10^{19}$  nvt. However, due to the low operating temperature, self-annealing may be reduced to a level where significant changes occur. This effect cannot be determined analytically and must be determined by tests. In case

**CONFIDENTIAL**

~~CONFIDENTIAL~~

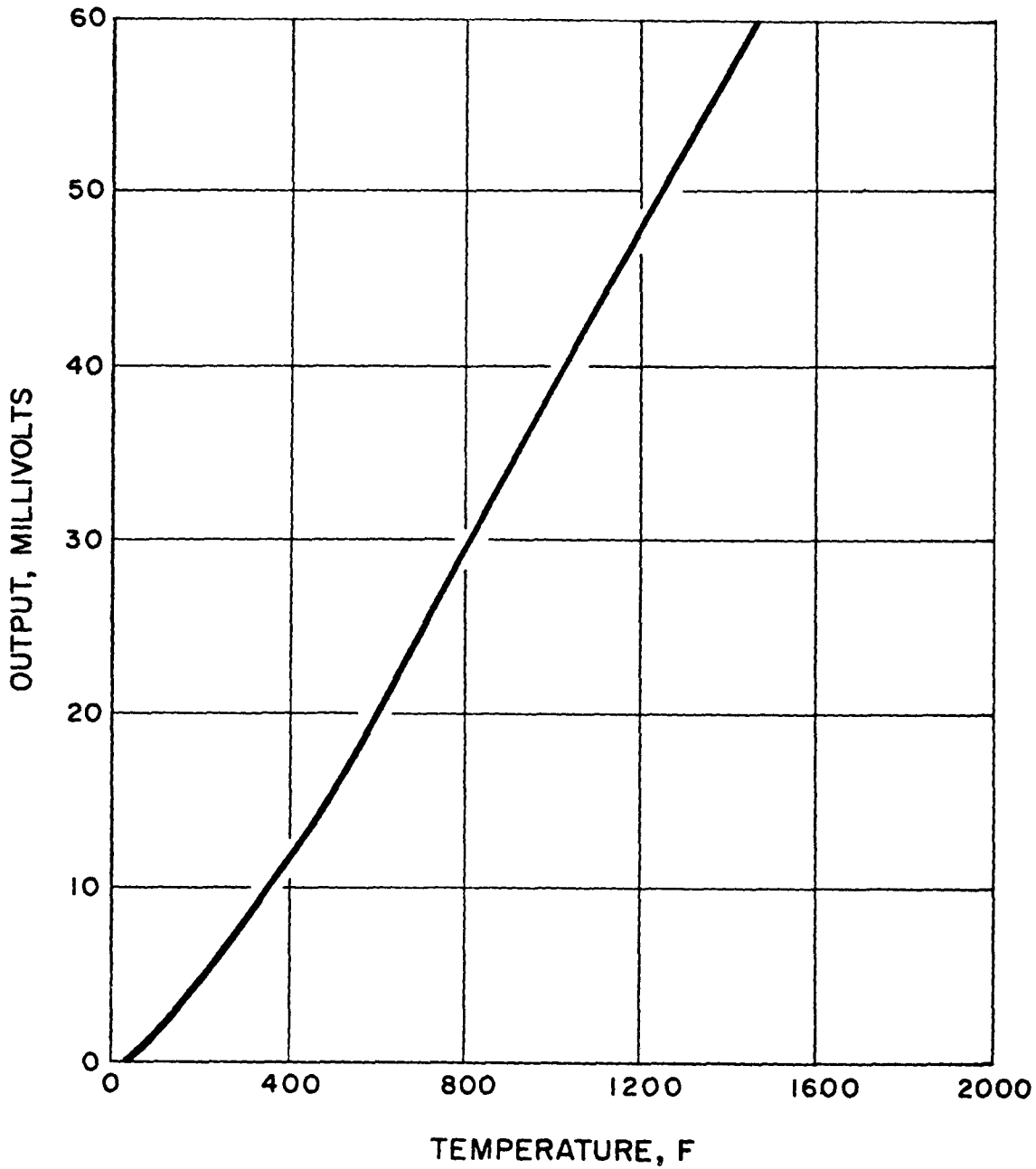


Figure 71 . Temperature-EMF Relationship for Chromel-Constantan (Reference Junction at 32 F)

~~CONFIDENTIAL~~

---

platinum resistance bulbs cannot maintain their stability in the nuclear radiation field, thermocouples must be considered for the propellant temperature measurements. Two thermoelectric alloy combinations can be considered for these measurements. They are gold cobalt-copper and copper-constantan. The sensitivity of a gold cobalt-copper thermocouple at 350 R is approximately  $18 \mu\text{v/R}$ , while the sensitivity of copper-constantan at the same temperature is approximately  $7 \mu\text{v/R}$ . These thermocouples do not have the stability of platinum resistance thermometers for cryogenic applications in nonnuclear environments, hence are not desirable.

#### Surface Temperatures Measurement Devices

Difficulty in analytically predicting the heat transfer characteristics and the nuclear heating rates on the components and the structural members will make a number of surface temperature measurements necessary to determine the operating temperatures of critical components. Thermocouples are the best choice of sensors for this class of measurements since they are relatively inexpensive, radiation resistant, can be attached to the component with the least amount of difficulty, and are adaptable to the broad range of temperature which is of interest.

#### Pressure Measurement Devices

As a part of the KEWB program, Atomics International conducted an investigation into commercially available pressure transducers suitable for use in nuclear environment up to  $10^{18}$  nvt. A summary table, showing the results of test conducted on 10 different transducers is reproduced herein as Table 15. Four of the 10 instruments tested show promising results in the radiation environment in which they were tested; three of the four

~~CONFIDENTIAL~~

TABLE 15  
TRANSDUCER CHARACTERISTICS

Manufacturer	Atlantic Research	Atlantic Research	Dynisco	Indevco	Irish Bros	Norwood	QIM(Kistler)	Statham	Statham	Omega
Model Number	LD-80	LD-77	P3A1M	2901-1000	6014	EPK-1000	PZ-14	PA-2177Cs-IM-350	PA-217s-IM 350	21-10
Type	Lead Zirconate Piezoelectric	Lead Zirconate Piezoelectric	Unbonded Strain Wire	Piezoelectric Ceramic	Quartz Piezoelectric	Bonded Strain Wire	Quartz Piezoelectric	Unbonded Strain Wire	Unbonded Strain Wire	Variable Capacitance
Natural Frequency	~1000 kc	~1000 kc	18 kc	100 kc	95 kc	44 kc	43 kc	27 kc	32 kc	80 kc
Response Time in Microseconds	0.5	0.5	8	2	4	8	4	10	10	3
Sensitivity (Approx) $\circ$	3 mv/psi	0.01 v/psi	45 $\mu$ v/psi*	25 mv/psi	2 mv/psi	40 $\mu$ v/psi	2.9 mv/psi	38 $\mu$ v/psi*	25 $\mu$ v/psi*	2.1 mv/psi*
N <sub>2</sub> Dynamic Sensitivity $\Delta$	1.07 mv/psi	No test	69.6 $\mu$ v/psi	0.97 mv/psi	2.55 mv/psi	62 $\mu$ v/psi	3.73 mv/psi	44 $\mu$ v/psi	No test	2.9 mv/psi
2H <sub>2</sub> + O <sub>2</sub> Dynamic Sensitivity $\Delta$	2.71 mv/psi	No test	71.2 $\mu$ v/psi	1.63 mv/psi	2.64 mv/psi	57 $\mu$ v/psi	4.45 mv/psi	42 $\mu$ v/psi	No test	1.9 mv/psi
Radiation Insensitive (yes - no)	No	No	Yes (with carrier)	No	No	No	No	Yes (with carrier)	No test	No
Cumulative Radiation Effects	10 <sup>16</sup> n/cm <sup>2</sup> 20-25% loss of output 10 <sup>17</sup> n/cm <sup>2</sup> Failed 10 <sup>18</sup> n/cm <sup>2</sup> No test	No test No test 90% loss of output	No test No test None	None None 93% loss of output	~10% loss of first peak No additional change No test	<10% loss of output None No test	No test No test None	None None No test	No test No test Failed electrically	10% loss of output 50% loss of output No test
Explosion Resistant	Yes	Yes	Yes	Yes	Yes	Yes	Yes	Yes	Yes	Yes
Temperature Effects	100° C No test (see LD-77) 150° C No test (see LD-77)	5% loss of output 40% loss of output	None 5% loss of output	15% loss of output No test possible	None No test possible	5% loss of output 5% loss of output	None None	10% loss of output 10% loss of output	30% gain in output No test	20% loss of output 50% loss of output
Corrosion Resistant in UD <sub>2</sub> SO <sub>4</sub> + H <sub>2</sub> SO <sub>4</sub>	Not available	Not available	Yes	Not available	Not available	Not available	Not available	Yes	No	Not available
"Clean" Ringing (yes - no)	No	No	Yes	No	No	Yes	Yes	Yes	Yes	Yes
Calibration (a) Static Means (yes - no) (b) Dynamic	No Yes	No Yes	Yes Yes	No Yes	Yes Yes	Yes Yes	Yes Yes	Yes Yes	Yes Yes	Yes Yes
Remarks		Superseded by LD-80		Maximum rated temperature is 110° C. Cable shorted before 150° C was reached	Cable fused at 130° C	Nitrogen cooled during temperature tests		Temperature compensated	First model	Has 25 mc carrier, saturation effects above 300 psi

\*Static calibration curve.

$\circ$  Sensitivities may vary a great deal depending upon applied voltage for strain wire types and cable capacitance for piezoelectric types.

$\Delta$  Dynamic calibration curves.

CONFIDENTIAL

CONFIDENTIAL



**CONFIDENTIAL**

---

were strain gage-type transducers and the fourth was quartz piezoelectric transducers. While the test conditions (flux rate and gamma heating) were not so severe as expected on the K-1 program, the results do indicate the types which have the greatest potential for being developed into satisfactory transducers for this program.

Variable Reluctance Transducers. A noticeable omission in the types of transducers tested on the KEWB program was the variable reluctance transducer. While this type of transducer has been successfully employed in a number of applications, alternating current operational devices are expected to be considerably more unstable in a high-radiation field than direct current devices. This is because of the change in dielectric constant and ionization currents for insulator materials located in a radiation field. Temperature-induced capacitance changes in the transducer and its electrical cable have also limited the precision of variable reluctance measurement systems on chemical rocket testing where the operating conditions are considerably more favorable.

Piezoelectric Transducers. Piezoelectric crystals, basically a charge device, are adaptable to making dynamic measurements but are of limited value in making static measurements. They have the additional disadvantage of having a high internal impedance which will accentuate any radiation-induced noise in the system.

Strain Gage Transducers. From the data available, strain gage-type transducers show the most promise. Two types of strain gage pressure transducers are available commercially; they are: (1) bonded strain gage pressure transducers and (2) unbonded strain gage transducers. The difference between the two is, as the names imply, the method utilized in attaching

~~CONFIDENTIAL~~

---

the strain element to the sensing element. While many of the operating characteristics of the two types are similar, there are basic variations which must be considered.

Bonded Strain Gage Transducers. Bonded strain gage transducers, manufactured by the Taber Instrument Corp., have been extensively employed at Rocketdyne for the measurement of pressure. These units were chosen, basically, because of their mechanical ruggedness and their calibration stability. While this transducer has been well proven in the nonnuclear environment, several modifications may be necessary for satisfactory operation in the nuclear environment which will be encountered on the K-1 engine. The two major areas of modification which can be foreseen are (1) the method of bonding strain gages and (2) extending the temperature operating range and/or providing cooling methods.

Bonded strain gage techniques utilized in nonnuclear environments have not proved entirely satisfactory in nuclear environments and must be modified for this instrument to perform in the K-1 environment. A more complete discussion of bonded strain gages is given under the Strain Measurements heading.

The present upper-temperature operating limit of the Taber pressure transducer is between 250 and 300 F which is far below the temperatures expected if the transducer is not shielded or cooled. While one of the factors limiting the upper temperature limit is the strain gage bonding material, whose temperature characteristics must be improved along with radiation resistance, it is very difficult to obtain stable zero and sensitivity characteristics during transient temperature operation. Therefore, shielding and/or cooling will be required on this program to obtain accurate information. Other modifications in the design should include the use of

~~CONFIDENTIAL~~

~~CONFIDENTIAL~~

---

spot-welded electrical junctions and elimination of organic materials throughout the system exposed to the nuclear environment.

Unbonded Strain Gage Transducers. Although it eliminates the bonding problem, the unbonded strain gage has limitations of its own. These limitations are: (1) the strain wire is not continuously supported, hence it is subject to high-frequency excitation from acoustical or mechanical sources, (2) the unsupported sections of the strain wire are difficult to cool-- particularly true when the strain element cavity is referenced to 0 psi, and (3) coolant gases cannot be passed around the unbonded strain gages. Coolant would cause extraneous stresses in the gages, possibly cause physical damage, and very likely change the transducer stability by changing the insulation resistance between elements of the bridge. Gas ionization around the uninsulated strain wires could also be a limiting factor in the application of unbonded strain gages.

In addition to the factors discussed above, Rocketdyne's experience on past chemical rocket engine programs has shown bonded strain gage transducers are more reliable than unbonded strain gage transducers, hence the bonded strain gage transducer should be given primary emphasis in this program. (Ref. 32).

#### Flow Measurement Devices

Flowmeters. The following types of flowmeters are promising in their present state of development:

1. Ultrasonic flowmeter
2. Turbine-type flowmeter

~~CONFIDENTIAL~~

---

3. Variable head flowmeter
4. Li radial flowmeter
5. Drag disk flowmeter
6. Axial momentum flowmeter

Each of the above types of flowmeter represents a method for mass flow measurement, but there are significant problems as well as advantages with each.

Ultrasonic Flowmeters. The ultrasonic flowmeter employs crystal drivers to propagate sound waves through the fluid. Vector addition to the fluid velocity to the propagation velocity produces an electronic signal proportional to the fluid velocity. Since the mass flowrate is proportional to both density and velocity, a separate determination of density must be made. The ultrasonic flowmeter requires relatively complex electronic circuitry and its operational characteristics depend upon the physical characteristics of the crystal units, including their holders, the coupling coefficient between the crystal and the fluid and the electronic circuitry. Radiation effects on the crystals and the electronic circuitry due to the K-1 nuclear field would complicate the use of this type flowmeter.

The advantages of the ultrasonic type are: (1) it integrates the effects of the fluid stream velocity profile, (2) it presents no flow obstructions in the fluid duct, and (3) it does not present a sealing problem.

Turbine Flowmeters. The turbine-type flowmeter contains an axially-mounted rotor which translates fluid velocity into rotor rotation. A detector, normally a magnetic proximity device, produces an ac electrical output which

~~CONFIDENTIAL~~  
DECLASSIFIED

~~CONFIDENTIAL~~

---

is proportional to rotor angular velocity. This type of meter has been widely used by Rocketdyne in cryogenic application where precisions of better than  $\pm 0.1$  percent have been demonstrated. The precision obtainable in a well designed installation is largely a function of the calibration capabilities. The principle of operation is relatively simple and no electronics or power supply are required.

The disadvantages of the turbine meter are: (1) it is slightly sensitive to fluid viscosity, (2) it is seriously sensitive to fluid phase, (3) it is subject to damage by excessive gas flows, and (4) it requires a separate determination of fluid density to obtain mass flowrate. Another variation of the turbine-type flowmeter is the double rotor meter manufactured by Potter Aeronautical Company. This device employs two rotors of different blade pitch mechanically coupled by a torsion member. By utilizing the angular displacement between the two rotors a relationship with mass flowrate can be derived. (A 4-in. flowmeter of this type is presently being procured by Rocketdyne for testing in liquid hydrogen over a flow range compatible with the K-1 requirements.) The results of these tests will determine if this technique is superior to a separate determination of density by pressure and temperature. The accuracy of this device appears to hinge upon the stability of the torsion member; this is particularly true in a radiation environment.

Variable Head Flowmeters. The variable head flowmeters use a restriction, usually of classic design, in the fluid duct. The conversion of fluid static head to velocity head is proportional to the liquid density and velocity squared (kinetic energy). The output is usually taken as the pressure drop across the restriction. In classical form, these devices are subject to fluid characteristics and to piping effects. Because of the  $\rho v^2$  dependency a separate determination of density must be made. Since the restrictor

~~CONFIDENTIAL~~

itself can be made relatively insensitive to the nuclear environment, the nuclear radiation will present problems only in measuring the differential pressure and in determining the density. These devices have been less precise than turbine flowmeter for measuring flowrate on chemical rocket engines.

Li Radial Flowmeters. In the Li radial flowmeter, the flow is directed radially outward using a vaned, driven casing much like a centrifugal pump. The fluid is then redirected inwards and reacts against another set of radial vanes. It can be shown that the torque generated at the second set of vanes is proportional to mass flowrate and the speed of rotation of the unit. If the casing is driven at constant speed, the torque is proportional to mass flowrate. The torque measurement depends upon the angular deflection of the rotor at its mount strains. Since the mount then becomes the measuring mechanism, its spring rate is important. The most serious problem with this flowmeter is the dynamic seals at each end of the casing, which are necessary for coaxial rotation. In addition, the unit must be driven at constant speed; a difficult task even where weight and complexity are not a factor and where a nuclear environment is not present. The salient feature of this device is that it depends upon integrated angular momentum, therefore its performance is not adversely affected by the fluid phase.

Drag Disk Flowmeters. In the drag disk flowmeter, a resistive element is suspended in the liquid conduit. The drag force acting upon the element is proportional to the fluid density and the velocity squared. In combination with either velocity measurement (such as the turbine-type flowmeter) or density measurement it yields mass flowrate. The practical feature of this device is that it can be made to have an essentially constant drag coefficient, which is an improvement over the single-valued discharge

~~CONFIDENTIAL~~

**CONFIDENTIAL**

---

coefficients of classical head-type devices. In addition, response is increased since the drag force is measured, usually by strain gages bonded to the drag disk support. The principle is simple and valuable; however, the device is subject to vibration, acceleration and temperature errors, all of which would be difficult to compensate for in this application.

Axial Momentum Flowmeters. The axial momentum flowmeter is similar in principle to the Li radial flowmeter, except the fluid is directed into the bladed annulus of a drum-shaped rotor which is driven at constant speed. As the fluid leaves the rotor it is traveling in a helical path with some angular momentum. Another drum-shaped bladed annulus, immediately downstream, receives the fluid and removes its angular momentum. In so doing it generates a torque in the compliant restraint attached to the downstream annulus. The generated torque is proportional to mass flowrate and rotor speed. The advantage and disadvantages of this flowmeter are similar to those of the Li radial flowmeter with one or two exceptions. These exceptions are: (1) there are no casing seals, only the dynamic seals for the impeller input (at least one company is attempting to eliminate this seal by installing a constant speed motor within the housing) and (2) there is the possibility of hydraulic coupling between the two annuli.

Flow Measurement Systems. To reiterate, all of these devices possess merits as well as serious problems. Hence, the most prudent approach is to select that system which in its present state of development is the most capable of reliable and precise flow measurements. Rocketdyne's experience shows this to be a volumetric flow measurement with the turbine-type flowmeter and a separate determination of density by the measurement of temperature and pressure. Such a mass flow measuring system for liquid hydrogen is presently under development for the J-2 program which has a nonnuclear environment.

~~CONFIDENTIAL~~

---

The problems presented by the nuclear environment will be present to some degree with the turbine-type flowmeter; however, there are several reasons why they may be easier to solve for this type flowmeter than any other transducer: (1) the flowmeter is cooled by the liquid hydrogen, hence nuclear heating will not be a serious problem, (2) since the device is displacement or velocity sensitive, it is not affected by changes in mechanical properties caused by neutron or gamma ray bombardment; and (3) since the output signal is frequency modulated, the measurement will not be subject to moderate change in the magnetic and electrical properties of either the detection device or the transmission system. However, special precautions in the design of the detector must be taken. These precautions include nonorganic insulation and welded terminals. Induced radioactivity should be considered in the selection of all the materials.

#### Strain Measurements

The literature contains a number of reports on different principles which have been investigated for use in making strain measurements and include resistance gages, inductance gages, capacitance gages, optical techniques and stress coatings. The resistance strain gage has been exploited the most, mainly because it is more adaptable to field installation than the other types. While some problems exist in the application of the resistance-type strain gage in the K-1 environment, it remains the logical choice.

Resistance Strain Gages. Strain is measured with the resistance strain gage by attaching a wire filament securely to the component being analyzed so a strain occurring in the test hardware is transferred to the filament. Strain in the filament changes the electrical resistance which is measured; usually the filament is connected into a Wheatstone bridge circuit.



**CONFIDENTIAL**

---

The five basic variables which enter into the resistance strain gage operational characteristics are (1) the material of the filament wire, (2) the filament construction, (3) the method of attaching the filament to the hardware under test, (4) the lead wire construction and (5) the circuit in which it must operate.

Filament Material. The best choice of filament material is dependent upon the environment in which it must operate. In the low and moderate-temperature range, up to 300 F, constantan has been widely employed. For higher temperature operation up to 700 to 1000 F, unannealed Karma wire has given satisfactory results. The effects of the K-1 nuclear environment on these materials is unknown at this time and must be determined by tests; it is not expected to be a serious problem, however, especially at the higher temperatures.

Filament Construction. Two methods are commonly employed in making the filament grid. One method is to employ a fine wire wound to form the grid shape desired. This form requires a carrier (grid holder) to retain the structural and electrical integrity of the grid. The grid holder may be paper, bakelite, mica, etc. While all of these materials are satisfactory in certain applications, the organic materials must be avoided on the K-1 program. Although the filament is normally bonded to the carrier with an adhesive or is embedded in the material, one company makes a resistance strain gage in which the filament is affixed to a metallic carrier by an extrusion process in which magnesium oxide is swaged completely around the strain wire to form the electrical insulation and the mechanical bond. This type of construction seems to be desirable for the K-1 environment; however, tests must be conducted to verify this conclusion. The second method of grid construction is accomplished by etching the grid from a

**CONFIDENTIAL**

~~CONFIDENTIAL~~

---

thin foil or film. In the case of the etched foil gage the filament can be attached to a permanent carrier, as in the case of the wire filament, or it can be attached to a temporary carrier and transferred during installation.

Gage Attachment. The most commonly employed method of attaching the gages (with or without holders) to the test hardware is with some type of bonding agent. A large number of adhesives have been tried and are being used with various results. Bonding is usually referred to as an art rather than a science since the results are influenced by the technique used in the mixing of the bonding materials, the method employed to prepare the surfaces to be bonded and the curing cycle. The nuclear environment and the high temperatures expected limit the number of adhesives which can be employed. Ceramic adhesives are the most promising, but in general they must be cured or applied at elevated temperatures. Long, high-temperature curing cycles, undesirable for shop or field applications, can be avoided by bonding the strain gage to a thin, metallic carrier of the same material as the test hardware. This is done in the laboratory under favorable conditions, before spot welding the carrier to the test hardware during the assembly period. This relatively new technique is very desirable since it allows laboratory-controlled conditions during the critical operation and reduces installation time during component or engine buildup. The one disadvantage of this technique is that it cannot be used on very thin components where the metallic carrier can alter the stress in the component under test.

Lead Wire Construction. The gage lead wire construction is important since it is the means of making electrical connections to the filament. The electrical junction must be capable of withstanding the environment; hence,

~~CONFIDENTIAL~~

---

spot welding or mechanical junctions must be used. One of the main causes of electric discontinuity in a resistance strain gage installation is lead wire failure caused by fatigue or tension which surpasses the yield strength. The lead wire must therefore be given particular attention and care to protect against damage.

Bridge Circuits. In general, gages will be wired to form complete four-arm-bridge circuits. If only one or two active gages are employed in the measurement, dummy gages mounted near the active gages will be used to complete the bridge. Even though the individual gages are temperature compensated, the additional compensation provided by this circuit arrangement will be required because of the temperature fluctuations expected on the K-1 engine components.

#### Acceleration Measurements

Rocketdyne has employed piezoelectric accelerometers exclusively on past chemical rocket engine development programs. These units were employed because of their small size, light weight and excellent frequency response capabilities. Weight and size are important since it is desirable that the instrumentation installation does not change the operating characteristics (mode or frequency of vibration) of the component under test. Size is of added importance since bulky units cannot be physically mounted in some of the locations encountered on a rocket engine.

Irradiation tests conducted on pressure transducers as part of the KEWB program by Atomics International indicate that quartz piezoelectric properties are unaffected by an integrated flux of  $10^{18}$  nvt, while other piezoelectric materials failed at equal or lower doses. Thus, while it can be reasonably expected that the quartz crystal will not be permanently

~~CONFIDENTIAL~~

~~CONFIDENTIAL~~

damaged by radiation imposed by the K-1 engine, little information exists to evaluate the magnitude of the dose rate effects. Transient radiation effects in a piezoelectric material may reasonably be expected. These effects along with the prompt radiation effects in the connecting cables, may prove to be very difficult to handle because of the high internal impedance of the crystal and the high input impedance required at the preamplifier. One additional disadvantage of piezoelectric devices is their temperature sensitivity. However, their small size may offset this disadvantage in some locations; if they are mounted on a cooled part, thermal conduction will dissipate the radiation-induced heat. Within the past year, an unbonded, air-damped strain gage accelerometer with improved frequency response characteristics has been introduced on the commercial market. These devices appear to be the most promising for operation in the K-1 environment. The effects of the nuclear environment on this instrument can be expected to be similar to that of the unbonded strain gage pressure transducers.

#### Permanent Damage in Mechanical Components

Reference to the radiation dose plot of Fig. 57 indicates that the accumulated radiation dose in certain areas of the engine system will exceed the tolerance of most organic materials. In the unshielded areas of the engine system, integrated radiation doses of  $4 \times 10^{16}$  nvt and  $5 \times 10^8$  r will accumulate in 1200 sec engine operation. In the shielded regions above the reactor core, doses of  $5 \times 10^5$  nvt and  $3 \times 10^7$  r can accrue. Indications are that certain organic materials will tolerate this dose in limited applications, but considerations of reliability and the desirability of later uprating to accommodate higher reactor power require that the K-1 engine system be as radiation resistant as possible. Wherever possible, components containing organic parts should be examined

~~CONFIDENTIAL~~

**CONFIDENTIAL**

---

for the possibility of substituting other materials or eliminating the organic parts altogether. Areas of an engine system which commonly employ radiation-sensitive materials are seals, electrical insulation and the reinforced Teflon bearing cages of liquid hydrogen-lubricated turbomachinery. It was previously mentioned that the combination of high-temperature and radiation damage dictate the replacement of organic insulating materials with ceramic counterparts. Other devices which are susceptible to integrated-dose radiation damage are described below.

#### Bearings

At the inception of Rocketdyne's program to develop liquid hydrogen pumps, the use of conventional lubricants for bearings and gears was recognized as impractical. The close proximity of the bearings to the low-temperature region would require large heat inputs to maintain fluidity, thereby imposing weight and complication on the system. The premise adopted was that a lighter, more compact and simple pump could be achieved by the elimination of an external lubrication and heating system.

An intensive program was conducted at Rocketdyne to develop the capability of bearing lubrication using the propellant being pumped. Liquid hydrogen was among the first of the various propellants studied, and test performance proved the feasibility of the concept. Subsequently, ball bearings with races and balls made of 440 CRES, and outer-land-riding cages made of glass-impregnated Teflon have been successfully tested during numerous component tests and during the Rover pump test program.

The liquid hydrogen-lubricated bearing demands a cage which will retain its anti-friction surface properties throughout a wide range of temperatures without being brittle or having other undesirable properties. Unfortunately, Teflon is one of the most radiation-sensitive engineering

~~CONFIDENTIAL~~

materials that can be used in this application. Reinforced Teflon possibly will be adequate in the K-1 application but its strength will rely entirely on the nature of the reinforcement. Also, the integrity of its surface has not been proven at the radiation dose expected. Advanced nuclear engines with higher powers and higher integrated doses must utilize a more radiation-resistant material than this, and it is therefore wise to develop a replacement as early as possible. Other promising materials include the calcium fluoride-Teflon and calcium fluoride-Kel-F "alloys", and radiation-resistant base materials with Teflon applied by a surface copolymerization process. Polystyrene might be used in this application as the base material. Graphite is perhaps the most resistant to radiation damage, although its brittleness presents design limitations.

In view of possible effects of radiation on the glass-impregnated Teflon cage material, a test program is being conducted to evaluate graphite cages. To date, three bearings have been tested in liquid hydrogen at shaft speeds of 26,000 and 33,000 rpm. One bearing was tested for 1-1/2 hr at 26,000 rpm. Two other bearings were tested at 33,000 rpm. One unit accumulated 6-1/2 hr of testing in six starts, while the second accumulated 5 hr of testing in five starts. The longest single-duration test was 2-1/2 hr and was made at 33,000 rpm. The tests have been performed at a radial load of 190 lb and an axial load of 400 lb.

#### Seals

Flanged joints requiring static seals should be kept to a minimum. They will probably be used only at the tank attach point and at the hot gas throttle valve.

~~CONFIDENTIAL~~

**CONFIDENTIAL**

---

The Naflex pressure-actuated seal (Fig. 72) developed at Rocketdyne is suitable for all flanged joints used in the engine system. This seal is currently operational in all cryogenic bolted joints in the Atlas and Saturn engine systems. Outstanding improvement in sealing of cryogenic liquids has been achieved by its use.

The operation of a pressure-actuated seal may be explained briefly by a schematic diagram. The figure shows a Naflex seal installed in a flange. The flange and seal tolerances are such that torquing of the flange bolts (not shown) causes the seal legs to deflect. This deflection causes the seal to exert a preload or spring force at A. As fluid pressure P is built up the unit loading at A is increased and at about 600 psi (depending on temperature and flange deflection) begins to exceed the spring load. The resulting high unit loads at A, in conjunction with the soft facing material, effects sealing. The success of the Naflex seal at low pressures and temperatures, compared with other pressure-actuated designs, is due to the combination of preload and facing material.

The standard Naflex seal has a thin Teflon facing. Since Teflon is subject to radiation damage, soft metal foil can be used in its place. An extensive development program now under way in connection with the Kiwi-B program has shown excellent results at temperatures from -320 F to 1200 F for the all-metal Naflex seal.

Naflex seals of Inconel X and Inco-718 with copper facing have accumulated a total of 14,000 sec sealing hot gas combustion products at 1200 F and 500 psi. During the 47 tests involved only a few cases of detectable leakage occurred, and in these cases the leakage was negligible. In laboratory tests, helium at 900 F and up to 1000 psi was sealed repeatedly using copper-faced Naflex seals. Equal success was experienced in sealing liquid nitrogen at pressures up to 2000 psi. In all test fixtures a

**CONFIDENTIAL**

~~CONFIDENTIAL~~

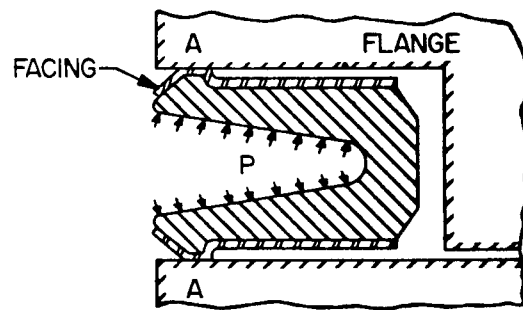
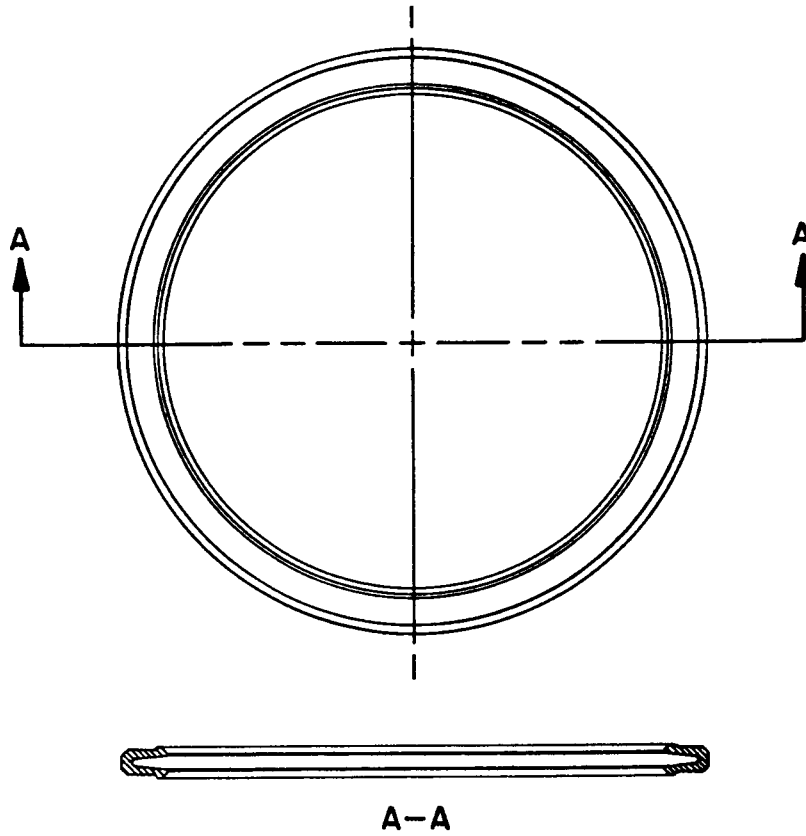


Figure 72. Pressure-Actuated Seal



**CONFIDENTIAL**

---

32-microinch finish with concentric machining grooves was used on the flanges.

Copper, nickel, silver and gold are being considered as materials for the foil facing; however, the present emphasis is on copper which has the desired softness, ductility and ease of handling. Plating with various soft metals offers an alternate method for coating the seal face. However, plating has these drawbacks which must be overcome: (1) plating is usually harder than foil and (2) it is difficult to maintain the close control on plating thickness, mechanical properties and finish which is needed for sealing.

The Naflex seal has been designed for maximum resilience through the use of high-strength metal and an optimum stress configuration. This resilience allows the use of minimum-weight flanges since the seal can accommodate some flange deflection. If heavier, more rigid flanges are used, the flexibility adds a margin of safety.

#### Explosive Devices

The safety system of the K-1 engine may employ destruction devices which utilize high explosives to break up and scatter the reactor core. These devices will probably be located in the region of highest radiation flux and must retain the highest degree of reliability in view of their critical importance to the engine test safety program. The effects of radiation on explosives are in two areas: (1) explosive efficiency may be decreased as the evolution of gas indicates changes in the chemical structure of the explosive and (2) the explosive may be made sensitive and unstable and may exhibit a tendency to predetonate.

~~CONFIDENTIAL~~

Studies reported by the Radiation Effects Information Center of Battelle Memorial Institute have shown that of the high explosives tested TNT exhibits the greatest radiation stability. Gas evolution, the predominant radiation-induced effect in these explosives, is shown in Fig. 73 which was excerpted from REIC Memorandum 2-C of June 15, 1959. TNT shows a flat, linear gas-evolution curve up to a total gamma dose of  $10^{10}$  ergs/gm (C). The maximum dose expected at the horizontal centerline of the K-1 pressure shell is  $10^{11}$  erg/gm (C), but the extrapolation of these data appears to be justified by the superior radiation resistance of TNT's aromatic structure. Neutron effects must also be considered but there is little hydrogen in TNT to absorb neutron energy and the  $N^{14} (n,p) C^{14}$  reaction appears to be insignificant, in view of the large gamma doses. Other studies have shown that Tritonal has approximately the same radiation resistance as TNT.

#### Solid Lubricants

Although solid-state lubricants have been shown to be more radiation sensitive than other nonorganic materials they appear to keep their lubricating properties up to doses far exceeding those expected in the K-1 application. The Radiation Effects Information Center of Battelle Memorial Institute indicates that a graphite-MoS<sub>2</sub> lubricant which is bonded to the bearing surface as a ceramic coating can withstand at least  $10^{16}$  nvt and  $10^8$  r.

Other methods of dry lubrication and lubricants which should be evaluated are carbide coating, nitriding and sintered metal surfaces. Selection of a material will be dependent upon its resistance to both temperature and radiation environments.

~~CONFIDENTIAL~~

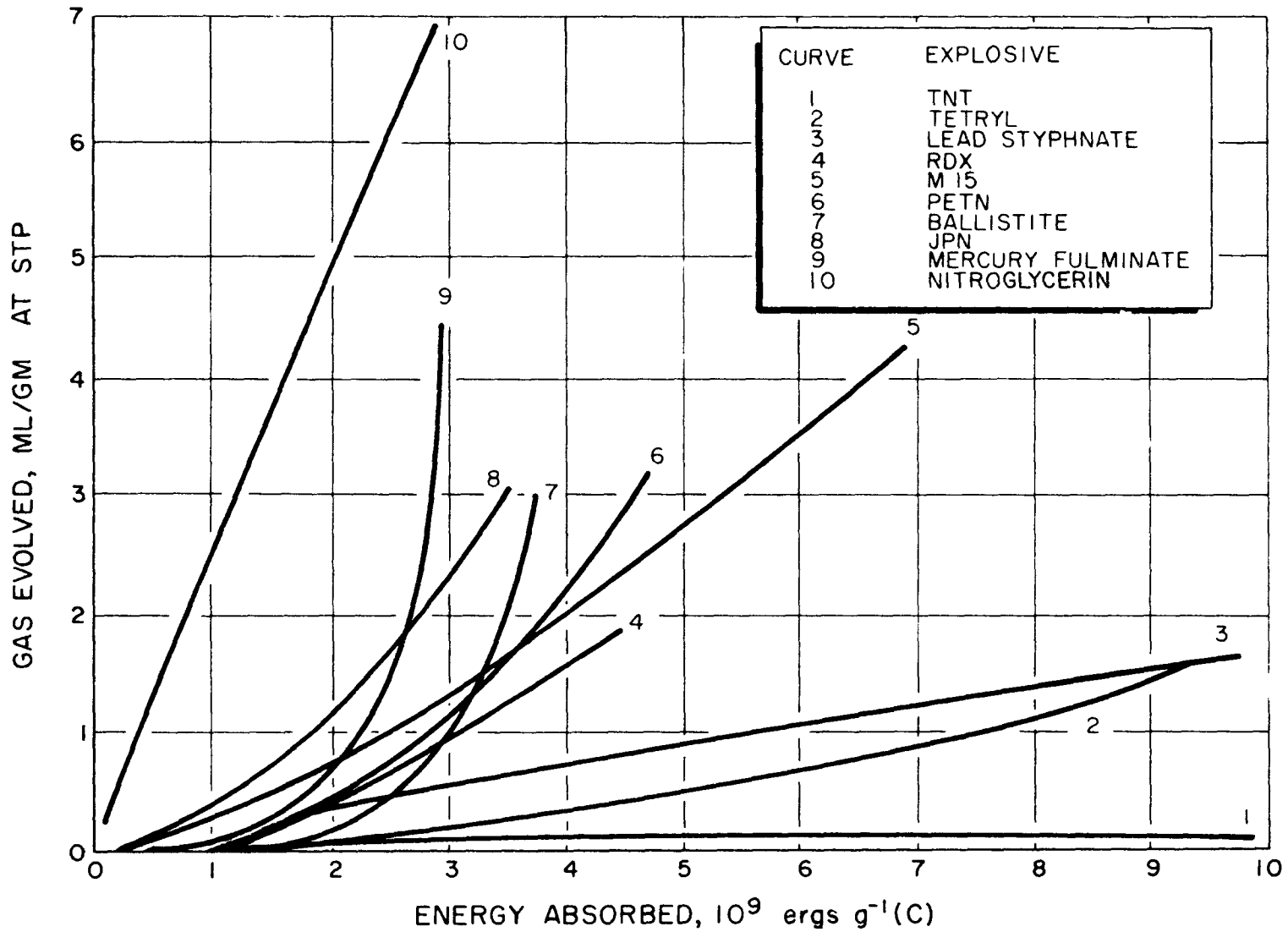


Figure 73. Gas Evolution by Irradiated Explosives at Ambient Temperatures

DECLASSIFIED

page blank

DECLASSIFIED

~~CONFIDENTIAL~~

TEST PROGRAMS

EXPERIMENTAL OBJECTIVES

There are two distinct types of experimental investigations which will be required in the development of a flight prototype nuclear engine system and its feed system components. The first type, research experiments, are for the purpose of obtaining basic data to verify calculated results and to furnish an empirical basis for further component analysis. The second type, developmental testing, serves to prove out the fully engineered feed system and its components and assures that they meet their design requirements. The tests outlined in this section cover both areas of experimentation, although more emphasis is placed on the final phases of component developments which will be performed in the radiation environment of the Kiwi-B experiments at NTS.

AREAS OF EXPERIMENTAL INVESTIGATION

Reactor Leakage Fluxes

Considerable uncertainties exist in the calculation of radiation leakage fluxes from a propulsion reactor. The magnitudes of all radiation effects depend on these fluxes and therefore an accurate knowledge of the environment is necessary for system development. Adequate instrumentation should be provided at all Kiwi-B experiments to record the magnitude and spectral distribution of neutron and gamma fluxes. Detectors should be placed relative to the reactor in positions which approximate the location of system components in the prototype engine. Other instruments should be included to provide data on heat generation rates in several engineering materials at different locations within the envelope of the engine system. These data will serve not only as a verification of calculated values but will be the empirical foundation on which to base further analysis and development.

~~CONFIDENTIAL~~

### Shield Performance

The radiation shield is of critical importance in controlling the vapor pressure of the tanked propellant, and therefore the NPSH at the inducer stage of the pump. It also determines the rate of radiation heating in the components of the engine system. The calculated performance of the shield must be verified by testing it in a highly directional radiation environment such as exists in the beam port of research reactors or in the leakage flux from the Kiwi-B reactor experiments.

Testing in the Kiwi-B environment would be the final phase of shield development. The test shield must be internally cooled with a cooling capacity designed to match the predicted heating rates, and it should be mounted as close to the reactor as is consistent with facility design and the available coolant supply. Instrumentation should be provided to record information on the heat fluxes and internal temperatures within the shield. Heat generation rates in shielded equipment should be recorded to determine the effectiveness of the shield, and the heat generation in shielded propellant is, of course, of primary interest. Temperatures of the hydrogen coolant should be recorded at various locations within the shield to provide additional data on heat fluxes and shield effectiveness.

As shield development continues, more advanced reactor experiments will employ the shield mounted in the bottom of the reactor assembly so that the propellant flow is directed through the shield just as it will be in the flight-type engine system. The shield coolant flow will issue from the reflector and will discharge directly into the reactor core. Instrumentation for this test will be as for earlier shield experiments; the leakage fluxes and heating rates will be determined and the shield temperatures will be recorded in order to calculate thermal stresses and heat fluxes within the shield.

~~CONFIDENTIAL~~

**CONFIDENTIAL**

---

Propellant Heating

Because of the importance of radiation-induced propellant heating, fast and thermal neutron fluxes and gamma radiation should be measured at various locations in the liquid hydrogen. Typical measurements in the propellant for fast neutrons, starting from the bottom of the propellant, are every 2 inches for the first 2 feet followed by one every foot for the next 2 feet. Thermal neutrons and gamma intensity would be measured every foot for the first 10 feet. Instantaneous measurements are required; therefore, ion chambers are necessary. Small "pencil" ion chambers have been developed for use at cryogenic temperatures and can be used for this purpose.

The Kiwi leakage flux data will supply valuable information concerning the magnitude of the propellant heating problem. However, knowledge of the convection currents and flow patterns of a propellant tank subject to radiation heating requires other means of investigation before an operating prototype may be built. Undoubtedly the final testing of the propellant tank design will be the flight configuration engine similar to the proposed K-1 engine system, but extensive research and development must be done first in order to design the developmental system. Experiments in early stages of development must be performed under controllable, repeatable conditions in which the test system may be easily varied and altered as more information is obtained concerning the phenomenon under study.

One such experimental facility is the propellant tank heating analog which has been constructed by Martin Denver. In this system a model tank is filled with fluid which simulates propellant and radiant energy is beamed into the tank by a bank of infrared lamps. The fluid which represents

**CONFIDENTIAL**

---

propellant is chosen to allow a visual study of convection patterns as well as to provide data through conventional instrumentation. Such experiments are valuable in uncovering the fundamental problem areas of tank design but are not sufficiently close to the actual propellant heating situation to be used in designing a prototype engine system. Difficulties in simulating the penetrating gamma radiation as well as the short-range neutron flux hinder the realistic simulation of reactor radiations. The properties of the fluid in the analog tank make it difficult to simulate the actual fluid dynamics of liquid hydrogen in a large rocket vehicle tank.

The next step in propellant tank development should be the utilization of a powerful testing reactor as a radiation source for studying the effects of radiation heating on a liquid hydrogen test loop. An obvious experiment would make use of a vacuum-jacketed model propellant tank suspended over a reactor such as that used by Convair Ft. Worth for shield testing during the ANP program. Although some of the ANP experiments were conducted with the reactor operating in the open air at ground level or suspended from cables to avoid ground scatter, the cryogenic propellant heating experiments might better be performed in a pool-type testing reactor such as the Convair 3 Mw unit. This reactor is capable of providing up to  $10^{11}$  n/cm<sup>2</sup> sec. In the vicinity of the reactor beam tube this flux is comparable to the flux calculated at the tank bottom in the proposed K-1 engine system. A large vacuum-jacketed tank instrumented for obtaining velocity and temperature data at several locations would be used to evaluate the effectiveness of different tank configurations, baffle designs and controlled boiling schemes.

The advantages of a pool-type reactor stem from the ease with which the test equipment may be serviced and replaced. A cryogenic loop can be lowered into the pool for testing, and removed again at the conclusion of the experiment. The displaced water then re-enters the pool to shield the reactor,

~~CONFIDENTIAL~~



~~CONFIDENTIAL~~

---

and development work on the test tank can proceed immediately.

A whole model tank need not be built for this test, because the phenomena of radiation-induced convection may be observed in a partial section of the tank which duplicates the conditions of radiation heating and propellant flow found in the real tank. The configuration of the tank's vacuum jacket can be designed to provide varying thicknesses of water between the reactor and points along the tank bottom, and in this way the distribution of radiation intensity may be altered to duplicate that of the real engine system. Instrumentation would provide temperature and flow velocity data at various points within the model tank.

A prototype tank which had been developed through these experimental programs would be ready for testing along with the rest of the engine system at the start of the nuclear engine test program at NTS.

#### Component Tests

Radiation testing will be required of those components which contain parts which are subject to deleterious effects in a strong radiation environment. The effects anticipated will consist of radiation damage to certain susceptible parts of the feed system components, and disruption of the functioning of electrical equipment through the generation of spurious voltages and leakage paths through insulation and surrounding atmosphere. A final and extremely important effect is that of radiation heat generation in components located close to the reactor core.

Preliminary testing in radiation sources other than the Kiwi experiments will aid in the early development of radiation-resistant feed-system components. Tests investigating radiation damage from integrated dose effects

~~CONFIDENTIAL~~

---

should be done in existing test reactors where the advantages of more convenient scheduling of tests, controllable and repeatable test conditions, and a large and variable integrated dose are more easily obtainable than with the Kiwi-B experiments. Initial research and development should be done in these test reactors on seals and on organic components. Certain electronic equipment should also be tested to ascertain the effects of integrated-dose damage. Final stages of component development may then be done in the environment of the Kiwi-B experiments to establish the effects of dose rate in components which otherwise will have been well proven.

To investigate the transient effect of high radiation dose rates, strong fluxes must be available in which to carry out component development tests. Rate effects are most predominant in electrical equipment, instrumentation, and control components where the voltages and leakage paths induced by ionization will have the most serious effect. Test reactors such as Godiva and KEWB are the only present sources of high-intensity radiation fluxes approaching that of a nuclear rocket engine system. These reactors should be utilized as much as possible during the early phases of the electrical system development, but the more advanced phases of development must be carried out with the Kiwi-B radiation environment.

Critical instrumentation and control components should be mounted as close to the radiation source as the facility permits so that the radiation levels of the flight prototype engine may be approximated. In the case of tests utilizing Kiwi-B radiation, the controls should be cycled both during and after the reactor test. Instrumentation equipment should be calibrated before, during, and after the reactor test. Later tests may incorporate complete electrical subsystems which would be operated in the radiation environment after each of their component parts has been proven through previous testing.

~~CONFIDENTIAL~~

**CONFIDENTIAL**

---

The radiation heating problem areas which arise in certain components require testing in a strongly directional, high-intensity source to prove out initial design calculations. Existing research reactors are not capable of the high fluxes required for realistic testing, and it is therefore necessary to utilize the fluxes from Kiwi-B. Testing in the latter's radiation is hampered by the presence of atmospheric convection cooling as well as air and ground scatter, but the most critical problem areas will probably not be alleviated. The results presented in the previous chapter show that the most serious heating problems exist in components which are forced to operate at high temperatures by the nature of their function, such as the turbine rotors and the hot gas throttle valve. In a ground test, these parts will absorb additional radiation from scattered radiation which bypasses the shield, although the atmosphere will scatter some radiation away from components as well. However, the parts most likely to become overheated lie within the components subjected to the hot gas stream and are not affected by the presence of atmospheric convection cooling.

Results of the early Kiwi-B experiments will furnish radiation flux information which will provide data on radiation heating and reduce the number of radiation heating tests required later in the engine program. In spite of the limited integrated neutron flux available, valuable data on induced radioactivity will also be provided by the test of a mock-up feed system. Induced radioactivity may be scaled with reactor power and run duration to determine the induced fluxes which will be experienced with the flight prototype engine.

~~CONFIDENTIAL~~

---

### Cavitation Studies

An understanding of the phenomenon of cavitation is important for performance optimization of any rocket engine which employs a propellant pump. Cavitation may occur if the pump inlet conditions do not meet required levels of net positive suction head, which is a function of fluid static pressure and velocity head less the vapor pressure. Low static pressure is a desirable design objective to achieve minimal tank weight and pressurant requirements. In a nuclear radiation field, propellant vapor pressure will tend to be undesirably high because of nuclear energy deposition, and this problem is better understood than others. Some adverse phenomena that may be theorized are associated with transitions of propellant state and phase. One possibility is that if liquid hydrogen is being pumped in a metastable state, nuclear radiation interactions may speed the transition to an equilibrium state, leading to point pressure discontinuities from which serious cavitation may arise. One may also theorize that the energy of nuclear interactions at the pump inducer inlet may counteract whatever benefits may be attributed to evaporative cooling, and will result in an increase in the tendency toward cavitation.

Cavitation data should be obtained during Kiwi-B reactor experiments by testing propellant flow hardware on an adjacent test car or pad. An experiment could be performed with a Rocketdyne Mark IX liquid hydrogen pump driven by a gaseous hydrogen-powered Mark III turbine as utilized in Rocketdyne's Kiwi-B1 Feed System. This test would provide specific data regarding cavitation as well as the performance of several other feed system components and assemblies. Figure 74 is a schematic representation of the proposed test, indicating orientation of the radiation effects assembly. The test car will hold the pump and turbine while other system components can be installed within the test cell.

~~CONFIDENTIAL~~

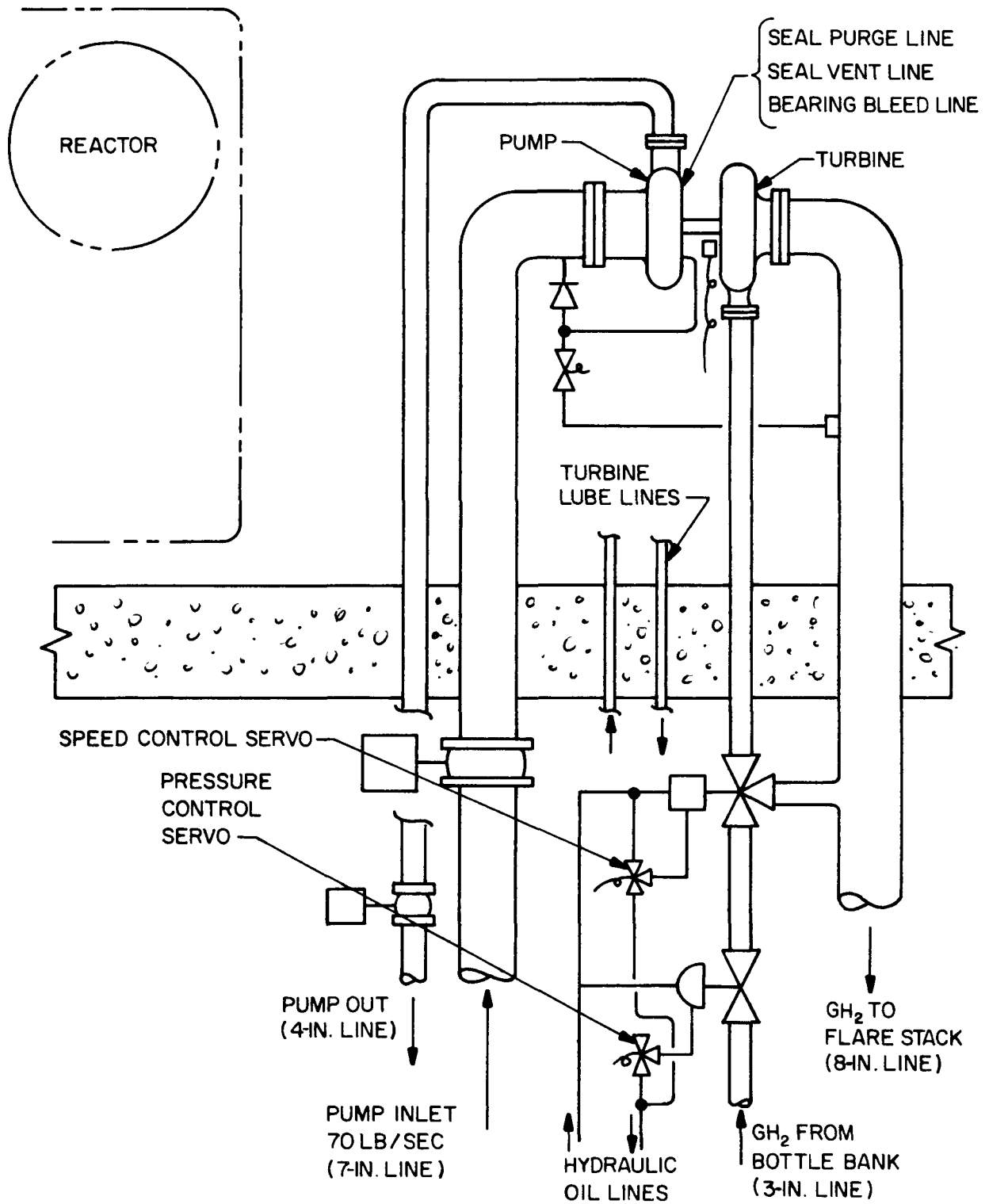


Figure 74. Cavitation Test Facility Schematic

~~CONFIDENTIAL~~

---

In the event that the test facility liquid hydrogen flow capacities and other modification requirements are not provided, an alternate test is proposed utilizing a cavitating venturi. The data obtained with this configuration will be only partially applicable to the problem, but will indicate the effects of radiation on cavitation tendencies of the hydrogen propellant. Figure 75 is a schematic of the alternate test mode. The merits of this test are based upon simplicity of the system and deletion of high liquid hydrogen flow requirements.

~~CONFIDENTIAL~~

**CONFIDENTIAL**

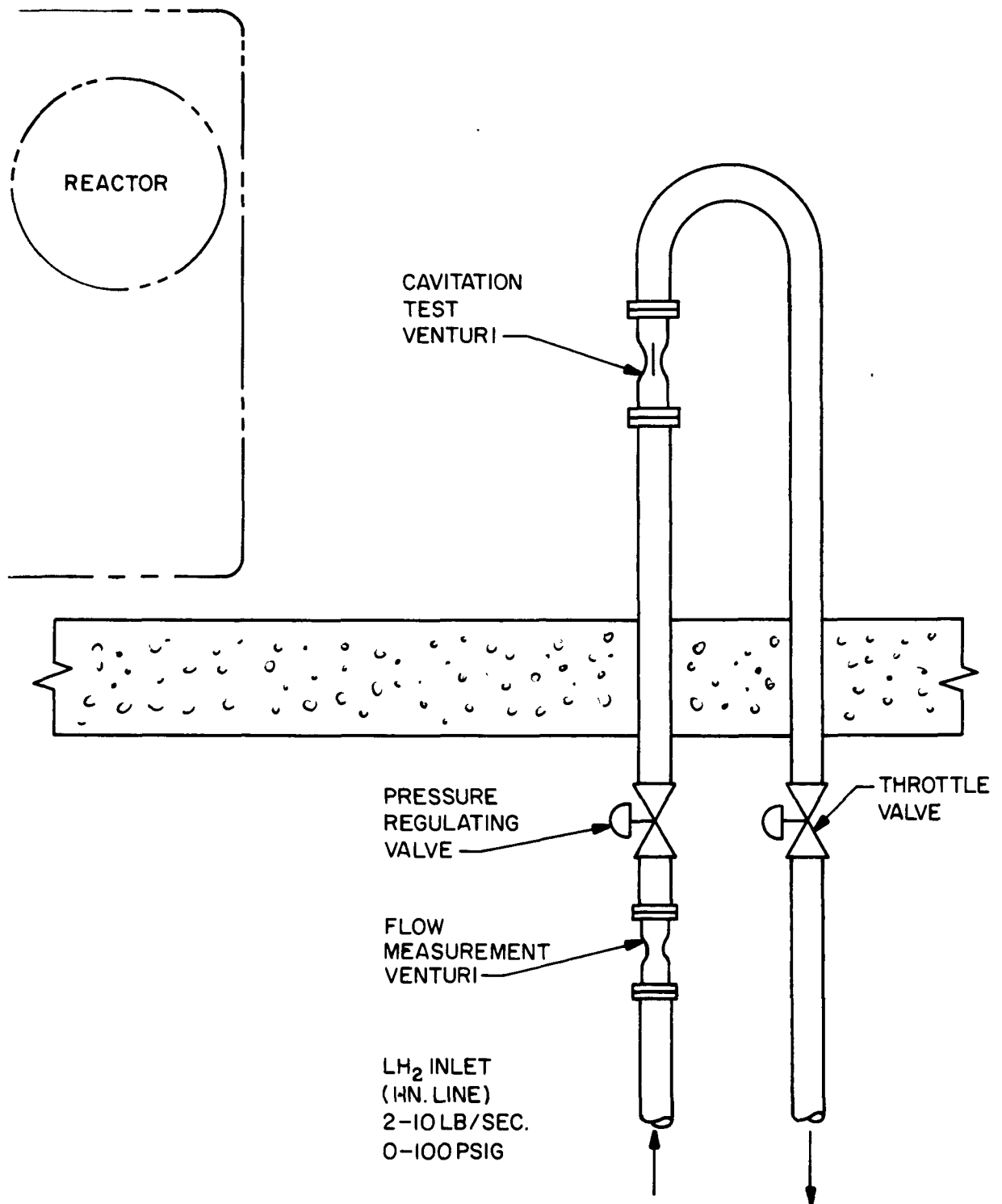


Figure 75. Cavitating Venturi Test Schematic

~~CONFIDENTIAL~~

## COMPONENT RADIATION TEST PROGRAMS

### High Speed Bearings

The liquid hydrogen feed systems developed by Rocketdyne will employ hydrogen-lubricated bearings in their high speed turbomachinery. This lubrication system answers the need for a simple, reliable lubrication system which can function at the extremely high speeds and low temperatures required for a high performance liquid hydrogen pump.

An essential feature of these antifriction bearings is the material from which their ball retainers are made. The bearing cages are constructed of glass-fiber reinforced Teflon at this stage of development. Teflon, unfortunately, is seriously weakened at the radiation doses expected from the K-1 engine system and a substitute material must be developed. Alternate cage materials were mentioned in the Radiation Damage section of this report, but it is not apparent at this time which of the alternate materials is superior. Many successful tests have been completed at Rocketdyne using cages made of graphite, and this material may be the best for this purpose.

However, the critical importance of the turbomachinery bearings from a system reliability standpoint make a complete development program necessary. Initial bearing cage development should provide for irradiation in materials testing reactors and subsequent testing in operating turbomachinery. It may eventually be of value to conduct bearing cage tests both under radiation and at cryogenic temperatures, but no indications exist at this time that the adverse effects of radiation and cryogenic temperatures in bearing cage materials may be synergistic.

~~CONFIDENTIAL~~



**CONFIDENTIAL**

---

Reactor Fragmentation Devices

Proposed reactor safety systems employ high-explosive shaped charges and explosive projectiles to break the reactor core into subcritical fragments in case of an aborted mission. The nature of this safety system makes it imperative that the explosives employed are thoroughly reliable during all stages of the vehicle's flight. The development program for these safety systems must be completed before their test in the environment of an operating reactor. It is evident that a premature detonation during a full reactor test would be extremely costly in terms of both time and money.

The effects of nuclear radiation on explosives include two possible deleterious effects: (1) decreased explosive efficiency, (2) change in sensitivity or possibility of predetonation. The developmental program should be conducted in a materials testing reactor to determine effects of radiation on the efficiency, brisance, sensitivity, and stability of the explosives under development. The effects of temperature on the functioning of shaped-charge explosive devices should also be the object of a development program. These data will provide information on the operating limitations of the reactor fragmentation safety system.

As mentioned in the radiation damage section, it appears that TNT is the most promising of these explosives but further experimentation and development is necessary. The irradiation test doses of small 5-gram samples of explosive should be equal to and above those expected in the K-1 application. The test apparatus should maintain the explosive within the anticipated K-1 temperature range and the gases evolved during and after irradiation should be analyzed. In addition, sensitivity to impact should be measured, and comparative determinations of the brisance of irradiated and unirradiated explosive should be made with a standard sand test device.

~~CONFIDENTIAL~~

---

### Control Components

Individual parts of the control system which may be sensitive to integrated-dose radiation damage should be tested separately before the components and subsystems are operated in the radiation fluxes of experimental propulsion reactors. When this preliminary development has been accomplished, the components and subsystems may undergo functional tests in the environment of Kiwi-B test reactors for resistance to radiation heating and disruption of electrical systems.

System development should be planned to include pre-exposure calibration testing as well as operational function testing in the Kiwi-B environment. The control elements will be tested again after the radiation test to obtain further information on transient and permanent effects.

The following list of presently available control elements mentions the radiation test objectives of particular importance for each device.

1. Solenoid valves and servovalves. Tests will incorporate checks for electrical noise level and insulation breakdown under operating voltage. This procedure will point out necessary design modifications for the solenoid valves and servovalves planned for use in the K-1 electropneumatic systems.
2. Feedback potentiometers. Operating loads should be imposed on these devices to check for insulation breakdown and excessive noise generation in the feedback signal.
3. Direct current motors. Several control devices employ dc motors for operation. Motors should be tested for electrical breakdown, maintenance of operating torque, and overheating.

~~CONFIDENTIAL~~

**CONFIDENTIAL**

---

4. Amplifiers. Control amplifiers, perhaps with built-in radiation and temperature compensation features, should be tested in fluxes equal to those encountered in engine operation. The proper functioning of the amplifiers and their compensation should be determined.
5. Voltage regulators. A test for proper functioning under radiation should be performed, and noise generation should be checked.
6. Step switches. These switches should be operated and checked for possible shifts in the triggering signal and for switch lockup caused by junction breakdown.
7. Electrical wiring in gaseous hydrogen-filled conduit. Tests should be made at maximum operating voltage to determine the noise level and leakage currents resulting from gas ionization and insulation breakdown.

The following are among the control system components which are not as yet available but must be tested in the high radiation fluxes of Kiwi-B before their reliability may be specified.

1. Rod actuator system
2. Engine gimbal actuator system
3. Pressure regulators
4. Electrical power supply

#### Flight Instrumentation

As in the case of control components, radiation-sensitive flight instrumentation should be tested in a materials testing reactor early during development.

~~CONFIDENTIAL~~

---

These tests will prove the equipment's resistance to integrated-dose radiation damage, and provide assurance of reliability for the full-power, full-duration K-1 engine run. Electrical disruption, the other aspect of radiation damage, must be examined under radiation conditions simulating a propulsion reactor, but few materials-testing reactors are able to supply these fluxes. Therefore, the sensitivity to radiation-dose rate of instrumentation and related circuitry must be tested in specialized reactors such as the prompt-critical test facilities of Godiva and KEWB. The radiation burst duration of these reactors will tend to limit the scope of tests for the slower transient effects. Final proof of the adequacy of flight instrumentation will be obtained through testing in the Kiwi-B reactor radiation in which suitable instrumentation will be calibrated before and after exposure, and data obtained during reactor operation will be analyzed in comparison to data obtained with reference instruments.

Equipment which should be included in the development of radiation-resistant flight instrumentation is listed below:

1. Chamber temperature thermocouples. These transducers are of extreme importance for the control of the engine system because they are a part of the primary engine control instrumentation. They must be checked under operating conditions for adequate output signal, electrical stability, and ability to withstand elevated temperatures and gas velocities. Thermocouple leads must maintain adequate resistance to radiation-induced voltages and leakage paths.
2. Turbine inlet thermocouples. Although the conditions of radiation and high temperature are not so demanding in this application as they are for thrust chamber temperature measurement, special attention should be paid to the thermocouples used here.

~~CONFIDENTIAL~~

---

Rapid response and a high degree of accuracy are necessary in these instruments which also provide inputs for the engine control system.

3. Cryogenic thermocouples. The combined effects of nuclear radiation and cryogenic temperatures may have an influence on cryogenic temperature measurement that is unknown at this time. The platinum resistance bulbs (or other devices) contemplated for use in measuring cryogenic temperatures must be tested at low temperatures and relatively high thermal neutron fluxes which will be found near the bottom of the propellant tank.
4. Pressure transducers. Several types of pressure measurement devices described previously may be sensitive to high-radiation dose rates. These instruments comprise a vital link in primary feed system control and must be highly reliable. Organic materials in these instruments should be avoided, or the transducer should be tested sufficiently to ensure successful operation. Transient effects will depend on the type of instrument and associated circuitry.
5. Flow meters. The turbine-type flow meter is seen as superior to the other varieties currently available. Nonetheless, this instrument must be tested for the ability of its electrical and magnetic components to resist radiation damage and for the maintenance of a usable signal-to-noise ratio under high radiation fluxes.
6. Strain gages. These instruments may possibly be sensitive to radiation damage through changes in the resistance of strain wires, degradation of the cement used to attach them, and electrical leakage in their insulation. Similar changes may occur in the rest of the strain gage circuit, and the high temperatures of the instrumented members under radiation may affect the performance of the gages.

~~CONFIDENTIAL~~

---

7. Accelerometers. Crystal accelerometers should be tested for permanent damage to the crystals as well as for transient effects manifested by the creation of spurious voltages and electrical leakage. Those accelerometers located in regions of high temperature and high-radiation dose rate will be subject to the additional problem of maintaining a safe operating temperature to avoid crystal damage.

#### Integrated Feed System Tests

The culmination of the various individual component and subsystem radiation tests would be the operation of a complete feed system in the radiation environment of Kiwi-B. It would be a final test of radiation resistance and would verify the component operating points. The test would be too short for accumulation of an appreciable integrated dose, and atmospheric convection would furnish unrealistic cooling for structural components, but the information on transient and rate effects would be extremely valuable. Unfortunately, limitations on existing facilities will make such a feed system test infeasible.

The propellant requirements for running a pump test simultaneously with a reactor experiment will require curtailing the duration of one or both tests. A large additional amount of vacuum-jacketed propellant lines would also be required. Another disadvantage of conducting a pump test during a reactor firing is that the possibility of a catastrophic failure of the turbopump under radiation testing would endanger not only the feed system but the reactor and test facility as well. Only an expensive, carefully designed blast shield and a fail-safe propellant cutoff system could provide absolute protection for the reactor in event of a serious malfunction.

~~CONFIDENTIAL~~

---

Difficulties in conducting a test of the complete turbopump system may be greater than the value of the test information which would be obtained in such a test. With the exception of certain feed system parts which might be susceptible to integrated dose radiation damage (and would have been replaced during the course of pump development) the pump is not critically sensitive to radiation. However, the turbine is a critical component from the standpoint of radiation heating and may experience overheating and consequent loss of strength in its second-stage rotor. If a test of the turbine alone could be conducted during reactor operation, the data obtained would provide important information on the functioning of the complete feed system under radiation. The results of this test, when combined with the results of radiation tests on other feed system components, will provide information which will assure the success of prototype engine system tests using the full feed system.

The turbine test would be accompanied by as much of the engine system control equipment as could be used, including the turbine inlet gas temperature control system. The turbine would be operated on gases from the bleed manifold on the nozzle under test, and all associated piping and valves would be included. This test has the advantage of allowing the reactor experiment to continue in case of turbine failure. Should it be necessary to terminate the turbine test, valves would be provided to direct the bleed gas from the reactor manifold to an orificed duct which would vent the gas to the atmosphere.

The turbine test with reactor bleed gas and as much of the associated control system as possible would very nearly simulate the operation of the full engine system. But there are also difficulties associated with the turbine test. It will require design and fabrication of special equipment if the turbine is to be rotating during the reactor test, and the development effort required for a device to absorb the turbine power will be considerable. The extremely high speed of the turbine plus the intensity of

~~CONFIDENTIAL~~

---

the associated radiation environment will make the design of rotor temperature instrumentation and a dynamometer or brake device very difficult. The possibility exists that a pump may be altered to pump liquid nitrogen instead of the liquid hydrogen for which it was designed, and, if this were done, a test would be obtained which might approach turbine operating loads and thermal stresses. The requirements of liquid nitrogen for this application will require additional equipment, although not so much as would be used for hydrogen.

It may be infeasible to actually run the turbine in the Kiwi-B radiation environment. If this is the case, valuable experimental data may still be obtained by performing a locked rotor test in which the turbine shaft is held stationary while the full turbine bleed gas flow is maintained. The locked rotor has the particular advantage of allowing temperature measurements over the turbine blades and wheels. Information on turbine operating temperatures in the radiation environment may be obtained in this way and conclusions drawn as to the probability of successful turbopump operation at high speed. The locked rotor test will be unrealistic in some ways because it will not provide the thermal contact at the blade roots that would be present at operating speeds, and the gas temperature at the second stage will be somewhat higher than under true operating conditions.

If calculations show the turbine stall torque to be excessive under full gas flow conditions, a dummy turbine rotor can be substituted which has blades with a zero angle of attack. Thermocouple leads would pass through the shaft and out the rear of the turbine. The operating temperatures of the turbopump can be simulated in radiation testing by providing a jacket of liquid propellant at surfaces where the turbine mates with the pump.

In spite of the difficulties associated with a turbopump or turbine test in the Kiwi-B environment, a certain amount of testing of these systems

~~CONFIDENTIAL~~



**CONFIDENTIAL**

---

under strong radiation must be accomplished before the feed system is entrusted to supply propellant to the K-1 prototype engine system. Considerable expenditure of effort is justified for the purpose of providing assurance against unforeseen failure of the reactor-turbopump system.

RECEIVED

page blank

252

RECEIVED

~~CONFIDENTIAL~~

REFERENCES

1. Maienschein, F. C., R. W. Peele, T. A. Love, and W. Zoble: "Energy Spectra of Fission-Associated Gamma Radiation," ORN - 2609, 1958.
2. Skliarevskii, V. V., D. E. Fomenko, and E. P. Stepanov: "Investigation of U<sup>235</sup> Fission Gamma Rays in the Energy Region up to 250 Kev," Soviet Physics 5. 2 pp 220-225, 1957.
3. Blomeke, J. O., and M. F. Todd: "U<sup>235</sup> Fission Product Production as a Function of Thermal Neutron Flux, Irradiation Time, and Decay Time," ORN 2127, 1957.
4. Perkins, J. F., and R. W. King: "Energy Release From the Decay of Fission Products," Nucl. Sci. and Engr. 3, 1958, pp 726-746.
5. Groshev, L. V., et al.: "Atlas of  $\gamma$ -Ray Spectra From Radiative Capture of Thermal Neutrons," International Series of Monographs on Nuclear Energy, Pergamon Press, 1959.
6. Deloume, F. E.: "Gamma-Ray Energy Spectra From Thermal Neutron Capture," APEX 407, 1958.
7. Groshev, L. V., et al.: "Thermal Neutron Capture Gamma-Ray Spectra and Nuclear Level Distribution," Presented as P/2029 in Geneva, 1958.
8. Flatt, H. P., and D. C. Baller: "The AIM-6 Code," NAA Program Description, January 1961.
9. Klein, O. and Y. Nashina, Z. Physik, Vol. 52, p 853, 1929.

**UNCLASSIFIED**

**ROCKETDYNE**  
A DIVISION OF NORTH AMERICAN ROCKET CORPORATION INC

~~**CONFIDENTIAL**~~

10. Albert, R. D. and T. A. Welton: "A Simplified Theory of Neutron Attenuation and Its Application to Reactor Shield Design," WAPD-15 (Del.), November 1950.
11. Duncan, D. S.: "Application to PIMG to Thermal Neutron Flux Calculations in Hydrogenous Shields," NAA-SR-Memo-5563, August 4, 1960.
12. Duncan, D. S. and H. O. Wittum, Jr.: "Application of Fast Neutron Removal Theory to the Calculation of Thermal Neutron Flux Distributions in Reactor Shields," NAA-SR-2380. July 1, 1958.
13. Duncan, D. S. and A. B. Speir: "GRACE I - An IBM 709 Program Designed for Computing Gamma-Ray Attenuation and Heating in Reactor Shields," NAA-SR-3719, June 30, 1959.
14. Duncan, D. S. and A. B. Speir: "GRACE II - An IBM 709 Program for Computing Gamma-Ray Attenuation and Heating in Cylindrical and Spherical Geometries," NAA-SR-Memo-4649, November 12, 1959.
15. Krumbein, A. D.: "Summary of NDA Unclassified Results of Moments Calculations for the Penetration of Neutrons Through Various Materials," NDA-92-2 (Rev.) August 30, 1957.
16. Chapman, G. T. and C. L. Storrs: "Effective Neutron Removal Cross Sections for Shielding," AECD-3978, September 1955.
17. Foderaro, A. and F. Obenshain: "Fluxes From Regular Geometric Sources," WAPD-TN-508, June 1955.
18. Gannon, M. J.: "SWAP-A," WAPD-P-701, May 1956.
19. Grodstein, G. W.: "X-Ray Attenuation Coefficients From 10 kev to 100 Mev," NBS 583, April 30, 1957.
20. Goldstein, H. and J. E. Wilkins, Jr.: "Calculations of the Penetration of Gamma Rays - "Final Report," NYO-3075, June 30, 1954.

**UNCLASSIFIED**

~~**CONFIDENTIAL**~~

21. Reactor Physics Constants: ANL 5800, July 1, 1958.
22. Schlichting, H.: Boundary Layer Theory, McGraw-Hill Book Co., Inc., 1955.
23. "Study of Supersonic Radial Compressors for Refrigeration and Pressurization Systems," WADC TR 55-257.
24. Graves and Streetman: "Propellant Heating and Payload Dose in Flyable Vehicles," Los Alamos Report N-2-1956.
25. Rockwell, T.: Reactor Shielding Design Manual, 1st Edition, USAEC, March 1956, pp 372-379.
26. Tommerhaus, K.: "Advances in Cryogenic Engineering," Vol. 5, 1960.
27. McAdams, W. H.: Heat Transmission," 3rd Edition, McGraw-Hill Book Co., Inc., 1954.
28. Eckert, E.R.G. and T. W. Jackson: "Analysis of Turbulent Free-Convection Boundary Layer on Flat Plate," NACA Report 1015.
29. Eckert, E.R.G. and R. M. Drake: Heat and Mass Transfer, McGraw-Hill Book Co., Inc., 1959, pp 235-236.
30. Acrivos, A.: "Combined Laminar Free- and Forced-Convection Heat Transfer in External Flows," AIChE Journal, 1, 285, 1958.
31. Randall, I. E., and A. Sesonske: "Effect of a Volume Heat Source on Free-Convection Heat Transfer, AIChE, Journal 5, 150, 1959.
32. Harris, S. P. and C. F. Bumpus, "Pressure and Temperature Instrumentation for Dynamic Measurements in the KEWB Program," NAA-SR-4709, 1 Nov. 1960.